# Coating stent materials with polyhedral oligomeric silsesquioxane-poly(carbonate-urea)urethane nanocomposites

**A thesis submitted in the partial fulfilment of the requirements for the degree of**

**Doctor of Philosophy (Ph.D.)**

**September 2009**

**by**

**Raheleh Bakhshi**

**University College London**

# ABBREVIATIONS

AB …….. Alamar Blue

APTT……...Activated partial theomboplastin time

γ-APS ……3-aminopropyltriethoxysilane

ATR-FTIR …….. Attenuated total internal reflection Fourier transforms infrared spectroscopy analyser

AFM ……... Atomic force microscopic

BMS……..Bare metal stent

CABG ……. Coronary artery bypass grafting

CAD …… Coronary artery disease

CE ……... Cholesterol esterase

COF…….Chronic outward force

CTB …… CellTiter-Blue

DES …… Drug eluting stents

DMAC …… N,N'-dimethylacetamide

DMEM …… Dulbecco's modified Eagle medium

DSC …… Differential scanning calorimetry

EC…….Endothelial cell

ECM ……... Extra cellular matrix

EDX …… Energy dispersive X-Ray

EHDA ……. Electrohydrodynamic spraying

EPs …….. Endothelial progenitor cells

FDA …….Food and Drug Administration

GPC …… Gel permeation chromatography

HUVECs ……. Human umbilical cord vein endothelial cells

ICP-MS …….. Inductively coupled plasma mass spectroscopy

ISR …….. In-stent restenosis

IVUS ……... Intravascular ultrasound

LMWH…….Low molecular weight heparin

LST ……. Late stage thrombosis

MDI …….4,4'-methylenebis(phenyl isocyanate)

MI ……... Myocardial infarction

MRI ……. Magnetic resonance imaging

NIH ……. Neointimal hyperplasia

NiTi ……. Nickel titanium alloy

PBS ……. Phosphate buffered solution

PCI …….. Percutaneous coronary intervention

PCU ……. Polycarbonate urea-urethane

PEG ……..Polyethyleneglycol

PEG ……..Polyethyleneglycol

PET ……..Polyethylene terephthalate

PLA ……..Phospholipase $A_2$

PLLA ……... Poly-L-lactide

PGA ……. Poly glycolic acid

POSS ……... Polyhedral oligomeric silsesquioxane

PTCA ……... Percutaneous transluminal coronary angioplasty

PU……..Polyurethane

PZC ……...Points of zero charge

RRF ……. Radial resistive force

SEM …….Scanning electron microscope

SMC …….....Smooth muscle cells

SQS ……. Silsesquioxanes

TCP…….. Tissue culture plastic

TVR …… Target vessel revascularisation

vWF…….. von Willebrand Factor

XPS ……. X-ray photoelectron spectroscopy

# TERMINOLOGY

**Angioplasty.** Angioplasty is the technique of mechanically widening a narrowed or obstructed blood vessel.

**Stent**. Stent is a man-made tube inserted into a natural vessel /conduit in the body to prevent, or counteract, a disease-induced, localized flow constriction.

**Restenosis** literally means the reoccurrence of stenosis, a narrowing of a blood vessel, leading to restricted blood flow. Restenosis usually pertains to an artery/large blood vessel that has become narrowed, received treatment to clear the blockage and subsequently become renarrowed.

**Intimal hyperplasia.** Intimal hyperplasia is the universal response of a vessel to injury. It is the thickening of the layer of a blood vessel as a complication of a reconstruction procedure.

**Magnetic Resonance Imaging**. Magnetic Resonance Imaging is primarily a medical imaging technique most commonly used in radiology to visualize detailed internal structure and limited function of the body.

**Haemostasis.** Haemostasis is a complex process which causes the bleeding process to stop. It refers to the process of keeping blood within a damaged blood vessel

# TABLE OF CONTENTS

## CHAPTER 3. Materials & Methods

# ABSTRACT

The long-term efficacy of coronary or peripheral stenting is limited by in-stent restenosis (ISR), which occurs in 15 to 30% of patients and is attributed primarily to neointimal hyperplasia. By adding a drug-eluting coating, this rate has been reduced to about 5% or less. However, recently longer-term follow-up data has highlighted problems with drug-coated stents, including late stage thrombosis. A bio-stable poly(carbonate-urea)urethane has been used for stent coating and the surface properties of the polymer have been optimised by incorporating the polyhedral oligomeric silsesquioxane molecule. These POSS polymers improve the adhesion and the growth of endothelial cells. The work described in this thesis, presents an innovative approach in self-expanding/balloon expandable coronary stent design that incorporates a NiTi/stainless steel alloy scaffold with a polyhedral oligomeric silsesquioxane- poly (carbonate-urea) urethane nanocomposite polymer (POSS-PCU) coating. Electrohydrodynamic spraying and ultrasonic atomization spraying of the non-biodegradable nanocomposite polyhedral oligomeric silsesquioxane (POSS) polymer have been investigated in detail for coating metallic stent materials and compared with dip coating. Because of the tight geometry of coronary stents, these new coating techniques have been shown to offer advantages over traditional coating techniques. These advantages include, reduced polymer consumption, precise coating thickness as low as 10 μm and a highly controllable spray which leads to consistent reproducible results. However, poor adhesion, or bond deterioration over the lifespan/ deployment of the device could reduces the efficiency and could impart even more complexity to the implant including formation of debris which can induce thrombus formation. Changing the surface physical property/chemical composition through the proposed protocol has been shown to increase the bonding strength by up to three times. This study has identified a new process and conditions which can be used in stent coating research.

# PUBLICATIONS AND PRESENTATIONS

1. R. Bakhshi, M.J. Edirisinghe, A. Darbyshire, Z. Ahmad, A. M. Seifalian; Electrohydrodynamic jetting behaviour of polyhedral oligomeric silsesquioxane nanocomposites. Journal of Biomaterials Applications, 2009; 23(4):293-309.

2. R. Bakhshi, J.Eaton-Evans, M.Edirisinghe, A.Darbyshire, Z.You, A.M.Seifalian, G.Hamilton; A novel nanocomposite polymer for the development of a new aortic stent graft. British Journal of Surgery (Abstract), 2009; 96(s1):5.

3. R. Bakhshi, M.J.Edirisinghe, J.Eaton Evans, A. Darbyshire, Z.You, J. Lu, A.M.Seifalian; Polymeric coating of surface modified nitinol stent with POSS-nanocomposite polymer using electrohydrodynamic spraying. Submitted to the Journal of The Royal Society Interface.

4. R. Bakhshi, M.J. Edirisinghe, A.Darbyshire, AM. Seifalian; Surface properties and biological behaviour of Polyhedral Oligomeric Silsesquioxane/poly(urea-urethane) carbonate hybrid nanocomposite. Final version is being finalized for submission to Biomaterials.

5. R.Bakhshi, A.Darbyshire, M.J. Edirisinghe, G. Hamilton, A.M.Seifalian; Novel nanocomposite polymer for cardiovascular devices. Nanoparticles 2008, Bradford (UK), February 2008.

6. R.Bakhshi, J.Eaton-Evans, M.J. Edirisinghe; Development of Abdominal Aortic Aneurysm stent graft with bioactive nanocomposite polymer. 8th World Biomaterial Conference, Amsterdam (Netherlands), May 2008.

7. R.Bakhshi, M.Edirisinghe, J.Eaton-Evans, A. Darbyshire, H.Salasinski, R.Kannan, A.Seifalian; Surface compatibility of a new origami based AAA

and coronary stents integrated with a nanocomposite polyurethane graft. British Cardiovascular meeting, Bournemouth (UK), November 2008.

8. R.Bakhshi, J.Eaton-Evans, M.Edirisinghe, A.Darbyshire, Z.You, A.M. Seifalian, G.Hamilton. Novel nanocomposite polymer for the development of a new aortic stent graft. Pearce Gould Visiting, UCL, London (UK), November 2008.

# ACKNOWLEDGEMENTS

I am forever grateful to Professor Mohan Edirisinghe for believing in my abilities and inspiring me to achieve my full potential. Thank you for giving me the opportunity to carry out this project and providing immense supervision and support.

I wish to express my deepest gratitude to Professor Alexander M Seifalian, whose unending supervision, help and patience have been invaluable. Thank you for giving me the opportunity to work on this project and for the constant support.

There are so many others in the Department of Mechanical engineering and Department of Surgery who have given me constant support and encouragement. My sincerest thanks to Dr. Zeeshan Ahmed, Dr. Bala Ramesh, and most particularly to Mr. Arnold Darbyshire. This thesis would have not been possible without all his help and advice.

I am very grateful to all staff and my colleagues at Department of Mechanical engineering and Department of Surgery for their constant support and most of all for their friendship.

I would also like to thank EPSRC for the financial support.

And lastly but most importantly my thanks go to my dearest parents for their sacrifice, love and support in numerous ways on my personal development. I would like to thank my dearest brother, Hamid Reza, who has always believed in me and whose support is an immense source of strength.

# LIST OF TABLES

# LIST OF FIGURES

Esterase; (C) Phospholipase A2; (D) Plasma fraction II; (E) Plasma fraction III; (F) $H_2O_2$ ; and G) t-butyl peroxide after 70 days.

**Figure 6.10.** Peel strength test of coated NiTi strip following 70 days immersion in different media. A) hydrolytic solutions, B) plasma fractions and C) oxidative/peroxidative solutions.

**Figure 6.11.** Ni release profiles from NiTi strips obtained from mass spectroscopy. Strips were incubated in DMEM.

**Figure 6.12.** Ni release profiles from NiTi strips obtained from sass spectroscopy. Strips were incubated in plasma fraction I.

# CHAPTER 1. Introduction

Since the introduction of stents to clinical cardiology, several researchers have shown the superiority of coronary stent implantation as compared to conventional angioplasty. However, restenosis still remains a major drawback of this technique. Basic research in animal models has identified stent-related factors including stent-material and stent-design as major determinants of intimal proliferation. The concept of stent coating has been developed to allow the combination of favourable biomaterial characteristics from different materials.

In this thesis a novel nanocomposite polymer for the stent coating application is being introduced. The properties of the nanocomposite for the application at the vascular interface are investigated. The application of new methodologies to coat bare metal stents including stainless steel and NiTi are investigated.

## 1.1. Contents of this thesis

In this thesis, a critical literature review on the conventional treatments for cardiovascular diseases is presented in Chapter 2. After a brief description of cardiovascular disease, conventional treatments of the disease are introduced. This chapter also discusses stents technology in more detail. The current development of stent technology is investigated. Then the problems with current stents either in clinical studies or research are discussed. It also discusses the possible role of nanotechnology in the development of stents, and finally it reviewes the different

coating methods in more detail, as stent materials coating is one of the main objectives behind this thesis research.

Chapter 3 gives a detailed description of the experimental procedures. This chapter discusses the materials and techniques used for the research carried out in experimental chapters 4, 5 and 6. The polymer characterization techniques and procedures are described. The equipment used for the electrohydrodynamic processing and ultrasonic atomization spraying is discribed in detail. A protocol for surface treatment of Nitinol (NiTi) is also described.

Chapter 4 discusses the characterisation of the developed nanocomposite introduced in this thesis. The bulk and surface properties of POSS-based nanocomposite are discussed in depth and compared to a carbonate based-polyurethane. The surface properties of the nanocomposite are of greatest importance as the application of the nanocomposite is investigated at the vascular interface.

Chapter 5 discusses the application of two methodologies, electrohydrodynamic spraying and ultrasonic atomization spraying techniques to coat bare metal stents including stainless steel and NiTi. The techniques have been optimised for both methodologies using POSS-PCU nanocomposites and best processing parameters selected.

Chapter 6 describes a new surface modification technique, developed to coat NiTi alloy. This alloy has been developed in development of stents. The morphological and topographical changes at the surface of the NiTi are also assessed upon surface

modification. The bond strength between the nanocomposite and the NiTi after surface treatment was also investigated and compared with un-modified NiTi.

In each experimental chapter, an extensive discussion has been carried out and a summary of the conclusions outlined in Chapter 7. Chapter 7 also set out the future plan of actions in order to further exploit the research development for biologically assessment of nanocomposite for stent application.

### 1.2. Hypothesis

Silsesquioxane-polyurethane nanocomposites possess the optimal characteristics as coating for cardiovascular stents, as they are biocompatible, biostable, strong, and have the surface characteristics with the potential of anti-thrombogenecity and endothelialisation properties.

### 1.3. Aims and objectives of the research

The primary aim of this study was to introduce a nanocomposite polymer for stents coating. For this reason, a range of silsesquioxane based-polyurethane nanocomposites were studied in order to select the most suitable polymer for further investigations. The selected nanocomposite should have good biostability and elasticity in the first step. Second, nanocomposites were studied to optimise the surface properties for blood-polymer interactions.

The secondary aim was to understand the fundamental of electrohydrodynamic processing and ultrasonic atomization spraying to use these techniques nanocomposite solutions. By understanding process parameters, optimum conditions for

electrohydrodynamic/ultrasonic atomization spraying for coating stents materials with nanocomposite is the one of the main objectives of this thesis.

Failure of the coating of the stents *in vivo*, reduces the efficiency and imparts even more complexity to the implant including formation of debris which can induce thrombus formation. Therefore, the other aim of this work is to increase the longevity of the coating of the stent materials by introducing a protocol for effective bonding of the nanocomposite polymer to NiTi.

# CHAPTER 2. Literature Review

## 2.1. Cardiovascular disease

Cardiovascular disease broadly covers a range of conditions affecting both the heart and the blood vessels. It is the leading cause of death in the aged western population (Hooi et al. 2004). In America alone, almost 2,400 deaths occur each day as a result of the disease, an average rate of one death every 37 seconds (Rosamond et al. 2008). When atherosclerosis which is described as the hardening and loss of elasticity of arteries occurs in the coronary arteries it is refered to as coronary artery disease (CAD). This causes about 2100 deaths annually per million of the population in England and Wales (about 110,000 deaths in total). The disease is typically caused by the deposition of atherosclerotic plaques (inflamed fatty deposits) on the inner wall of arteries (Mayer et al. 2007), which narrows the vessel lumen and obstructs the coronary arteries. This narrowing is commonly referred to as a stenosis and leads to a consequential restriction of the blood supply to the muscle cells surrounding the heart. Coronary artery stenosis may be asymptomatic or may lead to shortness of breath and angina, a chest pain. A critical reduction of the blood supply to the heart may result in myocardial infarction (MI) or death.

The atherosclerotic lesions that form may also become fragile and rupture, resulting in thrombus formation and a further restriction of blood flow. The symptoms and treatment depend on which set of arteries are affected. Peripheral artery disease mainly relates to vessels of the lower limbs (Kirkpatrick 1999). However, the symptomatic prevalence is mainly in vessels smaller than 6 mm internal diameter.

## 2.2. Vessel structure and function

Oxygenated blood is distributed to the heart via the coronary arteries which are on the surface of the heart. The two primary coronary arteries are the left and right main coronary arteries. These originate near the cusps of the aortic valve. Additional arteries branch off the two main coronary arteries to supply the heart muscle with blood. Since coronary arteries deliver blood to the heart muscle, any coronary artery disorder or disease can have serious implications by reducing the flow of oxygen and nutrients to the heart, which may lead to myocardial infarction and possibly death. The vascular system is composed of arteries, capillaries and veins. Differentiation of arteries and veins results in their anatomic layers.

The wall of an artery consists of three layers. The innermost layer, which is in direct contact with the flow of blood, is the tunica intima. This layer is lined with endothelial cells (ECs) which form flat pavement-like patterns on the inside of the vessels and are surrounded by a connective tissue basement membrane. The basement membrane separates endothelium from the underlying layers. ECs act as protective barrier and control the exchange of nutrients and fluid between blood and tissue, which is the basis for the maintenance of the stability of the physiological environment essential to cell survival. The middle layer is the tunica media and it is usually the thickest layer. It is composed of smooth muscle cells (SMC) and extracellular matrix (ECM). It not only provides support for the vessel but also changes the vessel diameter to regulate blood flow and blood pressure. The outermost layer, which attaches the vessel to the surrounding tissue, is the tunica adventitia. It is composed of connective tissue and contains primarily fibroblasts, elastic and

collagenous fibers. These fibres allow the vessel to stretch whilst preventing overexpansion due to the pressure that is exerted on the walls by blood flow.

Blood passes through capillaries into venules, it then flows into progressively larger veins until it reaches the heart. The walls of the veins have the same three layers as the arteries, but develop thinner walls. The tunica media (smooth muscle) and tunica externa (connective tissue) are much reduced and have the media composed primarily of SMC with relatively low amounts of elastic tissue.

## 2.3. Conventional treatments of cardiovascular disease

The symptoms and health risks that are associated with a stenosed (narrowed) artery may be treated medically by modification of risk factors and/or by drug treatment. If these medical treatments fail or are inappropriate, two invasive therapies are available for improving the blood flow in occluded vessels. The first is called percutaneous transluminal coronary angioplasty (PTCA) - or simple balloon angioplasty- and it involves a non-surgical widening from within the artery using a balloon catheter (Gruentzig et al. 1979). The first clinical application of coronary angioplasty using a balloon catheter was performed more than 20 years ago by Gruentzig (Gruentzig 1978). In PTCA a balloon-tipped catheter is inserted into the body, typically via the femoral artery located in the groin and negotiated to the site of occlusion. Balloon inflation within the stenosed section compresses the plaque against the vessel wall, increasing the internal diameter of the lumen and hence, increasing blood flow. The balloon is subsequently deflated and the catheter removed (Figure 2.1).

The second therapeutic option left is coronary artery bypass grafting (CABG) (Cook et al. 2007) and it involves major cardiac surgery. In coronary artery bypass surgery, the affected artery is bypassed by grafting another blood vessel (usually saphenus vein (Kunlin J. 1949) from the leg) to carry blood around the obstruction, thereby improving myocardial blood supply (Figure 2.2). In the 1970's and 1980's, an artery from the inside of the chest wall, the internal thoracic artery was used as an alternative to vein for the bypass grafts (Berroeta et al. 2006). Bypass grafting typically requires open-chest surgery and the use of a heart-lung bypass machine to circulate and exygenate the blood. The patient may need to stay in the hospital for a few days after open-chest bypass surgery, and possible complications may develop from the surgery.

Bypass surgery is usually performed for heart attack only when other treatments, such as medicine and angioplasty, are unlikely to be effective because of the location or extent of the blockage. Bypass may be a better option for people with diabetes or with two or more blocked coronary arteries. Generally, the greater the extent of coronary atherosclerosis, the greater the benefits of bypass surgery over angioplasty (Smith, et al. 2006). CABG is offered when there is a blockage of 50% or more in the left main coronary artery, alone, or 70% or more in all three other major coronary arteries. For patients who do not have suitable vein or are not able to tolerate general anaesthesia, CABG is not usually practible.

Although PTCA is of lower cost and is far less invasive than CABG surgery, restenosis of the artery is an associated problem (Dorros et al. 1983). Restenosis is a narrowing at the site of balloon dilatation (Waller et al. 1991). It develops rapidly following the procedure. The precise mechanisms for restenosis probably vary

between patients, but a combination of artery wall remodelling and intimal hyperplasia is likely involved (Austin et al. 1985). Restenosis has three main causes (Lafont et al. 1995; Schwartz et al. 1998). The first, recoil of the artery, happens when the balloon is deflated. It usually occurs immediately or after 24 hours of completion of the procedure, and may require emergency CABG. The subsequent problem - negative remodelling- mostly arises during the first six months and is a contraction of the adventitia secondary to an injury reaction (3-6 months). In the case of negative remodeling, this contraction is non-uniform, leading to areas of sagging or bulging within the vessel, resulting in a restenosis of the vessel lumen. The third subsequent problem that can result from the mechanical process of balloon inflation within the target vessel is vascular injury, initiating an inflammatory response that stimulates the migration of smooth muscle cells to the site of trauma (4-6 months) (Hou et al. 2000). This migration of cells is coupled with rapid proliferation, resulting in the uncontrolled build up of cellular (scar) material. This process of rapid cell proliferation is commonly termed neointimal hyperplasia (NIH). The elastic nature of an artery means that expansion during balloon inflation is followed by a subsequent contraction as the balloon is deflated. As a consequence of these physiological responses to balloon induced arterial injury, PTCA has associated with it a 30 to 50% restenosis rate (failure rate) within a year of the procedure (Serruys et al. 2002). A repeat procedure is required consequently in approximately 20% of patients with simple lesions. The rate of re-intervention is much higher (up to 50%) for arteries of small calibre (≤3mm), long lesions, total occlusion and in people with diabetes.

Interventional cardiologists have employed a number of approaches in order to reduce the rates of restenosis following vascular interventions. In the mid-1990s, balloon

angioplasty with a procedure known as stenting, revolutionized the treatment of coronary artery disease. The main advantage is that it is carried out as an outpatient procedure, reducing costs and recovery time significantly. With a success rate of 70-75% in terms of vessel patency, it is replaced by bypass surgery except for multiple blockage cases (van Domburg et al. 1999).

## 2.4. Stents

Since 1996, implantation of stents in blood vessels has been performed in humans after angioplasty to prevent occlusion and restenosis of coronary arteries (van Domburg et al. 1999). A stent constitutes the most effective way to treat stenosis since they act as permanent prosthetic linings to keep the artery inflated and maintain its patency.

Coronary stents are small cylindrical wire mesh tubes, range from 8 to 38 mm in length and from 2.5 to 4 mm in diameter (Vaina & Serruys 2006). Stents differ in inetrunit connections, flexibility, radiopacity, surface area coverage and composition. Because of the mechanical strength required to properly support vessel walls, stents are typically made of metallic materials including stainless steel, cobalt and tantalum alloys (Kang et al. 2007; Liu et al. 2006; Mani et al. 2007). Stents are deployed in conjunction with balloon angioplasty, whereby the stent is crimped over the deflated balloon located at the end of the catheter and expanded *in situ* as the balloon is inflated (Figure 2.3).

The stent device is not attempting to remove the obstruction, but instead, to create a larger lumen within the lesion. Thus the ideal stent should capitalize on the

development of a purposeful, localized dissection and plaque disruption. An ideal stent should expand the artery stenosis mechanically and propagate pulsatile blood flow. Second, the material itself needs to be biocompatible, corrosion resistant, resistant to thrombus, stenosis and external compression, visible using standard x-ray and magnetic resonance imaging (MRI) methodology. The material also needs to be fatigue resistant because, the device is subjected to continuous cyclic loading induced by systole/diastole blood pressure after the implantation (Poncin & Proft 2003; Whittaker & Fillinger 2006). Selection of a specific stent for a patient is generally made based on the operator's experience with that stent, lesion characteristics (i.e. ease of stent deliverability, need for side-branch access, size of the target vessel, lesion length) and the stent delivery system.

Currently there are two broad categories of stents: balloon-expandable and self-expanding. 316L stainless steel, an alloy of iron, chromium, and nickel is frequently used for the balloon expandable stents. Examples of balloon expandable stents are the Palmaz stent (Cordis Corp., Warren NJ) made from stainless steel and the Strecker stent (Medi-Tech, Watertown MA) made from tantalum (Figure 2.4A). If the stent is to be balloon expanded, it must exhibit plastic deformation in the strain range corresponding to the balloon expansion to avoid recoil.

Although nickel-titanium alloy (Nitinol/NiTi) was first developed for aerospace technology (Nickel Titanium Naval Ordinance Laboratory) (Whittaker & Fillinger 2006), it is being utilized in medical applications. The use of NiTi in medical devices ranges from orthodontic dental arch wires, medical guide wires for diagnostic and more recently in self-expanding endovascular stents (Tan, Dodd, & Crone 2003).

Nitinol exhibits a combination of properties (which will bw discussed later in thi section) which makes these alloys particularly suitable for self expanding stent. Examples of the self-expanding stents are the Wallstent (Schneider and Minneapolis MN, USA) made from Ni-Co-Ti-Steel, the Gianturco Z-stent (Cook, Bloomington IN) made from stainless steel and the Symphony stent (Boston Scientific/Vascular, Natick, MA) made from Nitinol (Figure 2.4B). If the stent is to be self-expanded, it needs a shape memory effect (see section 2.4.1.2) at body temperature.

### 2.4.1. Application of NiTi in biomedical application

The growth of NiTi in the medical industries has exploded in the last 20 years. Currently available stent metals like stainless steel and tantalum have limitations such as suboptimal radiopacity and mechanical properties which may complicate insertion and positioning of the stent at the site of obstruction. In contrast, NiTi alloy (with nearly equiatomic nickel and titanium distribution) has attracted considerable attention for such an application. This is because of its several advantages, including optimal radiopacity, superelasticity and shape memory characteristics and good biocompatibility (Poncin & Proft 2003; Stoeckel et al. 2004; Whittaker & Fillinger 2006). In this section, after a brief explanation of the fundamental mechanisms of shape memory and superelasticity is followed by a describtion of how they relate to the characteristic performance of self-expanding stents.

#### 2.4.1.1. Superelastic properties

Superelasticity refers to the ability of certain metals to undergo large elastic deformation. Conventional stent materials, such as stainless steel or cobalt-based alloys, exhibit different elastic deformation behaviour from that of the structural

material of the living body. The elastic deformation of conventional stent materials is limited approximately to 1% strain, and elongation typically increases and decreases proportionally with the applied force. In contrast to this material, Nitinol alloys can be elastically deformed.

A stress-induced phase transformation is accompanied by strains in excess of 8% that can be fully recovered through a reverse phase transformation if the material is unloaded (Figure 2.5). The loading and unloading show plateaus, along which large deflections (strains) can be stored during loading or recovered during unloading with small changes in loads (stress). After an initial linear increase in stress with strain, a large strain can be obtained with only a small further stress increase. This is called the loading plateau. The end of this plateau is reached at approximately 8% strain. Unloading from the end of the plateau region causes the stress to decrease rapidly until a lower plateau (unloading plateau) is reached. Strain is recovered in this region with only a small decrease in stress. The last portion of the deforming strain is finally recovered in a linear fashion. Because more than 8% deformation is elastically recovered, this behaviour is called superelasticity.

Stainless steel, titanium and other metals are very stiff relative to biological materials, yielding little in response to pressures from surrounding tissue. The extraordinary compliance of NiTi clearly makes it the metal most mechanically similar to biological materials (Figure 2.6).

#### 2.4.1.2. Shape memory properties

An additional unique attribute of superelastic devices is that they can be deployed using the shape memory effect. This character is due to their ability to revert to a pre-deformed shape on heating. While superelasticity is the result of a stress-induced phase transformation, shape memory is the result of the thermal phase transformation. In fact, when the superelastic NiTi is cooled to below a critical temperature, which is called the transition temperature and is dependant on the alloy composition and processing history, it also changes its crystal structure. If no force is applied, this phase change is not accompanied by a shape change. The material can be plastically deformed in the 'low temperature' state and can be restored by heating above the transition temperature (Stoeckel e al. 2004).

Self expanding Nitinol stents manufactured with a diameter larger than that of the target vessel. The transition temperature is set at 30°C (below body temperature); where it is called martensitic state which is the phase state below transition temperature. The stent can be easily crimped at or below room temperature and placed in the delivery system. The device is received by the physician preloaded in a catheter and in its martensitic state. It will stay compressed while positioning to the deployment site until temperature is raised to above 30°C. At the desired location it will be released from the catheter and warm up to body temperature. It recovers its 'pre-programmed' shape and expands until it hits the vessel wall. Now, at body temperature the stent is superelastic. All the self expanding stents, therefore, are constrained in the delivery systems to prevent premature deployment.

Advantages over current balloon expandable stents include a greater resistance to crushing in exposed vessels (such as the femoral or carotid arteries), explain lower bending stresses when situated in tortuous paths, more flexible delivery systems and the elimination of recoil.

#### 2.4.1.3. Dynamic interferences

Self-expanding stents take advantages of another important feature of super-elasticity; which is called dynamic interference. Following balloon expansion, the balloon is deflated, causing the stent to spring back towards its smaller, undeformed shape. This spring back or loosening is an undesirable feature. In order to fill a 5 mm lumen, the stent might have to be expanded to 6 mm so that it springs back to 5 mm. This potentially damages the vessel and leads to restenosis. In contrast, the NiTi stent expands directly to its pre-programmed diameter with no recoil (Stoeckel, 2004).

The delivery of a stent made from super-elastic Nitinol is illustrated in Figure 2.7. The stent is delivered through the loading curve to point A. Upon release form the delivery system inside the vessel, it expands following the unloading path of the stress/strain curve, at point B it reaches the diameter of the vessel lumen, positioning itself against the vessel wall with a low outward force (Chronic outward force, COF). This force remains nearly constant even if the vessel increases in diameter. If the vessel contracts through spasm or is compressed from outside, the stent resists deformation by a higher force (Radial resistive force; RRF). This hysteresis stress of the NiTi allows for the design of self-expanding stents that exert only low outward force but resist deformation with a much higher force. After deployment, the NiTi continues to gently push outwards the vessel wall, helping to prevent undesirable changes in position

despite movements in the vessel. After deformation is completed, it is deployed by releasing from the catheter until the lumen is filled and expansion stopped (point B). The gentle pressure against the vessel wall is controlled by the unloading arrows, but effort to reclose the vessel is restricted by the stiffness indicated by the unloading arrows.

## 2.5. Problems with bare metal stents

Stents decrease restenosis by providing the largest initial expansion diameter and by preventing the early recoil which occurred with angioplasty and late negative remodelling of the treated vessel (Kuntz et al. 1993; Kuntz et al. 1992). Despite the wide use of intracoronary stents, biocompatibility still remains limited by in-stent restenosis (ISR) which occurs in 15 to 30% of patients. The lesions or cases in which stenting is of unproven benefit include: small vessels (<3 mm lumen), long lesions, left main coronary artery disease and bifurcation lesions. Lesions and cases for which stenting is beneficial include; native coronary artery lesions in vessels ≥ 3mm in lumen, chronic total occlusions, restenotic lesions, acute MI and treatment of threatened artery closure.

Histological studies following coronary stenting have shown ISR can be attributed primarily to neointimal hyperplasia. Neointimal proliferation occurs principally, but not exclusively, at the site of the primary lesion within the first six months after stent implantation. The bulk of ISR consists of extracellular matrix, proteoglycans, and collagen, with only 11% cells. Stents-induced arterial injury and lipid core penetration that occurs during stent deployment leads to increased acute and chronic inflammation of the vessel wall (Farb et al. 1999). This in turn leads to the elaboration

of cytokines and growth factors that induce multiple signalling pathways and activate the migration and proliferation of smooth muscle cells (Kornowski et al. 1998; Suzuki et al. 2001). Extra cellular matrix (ECM) is deposited by activated fibroblasts resulting in luminal narrowing, resulting in the deposition of platelets and fibrin at the site of injury, forming thrombus and causing leukocyte migration (Fattori & Piva 2003a).

In addition to ISR, bare metal stents (BMS) also have associated with them the risk of acute and subacute thrombosis within the first month following stenting (Bertrand et al. 2000). Several factors increase the risk of stent thrombosis, including the damage of the vessel wall during delivery of the stent, the resistance of the body to having a foreign material within the vascular system, which can release metal ions; that is, chromium and molybdenum leached from stainless steel reacts with hydrogen peroxide and superoxide anions producing free radicals and further inflammation (Koster et al. 2000). Vascular trauma and/or the presence of artificial prostheses within the vascular system incite a series of complex reaction mechanisms. An aggressive physiological response is elicited by the body in order to restore 'normality' throughout the entire vascular system and regain what is commonly referred to as haemostasis.

In the clinical setting, neointimal formation and in-stent restenosis are related to patient-specific factors such as genetic predisposition or diabetes mellitus (Sobel 2001), to lesion-specific factors such as vessel calibre (Mintz et al. 1996), lesion length or plaque burden (Prati et al. 1999) and to procedure-specific factors such as the extent of vessel damage, residual dissections (Kornowski et al. 1998), number of

stents, minimal stent diameter or minimal stent area. Patient-specific factors can not be influenced to any extent. Attempts to modulate lesion-specific factors by pharmacological therapy have not been successful so far. Procedure-specific factors may be favourably affected by the stent implantation technique and stent characteristics. This has resulted in a huge variety of stents, differing in design, material, surface, radioactivity and coatings (Gunn & Cumberland 1999).

Stent design varies in the geometry (number of intersections and interstrut area), in the strut configuration and the surface metal-to-artery tissue ratio. These are the major determinants of stent profile, flexibility, radial strength and (elastic) expansion characteristics. The elastic modulus- or stiffness- of the material affects stent expansion properties as late as eight weeks after deployment (Hofma et al. 1998). Reduction of strut–strut intersections can reduce the vascular injury, thrombosis and neointimal hyperplasia (Rogers & Edelman 1995). Surface characteristics can be modulated by (electromechanical) polishing, ion implantation or coating. Surface characteristics include chemistry, charge, and texture (Edelman et al. 2001) modulate cellular vessel response (plasma proteins, inflammatory and proliferative mediators, platelet and leukocyte activation). Suitable stent materials are metals, metal-alloys or polymers. Stent coatings can dramatically reduce protein deposition and platelet adhesion in experimental settings (Regar et al. 2001).

## 2. 6. Bare metal stent coatings

Whilst there is considerable literature on the effects of coating stents much of this is flawed by poor experimental design as comparative uncoated stents are not included in trials. Coatings are various and can be classified in different categories. A variety

of biologically inert coatings have been investigated to render the stent surface less thrombogenic.

### 2.6.1. Metallic stents and surface treatments

In addition to the choice of material, metallic coatings and surface treatments have been investigated for their ability to add functionality and improve the haemocompatibility of stents. De Scheerder *et al.* have evaluated the effect of metal surface treatment, using electrochemical polishing on stent thrombogenicity and neointimal hyperplasia in both a rat arteriovenous model and a porcine coronary model (De Scheerder et al. 2000). Electrochemical polishing decreased early thrombus formation (7 days) and reduced neointimal hyperplasia by 40% (6 week follow-up) after stent implantation when compared to un-polished stents. The pathophysiological mechanism that most likely explains the decrease of thrombus formation is that electrochemical polishing results in a decreased surface area, resulting in less platelet adhesion and fibrinogen binding. In addition, both polished and un-polished NiTi stents displayed significantly less thrombus formation in comparison to stainless steel stents. This may be because of the unique stress-strain relationship of the alloy that allows uniform stent expansion at low pressure. So, the thermoelastic Nitinol stent induced less acute arterial injury during deployment than the balloon expandable stainless steel and therefore is associated with less thrombus formation (Carter et al. 1998; Sheth et al. 1996).

### 2.6.2. Inorganic/Ceramic coating materials

Gold is biocompatible and more radio-opaque than stainless steel. Initial *in vitro* and animal studies demonstrated improved patency resulting in reduced rates of thrombus

formation, neointimal hyperplasia and improved re-endothelialisation (Vom et al. 2002). These results were not reproduced in subsequent clinical trials and significantly increased angiographic restenosis and less favourable one year event free survival was reported. A comparison of gold coated versus uncoated stainless steel NIR™ stents (Medinol, Inc.), concluded that gold coating triggers an exaggerated vascular response resulting in increased risk of restenosis, possibly by gold allergy (Svedman et al. 2005) but no increased risk of acute thrombosis (Park et al. 2002b). Gold-plated stent restenosis has been found to be diffusing that involves the overall stent length indicating a great proliferative neointimal response (Danzi et al. 2002). Some randomized studies showed that gold-coated stents are associated with an increased neointimal proliferation.

Silicon carbide is an inert semiconductor. In part the thrombogenicity of bare metal stent (BMS) is due to electron transfer between blood and the stent. Silicon carbide reduces this electron transfer resulting in reduced thrombogenicity and improved biocompatibility. It has been demonstrated to reduce platelet and leukocyte activation *in vitro* compared to stainless steel and tantalum stents. Initial clinical trials have not demonstrated any benefit over uncoated stents (Unverdorben et al. 2003).

Titanium nitric oxide (TiNOX) does not produce the reduction-oxidation reactions, hydrolysis or metal-organic ion complex formation demonstrated by the nickel component of stainless steel (Kandzari et al. 2002). Porcine studies compared TiNOX-1 (ceramic) or TiNOX-2 (metallic) with uncoated stainless steel stents. Initial findings demonstrated reduced neointimal formation and platelet adhesion (Windecker et al. 2001b). A reduced neointimal hyperplasia up to 50% at 6 week

follow-up (Windecker et al. 2001a) has been observed. It has not yet been used in clinical trials.

Diamond–like carbon is one of the most commonly used coatings; it has improved biocompatibility *in vitro* (Gutensohn et al. 2000). Porcine studies have demonstrated reduced thrombogenicity and reduced NIH but clinical trials have demonstrated no significant benefits (Airoldi et al. 2004).

### 2.6.3. Synthetic and biological polymeric coatings

Phosphorylcholine is a naturally occurring neutrally charged phospholipid, a component of the plasma membrane. It causes less platelet activation than stainless steel. Stents coated with phosphorylcholine have been shown to be non-inflammatory and non-thrombogenic *in vitro* and *in vivo* for six months or longer (Lewis et al. 2002). Phosphorylcholine also provides a basis for a drug eluting coating. Porcine studies demonstrated no significant benefits for NIH (Whelan et al. 2000) although clinical trials have shown good tolerance and low levels of restenosis (Galli et al. 2000;Galli et al. 2001).

The most widely used materials for resorbable stents or stent coatings are the aliphatic polyesters including poly-L-lactic acid, polyglycolic acid, poly-DL-lactic acid and poly-ε -caprolactone. A porcine model using poly-L-lactic acid demonstrated minimal inflammatory and thrombotic response with good initial radial strength. Clinical trials with this and other polymer-based stents to date have yielded highly variable results. The major disadvantage with bioabsorbable stents are the induced marked inflammatory response during degradation (Vaina & Serruys 2006). Two new

bioabsorbable coatings including one with bioabsorbable oil (consists of a very lipophilic, omega-3 fatty acid blend that is applied after the stent has been crimped on the balloon). The other is with hydroxyappatite which is a bioactive porous material that is normally found in the bones and the matrix of teeth (Vaina, S. & Serruys, 2006).

### 2.6.4. Immobilized drug coatings

Heparin - The molecular target of heparin is antithrombin III (ATIII) (Xiao,Z., Théroux, P. 1998). Once activated by heparin, ATIII inactivates thrombin and/or activated factor X (Xa) resulting in its anticoagulant activity. Low molecular weight heparins (LMWH), for example enoxaparin, are produced by degradation of unfractionated heparin and consist of smaller polysaccharide chains. LMWH are unable to simultaneously bind ATIII and factor Xa and preferentially bind to factor Xa (Kidane et al. 2004). *In vitro* studies demonstrate delayed onset of thrombus formation. Heparin coated stents were well tolerated in clinical trials but demonstrate no significant benefit (Semiz et al. 2003; Vrolix et al. 2000; Wohrle et al. 2001).

The heparin-modified stent grafts displayed superior blood compatibility compared to the unmodified stent grafts and it was further improved by the addition of Abciximab (Christensen et al. 2001; Christensen et al. 2005).

Although a heparin-coated stents (Wiktor GX HepaMed) are effective in the prevention of late stent restenosis in a porcine coronary (Ahn et al. 1999), heparin-coated Dacron- covered stent-grafts was not promising with regard to neointimal thickening and related stenosis in the iliac arteries in sheep (Schurmann et al. 1997).

Other categories of stents that have been studied, include autologous vein graft wrapped stents, polymeric stents and biodegradable stents. An autologous vein can feed through the lumen of a stent providing an intact endothelial surface. Porcine trials have demonstrated that the procedure is feasible and initial results are promising (Stefanadis et al. 1996). However, studies have not proven that the endothelium of these vessels remains intact. This has yet to be tried clinically.

Murphy et al (Murphy et al. 1992) have demonstrated the technical feasibility of percutaneous deployment of polyethylene terephthalate (PET) polymeric stents (Figure 2.8A) *in vivo* in the coronary artery, although they ere associated with an intense proliferative neointimal response that resulted in complete vessel occlusion. A marked inflammatory and neointimal response to an array of biodegradable as well as nonbiodegradable polymeric stents have been observed in the porcine coronary artery (van der Giessen et al. 1996).

The pioneering work on biodegradable stents was carried out by Zidar and coworkers at Duke University based on poly-L-lactide (PLLA) (Tamai et al. 2000), followed by biodegradable stents made from poly-L-lactide by Colombo et al (Colombo & Karvouni 2000). The Igaki-Tamai stent which is a high-molecular weight poly-L-lactic acid stent was the first biodegradable stent implanted in humans (Figure 2.8B). six-months follow up results by intravascular ultrasound (IVUS) showed it does not stimulate intimal hyperplasia compared to stainless steel stents (Palmaz-Shwartz) (Colombo & Karvouni 2000), although it lacks a demonstration of complete reabsorbing within a few months suggesting the need for a longer-term investigation (Tamai et al. 2000). Quick endothelialisation of biodegradable stents is necessary to

eliminates the chance of pieces of the degrading stent breaking off into the lumen. This also dictates that the degradation time of the stent be at least longer than the endothelialisation time. Two biodegradable stents are being clinically tested: BVS (Abbott Vascular) and tyrosine–polycarbonate (REVA Medical/Boston Scientific) (Venkatraman et al. 2008).

Table 2.1. Commercially coated stents (Wieneke et al. 2002).

| **Stent** | **Coating** | **Company** |
|---|---|---|
| BiodivYsio | Phosphorylcholine | Biocompatibles Cardiovascular Farnham, UK |
| Carbostent | Pyrolytic carbon | Sorin Biomedica Saluggia, Italy |
| Arthos Inert | Ion implantation (no coating in the close sense) | Amg Raesfeld-Erle, Germany |
| Tensum III / TENAX Lekton | Silicon carbide | Biotronik, Berlin, Germany |
| NIRoyal | Gold | Boston Scientific SCIMED Maple Grove, USA |
| LUNAR Stent | Iridium-oxide | InFlow Dynamics AG Munchen, Germnay |
| Cypher-Stent | Poly(ethyl methacrylate)/ n-butylmethacrylate | Cordis, Warren, USA |
| Yukon | Diamond-like carbon | Translumina, Hechingen, Germany |

### 2.6.5. Drug-eluting stents

Drug eluting stents (DES) were developed and approved first in 2003, with significant initial success (Valgimigli, M. et al. 2005). By adding a drug-eluting coating, the rate of restenosis has been reduced to about 5% or less. Longer-term follow-up has

highlighted problems with drug-coated stents (McFadden et al. 2004; Virmani et al. 2004) significantly reducing their usage after 2005.

DES deliver drugs at the site of the lesion, releasing single or multiple doses of a bioactive agent resulting in accumulation in tissues adjacent to the device (Fattori & Piva 2003b). Initial studies were aimed at the systemic administration of a variety of active agents to ameliorate the inflammatory response to stenting. However, this approach provided inadequate cessation of ISR and increased the risk of systemic side-effects (Meurice et al. 2001). This lack of success was attributed primarily to insufficient drug concentrations at the site of trauma, thus prompting the idea of localised drug delivery.

Investigations have culminated in the development of DES, which utilise the stent struts as the delivery platform for the localised administration of an array of active agents and to provide a vehicle for the release of therapeutic drugs (Table 2.2). The advantages of DES include the prolonged deposition of therapeutic agent directly into the vessel wall, at high concentrations and at the time of injury. Because of local delivery, systemic concentrations are minimised, reducing the risk of remote systemic toxicity (Klugherz et al. 2002).

Although a multitude of drugs and delivery platforms have been studied for application as drug/device combinations in DES, only two products, Cypher and Taxus, have gained Food and Drug Administration (FDA) approval for use in the treatment of coronary stenosis at the outset of this project. The use of either Cypher (sirolimus-eluting) or Taxus (paclitaxel-eluting) stents is recommended for patients

with symptomatic coronary artery disease, in whom the target artery is less than 3 mm in calibre (internal diameter) or the lesion is longer than 15 mm.

Sirolimus (Rapamycin) is a macrocyclic lactone (Figure 2.9A) that has demonstrated potent anti-fungal, immunosuppressant and anti-proliferative activity and was approved by the FDA in September 1999. Paclitaxel (Taxol®) (Figure 2.9B) is an anti-tumor drug, originally extracted from the bark of the Pacific yew Taxus brevifolia. The list of DES introduced are elucidate in Table 2.3.

Table 2.2. Overview of drug delivery vehicle (Regar et al. 2001).

- Polyvinyl pyrolidone/cellulose esters
- Polyvinyl pyrolidone/polyurethane
- Polymethylidene maloleate
- Polylactide/glycocoide co-polymers
- Polyethylene glycol co-polymers
- Polyethylene vinyl alcohol
- Polydimethylsiloxane (silicone rubber)

### 2.6.5.1. Problems of currently commercialised DES

The clinical success of commercially available DES, such as Cypher and Taxus, has been demonstrated (Regar et al. 2002; Tanabe et al. 2003). The development of DES for the treatment of coronary stenosis has undoubtedly revolutionised the area of interventional cardiology. Both Cypher and Taxus have demonstrated excellent results with regards to inhibition of neointimal hyperplasia and the associated ISR when compared to bare metal stents, with a subsequent reduction in the need for target vessel revascularisation (TVR) procedures (Oberhoff, M., 2002, Sousa, J. E., 2001). In addition, the problem of subacute thrombosis (within the first 30 days) has been

demonstrated to be low (<1.0%) and equivalent between Cypher, Taxus and bare metal stents (Leon 2007).

Table 2.3. Drug eluting stents (Vaina & Serruys 2006).

| Name of stent | Stent platform | Coating | Drug | manufacturer | status |
|---|---|---|---|---|---|
| CYPHER® | Stainless steel | Durable polymer | Sirolimus | Cordis | CE Mark |
| TAXUS® | Stainless steel | Durable polymer | Paclitaxel | Boston Scientific | CE Mark |
| Endeavor™ | Cobalt alloy | Durable polymer | Zotarolimus | Medronic | CE Mark |
| Zomaxx™ | Stainless steel-tantalum | Durable polymer | Zotarolimus | Abbott Vascular | CE Mark |
| Xience™ | Cobalt chromium | Durable polymer | Everolimus | Guidant Corporation | CE Mark |
| Dexamet™ | Stainless steel | Durable | Dexamethasone | Abbott Vascular | CE Mark |
| BVS | biodegradable | Bioabsorbable | Everolimus | BVS, Guidant | - |
| Biomatrix™ | Stainless steel | Bioabsorbable | Biolimus A9 | Biosensors | CE Filed |
| Nobori™ | Stainless steel | Bioabsorbable | Biolimus A9 | Terumo | - |
| Champion™ | Stainless steel | Bioabsorbable | Everolimus | Guidant Corporation | - |
| Infinnium™ | Stainless steel | Bioabsorbable | Paclitaxel | Sahajanand | CE Mark |
| Supralimus™ | Stainless steel | Bioabsorbable | Sirolimus | Sahajanand | CE Mark |
| CoStar™ | Cobalt chromium | Bioabsorbable | Paclitaxel | Conor Medsystems | CE Mark |
| Nanoporous stent | Stainless steel | Alumina/aluminium oxide/$Al_2O_3$ | Tacrolimus | Jomed | - |
| Yukon DES™ microorous stent | Stainless steel | Aluminium oxide | Sirolimus | Translumina | CE Mark |
| Janus ™ | Stainless steel | - | Tacrolimus | Sorin | CE Mark |

However, this success has been overshadowed to some extent by recent concerns regarding late stage thrombosis (LST) (Ong, et al. 2005). They can potentially result in thrombosis once the stent platform has ceased eluting drugs or localized tissue concentration is insufficient. The Cypher and Taxus DES result in delayed arterial healing when compared with BMS of similar implant duration (McFadden et al., 2004). This results obtained in the study by Joner et al (Joner et al. 2006) who were the first group to examine systematically the effects of DES the on human coronary pathology. The delay in arterial healing characterized by persistent fibrin deposition

and delayed re-endothelialization when compared with sites of BMS implantation. The cause of DES LST is multi-factorial with delayed healing in combination with other clinical and procedural risk factors playing a role.

Further investigations into the biological mechanisms and clinical implications of DES and coronary thrombosis have recently been carried out by Lüscher *et al*. (Luscher et al. 2007). The report identified several factors which contribute to an increased risk of LST, including the procedure itself (stent malapposition and/or under-expansion, the number of implanted stents, stent length, persistent slow coronary blood flow and dissections), patient and lesion characteristics, stent design and premature cessation of anti-platelet drugs. It is apparent from these studies that LST is the result of numerous mechanisms, with significant emphasis on the discontinuation of dual anti-platelet therapy. It has been shown that DES delay arterial healing and endothelialisation of stent struts as a result of the active agents employed and as such, once anti-platelet therapy has ceased, the stent is susceptible to a foreign body response (Venkatraman & Boey 2007). In particular, it appears that the polymers currently used to coat stents increase the risk of contact activation and hypersensitivity reactions, which may result in localised inflammation and lymphocyte infiltration.

The techniques which facilitate endothelialisation include physical methods such as pore creation (Deepa & Venkatraman 2009) and lithography to create nanosized surface features, which have been shown to enhance endothelialisation rates *in vitro*. Chemical modification has also been introduced to attach ligands and thus directly influence ECs (Venkatraman et al. 2008). However, the effectiveness of these

modifications to accelerate endothelialisation rates *in vivo* remains to be demonstrated. Finally, new stent platforms, such as endothelial progenitor cell capturing stents may provide in the near future a more "physiological" answer to stent implantation, reducing vascular injury and accelerating vessel healing with consequent improvements in clinical outcome. Another technique is to anchor an antibody that captures floating endothelial progenitor cells (EPs) from the bloodstream. In clinical trials, the Genous stent -which is not drug-eluting- was reported to have fared as well as the paclitaxel-eluting stent (Genous stent) ( 2009). The concern that it is successful in a subsection of patients with a high level of floating EPs, needs to be addressed.

The concerns raised with regards to the current coatings employed for stent coating, highlights the requirement for biocompatible, long-term non-thrombogenic/anti-thrombogenic coatings, with long-term adhesive stability without the occurrence of polymer delamination or cracking, which also promote endothelialisation.

## 2.7. Possible role of regenerative medicine and nanotechnology for cardiovascular implants

This endothelial monolayer that lines the normal blood vessel serves as a bio-regulator of cardiovascular physiology. The vascular endothelium is versatile and multifunctional with many synthetic and metabolic properties. These include the regulation of thrombus and platelet activation, adhesion and aggregation (Autio et al. 1989) as well as modulation of vascular tone and blood flow (Furchgott & Zawadzki 1980). It also controls SMC migration and proliferation (Casscells 1992). EC secrete and express numerous growth factors, extracellular matrix products, anti-thrombotic

and pro-coagulant factors. ECs are intimately involved in maintaining a non-thrombogenic blood-tissue interface. Re-endothelialized segments of artery are often associated with less neointimal thickening the absence of intact EC lining therefore predisposes cardiovascular implants; including bypass graft and stents; to platelet deposition, thrombus and implant failure. As a result, investigators have developed methods to promote the endothelialisation of vascular grafts prior to implantation by transplantation of ECs *in vitro*, a process called EC seeding. The cellular engineering approach called 'seeding' involves lining the lumen of the graft *in vitro* with EC (Herring et al. 1978; Zilla et al. 1987).

Recent advances in science and technology, especially progressive development in nanoscience and nanotechnology, offer novel nano-structured materials with enhanced characteristics which make them the the material of choice for various applications. The enhanced characteristics include: greater strength, higher resistance to permeability and higher heat stability (Wahab et al. 2008; Zeng et al. 2009). Nanotechnology is concerned with manipulation at the molecular or atomic level to provide useful applications (Ghalanbor, et al. 2005; Kubik et al. 2005). The main unifying theme is the control of matter on a scale smaller than 1 micrometer, normally between 0.1-100 nanometers, as well as the fabrication of devices on this same length scale (Figure 2.10). For comparison, the typical carbon-carbon bond length, and the spacing between these atoms in a molecule, is in the range 0.12-0.15 nm, and a DNA double-helix has a diameter around 2 nm. The smallest cellular life forms; the bacteria of the genus Mycoplasma; are around 200 nm in length. Materials reduced to the nanoscale can show very different properties compared to what they exhibit on a macroscale, enabling unique applications (Kubik et al. 2005). For instance, opaque

substances may become transparent (copper); inert materials become catalysts (platinum); stable materials turn combustible (aluminum); solids turn into liquids at room temperature (gold); and insulators become conductors (silicon). A material such as gold, which is chemically inert at normal scales, can serve as a potent chemical catalyst at nanoscales. Much of the fascination with nanotechnology stems from these unique quantum and surface phenomena that matter exhibits at the nanoscale.

The difficulties involved in fulfilling the numerous ideal characteristics using traditional synthetic materials have lead biomaterials research towards the fields of nanotechnology and tissue engineering. Nanotechnology is concerned with the incorporation of man-made molecules into traditional materials to express novel advantageous properties such as anti-thrombogenecity and biostability (Habal 1984).

Hybrid inorganic–organic composites are an emerging class of new materials that hold significant promise. Materials are being designed with the good physical properties and the excellent choice of functional group chemical reactivity associated with organic chemistry. Such models start with an established polymer system model and an assignment of dimensionality to the nanofiller. The most promising nanofillers and their dimensionality include clay layered silicates, single and multi-walled nanotubes, carbon nanofibers and polyhedral oligomeric silsesquioxane (POSS)-nanostructured chemicals (Phillips et al. 2004).

### 2.8. Nanocomposite

The term "nanocomposite" was first coined by Roy and Komarneni in the early 1980s (Komarneni 1992) signifying a major paradigm shift in the understanding of the sol-

gel process (Hoffman, et al. 1984). This involved using the solution sol-gel process to create maximally heterogeneous rather than homogenous materials. Nanocomposites should be clearly differentiated from “nanocrystalline “and "nanophased" materials, which refer to single phases in the nanometer range. Nanocomposites refers to composites of more than one independent solid phase where at least one dimension is in the nano-meter range with all solid phases in the 1-20 nm range. These solid phases may be amorphous, semi-crystalline/crystalline or combinations thereof. They can also be inorganic or organic or both (Komarneni 1992).

Due to their nano-scale sizes, nanocomposites can serve as bridges between molecules in the polymer. This nature allows them to exhibit different properties from conventional microcomposites (Alivisatos 1996). Examples of this in nature are shells, bones, and teeth. Composite shells or nacre are composed of alternating calcium carbonate ($CaCO_3$) and nanoscale aragonite asperities (Zaremba et al. 1996) and, in so being, are 3000 times stronger than monolithic $CaCO_3$ crystals (Gao et al. 2003). Man has since endeavored to synthesize nanocomposites, and it has been found that these synthetic nanocomposites have immense potential because they possess increased conductivity, mechanical strength, optical activity, and catalytic activity (Merkel et al. 2002b). Their behaviour is governed by the method of nano-reinforcement, the nano-interface, the synthetic process utilized, its microstructural effects, and the interaction between the polymeric and reinforcing component (Lee & Lichtenhan 1998).

### 2.8.1. Structure of nanocomposites

Conventionally when the components of a composite are mixed, phase separation occurs resulting in the formation of microcomposites. In nanocomposites however, the nanofillers are able to intercalate between the layers of the matrix (intercalated type) or be even further dispersed uniformly within the matrix to form exfoliated nanocomposites thus maximizing the surface area for component interaction. While intercalated nanocomposites have regular interlayers, exfoliated ones have larger interlayers (Figure 2.11).

### 2.8.2. Polyhedral oligomeric silsesquioxane nanocomposites

Polyhedral oligomeric silsesquioxanes (POSS) have an inorganic silicon oxygen core that is thermally and chemically robust. The term silsesquioxane refers to all structures with the stoichometric formula $RSiO_{1.5}$. This central core is externally bonded with organic groups. These substituents can be totally hydrocarbon in nature, or they can embody a range of polar structures and functional groups, able to provide compatibility of the nanostructure with man-made polymers or biological systems. So, each POSS nanostructure can be manufactured to contain a chemically precise number of reactive groups that impart specific functionality to them. The average diameter of a POSS molecule is 1.5 nm. Thus POSS can be used as a monofunctional or graftable monomer, a dysfunctional comonomer, a surface modifier, or a polyfunctional crosslinker for polymers (Figure 2.12).

In complete contrast to siloxane, silsesquioxanes (SQS) exist as ladder- or cage-type nano-structures (Tran et al. 2001), as illustrated in Figure 2.13. Scott, in 1946, first isolated oligomeric organosilsesquioxanes, $(CH_3SiO_{1.5})_n$ along with other volatile

compounds through thermolysis of the polymeric products obtained from methyltrichlorosilane and dimethylchlorosilane co-hydrolysis (Li et al. 2001a).

Ladder-like polysilsesquioxanes include poly (phenyl silsesquioxane) (Li et al. 2000a; Li et al. 2000b), poly(methyl silsesquioxane) (Maciel, Sullivan, & Sindorf 1981) and poly (hydridosilsesquioxane) (Frye & Collins 1970). Having an outstanding thermal stability, oxidative resistance even at temperatures of more than 500°C, good insulating properties and gas permeabilities, these ladder-like silsesquioxane polymers have a variety of applications in areas such as electronics and optical devices, semiconductor devices, optical fiber coatings, gas separation membranes and drug delivery (Li et al. 2001b).

In 1995, Lichtenhan and co-workers (Lichtenhan et al. 1998) developed and patented a closed-cage SQS, POSS or molecular silica (Lichtenhan 1995). POSS with the formula of $(RSiO_{1.5})_n$ where n= 8,10,12 are compounds that embody a truly hybrid (inorganic–organic) architecture(Li et al. 2001c). One or more of theses R can be replaced by a reactive functional group to form homosilsesquioxanes (Suresh et al. 2004), or can be formed into dendrimers or used as nanobridges (Dijkstra et al. 2002; Moreau et al. 2003b; Wada et al. 2005). A typical POSS molecule with the silica-like core (0.53 nm in diameter), externally covered by eight organic corner group with the general sizes of from 1 to 3 nm in diameter, can be thought of as the smallest possible particles of silica. In this way, POSS can be incorporated into linear or thermosetting polymers thereby improving their thermal and oxidation resistance and reducing their flammability. In addition, they can be used in biomedical applications such as scaffolds for drug delivery, imaging reagents (Chiacchio et al. 2005).

POSS are increasingly being used to synthesise hybrid nanocomposites due to their chemical versatility over silica, silicones or other nanofillers such as carbon nanotubes and nanoclays (Joshi & Butola 2004). Depending on the number of side groups, they may exist as pendant cages, be part of a polymeric backbone, or be cross-linked. Researchers have since shown that these nanocomposite cubes may be incorporated as building blocks (Sanchez et al. 2001a) of controllable shapes (Moreau et al. 2003a) into other polymers to form hybrid materials (Choi et al. 2001; Wada et al. 2005) with improved miscibility and elasticity (Haddad et al. 1999; Sanchez et al. 2001b). This is achieved as monodispersions in polymers such as epoxide, acrylate, norborne, styrene, acetoxystyrene (Xu et al. 2002b) and polyurethanes.

The nanoscale size of the POSS molecules, as well as the degree of control and opportunity to tune the interactions through substituents on the POSS cage, differentiate these materials from conventional additives (Misra et al. 2007). They can be easily functionalized with a wide variety of organic groups such as – $NH_2$, –SH, –OH and –COOH and can be incorporated into polymer systems via polymerization, grafting, blending, and so improving polymer properties. In hybrid nanocomposites, the judicious choice of functional moieties may change the dispersion behaviour of POSS molecules in the polymer matrix, enhance the processing parameters, and impart desired physical and thermomechanical properties of the final hybrid materials. Different POSS molecules have been successfully incorporated into many kinds of polymers, such as styryls, acrylics, liquid crystalline polyesters, siloxanes, and polyamides (Fu et al. 2000) via polymerization, grafting, blending.

POSS's composition is truly a hybrid. It is not just a mixture of an inorganic particle with a polymer, rather POSS represents a physical union of two dissimilar material types into a single molecular package that has characteristics imparted to it from each of the two dissimilar materials. That is the reason for the fact that POSS enhances the physical properties of polymers to a degree that is not possible via the blending of polymers with silsesquioxane resin or inorganic particles.

Physical properties in materials begin to manifest themselves from structures formed at the 1 nm to 10 nm level. Therefore, it is highly relevant to ensure that the nano-reinforcing agents are fully dispersable, and compatible at this length scale. Otherwise, physical properties cannot be fully controlled.

#### 2.8.2.1. POSS polymers-copolymers

In general, there are three ways that POSS building blocks can be incorporated into materials. Method I is as an alloying agent, where POSS is blended into a material using high shear mixing/blending With method II, POSS can be polymerizable into a material using standard copolymerization or reactive grafting techniques. With method III, POSS can be utilized as a surface modifier.

When working with amorphous materials such as polystyrene, POSS is alloyed into the amorphous phase. But when working with semi-crystalline or other multiphase or multi-compositioned plastics or biological systems, depending on the types of R-groups, POSS cages have relative affinity for the amorphous region in a polymer or for the crystalline region.

Previous studies have shown that the resultant polymers are hybrid organic–inorganic nanostructured composites with dramatically improved bulk properties, including decreased dielectric constant (Leu et al. 2003), decreased oxygen permeability (Isayeva & Kennedy 2004), increased flammability retardation, increased mechanical strength (Gao et al. 2001; Kim et al. 2003; Laine 2005), increased thermal stability (Liu et al. 2005; Neumann et al. 2002; Zheng et al. 2001) and increased chemical resistance (Laine 2005) and increased glass transition temperature (Kuo et al. 2006; Lee & Lichtenhan 1999; Oaten & Choudhury 2005; Patel et al. 2006).

A special field is represented by POSS-modified polyurethanes because these polymers encompass a huge number of specialized applications. Some papers have appeared in recent years describing synthesis, morphological characterization, and deformation behaviour of POSS-modified thermoplastic PU elastomers (Fu et al. 2000; Hsiao et al. 2000b; Madbouly et al. 2007; Nanda et al. 2006).

It is well known that the properties of polyurethane are primarily related to the formation of a microphase separation from the thermodynamic incompatibility (immiscibility) of solid like hard segments and rubbery soft segments. The hard segments usually involve interchain interactions by means of van der Waals forces and hydrogen bonding, which determine the macroscopic properties. Being constituted with two thermodynamically incompatible soft and hard blocks, segmented PU are characterized with a unique combination of mechanical and thermal properties. Variation of the chemical nature of one of the segments or both is a powerful tool for the control of the structural and properties of these polymer

materials. Such characteristics of the segmented PU can be helpful in the creation of nanostructured organic–inorganic hybrid materials (Kickelbick 2003).

POSS could also be incorporated into PU by various methods to improve the performance of the latter. For example, Liu et al used octaaminophenyl POSS as a cross linking agent for PU pre-polymer to prepare PU hybrid networks, and these displayed increased glass-transition temperature, storage modulus, and thermal stability (Liu et al. 2006). Neumann et al reported a new type of POSS macromer with eight reactive isocyanate groups for the synthesis of hybrid organic-inorganic urethane nanomaterials, and this showed thermal stability up to 190 °C (Neumann, D. et al. 2002). Synthesis of amphiphilic telechelic oligourethanes with terminal POSS groups through reaction of monoisocyanate substituted POSS and oligo(oxyethylene diol) and investigation of the structure of such polymers in solution have been reported recently. Interestingly, chemical reaction of monoisocyanate substituted POSS fragments with polyamidoamine of a dendritic nature (polyamidoamine PAMAM dendrimers) leads to the formation of several organo-inorganic core–shell type nano-hybrids. Application of dihydroxy-containing POSS with isocyanate pre-polymers can yield linear segmented PU with POSS fragments as a side group of the hard segments. By analogy with this method diamino-POSS has been used to prepare nanostructured PU–POSS hybrid aqueous dispersions. As demonstrated, reaction of the silanol groups of an open cage POSS with isocyanate moieties gave segmented PU with POSS incorporated in the polymer main chain as a part of the hard segment. Cross-linked PU could also be synthesized through the reaction of octafunctional POSS with either isocyanate or amine groups (Bliznyuk et al. 2008). All these studies demonstrated that incorporation of POSS had a dramatic effect on the structure and

physical properties of segmented polyurethane. Recently Nanda et al. (Nanda et al. 2006) synthesized well dispersed polyurethane/POSS hybrid materials utilizing a solution polymerization process. Ordered morphologies with homogenously distributed POSS domains (100–150 nm) were observed. The authors reported significant increases in physical properties, including tensile strength, storage modulus, complex viscosity, surface hydrophobicity, and glass transition temperature.

POSS molecules are believed that reduce the viscosity during processing. It is true that plasticizers can also be used to reduce viscosity, but modulus and $T_g$ are also reduced as a result. This is not the case for POSS incorporation. Increase in glass transition temperatures are common and result for the incorporation of POSS directly into the polymer backbone. Depending upon how the POSS is incorporated (random or blocky), one or more glass transitions may be observed. Increase in glass transition has been attributed to chain motion reduction. Based on the study by Professors Laine and Feher, it has been proved that when a number of cell targeting receptors are placed on a POSS very specific cell location and binding can be achieved. In summary, POSS bridges a gap between monomers and fillers in terms of size and in terms of reinforcement characteristics. Variation of the R-group on POSS can afford either plasticization or reinforcement.

The framework of POSS, constituted by Si-O and Si-C bonds, is similar to silicone, which is a favored option in biomaterials and first introduced into breast surgery in the 1960s due to its inert nature and low inflammatory response. Its biocompatibility can be ascribed to the foci of silicon-rich areas with decreased surface free energy (Silver et al. 1999). Unlike carbon nanotubes (Cui et al. 2005) POSS moieties are

non-toxic and cytocompatible (Kim et al. 2007). Additionally, it has been confirmed that POSS cages, as nanoscale building blocks, can be incorporated into other polymers with improved mechanical and viscoelastic properties. Thus, materials scientists are motivated to extend POSS-based polymeric nanocomposites to tissue engineering and biomedical applications. Cationic POSS (e.g. ammonium-POSS) has been given more and more attention because it can form a complex with anionic molecules with great potential application in DNA/gene delivery, drug delivery, and DNA/protein detection.

## 2.9. Coating stent metals

Various approaches have been previously used to include polymers in stents including dipping (McGillicuddy et al. 2006a; Sharkawi et al. 2005), spraying (Sharkawi, et al. 2005), solution casting and chemical vapour deposition (Hanefeld et al. 2006; Lahann et al. 1999). However, these methods have significant disadvantages. With casting, dipping and chemical vapour deposition, the final surface morphology is smooth (Hanefeld et al. 2006a; Lahann et al. 1999a; McGillicuddy et al. 2006b; Sharkawi et al. 2005a), resulting in a platform that does not promote endothelial progenitor cells (EPC) growth and migration. In addition, solvent-based coating techniques have some disadvantages, such as bridging, pooling and lack of uniformity or inability to apply different thicknesses with precise process control, in particular when coating thicknesses of <0.5 mm are to be prepared (Lahann et al. 1999b; Loeffler et al. 1999; Okner et al. 2007). Chemical vapour deposition is unfavourable as it requires high temperature and pressure environments and complex equipment (Okner et al. 2007a). Considering these disadvantages, a new approach is needed to apply a thin polymeric film on the metallic stent surface with a high degree of precision. Spray-coating is

usually reserved for devices and surfaces where a consistent coating thickness is especially important. Stents are commonly spray-coated to minimize pooling and drip spots that could occur with a dip process. Therefore, alternatives were sought to coat stent material, namely electrohydrodynamic spraying and ultrasonic atomization spraying, the experimental details of these were given here.

### 2.9.1. Electrohydrodynamic spray deposition

Electrohydrodynamic spraying (EHDA) is a process in which an electric force is generated at the surface of the liquid by applying a potential difference of the order of kilovolts between the needle, which perfuses the liquid, and the collection electrode, which gathers the product droplets of a jet that forms due to the electric field (Pareta et al. 2005; Zhang & Edirisinghe 2006; Zhang et al. 2006). In this way, a polymer solution undergoes deformation to a meniscus at the outlet of a capillary and/or elongates to a jet which subsequently breaks up into droplets. Compared to other spraying techniques of liquids, electrohydrodynamic processing has some significant advantages, e.g. relatively easy generation and avoiding coalescence of droplets due to electric charge of the same polarity in the droplets, and achievement of a narrow size distribution of droplets in the stable cone-jet mode (Watanabe et al. 2003).

#### 2.9.1.1. Modes of electrohydrodynamic spray deposition

EHDA occurs in many modes (Jaworek & Krupa 1999b) considering different influencing properties such as the physical properties of the liquid (e.g. surface tension, density, conductivity and viscosity) and processing parameters (e.g. flow rate and electric field strength, which is determined by the applied voltage and the distance between the needle and the collection point) (Edirisinghe & Jayasinghe 2004) (Figure

2.14). The modes of electrohydrodynamic processing has been characterised by two criteria:

1. The geometrical form of the liquid at the outlet of the capillary.
2. The nature of the jet behaviour in its disintegration into droplets.

Based on these two criteria, the spraying modes can be divided into two groups. The first group comprises the modes in which only fragments of liquid are ejected from the capillary without a continuous jet; that is, the dripping, micro-dripping, spindle, multi-spindle, and ramified-meniscus modes. The second group consists of the modes, in which the liquid characteristically issues from the capillary in the form of a long continuous jet which disintegrates into droplets after travelling for some time and distance, usually a few mm from the outlet of the capillary. Stable cone-jet, procession, oscillating, multi-jet and ramified-jet modes are included in the second group (Jaworek & Krupa 1999b). The meniscus and the jet in the second group can be stable, variable, or rotate spirally around the capillary axis, or whip irregularly.

#### 2.9.1.1.1. Dripping mode

The dripping mode of electrospray is commonly obtained at lower applied voltage. It is similar to dripping when no voltage is applied to the capillary. The dripping mode in the electrohydrodynamic processing is very similar to the dripping observed for electrically neutral conditions. The drops take the shape of regular spheres at the capillary exit and detach from the capillary as the gravity force and the electric force overcome the surface tension force. After the drop detachment, the meniscus contracts back to form a hemispherical-like meniscus. With increasingly applied voltages, the

meniscus elongates due to electrohydrodynamic forces, which cause the droplets to grow smaller as they detach from the meniscus. This is attributed to two different reasons: one is the reduction in the surface tension of the liquid because of the electric charges on the surface create an electrostatic pressure opposite to the capillary pressure; the other is the attraction of liquid towards the plate due to the action of the electric field and the charges located at the end of the hanging droplet (Cloupeau & Prunet-Foch 1990). For further increase of the voltage the drop can for some time, be connected with the capillary by a thread, which next breaks of as the drop falls down.

#### 2.9.1.1.2 Micro-dripping mode

When the applied voltage is increased further than the value it has in the dripping mode, the electric force close to the capillary exit becomes sufficiently high to keep a stable hemispherical or ellipsoidal meniscus. The micro-dripping mode differs from the dripping mode as the meniscus does not contract back after droplet detachment. The droplet production frequency is usually two orders of magnitude higher than that of the dripping mode and it ranges from a few droplets up to a few thousand droplets per second. A small droplet -much smaller than the capillary diameter- is formed at the tip of the meniscus, where the electric field is much stronger. The droplet gets detached from the meniscus and does not undergo further disruption. The micro-dripping mode is usually observed at < 4 kV. The size of the droplets can range from a few tens up to about a hundred of micrometer in diameter.

#### 2.9.1.1.3. Spindle mode

The spindle mode is generated at high flow rate with sufficiently high electric field where the liquid can elongate in the direction of the electric field, taking the shape of

a thick jet which detaches as a vast spindle-like fragment. Spindle mode differs from dripping and micro-dripping modes because it is generated at higher voltages and such high voltages detache a fragment of liquid before a continuous jet is formed. Second, there is no regular droplet is ejected from the meniscus but only elongated fragments of liquid. Third, after its detachment the spindle can disrupt into several smaller droplets of different sizes, ranging from 300-1000 μm, depending on the electric field stength. The meniscus contracts to its initial shape, and a new jet starts to be formed. Finally, the characteristic time that liquid is provided to the capillary is nearly equal to or shorter than the jet formation time. Increase in the applied voltage causes the single jet to become multiple jets.

#### 2.9.1.1.4. Unstable cone-jet mode

A traditional mode which lies between the spindle/multi-spindle mode and stable cone-jet mode (described later in this section) can be observed under the condition of certain flow rates and applied voltages. It is an intermittent mode, namely unstable (or intermittent) cone-jet mode. In this mode, the liquid escapes the capillary in the form of a skewed cone and smoothly changes into a thin jet at the tip, which is similar to the configuration of the cone-jet mode. However, both the cone and the jet rotate regularly round the capillary axis, taking the shape of a fragment of a spiral. Compared with the spindle mode, the unstable cone-jet mode has a thinner jet of diameter smaller than 100 μm, of which the end part winds round the mother spiral. The jet disintegrates into droplets due to repulsive electrostatic forces and possibly centrifugal forces too.

#### 2.9.1.1.5. Cone-jet mode

In the cone-jet mode the liquid issues from the capillary in the form of a regular, axi-symmetric cone with a thin jet at its apex, stretching along the capillary axis and breaking up into fine droplets.

The shape of the liquid cone is a result of the balance of liquid pressure, liquid surface tension, gravity, electric stress in the liquid surface, liquid inertia, and liquid viscosity (Hartman R.P.A et al. 1999). The applied electric field accelerates the surface charge toward the cone apex.

A thin jet of diameter ranging from a few micrometers up to a few tens of micrometers is formed at the tip of the cone and the jet remains stable to the length of a few mm from the capillary exit because of the weak lateral electric field. The space charge in the cone-jet mode is much more stable than in other spraying modes because the droplets are smaller and of lower mobility. The space charge reduces the electric field near the end part of the jet, so the jet undergoes instabilities at the bottom end. As the result, the jet breaks up into a number of primary or main droplets and a number of secondary droplets and satellites (K.Tang & A.Gomez 1994c). There are two types of instability, namely varicose and kink. In the varicose instability case, the axis of the jet is not deflected and the jet disintegrates into equal droplets. In the kink instability case, the end of the jet moves irregularly and breaks up into a series of droplets due to electrical and inertial forces. Unlike unstable cone-jet mode, the cone is axi-symmetrical and both the cone and the jet at its initial fragment remain (Jaworek & Krupa 1999a). Secondly, the cone to jet transition zone is very smooth in stable cone-jet mode.

#### 2.9.1.1.6. Multi-jet mode

On further increase of applied voltage or liquid flow rate, the cone-jet mode changes to the multi-jet mode. When the applied voltage increases in the cone-jet mode, the cone depth and the jet diameter becomes smaller until a critical level at which the Taylor cone becomes skewed, leading to a single jet at the rim. This situation is unstable and two jets at opposite sides relative to the axis, or three gets symmetrically distributed on the rim of the capillary, are formed. The diameter of the jets is smaller than a few tens of micrometers. The jet disintegrates due to kink instabilities, into small droplets, forming a fine mist around the capillary axis. As has been observed, 2-8 such jets are ejected from capillary. The number of emission points increases to a certain number with the increase in voltage or flow rate, and each jet is formed faster and becomes thinner due to increasing shear stresses.

The reason for the formation of multi-jet mode from stable cone-jet mode is the limited velocity of the jet formation as compared to the liquid velocity at the outlet of the capillary, resulting from the flow rate. The diameter of the jets also increases with the increase in flow rate. As a result, an excess volume of liquid that can not be removed by electrical forces accumulates at the outlet of the capillary. The multi-jet mode disappears then, changing to ramified meniscus mode. In this mode, the meniscus becomes perfectly flat with only short cones at the emission points.

#### 2.9.1.1.7. Corona discharge

When the electric field between the capillary and ground electrode becomes greater than the electrical breakdown threshold of the interfacial surface tension of liquid-

surrounding air interface, corona discharge occurs and in this situation none of the regular modes can be observed (Cloupeau & Prunet-Foch 1989).

### 2.9.1.2. Mechanism of stable cone-jet mode

The stable cone-jet mode is most desirable as it generates near mono-dispersed droplets (Edirisinghe & Jayasinghe 2004) at a relatively reasonable frequency and the size from sub μm to several tens of μm can be obtained. By such a method, a very precisely controlled thickness of polymer can be applied to a selected surface of a stent without it interfering in the deployment of the stent. As discussed in section 1.8.1.1.5, this process can be classified into two stages: 1) liquid acceleration and cone forming; and 2) the break-up of jet into droplets.

The liquid acceleration and the shape of the liquid cone process result from the balance of several forces involved; these are liquid pressure, liquid surface tension, gravity and electric strengths in the liquid surface. The conical shape is sometimes refered to as a 'Taylor cone' form when the outward stress due to an applied electric field balances the inward stress due to the liquid surface tension. Hartman has presented a cone-shape model in which forces that have to be taken into account are illustrated (Figure 2.15) (Hartman et al. 1999).

### 2.9.1.2. The effect of the physical properties of the solution over electrohydrodynamic processing in stable cone-jet mode

The predominant property which can control droplet size and morphology of the film produced is the concentration of the polymer in the solution which governs its viscosity, surface tension and electrical conductivity, and these are key EHDA

properties (Jayasinghe & Edirisinghe 2004b;Zhang & Edirisinghe 2006) (A.M.Gañán-Calvo eta l. 1997;Hartman R.P.A et al. 1999). Each of these properties is discussed briefly.

#### 2.9.1.2.1. DC electrical conductivity

Among the properties of liquids, conductivity is the most important property for electrospraying in the cone jet mode. Liquids with low conductivity (insulators), such as olive oil, can not be processed in the cone-jet mode, as there is not enough charge build-up in the liquid. In such cases, electrospraying of liquids in cone-jet mode can be achieved by artificially increasing their conductivities with additives like salt (J.M.López-Herrera et al. 2003). For liquids with very high conductivity, the electrohydrodynamic processing would , again, not occur, unless the flow rate is lowered. The value of liquid conductivity influences the morphology of the liquid issued in a stable cone jet mode. As conductivity increases, the filament width, length, flow rate for cone jet mode and droplet size all decrease (A.M.Gañán-Calvo et al. 1997).

Relative permittivity or the dielectric constant is a measure of the polarisability of a material in an electric field. The polarization reduces the magnitude of the electric field inside the liquid. Relative permittivity along with vacuum permittivity and conductivity determines the electrical relaxation time, $t_e=\beta\varepsilon 0/K$. Electrical relaxation time is the time required to smooth a perturbation in the electric charge, where $\beta$ is the relative permittivity, and $\varepsilon_0$ and K are the vacuum permittivity and electrical conductivity, respectively (A.M.Gañán-Calvo et al. 1997).

#### 2.9.1.2.2. Surface tension

Electrohydrodynamic spraying occurs when the electric forces overcome the surface tension forces of the liquid. The major role of surface tension in drop formation is to control the size, or volume and shape of the drop. The onset voltage for a stable cone-jet mode increases with the liquid surface tension, and this also results in greater probability of electrical discharge occurring due to surrounding air. It is easier to establish a stable cone-jet with sufficient electrical conductivity and moderate surface tension (K.Tang & A.Gomez 1994b; Tang & Gomez 1995). Tang and Gomez (1995) used $CO_2$ and $SF_6$ (gases with higher electrical break-down threshold) instead of air as a surrounding fluid to obtain cone-jet mode for deionised water with conductivity $1.02 \times 10^{-6}$ $Scm^{-1}$.

#### 2.9.1.2.3. Liquid viscosity

For liquid with viscosity below 100 mPa s, the droplet size in the cone-jet mode has been found to be directly proportional to the viscosity (Hartman R.P.A. et al. 2000). The droplet size of the glycerol in the cone-jet mode has been found to double when the viscosity is increased from 1225 mPa s to 1325 mPa s (Jayasinghe & Edirisinghe 2002). However, higher viscosities help to produce the stable cone-jet mode as the electrical stresses acting on the liquid-air interface can easily be dssipated into liquid bulk when the viscosity is sufficiently high (J.M.López-Herrera et al. 2003).

#### 2.9.1.2.4. Density

The density of the liquid plays an important role in determining the jet diameter in the cone jet mode. When the viscosity and conductivity of the liquid are large enough, the electrical charge is efficiently transmitted across the jet section by viscous forces.

However, the viscous forces depends on the density of the liquid (A.M.Gañán-Calvo et al. 1997).

### 2.9.1.3. Droplet production in stable cone-jet mode

The stable cone-jet mode is the most studied and understood mode due to its capability to produce near mono-dispersed droplets over a wide size range (sub-micron to hundreds of micron). The droplet size produced in the cone jet mode depends on a few parameters.

1- Effect of flow rate on cone jet mode: the size distribution produced in electrohydrodynamic spraying in the cone-jet mode depends on the diameter of the jet, and on the break-up of this jet into droplets. Every liquid has a minimum flow rate, below which a stable cone-jet mode can not exist. At this minimum flow rate the jet breaks up due to axi-symmetric instabilities.

2- Effect of applied voltage on cone jet mode: the electric field between the capillary and the ground electrode is an important parameter in controlling the process of electrohydrodynamic spraying. This is determined by the applied voltage and other factors such as the configuration of the ground electrode and the inter-electrode spacing. The spraying of the liquid takes place mainly due to electrical forces produced by this field, therefore a higher applied voltage leads to a stronger spraying effect on the liquid. Within a well defined voltage range, the meniscus of the liquid becomes conical and stationary. Below this voltage range, the spray always operates in pulsatiling mode (A.M.Gañán-Calvo et al. 1997). With a given inter electrode spacing, different modes of spraying can be observed if the voltage is gradually

increased from lower values to higher values. Applied voltage is a key variable in establishing the cone-jet mode and the cone-jet mode can prevail within a range of applied voltages of higher values (K.Tang & A.Gomez 1994a). Within this range of applied voltage of cone-jet mode, droplet size reduces with the increase of applied voltage from the lower value of range to higher values. As the droplet size decreases with the applied voltage and increases with the flow rate, it is necessary to select the highest possible value of applied voltage and the lowest possible value of flow rate to achieve the minimum droplet size (Jayasinghe & Edirisinghe 2004a). For highly conducting and viscous liquids, the sizes of the droplets electrosprayed from the cone-jet mode are found to be relatively insensitive to applied voltages (Ku & Kim 2002).

The flow of liquids in a high voltage electric field has received much attention in the last two decades because of the phenomenen of jetting and droplet generation, which have numerous applications in agriculture, bioengineering, environmental engineering and materials science (Fenn et al. 1989; Zhang et al 2006). The technique has been applied to emulsion production, mass spectroscopy (Whitehouse et al. 1985), processing of nano-biomaterials (Huang et al. 2004), microincapsulations, formation of powders, thin-film formation (Jaworek & Krupa 1999c) and ceramic electrostatic atomization printing (Jayasinghe et al. 2002). EHDA has some significant advantages, for example it is relatively easy to generate droplets and avoid coalescence of droplets due to electric charge of the same polarity in the droplets, and to achieve a narrow size distribution of droplets via the cone-jet mode (Pareta et al. 2005).

### 2.9.2. Ultrasonic atomization spraying

The first application of ultrasonic waves to the generating of sprays was proposed by Wood and Loomis in the beginning of 20$^{th}$ century (Wood & Loomis 1927). The principle is based on employing high frequency sound waves, beyond the range of human hearing. Ultrasonic atomizer nozzles convert low viscosity liquids into ultra fine sprays. The radiating-wave frequencies most commonly used in ultrasonic cleaning, 18-120 kHz, lie just above the human audible frequency range.

An ultrasonic power supply (generator) converts DC voltage to high frequency electrical energy. Ultrasonic nozzles operate by converting a high frequency electrical signal, fed into two electrodes sandwiched between two piezoelectric transducers. Disc-shaped ceramic piezoelectric transducers convert electrical energy from the power generator into mechanical vibrations at the same frequency. The vibrations from the transducer are intensified by the titanium probe (horn), creating pressure waves in the liquid, ultrasonically vibrating at the nozzle's atomizing tip.

Ultrasonic atomizers work at many different frequencies and are very good at converting various liquids into fine particles. Without the use of air pressure, liquids enter either the rear or side of the atomizing converter, where they are pumped to the vibrating surface. Liquid emerging onto the atomizing surface is broken into a spray by the ultrasonic energy concentrated there (Figure 2.16). The vibrating surface has many possible shapes and styles for different coating and process applications (Figure 2.17).

#### 2.9.2.1. Advantages of ultrasonic atomization spraying

The process of ultrasonic atomization spraying has some specific characteristics that give it advantage over other traditional mechanical methods, like pressure or gas-assisted systems, to generate sprays of very small droplets. The factors that distinguish pressureless, ultrasonic atomizing nozzles from other spray nozzles include:

1. In particular, the resulting droplet produced has very narrow size distribution, and the droplet diameter is essentially controlled by the ultrasonic frequency (Lang 1962; Lozano et al. 2003). Median drop sizes range from 18-68 microns.

In an ultrasonically produced spray, drop size is governed by the frequency at which the nozzle vibrates, and by the surface tension and density of the liquid being atomized. Frequency of the specific type of nozzle is the predominant factor. These droplets are larger with low frequency probes and smaller with higher frequency probes.

For uniform particle size distribution, ultrasonic atomizers have to be adjusted in order to hit the "sweet spot" so that the liquid being processed is efficiently converted to spheres for the application. Resulting droplet size distributions are very narrow and the mean diameter is essentially only controlled by the excitation frequency. Generation of droplets in the micron range requires MHz waves, with voltages around 30 V, which translates into power requirements on the order of 10 W.

2. An important feature is ultra-low flow rate, soft and low-velocity spray, typically on the order of 7.6-12.7 cm per second. Other common spraying techniques, which use pressure in order to generate a spray, generally produce drops with velocities well over 100 times that generated by ultrasonic atomization spraying. This velocity differential means that pressure sprays generate the order of 10,000 as much kinetic energy as do ultrasonically atomized sprays. This striking contrast in spray energy has important, practical implications:

2.1. In coating applications, the unpressurized, low-velocity spray significantly reduces the amount of overspray since the drops tend to settle on the substrate, rather than bouncing off it. This translates into substantial material savings and reduction in emissions into the environment.

2.2. The spray can be controlled and shaped precisely by entraining the slow-moving spray in an ancillary air stream. Spray patterns from as small as 0.177 cm wide to as much as 30.5-60.1 cm wide can be generated.

2.3. This ultrasonic nozzle design provides an easily controllable atomized spray that cannot clog because of the large liquid feed orifice and the self-cleaning ultrasonic vibration.

For these reasons, the use of ultrasonic atomizing devices is becoming increasingly popular for a number of applications, for example in domestic humidifiers or medical nebulisers (Albertini et al. 2005). It is usually recommended for use in applications where flow rates are very low and narrow spray patterns are needed.

Ultrasonic atomization spraying as a possible spray coating on a moving surface has been previously studied. It was found that the percentage area of the covered surface increased with an increase in the height of the ultrasound atomiser from the surface and the vibrational amplitude of the atomiser, while the liquid film thickness on the coated surface decreased with an increase in the height of the ultrasound atomiser, vibrational amplitude of the atomiser and the linear velocity of the moving surface. Also, it was observed that the percentage area as well as the liquid film thickness increased with an increase in the liquid flow rate irrespective of changes in other parameters. The increase in the viscosity of the spraying liquid reduced the area covered by the spray for surface coating, while it increased the coating film thickness (Gaikwads et al. 2005).

Ultrasonic atomization spraying has also been used for the production of protein-loaded biodegradable microspheres. It does not produce degradation of the polymer matrix and the particle characteristics can be modified by adjusting formulation parameters and spraying conditions (Felder et al. 2003). Dirix et al (1993) reported the preparation of protein loaded biodegradable microspheres using an ultrasonic nozzle, collecting the particles in the non-solvent bath to remove the organic solvent and to harden the embryonic microsphere. Bovine serum albumin loaded microspheres with a spherical shape and smooth surface structure were successfully prepared from poly(lactide-co-glycolide) using an ultrasonic nozzle. Process and formulation parameters were investigated with respect to their influence on microsphere characteristics, such as particle size, loading capacity, and release properties. In conclusion, ultrasonic atomization spraying represents a versatile and

reliable technique for the production of protein loaded biodegradable microspheres without inducing degradation of the polymer matrix (Bittner & Kissel 1999). Ultrasonic atomization spraying was evaluated as a new approach for the preparation of ionically cross-linked controlled-release chitosan microparticles (Beatrice, Nadia, & Lorenzo 2005).

With the best matching of polymer characteristics (Pavanetto et al. 1993), liquid and the solute molar fraction (Yasuda et al. 2005) and process of spray drying and coacervation (Blanco-Prieto et al. 2004), ultrasonic driven atomizers can provide a mist-like spray with a particularly narrow droplet size distribution and very low spray velocity. Other studies include microencapsulation (Yeo & Park 2004), fabrication of porous carbon nanotube (Su et al. 2008), delivery of drug for lung inhalation (Zhang et al. 2008). Ultrasonic atomization spraying was used to produce a thin continuous polymer coating (Pan et al. 2007b; Pan et al. 2006) and also polymeric coating incorporating monoclonal antibody for stents (Wang et al. 2009)).

The introduction of foreign material into a living organism, creates an interface between the material and tissue. This means that the surface free energy, morphology (roughness, porosity), electrical properties, hydrophilicity, the presence of ionic groups and surface contamination of a polymer, will all affect tissue-polymer interaction (Gosolewski 1989).

The introduction of a foreign material into a living organism creates an interface between the material and tissue. Many different types of nonporous materials are used in the vascular system including natural rubber latex, neoprene rubber,

poly(tetrafluoroethylene) (PTFE), poly(ethylene terephtalate) (Dacron), silicone rubber and polyurethanes. All foreign substances when exposed to the blood show some degree of thrombosis at the vascular interface (SHARP & TAYLOR 1971). So, the antithrombogenic properties of these biomaterials are still not good enough for the demanding applications such as cardiovascular implants and devices (Aiping & Tian 2006c) and require the introduction of anticoagulants.

Stainless steel and NiTi alloy was used in this thesis as the material of choice for balloon expandable and self-expanding stents. NiTi was used because of its several advantages, including optimal radiopacity, superelasticity and shape memory characteristics. According to the concerns raised with regards to the current coatings employed for stent coating, a novel POSS incorporated poly(carbonate-urea)urethane nanocomposite was introduced for stent materials coating. Hybrid inorganic–organic nanocomposites hold significant promise because of the enhanced characteristics of the materials in nano-scale. In order to obtain materials with improved blood compatibility for a short and long term blood reaction a better understanding of the complex parameters of the interactions between blood and the biomaterial is required. The chemical and physical characteristics of the biomaterial's surface which are responsible for the biological reactions at the interface are certainly of great importance. Surface characteristics of the nanocomposite were measured comprehensively in this study. Electrohydrodynamic spray deposition and ultrasonic atomization spraying were investigated in this thesis as coating techniques. Processing parameters of the two techniques were optimised.

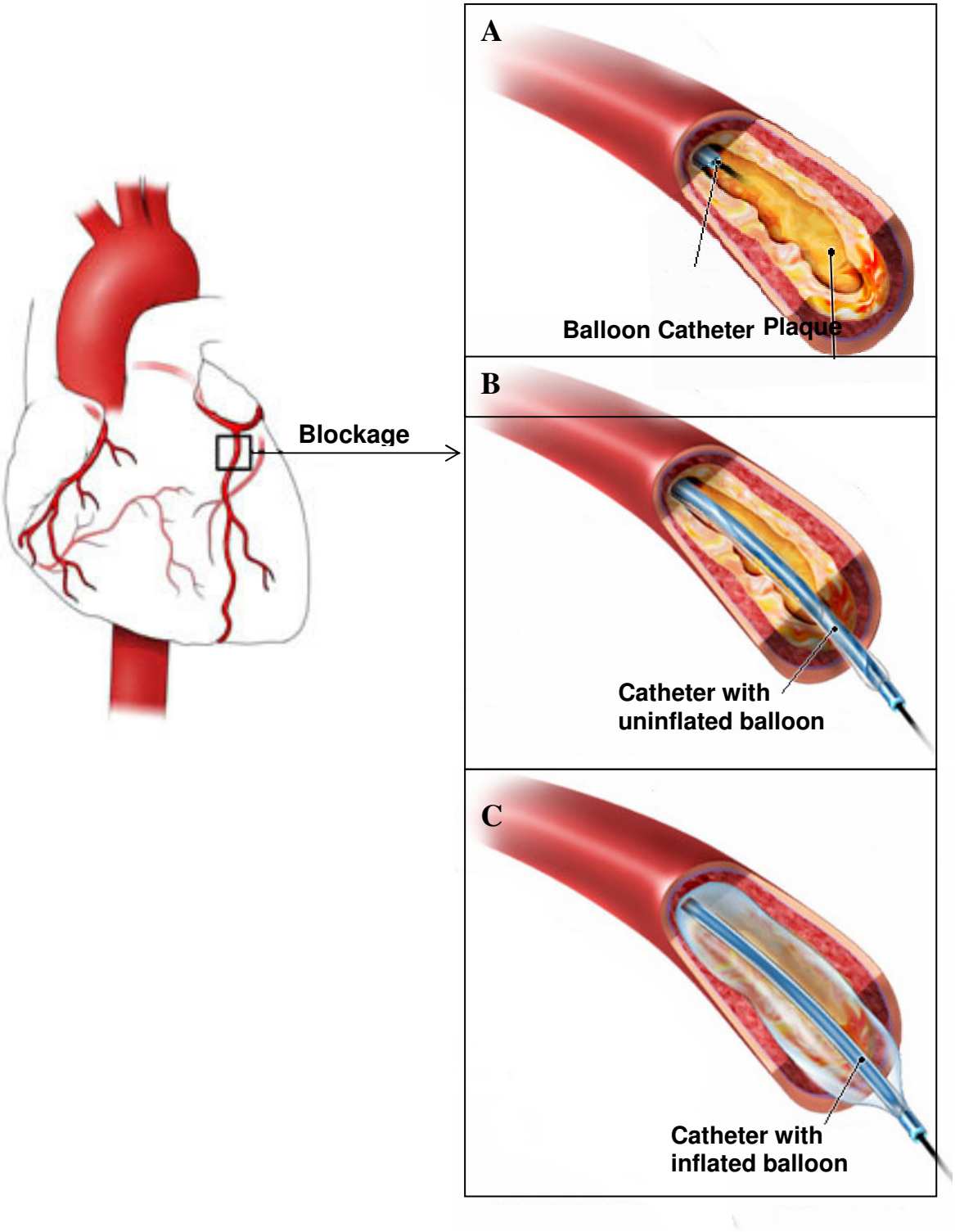


Figure 2.1. Balloon angioplasty. (A) a guide wire with a deflated balloon is passed through the catheter in the narrowed artery; (B) the balloon is then inflated to push the plaque against the artery wall; (C) the balloon is then removed (http://www.orlandocvi.com/procedures_catheter.html)

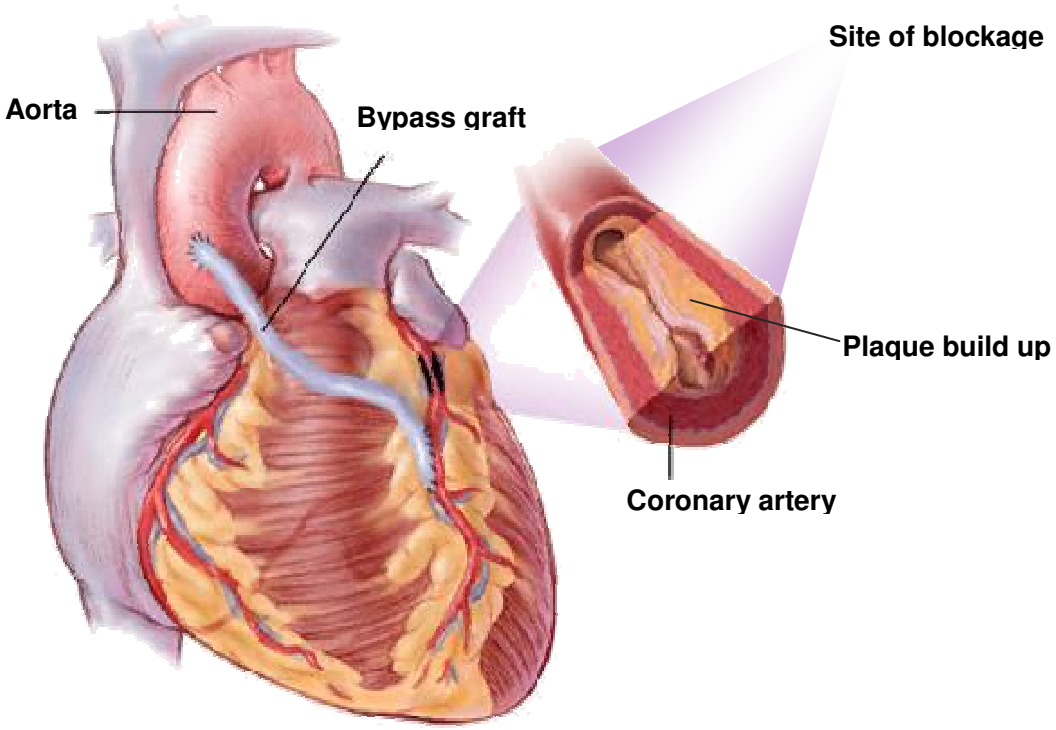


Figure 2.2. Coronary artery bypass grafting

(http://www.bostonscientific.com/templatedata/imports/HTML/lifebeatonline/winter2006/learning.shtml).

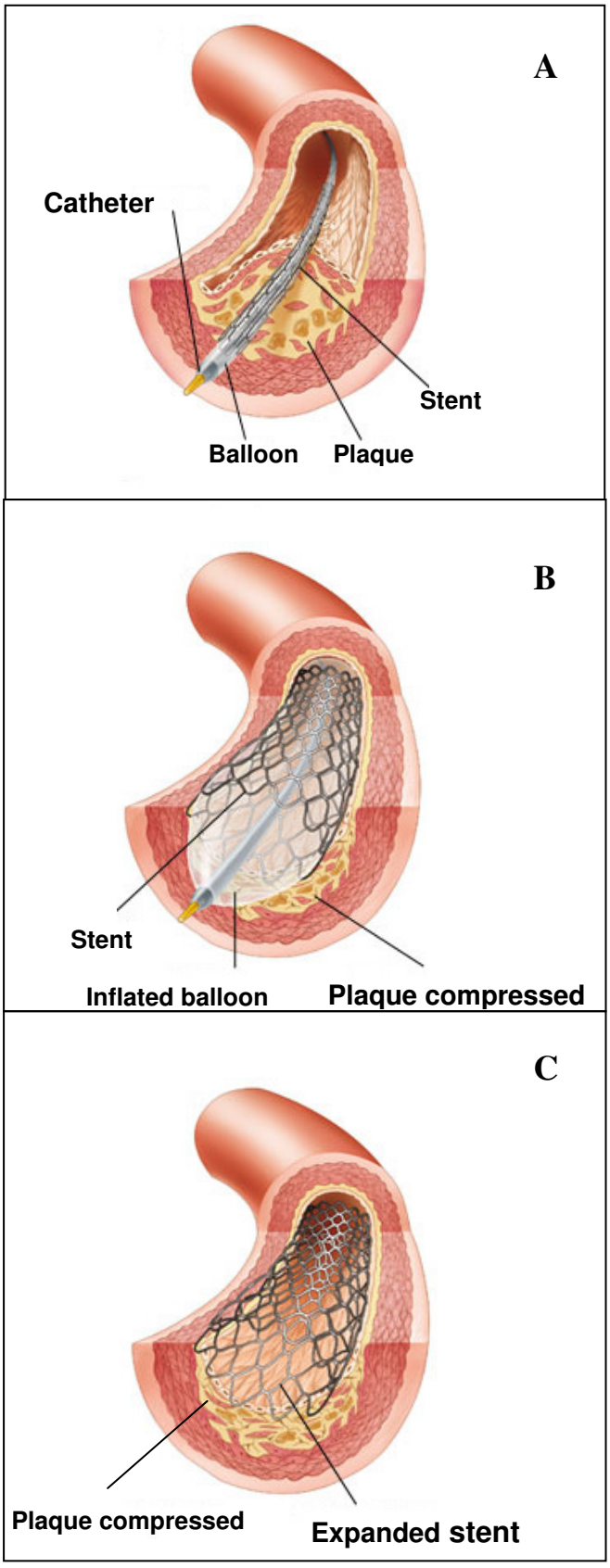


Figure 2.3. Stenting procedure. After removal of the balloon the stent is left in place to keep the artery open (http://www.britannica.com/EBchecked/topic-art/40908/95218/Balloon-angioplasty-and-stent-insertion-In-a-coronary-artery-where).

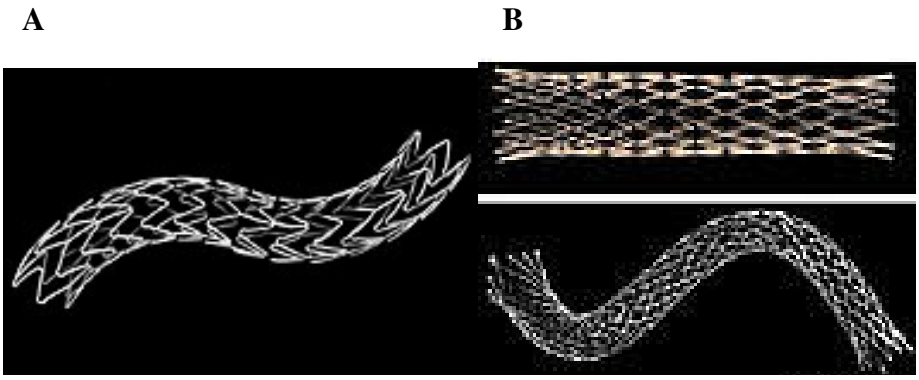


Figure 2.4. (A) Palmaz stent made from stainless steel; and (B) Symphony stent made from Nitinol.

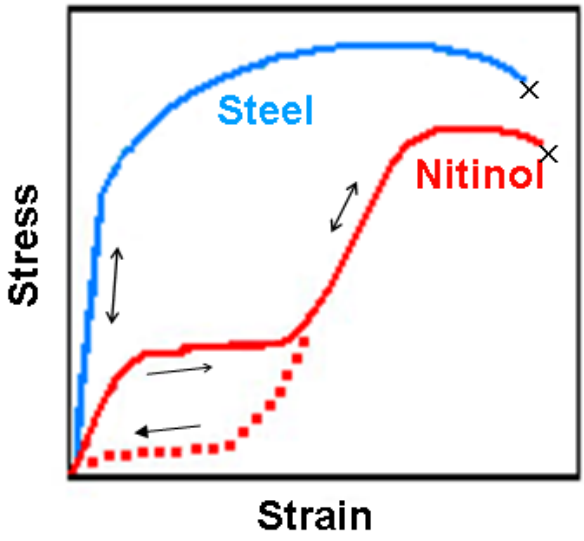


Figure 2.5. Schematic stress-strain diagram for Nitinol and stainless steel (Stoeckel, Pelton, & Duerig 2004).

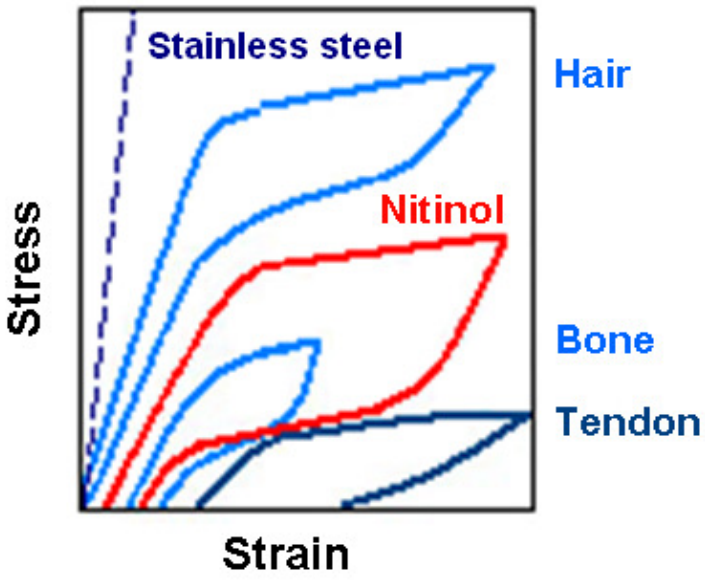


Figure 2.6. . Stress-strain curves comparing with biomaterials.

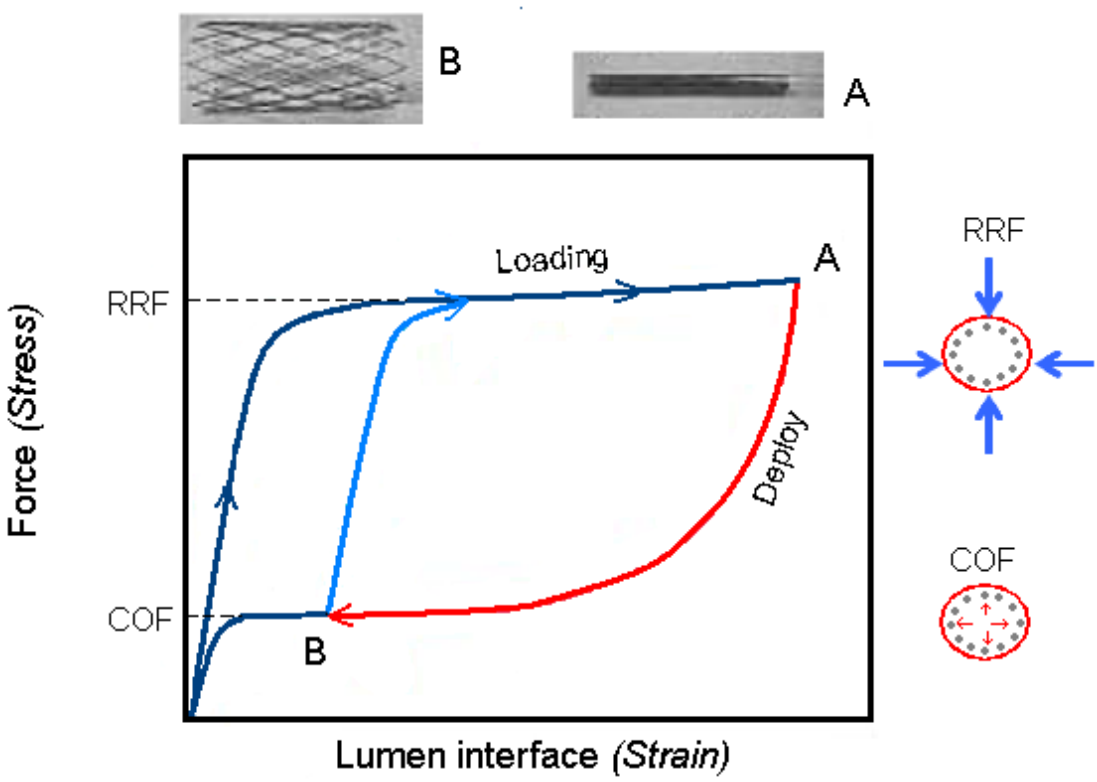


Figure 2.7. Delivery pattern of a super-elastic stent. A stent is manufactured in the open configuration (state B), and deformed to a close position (Satate A).

Keys: RRF: Radial resistive force

COF: Chronic outward force

State A: Stent scaffold

State B: Post-deployment

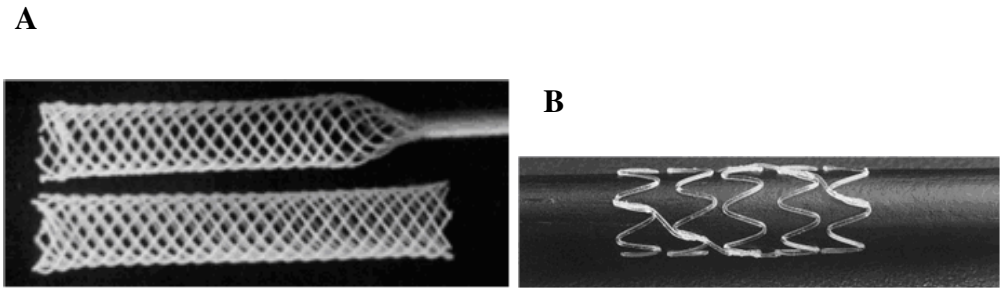


Figure 2.8. (A) Photograph of self-expanding biostable polymeric polyethylene terephthalate (PET) stent; (B) the Igaki-Tamai stent is a premounted, balloon expandable PLLA stent that also has the ability of self-expansion (Tamai, Igaki, Kyo, Kosuga, Kawashima, Matsui, Komori, Tsuji, Motohara, & Uehata 2000).

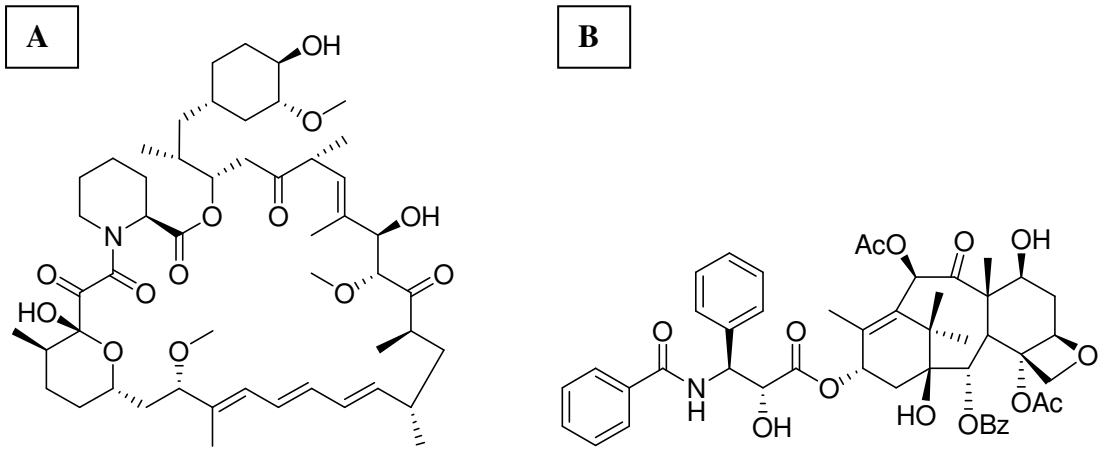


Figure 2.9. (A) Chemical structure of rapamycin; (B) chemical structure of paclitaxel.

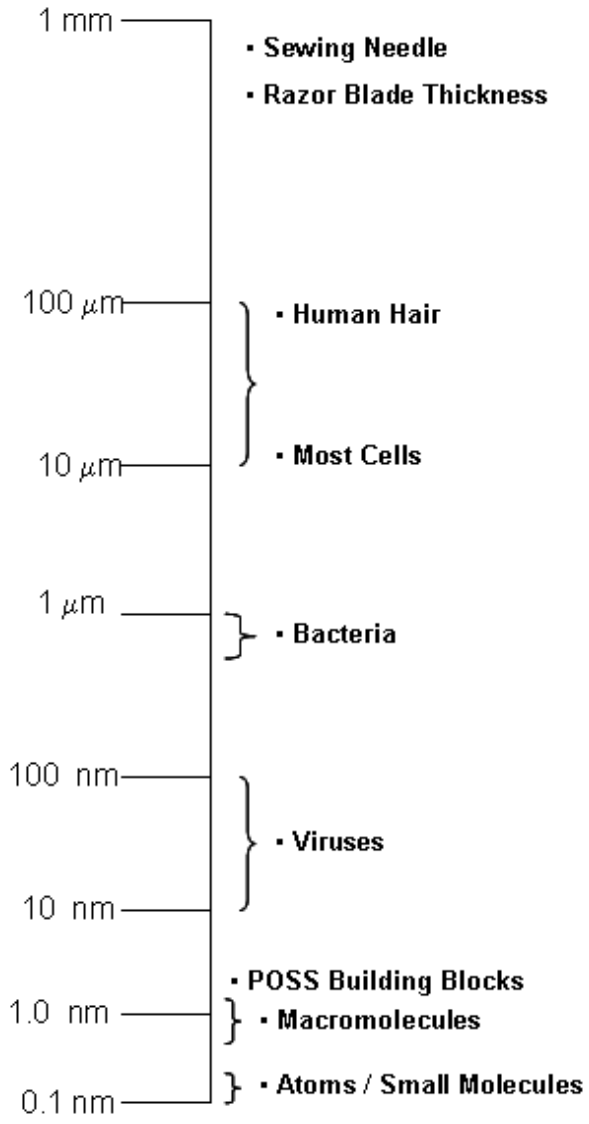


Figure 2.10. Critical length scale for different materials (Lichtenhan & Hibrid Plastics 2003)

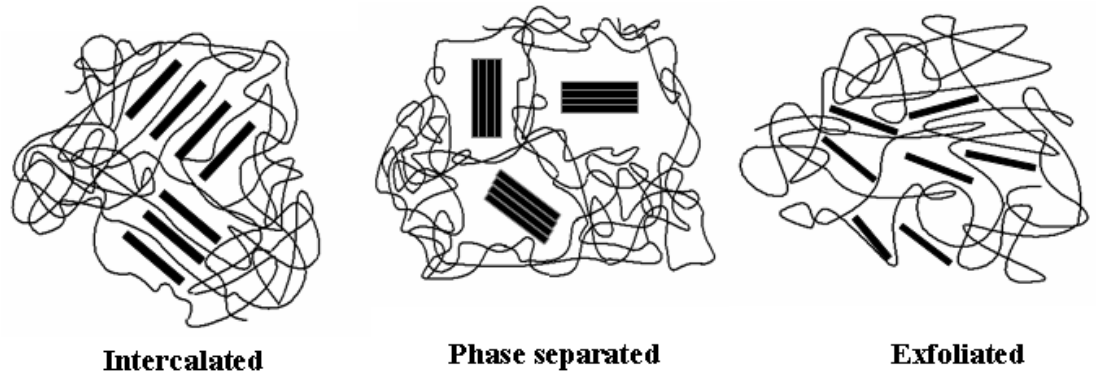


Figure 2.11. Types of synthesized nanocomposites.

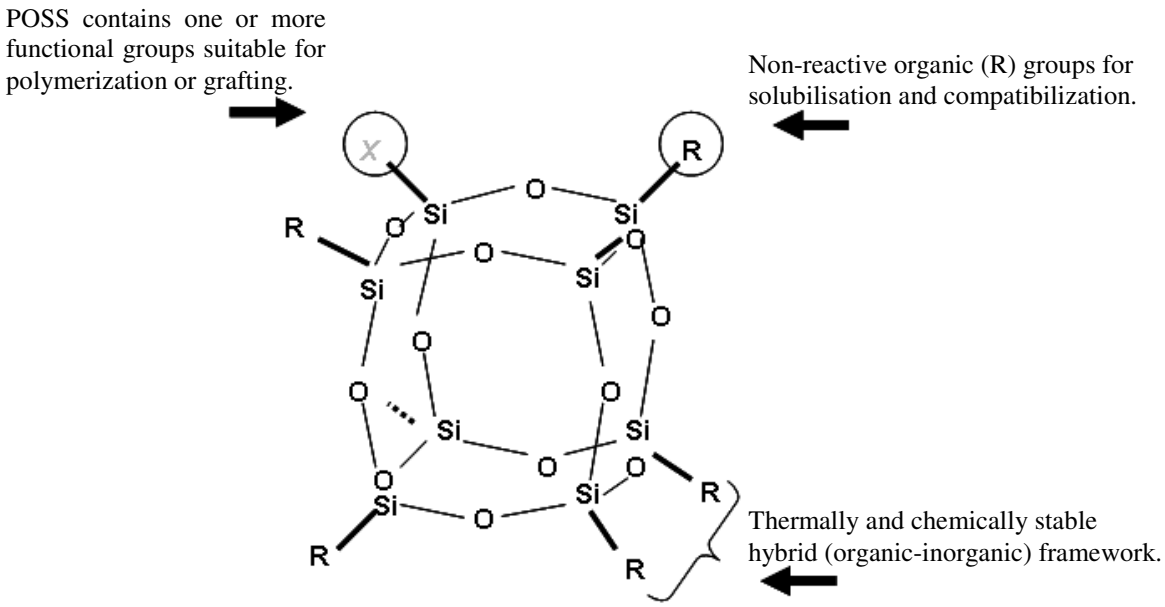


Figure 2.12. Three-dimensional structure of polyhedral oligomeric silsesquioxane molecule.

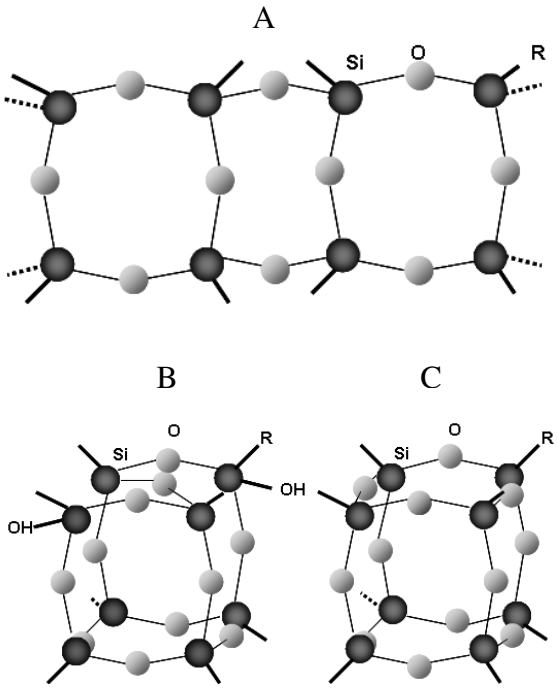


Figure 2.13. Different structures of silsesquioxanes. (A) ladder structure; (B) Partial cage structure; (C) cage structure.

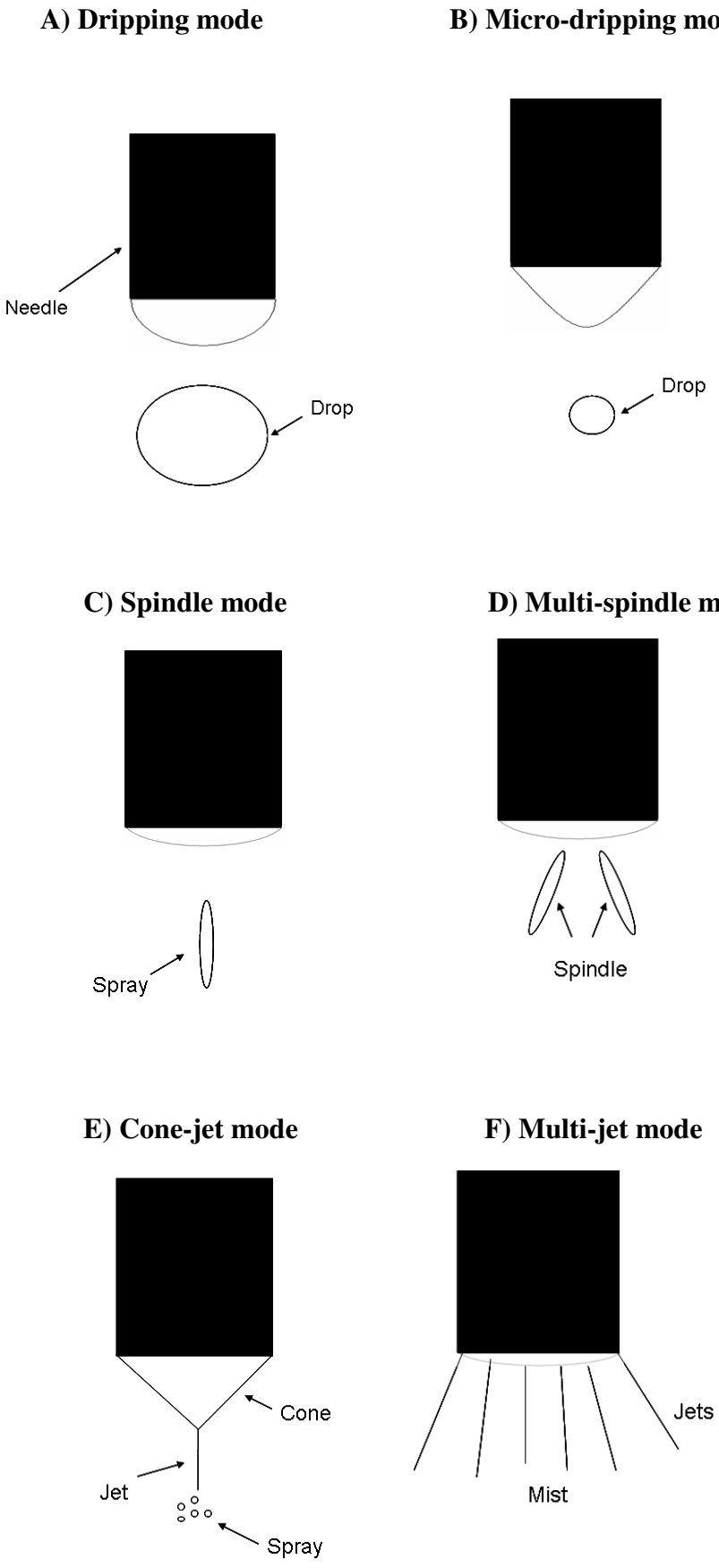


Figure 2.14. Different modes observed in electrohydrodynamic spray deposition.

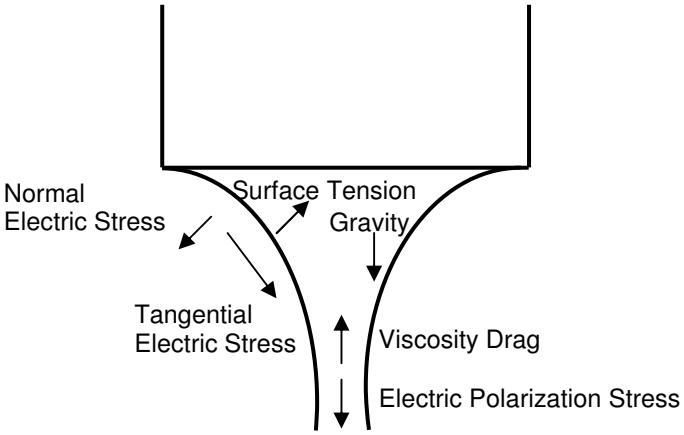


Figure 2.15. Forces acting on a Taylor cone (Hartman et al. 1999).

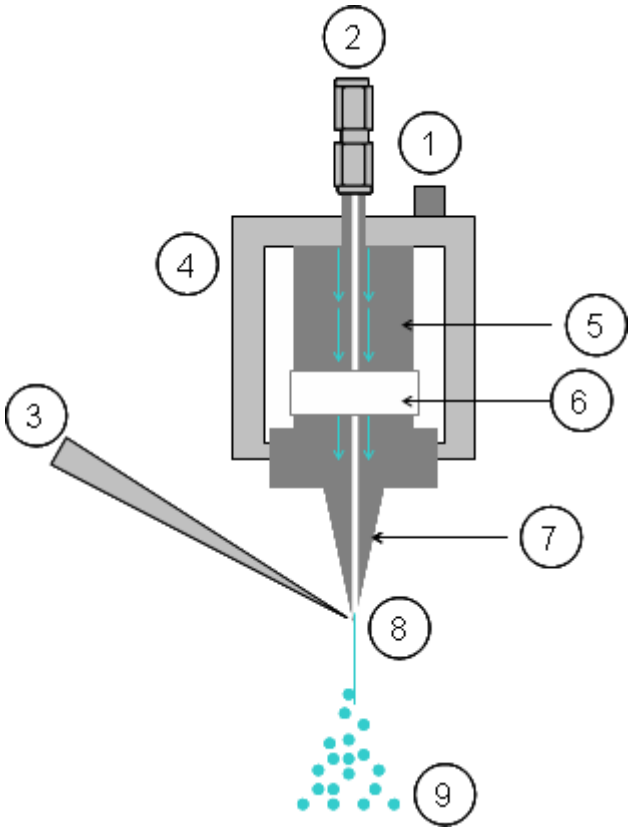


Figure 2.16. Schematic diagram of the ultrasonic atomizer: (1) electrical connection to the broadband ultrasonic generator connection of oscillator; (2) connection for nitrogen; (3) connection for liquid solution; (4) protecting cap; (5) Titanium amplifying section; (6) Piezoceramic element; (7) Nozzle; (8) Atomizing surface; (9) atomizer jet.

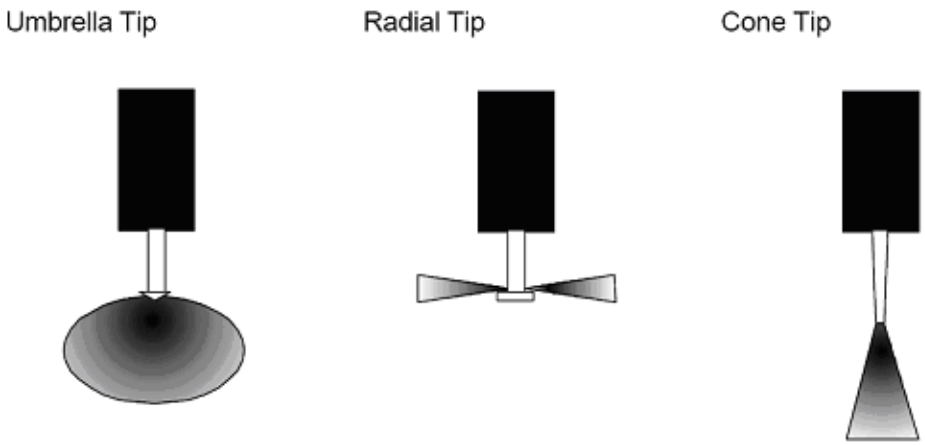


Figure 2.17. Different nozzle design for ultrasonic atomization spraying.

# CHAPTER 3. Materials & Methods

This chapter describes the various experimental techniques used to characterize the nanocomposite polymer. It also describes the different techniques employed for coating of NiTi and stainless steel alloy material with nanocomposite. It also discusses the specific techniques used for surface treatment of the alloy to enhance the integrity between the alloy and the nanocomposite for long time.

## 3.1. NiTi superelastic alloy

Mechanical tests were conducted on a strip of NiTi alloy that was 5.7 mm in width and 0.5 mm in thickness. The nearly equiatomic NiTi alloy (55.8 wt % Ni) strips used in this study were provided by Memry Corp., Bethel, USA. The material had been rolled and subsequently annealed to restore its superelastic properties. An Instron static test machine, equipped with 2000 ±20 kN load cell, was used to apply a tensile load to the specimen with a constant corss head rate of 20 mm/s. The gauge length was set at 143 mm. A schematic view of the set up is shown in Figure 3.1. A preload of 100 N was applied to remove any slack from the system. The test was conducted in two steps: 1) the specimen was loaded and unloaded to characterize the superelastic behaviour; and 2) the same specimen was then loaded to failure to determine the tensile strength and the failure characteristic of the material.

## 3.2. Synthesis of POSS-PCU nanocomposite

The simplified reaction scheme for the POSS-PCU synthesis process is shown in Figure 3.2. 72g of dry polycarbonate polyol (2000$M_w$) and 2g of cyclohexane

chlorohydrine-polyhedral oligomeric silsesquioxane (POSS) (Hybrid Plastics, Hattiesburg) were placed in a 250ml reaction flask equipped with a mechanical stirrer and nitrogen inlet. The mixture was heated to 135°C to dissolve the POSS cage into the polyol and then cooled to 70°C. Flake 4,4'-methylenebis(phenyl isocyanate) (MDI), were added to the polyol blend and then reacted, under nitrogen, at 75-85 °C for 90 minutes to form a pre-polymer. 156g of N,N'-dimethylacetamide (DMAC) was added slowly to the pre-polymer to form a solution and the solution was cooled to 40°C. Chain extension of the pre-polymer was carried out by the slow drop-wise addition of a mixture of 2g of ethylenediamine and 0.05g of diethylamine in 80g dimethylacetamide to the pre-polymer solution. In this manner, a solution of polycarbonate urea-urethane (PCU)- with the hard segments being molecularly modified by nanostructured molecules-polyhedral oligomeric silsesquioxanes (POSS-PCU nanocomposite) with 2 wt% cyclohexane chlorohydrin-silsesquioxane- was synthesised. Similarly, by increasing the ratio of POSS to ethylenediamine, 2 wt%, 4 wt% and 8 wt% POSS-PCU nanocomposites were obtained.

Liu et al. have shown that when the concentration of Octa(propylglycidyl ether) POSS is 10 %wt or more, the concentration of POSS moiety on the surface was no longer increased(Liu, Ni, & Zheng 2006). Therefore, nanocomposites with the POSS concentration less than 8 wt% were investigatede in this study. The amount of ethylenediamine decreased accordingly with increasing the POSS amount, therefore, the stiffness of the nanocomposite reserved even at higher POSS concentrations. Hereafter, these nanocomposites are referred to as POSS-PCU2, POSS-PCU4 and POSS-PCU8. For comparison, a pure PCU was also synthesised. All the chemicals,

reagents, glassware and associated relevant equipments were purchased from Sigma-Aldrich Ltd. (Dorset, UK).

## 3.3. Characterization of physical properties of POSS-PCU solution

Measurements were carried out to determine the physical properties governing the electrohydrodynamic processing behaviour of the solutions for the research discussed in chapter 5. Each instrument was calibrated before use and cleaned and dried thoroughly taking measurements on different samples. A 20 wt% POSS-PCU2 solution was dissolved in extra DMAC and was left overnight at room temperature making sure the polymer had completely dissolved. By varying the dilution of this polymer solution, several concentrations were obtained for electrospraying. DMAC was characterized in the same way as the POSS-PCU solutions. All measurements were carried out at ambient temperature. All experiments were repeated five times and the average was reported in this thesis.

### 3.3.1. Density

The density of the samples was measured using a standard 25 ml density bottle (VWR, Lutterworth, UK). Calibration was carried out by measuring the density of de-ionised water and ethanol. The weight of the density bottle was set to zero and then the net weight of the solution was measured and density of that solution was reported by dividing the net weight by the specific volume of the density bottle.

### 3.3.2. DC electrical conductivity

DC electrical conductivity was measured using a HI-8733 conductivity meter (Hanna Instrument Ltd., Bedfordshire, UK). The conductivity probe was calibrated using the

ethanol with known conductivity value. The meter is always used at ambient temperature. Before each measurement the probe was rinsed with de-ionised water and dried. About 50 ml of solution was required for this probe. The probe was agitated to remove any bubbles on the probe. The measuring range of this meter is 0.0 to 199.9/ 0 to 1999 µS/cm and 0.0 to 19.99/0 to 199.9 mS/cm.

### 3.3.3. Viscosity

Viscosity was determined using a ViscoEasy-L concentric cylinder rotational viscometer (Schott, Camlab Ltd., Cambridge, UK) working at 100 rpm at ambient temperature

### 3.3.4. Surface tension

Surface tension was measured using a Kruss Tensiometer K9 (Kruss GmbH, Germany). Wilhelmy's plate method was used. The ring and plate were lowered till the surface of the liquid and pulled on the liquid surface without breaking the surface. The value increased first and suddenly dropped to zero when the ring was separated from the liquid completely. The maximum value calculated from this procedure is the surface tension. The average of five consecutive values is reported as the final result. The plate was cleaned and dried after each test to minimize the error. The instrument was calibrated with de-ionised water and ethanol.

## 3.4. Characterization of POSS-PCU films

For the research in chapter 4, nanocomposite solutions (POSS-PCU2, POSS-PCU4, and POSS-PCU8) and PCU as the control were weighed onto a glass plate/petri dish.

The solvent from the polymer solutions was then allowed to evaporate in an oven overnight at 60°C prior to further characterization.

### 3.4.1. Gel permeation chromatography

The molecular weight distribution of the polymers was measured by gel permeation chromatography (GPC) at RAPRA Technology, Shrewsbury, UK. A single solution of each sample was prepared by adding 15 mL of eluent to 30 mg of sample and warming at 80°C, with shaking, for 30 minutes and then filtered through a 0.45 μm PTFE membrane into autosampler vials. Gel permeation chromatographic analysis was carried out at 80 °C on a PL-GPC 120 (Polymer Laboratories) liquid chromatography system equipped with a PL-AS-MT autosampler, PLGel guard column (Polymer Labs), two mixed bed-B columns ; 30 cm and 10μm; and a differential refractometer. DMAC (with 0.01M lithium bromide) was used as an eluent at a flow rate of 1 mL/min. Poly(methyl methacrylate) standards were used to calibrate the GPC system. The results are expressed as the "PMMA equivalent" molecular weights and it should be appreciated that there could be a significant difference between these PMMA equivalents and the true molecular weights. The data was collected and analysed using Polymer Laboratories 'Cirrus' software. Test were done in duplicate.

### 3.4.2. Stress–strain analyses

A tensometer (Instron 5565, UK) equipped with a 500 N load cell was used to determine the mechanical properties at room temperature. Dumbbell shaped test specimens were cut from the nanocomposite films for stress-strain testing, in accordance with DIN 53504 (DIN 53504, 1994). Thickness of the dumbbell shape

samples was measured using a digital micrometer (IP54 RS). The initial clamp distance was 20 mm. The applied stretching speed was 100 mm/min. Five replicates were tested for each thickness.

### 3.4.3. Differential scanning calorimetry

The POSS-PCU nanocomposites were studied using differential scanning calorimetry (DSC) in order to determine the glass transition temperature ($T_g$) and melting temperature ($T_m$). Calorimetric measurements were performed on a heat-flux differential scanning calorimeter (DSC-60 Shimadzu Ltd., Japan), in a dry nitrogen atmosphere achieved with the help of a liquid nitrogen cooling unit. Samples about 10 mg in weight were used for $T_m$ measurements and about 20 mg was used for $T_g$ measurement to improve the quality of the results and to obtain the sharp peaks. The DSC was calibrated using an indium standard. The thermal cycle applied for glass transition temperature was heating from -100°C to 50°C at a heating rate of 20 °C/min, while melting temperatures were measured by reheating from 50 to 300 °C at 10 °C/min. The glass transition $T_g$ was calculated as inflection in the $C_p$ change. In order to achieve consistency, measurements were repeated three times.

### 3.4.4. Rheological measurements

All rheological measurements were carried out using a rheometer (CVO 100, Bohlin Instruments Ltd, UK), at shear rates ranging from 0 to 200 $s^{-1}$. The temperature was maintained at 25±1 °C using a control bath (Bohlin Peltier system). The experiments were carried out on as-prepared polymer solution using cone-plate geometry (upper plate diameter 40 mm) with 150 μm gap. The rheometer was computer-driven using a software package (Bohlin software CVO 100).

### 3.4.5. Scanning electron microscopy

Surface morphology of the films was examined using a JEOL JSM63101F scanning electron microscope (SEM) (JEOL Ltd., UK). For this observation, samples were placed on aluminium stubs and the surfaces to be examined were gold coated using an Edwards 5150B sputter coater prior to microscopy. SEM was carried out at an accelerating voltage of 10 kV. Samples were viewed under low magnification and images were captured at ×200 magnification. For the research in chapter 6, the morphology of the interface and the thickness of the surface layer formed on the NiTi samples were determined by SEM using a sample size of 10 mm.

### 3.4.6. Zeta-potential

The ζ-potential determinations were done with the adjustable gap cell unit of the SurPass Electrokinetic Device (Anton Paar, Graz, Austria). Two rectangular specimens (10 × 20 mm) were cut from the polymer foils and glued by double sided adhesive tape on the sample holder blocks. The two sample holder blocks were mounted into the gap cell to achieve an initial slit width of approximately 0.1 mm. The final slit width was fine-adjusted by measuring the flow rate during of the electrolyte in the range between 100 and 150 ml/min. The electrolyte was a $10^{-3}$ M aqueous KCl solution. The change of the pH–value was done by the automatic titration routine, using 0.1 M HCl for titration, beginning at pH 10 (adjusted by addition of NaOH). Surface potentials were calculated by software of SurPass based on Helmholtz-Smoluchovsky equation shown below.

$$\varsigma = \frac{dU}{dp} \cdot \frac{\eta}{\varepsilon . \varepsilon_0} \cdot \frac{L}{A.R} \qquad 3.1$$

In which $\zeta$ is the zeta potential; *dU/dp* is the slope of the streaming potential versus pressure; $\eta$ is the viscosity of the electrolyte; $\varepsilon$ is the dielectric constant of the electrolyte; $\varepsilon_0$ is the vacuum permittivity; *L* is the length of the streaming channel; *A* is the cross section of the streaming channel; and *R* is the AC resistance inside the measuring cell.

### 3.4.7. Contact-angle

To prepare the samples for contact angle measurements, POSS-PU films about 50 µm thick were cast-coated on well-cleaned glass slide substrates and oven-dried at 60 °C overnight. Dynamic contact angles were measured at ambient humidity and temperature on a Drop Shape Analyser (DSA 10 MK2, Krüss, Hamburg, Germany). Water, diiodomethane, ethylene glycol and formamide were used as probe liquids. The polymer films were fixed horizontally and immersed in a chamber containing probe liquid. A motorised syringe was used to increase or decrease the bubble volume. Surface energy was calculated by measuring the contact angle between the sample surface and test liquid, which will be discussed in the results. Contact angle hysteresis was calculated by measuring advancing and receding contact angles using the tilting plate technique.

In the tilting plate method a contact angle sample is slowly tilted until the sessile drop on it begins to move in the downhill direction. At that time, the downhill contact angle is the advancing angle and the uphill angle the receding contact angle. Measurement has been done immediately before actual motion takes place, because once motion starts, the system is no longer in thermodynamic equilibrium. Six different measurements were done and averaged for each sample.

### 3.4.8. Attenuated total internal reflection Fourier transform infrared spectroscopy

To analyze the surface composition of the nanocomposites using an Attenuated total internal reflection Fourier transform infrared spectroscopy analyser (ATR-FTIR) (Advance 2000, Perkins-Elmer Ltd., US), the surfaces of the polymeric films were exposed to infra-red radiation of 4200–600$cm^{-1}$ wavelengths at an incident angle of 301° and at room temperature (25 °C). A total of 16 scans were performed per sample. The analysis was repeated five times and the results averaged. The surfaces of each specimen were analyzed using a 2-mm germanium (Ge) crystal with a 458 angle maintaining constant contact pressure between the crystal and the specimens.

### 3.4.9. Atomic force microscopy

The structure of POSS-PCU films on glass substrate was studied with an atomic force microscopic (AFM) using a Digital Instruments NanoScope (Digital Instrument Inc., USA) in the tapping mode. A silicon probe with 125 µm long silicon cantilever, nominal force constant of 40 N/m and resonant frequency of 275 kHz was used for tapping mode surface topography studies.

## 3.5. *In vitro* assessment of the resistance of POSS-PCU nanocomposites to oxidative and hydrolytic stress

The resistance of the POSS-PCU nanocomposite to chemical degradation was investigated by incubating the specimens in a variety of chemically aggressive/biological solutions at 37°C. These accelerated *in vitro* tests have shown good correlation with human and animal model results.

### 3.5.1. Plasma protein fractions

The procedure for plasma fractionation with polyethylene glycol (PEG) was adopted from the method described by Hao et al. (Hao 1979). Citrated human plasma (200 mL) derived from fresh frozen human plasma obtained from the Blood Transfusion Department at Royal Free Hospital, London, UK was placed in a beaker in a cold room (4°C). Polyethyleneglycol (PEG, MW=3350, Sigma Chemical Ltd., Dorset, UK) was added slowly, while stirring, to the plasma in the amount 10 g/100 mL. After 60 min of stirring, the 10% PEG precipitated, designated fraction I, was removed by centrifugation at 2000 rpm for 30 min. An additional 10 g of PEG was then added to the supernatant liquid to reconstitute a 10% mixture, followed by centrifugation to obtain fraction II (10–20% PEG precipitate). The process of mixing and centrifugation was then repeated to obtain four plasma protein fractions with the corresponding plasma fractions. The precipitates were reconstituted to the original volume of plasma (200 mL) with PBS. The distribution of plasma proteins in plasma fractions I-IV is illustrated in Table 3.1.

### 3.5.2. Hydrolysis with lysosomal enzymes

A solution of cholesterol esterase (CE) was prepared by dissolution of CE powder (Sigma Chemical Ltd., Dorset, UK) in a pH 7.0, 0.05 M phosphate-buffered solution (PBS) at a concentration of 1 U $mL^{-1}$, which was then sterile filtered using a 0.22 μm filter. The standard 1 U is characterizeed by its ability to hydrolyse 1 mM $min^{-1}$ phosphatidylcholine at pH 8.0 at 37°C. The other hydrolytic solution is phospholipase A2 solution (porcine pancreatic phospholipase, PLA, Sigma Chemical Ltd., Dorset, UK), which was prepared in buffer solutions (50 mM Tris, pH 8.0, containing 6.8 mM $CaCl_2$) at a concentration of 0.18 U $mL^{-1}$.

Table 3.1. Distribution of selected plasma proteins in the PEG fraction (Hao 1979).

| Plasma Proteins | Fraction wt%(mg/dL) I | II | III | IV | Amount (mg/dL) |
|---|---|---|---|---|---|
| Albumin | 6 (206) | 4 (138) | 86 (2958) | 100 | 3440 |
| IgG | 88 (651) | 15 (111) | 1 (7) | 1 | 740 |
| Transferrin | 6 (13) | 22 (49) | 58(129) | 99 | 223 |
| α2-Macroglobulin | 35 (66) | 65 (123) | — | — | 189 |
| Fibrinogen | 88 (158) | — | — | — | 179 |
| Ig (+) | 34 (53) | 58 (91) | 20 (31) | — | 157 |
| Haptoglobin | 2 (2) | 40 (43) | 56 (61) | 86 | 108 |
| a-Lipoprotein | 15 (10) | 25 (16) | 50 (32) | 50 | 64 |
| C-3 component | 93 (52) | 7 (4) | — | — | 56 |
| a1-Acid glycoprotein | — | — | 100 ± 54 | — | 54 |
| Ceruloplasmin | 14 (3) | 23 (5) | 73 (16) | 100 | 22 |
| Plasminogen | 69 (11) | 19 (3) | — | 89 | 16 |
| β-Lipoprotein | 100 (16) | — | — | — | 16 |
| Prothrombin | 25 (2) | 50 (4) | 25 (2) | — | 8 |
| C-1 esterase inhibitor | — | — | 100 (4) | 100 | 4 |

### 3.5.3. Oxidation and peroxidation

As described by Zhao (Zhao 1993) an oxidising systems can be made by combining hydrogen peroxide (Fluka Chemicals, Buchs, Germany), cobalt chloride (Sigma Chemical Ltd., Dorset, UK) and t-butyl peroxide (Sigma Chemical Ltd., Dorset, UK). Therefore, solutions were made of (i) 1.63 M of hydrogen peroxide ($H_2O_2$) and 0.1M $CoCl_2$ .$6H_2O$ ($H_2O_2$/ $CoCl_2$) to induce formation of hydroxyl radicals, (ii) 1.63 M t-butyl hyrdoperoxide and 0.1M $CoCl_2$.6 $H_2O$ (*t*-but/$CoCl_2$) to induce peroxidation i.e. generation of alkyl and hydroxyl radicals.

### 3.5.4. Control

Both modified and non-modified NiTi was incubated in distilled water under the same conditions to act as a negative control (Phua 1987; Salacinski et al. 2002b).

All the degradative solutions contained 10mg streptomycin, 10000U penicillin per millilitre to minimise bacterial and fungal infections, which could affect the outcome of the results. For the research in chapter 4, five POSS-PCU2 films were incubated in each solution at 37°C for 70 days on a shaker platform, and solutions were replaced weekly. After completion of the experiments, the samples were rinsed in distilled water, dried in air prior to GPC and tensile testing. For the research in chapter 6, five POSS-PCU2-coated NiTi strips incubated in the solutions. After completion of the experiments, the samples were rinsed in distilled water and dried in air prior to microscopy and peel strength assessment.

## 3.6. Endothelialisation of POSS-PCU: An *in vitro* study

### 3.6.1. Extraction of human endothelial cells

Endothelial cells were obtained from human umbilical cord veins (HUVECs) by an adaptation of the method of Jaffe (Jaffe et al. 1973). A sterile technique was utilized in all manipulations of the cord. Human umbilical cords were obtained from the labour ward of the Royal Free Hospital, Hampstead. The cord was severed from the placenta soon after birth, and stored in a sterile container filled with 40 ml of Media 199 (Invitrogen Ltd, Paisley, UK). The cord was inspected, and all areas with clamp marks were cut off. The umbilical vein was cannulated with a blunt 14 gauge needle, 2 cm long, and the needle was secured by clamping the cord over the needle with an umbilical cord tie. The vein was perfused with 100 ml of PBS to wash out the blood and allowed to drain. 25 ml of warm filtered collagenase A2 (Sigma-Aldrich Ltd, Dorset, UK) solution (12.5 mg in 25 ml media) was then infused into the umbilical vein from the other end through another clamped syringe. The umbilical cord, suspended by its ends, was placed in the incubator at 37°C for 10 min. After

incubation, the cord was massaged gently prior to collecting the collagenase suspension containing the endothelial cells by perfusion with 30 ml of PBS. The effluent was collected in a sterile 50 ml conical centrifuge tube containing 10 ml of complete medium obtained from the stock made up of 157 ml Medium 199, 40 ml foetal bovine serum, 3.4 ml of 200mM L-glutamine solution and 1% penicillin/streptomycin (Invitrogen Ltd, Paisley, UK) to neutralize the collagenase. The cells were sedimented at 250 g for 10 minutes, and the cell button was resuspended in 5 ml of warm complete culture medium. The cell suspension was added into 5 $cm^3$ flasks and was incubated at 37°C under 5% $CO_2$. 24 hours later, the flasks were gently washed with 4 ml PBS to remove red blood cells and fed with 5 ml of complete medium.

### 3.6.2. Primary endothelial cell culture

The HUVECs in flasks were viewed daily under high power transilluminated microscopy and the presence of endothelial cells (EC)'s verified by confirmation of their characteristic cobblestone morphology. Once a confluent monolayer was achieved cultures were passaged by removing the cell culture medium, washing with 4 ml PBS and then adding 3 ml of 10% trypsin solution (Invitrogen, Paisley, UK). The flask was then incubated for three minutes prior to gentle tapping in order to loosen all the cells. The trypsin was then neutralised by the addition of 5 ml complete medium. The cell suspension was spun at 250 *g* for 10 minutes before discarding the supernatant, resuspending the cell pellet in 7 ml complete medium, and placing in a 75 $cm^3$ flask. The cells were fed twice a week with a complete change of fresh culture medium. Cultures were passaged every 2-3 days and split in at a ratio of 1:2. Confluent HUVECs from passage 6 was used for the experiments.

### 3.6.3. Cell viability analysis

#### 3.6.3.1. Alamar Blue assay

Alamar Blue (AB, Biosource Ltd., London, UK) is an assay designed to measure quantitatively cell metabolism and viability through calorimetric oxidation reduction of resazurin and resarufin indicatore resulting from cell metabolism. The data may be collected with either fluorescence-based or absorbance-based instruments. Resazurin has a much higher electrochemical potential than the carriers on the cell membrane, and on contact with the membrane, it is reduced to resarufin. Resazurin acts as an intermediate electron acceptor in the electron-transport chain between the final reduction of $O_2$ and cytochrome oxidised by substituting for molecular oxygen as an electron acceptor. The rate of bio-reduction is related to the level of redox potential on the cell membrane, which in turn characterises the constitutive part of the metabolic activity of a given cell type.

AB has certain properties that make this assay attractive. It is soluble in culture media in oxidative form as well as in the reduced one, stable in solution and minimally toxic to cells, and produces changes that are easy to measure. AB allows a continuous assessment of the metabolism and viability of seeded cells, is simple to perform, and does not destroy the cells. So, it is possible to achieve a long term monitoring of cells in culture without any negative effects. Some studies on the long-term culture of plant cells, fibroblasts, osteoblasts, epithelium cells, lymphocytes and transformed cell lines show that the reduction of AB correlates with the viability and proliferative activity of cells (Petrenko et al. 2005). Limitations of AB are few. If prolonged incubation times are used (> 24 h), reversal of the reduction process occurs via a secondary redox step, resulting in a colourless solution, particularly when very high cell concentrations are

used. Microbial contamination would also reduce AB, thus yielding erroneous results, but this would affect any other assay of ECs as well.

For the experiment in Chapter 5, POSS-PCU2 nanocomposite has been cast/sprayed coated on Melinex film (TAAB, Berkshire, UK) and left overnight in an oven at 60°C to evaporate the solvent. In particular, the hybrid materials were cut into disks of opportune diameter, to fit inside the 96-well plates (Invitrogen, Paisley, UK). All sets of samples were sterilized by autoclaving. Three wells for each sample were plated with $2\times10^4$ cells/well. HUVECs were seeded and monitored for attachment to nanocomposite polymer surfaces. The AB assay can be adapted providing the 1:10 ratio of AB reagent volume to medium volume is preserved; that is, 20µl AB reagent to 200µl of medium. After a 24 hours incubation, 20 µL AB was placed in each well and incubated for 4 hours. The fluorescent was measured using a fluorescence spectrophotometer (Fluoroskan AscentFL, ThermoLabsystems, Virginia, USA) at 530 nm excitation and 620 nm emission. The fluorescence signal from each sample was isolated by subtracting from raw background fluorescence signal, the background control signal. Each absorbance was measured and displayed compared with the control. The experimental process was repeated three times, and the average of the results was reported.

#### 3.6.3.2. CellTiter-Blue assay

The cell vitality and proliferation were also evaluated by CellTiter-Blue (CTB, Promega, Hampshire, UK) assay for the research in chapter 4. The CellTiter-Blue cell viability assay (CTB) provides a homogeneous, fluorometric method for estimating the number of viable cells. The assay is based on the ability of living cells to convert a

redox dye (resazurin) into a fluorescent end product (resorufin). Nonviable cells rapidly lose metabolic capacity and thus do not generate a fluorescent signal. The homogeneous assay procedure involves adding the single reagent directly to cells cultured in serum-supplemented medium. After an incubation step, data are recorded using either a plate-reading fluorometer or spectrophotometer.

This set of experiments was performed using polystyrene culture plates as the standard and POSS-PCU with different concentrations of POSS to elicit the difference in EC adhesion between different nanocomposites as well as to compare the endothelialization properties of silsesquioxane-containing nanocomposite to pure PCU. For the research in chapter 4, each polymer (PCU and POSS-PCU nanocomposites) was coated on Melinex film, dried in an oven overnight and then cut into disks of opportune diameter for the 96-well plates. All sets of samples were sterilized by autoclaving the samples. Cell vitality and proliferation were evaluated using CTB assay in this set of experiment. The recommended quantity of CTB reagent to use is 1:5 dilution of the original stock of CTB; that is, 20µl of reagent to each 100µl of medium in a 96-well format. Three wells per sample were seeded and the experiment was repeated three times per sample. After 48 hours incubation, the fluorescent was measured using a fluorescence spectrophotometer at 530 nm excitation and 620 nm emission.

Under most experimental conditions, the fluorescent signal from the AB/CTB reagent is proportional to the number of viable cells. For individual calibration curves for each cell type, known numbers ($0.5\text{-}2.5 \times 10^4$) of cells were plated in triplicates in multi-well cell culture plates. After letting the cells adhere to the plates for 24 h, 2:10

dilution of the original stock of CTB (1:10 dilution in the case of AB) was added to the medium. The plates were incubated for another 4 h at 37 °C. CTB bioreduction was assessed by measuring the fluorescence in the cell culture supernatant using a spectrophotometer at 530 nm excitation and 620 nm emission.

### 3.6.4. Cell confluence morphology

#### 3.6.4.1. Light microscopy; cellular characterization by immunostaining

The von Willebrand Factor (vWF) expression specific to mature endothelial cells was evaluated in this study. Observations of cytoskeleton and nucleus were carried out to check their development on POSS-PCU.

HUVECs were cultured on POSS-PCU2 nanocomposite films for 48 hours. Prior to immunolabeling with the vWF antibody, the cells were fixed by incubation with 1% paraformaldehyde at 37 °C for 20 min following two washes with Dulbecco's modified Eagle medium without red phenol (DMEM). The cells were made permeable in the presence of 0.5% Triton X100 followed by 40 min incubation at room temperature with 500 lL primary goat polyclonal antibody anti-von-Willebrand-factor (Abcam Ltd. Cambridge, UK) diluted to 1/50 in 0.1% Triton X100 containing 0.5% bovine serum albumin (BSA). Subsequently, the cells were washed twice with 1 mL DMEM without red phenol/BSA to remove the excess antibodies. These cells were then incubated for 30 min at room temperature with the secondary antibody, 500 lL of polyclonal donkey anti-goat-immunoglobulin G conjugated with Alexa-Fluor 488 (Invitrogen Ltd, Paisley, UK) diluted to 1/100. After three washes in DMEM without red phenol, the sample was imaged by confocal laser scanning microscopy (Leica DMIRE2 HC Fluo TCS 1-B, Germany), using the 488 nm spectral

line. The morphology of the proliferating ECs was also studied using optical microscopy.

For immunostaining of the Cytoskeleton and Nucleus, as for vWF immunostaining, cells were fixed with 1% paraformaldehyde for 20 min and permeabilized with Triton X-100 (0.5%) for 40 min. The cells were then incubated for 30 min at 37 °C with propidium iodide labeled with Alexa-Fluor 488 (Invitrogen, UK) diluted to 1/100 in Triton X-100 (0.1%) and followed by two rinses with DMEM without phenol red. The cells were observed by fluorescence confocal microscopy using the 488nm and 594nm spectral lines.

#### 3.6.4.2. Electron microscopy

Seeded polymer films for electron microscopy were washed carefully with PBS and the seeded samples were fixed in 4% formaldehayde in PBS for two hours at room temperature. The samples were then dehydrated with ethanol/distilled water (10% ethanol increments) at 41 ºC. The discs were observed using a scanning electron microscope (Philips SEM Model 501, Netherlands). Before imaging, samples were attached to aluminium stubs and coated with gold using an SC500 (EM Scope) sputter coater.

The parameters assessed were the presence of cell retraction, loss of filopodia and a rounded cell appearance; indicators of impaired cell motility and morphogenesis (Park et al. 2002a).

## 3.7. Coating NiTi with POSS-PCU

### 3.7.1. Casting

A casting method was used to prepare polymer films. For cast films, the polymer solution was diluted with extra DMAC to reach the final concentration of 15 wt% and centrifuged for 45 minutes. It was then brushed onto the substrate. The polymer solution was then allowed to evaporate in oven overnight at 60 °C.

### 3.7.2. Electrohydrodynamic spray deposition

In a typical electrohydrodynamic spraying process (Figure 3.3), the equipment used consists of a stainless-steel needle with an orifice diameter of 330 μm held in resin and connected to the positive terminal of the high voltage power supply (Glassman Europe Ltd., Tadley, UK) capable of applying an electric field between the needle and grounded plate electrode. Polymer solution was released to the needle through a silicone rubber tube by an infusion pump (Harvard, Apparatus Ltd., Edenbridge, UK). A jet was ejected from the surface of the charged polymer solution when the applied electric field strength overcomes the surface tension. A microscope lens in conjunction with a high-speed camera, which was connected to a computer, was used to observe the jet move toward the substrate and capture images. The jet breaks up into charged droplets which were collected on the stainless steel substrate located at a distance of 25 mm from the needle exit and fixed to a rotating plate (Pareta & Edirisinghe 2006).

Electrohydrodynamic spraying (EHDA) of POSS-PCU2 solution on a stainless steel substrate was investigated over a wide applied voltage-flow rate parametric space and in order to study the effect of varying the polymer concentration in the solution and

the electrospraying time studied. Modes of spraying of the polymer solutions were established for 20 wt%, 15 wt% and 10 wt% polymer concentration solutions. A sample of the 15 wt% polymer solution was subjected to EHDA at 5.8 kV and 4 µl/s in the stable cone-jet mode. The films produced with the above mentioned set up were collected after 1, 2 and 3 hours, to study the effect of electrospraying time on the film thickness. The films were kept overnight in an oven held at 60°C to let the solvent present in the film to evaporate.

### 3.7.3. Ultrasonic atomization spraying

The POSS-PCU2 nanocomposite coating was applied using an ultrasonic atomising spray (MicroMist™, Sono-Tek Co. Ltd., Milton, NY) as shown in Figure 3.4. A MicroSpray nozzle is used in the set up of this study with the orifice size of about 0.5 mm. This orifice size is usually recommended for use in applications where flow rates are very low and narrow spray patterns are needed as required with current application.

The spray solutions were prepared by dissolving POSS-PCU2 in more DMAC. The liquid ejected from the micro-syringe was atomized and focused by ultrasonic atomization spraying equipment, and then the focused liquid beam was sprayed onto the surface of NiTi strips. The strip was kept rotating and moving during the spraying process to get a homogeneous coating. Adjucement of the nitrogen level and voltage applied allowed ultrasonic atomization spraying of the polymer, provided an even spray of polymer. Power is controlled by adjusting the output level on the power supply. The heater was used to evaporate the solvent on contact with the sample, leaving a polymer layer.

#### 3.7.3.1. Parameter optimisation

POSS-PCU2 films were prepared by spraying in the arrangement described above under certain conditions. The parameters varied were: polymer flow rate, voltage applied, time sprayed, temperature, distance from spray nozzle, polymer concentration, gas flow rate and drying conditions. These parameters were changed in accordance with the Taguchi method (Taguchi 1986). The Taguchi method for parameter optimisation allows the effect of multiple parameters on a performance characteristic to be assessed in a condensed set of experiments. This will be further discussed in chapter 5.

## 3.8. Surface treatment of NiTi

Surface treatment is used to promote bond strength between the POSS-PCU2 nanocomposite and the surface of NiTi strips. This protocol was done in different steps.

### 3.8.1. Surface roughening

Rectangular NiTi samples (50 mm × 5 mm) were cut from 0.5 mm thick strips of the material. An oxide layer already exists on the alloy surface as a result of the manufacturing process. Sand blaster at a working distance of 200 mm was used to remove most of the existing oxide layer and to produce a macroscopically rough surface.

### 3.8.2. Surface anodization

Electrochemical reactions are successfully used for degreasing, etching and oxidising metal surfaces, where the metal acts as an anode (Ramani, Weinder, & Kumar 1998).

A new electrochemical method, based on the work of Cheng et al. (Cheng, Shi, & Man 2005), was used to produce a titanium oxide ($TiO_2$) coating on NiTi that involved anodizing the Ti alloy in a methanolic electrolyte. The NiTi sample was immersed in an electrolyte prepared by dissolving 10 g of $NaNO_3$ (99.9%) in 1 litre of methanol (Sigma-Aldrich Ltd., Dorset, UK). The sample was then galvanostatically anodised at the ambient temperature (20°C) using a current density of $3\times10^{-2}$ $mA/mm^2$ for 3 hours with a pair of graphite rods as the cathode. The distance between anode NiTi and cathode was set at 20 mm for the anodisation process. The anodized samples were then left in the oven for 1 hour at 600°C. This step has been called heat treatment. The schematic view of the anodisation set up is shown in Figure 3.5.

### 3.8.3. Silanisation

3-aminopropyltriethoxysilane (γ-APS) (Sigma-Aldrich Ltd., Dorset, UK) (Figure 3.6) was applied to the surface as the coupling agent to chemically improve the adhesion between NiTi substrate and POSS-PCU2 film. It has three ethoxy groups and an amine group as an organofunctional group bound via a propyl group (-$CH_2$-$CH_2$-$CH_2$-) link to the silicon atom. Prior to immersing in the silane solution, the anodized NiTi samples were cleaned by ultrasonic vibration (Kerry Ultrasonic machine, North Yorkshire , UK) for 5 min in ethanol and then in acetone. The cleaned metals were then immersed in sodium hydroxide (NaOH) alkaline cleaner at 60°C for 15 min to make sure there were sufficient OH groups to react with alkoxy functional groups, then rinsed with distilled water and dried in air. Solutions of 2 and 5 vol% γ-APS were prepared by diluting with ethanol/deionized water (95/5 vol%). The natural pH of the γ-APS solution was ~8 and the reaction can be catalysed with $H^+$ or $OH^-$. Acetic acid was used to adjust it to pH~4. These solutions were then activated and

hydrolyzed either for 15 min or for 60 min at the ambient temperature (23°C). Concentration, pH and hydrolysis time are believed to have a significant effect on the effectiveness of the modification process (Blum et al. 1991; Tesoro & Wu 1991).

The samples were then dipped into the freshly prepared silane solution, allowed to dry in air for 15 min and then cured at 110 ºC for 20 minutes to crosslink the silane films. Thermal curing is well known to increase the crosslinking of silanes to form siloxane film on the NiTi surface. Aminosilane bonds to the oxide layer and also provides a reactive amine group for subsequent reaction of isocyanate pre-polymer coat. With the formation of chemical bonds between silane molecules and NiTi substrate, Si-O-Ti bonds are formed. The amine end of the silane molecule can polymerize with the isocyanate group of the POSS-PCU2 to form a urea group. The simplified reaction is drawn in Figure 3.7. The silanised strips were then primed with pre-polymer. Finally, the silanised NiTi strips were coated with polymer and placed in an oven overnight at 60 ºC to remove any solvent.

### 3.8.4. Energy dispersive X-ray

The chemical composition of the coating was obtained using the Energy Dispersive X-Ray (EDX) analysis system (JEOL Ltd., UK) equipped with SEM. The morphology of the interface and the thickness of the surface layer formed on the NiTi samples were determined by SEM. Topographic analysis of the modified NiTi surface was carried out by a scanning probe microscope operated in atomic force microscopy (AFM) contact mode.

### 3.8.5. X-ray photoelectron spectroscopy

The samples were analyzed by X-ray photoelectron spectroscopy on a VG Scientific ESCALAB 5 spectrometer with monochromatic Al Ka (120 W) X-ray radiation. The base pressure in the analysis chamber was better than $10^{-8}$ mbar. Survey spectra were acquired at 160 eV. High resolution scans were acquired at 40 eV pass energy to determine the chemical states and concentrations. The XPS depth profiles were obtained by using a rastered (2 $mm^2$) 4 keV Argon ions beam. The system boasts a Quartz Catalytic Cell capable of pressures up to 6 bar at 400 °C or 1 bar at 1000 $^oC$.

### 3.8.6. Peeling test

An Instron 5565 tensometer equipped with a 500 N load cell was used to measure the peel strength of the POSS-PCU2 coated NiTi strips. The coated specimens were loaded in the test machine as shown in Figure 3.8. The approach in this study is based on the ASTM D413 standard (ASTM D413 2007), which is used to determine the force per unit width required to separate a rubber layer from a flexible substrate such as fabric, fibre, wire, or sheet metal. The standard details methods for peeling the strip with the unpeeled portion held such as to give $\alpha^\circ$ separation with moving grips. The adhesion strength is equal to the mean force recorded during the test. The peeling process was initiated manually. The lower machine grip was used to clamp the NiTi strip and the upper grip held the polymer film, with an initial distance of 10 mm between the grips. The test was conducted with a crosshead displacement rate of 5 mm/min to a final extension of 40 mm. Tests were conducted on specimens subjected to the surface modification and on an unmodified strip, which acted as a control. Both electrosprayed and cast samples with the same thickness used for testing for comparison. For each type of sample, experimentation was done in triplicate.

### 3.8.7. Inductively coupled plasma mass spectrometry

Rectangular (30mm x 5mm) samples were cut from 0.5mm thick NiTi strips. The surface modified NiTi strips were then primed with pre-polymer by ultrasonic atomization spraying as discussed in detail in section 3.7.3, and finally coated with polymer using the same parameters. Plasma protein fraction I (prepared as discussed in section 3.5.1) and Dulbecco's modified Eagles' medium (DMEM) was used as the release medium to further express the Ni release characteristics of NiTi. The samples were then incubated at 37°C in 15mL conical centrifuge tubes were filled with 5mL of the plasma protein fraction I / DMEM. One NiTi sample from each group removed at 1, 24, 48 and 72 hours. The centrifuge tubes containing plasma fraction I or DMEM were then sent to the Mass Spectrometry Facility, King's College London for Inductively Coupled Plasma Mass Spectroscopy (ICP-MS) using a PerkinElmer Elan DRC+ with an AS93 autosampler. Data was managed using the PerkinElmer Elan v3.2 software. The experiments repeated three times and results averaged.

The Ni release from these samples is compared to the Ni release from unmodified NiTi strip and bare NiTi as the control.

## 3.9. Statistical data analysis

The data from each experiment obtained was plotted and analysed using GraphPad Prism 4 software (GraphPad, San Diego, CA, USA). The data are presented as means and standard deviation (n=5). Statistical analysis of tests was carried out using the one-way ANOVA test with post-hoc Bonferroni analysis.

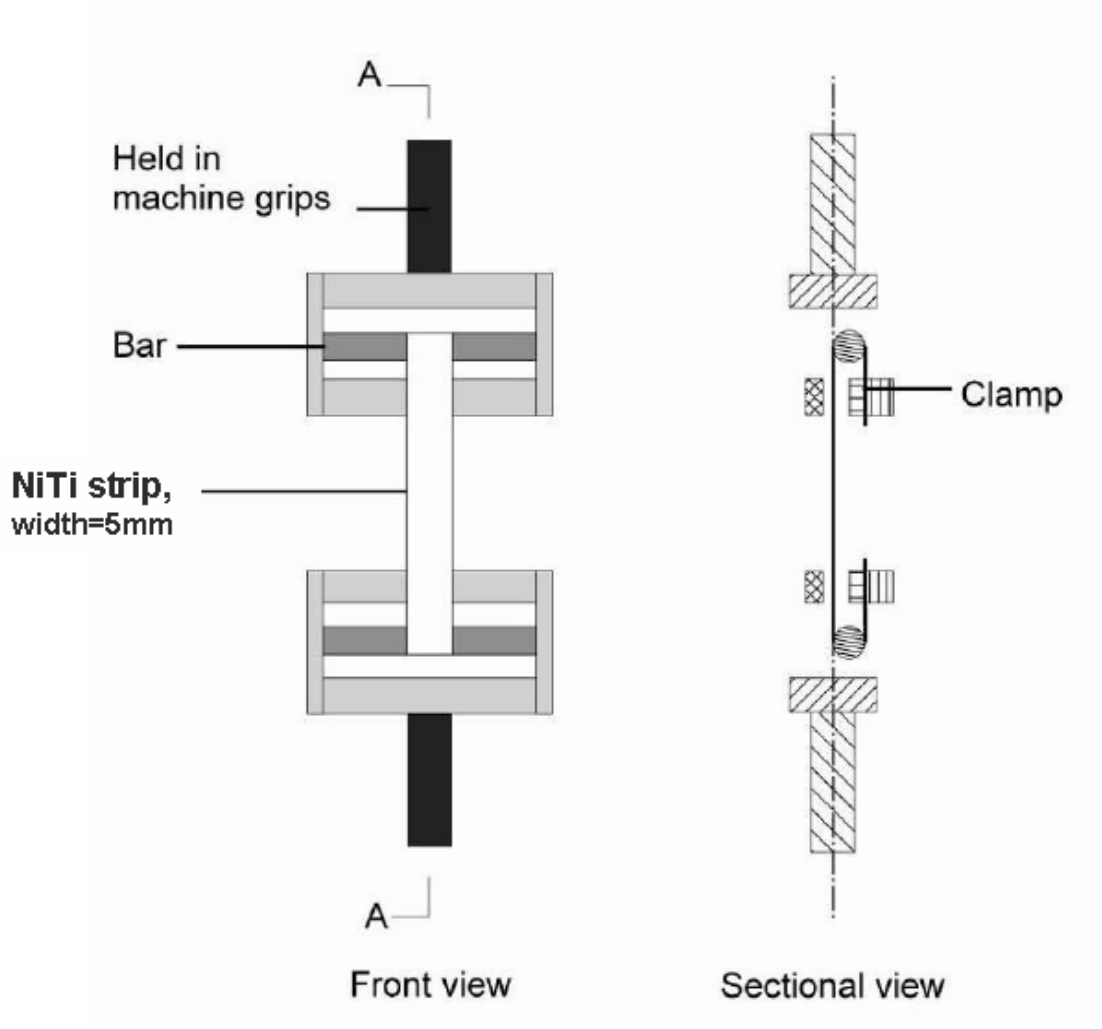


Figure 3.1. Tensile testing of NiTi strip arrangement using tensometer.

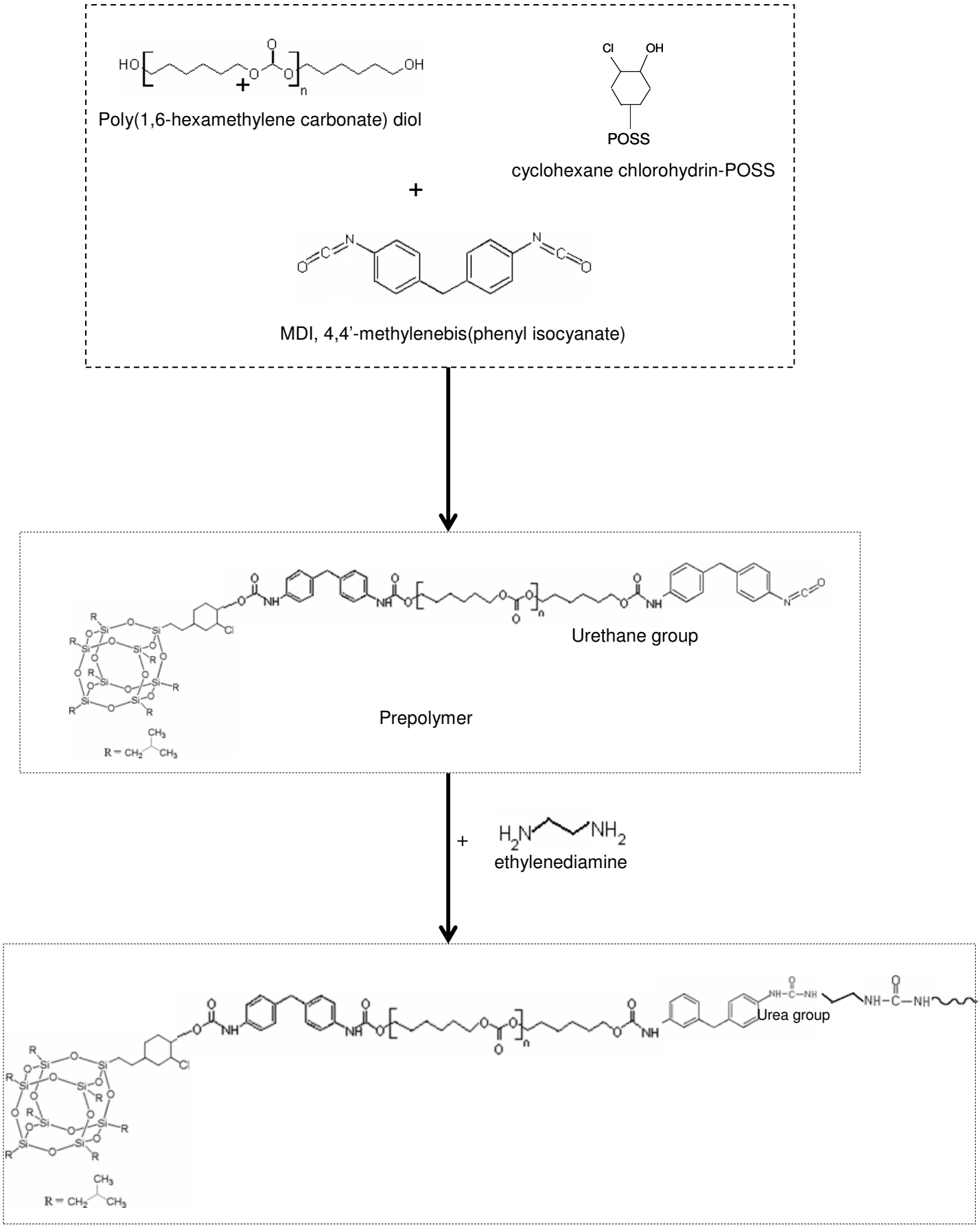


Figure 3.2. Simplified reaction scheme of nanocomposite synthesis.

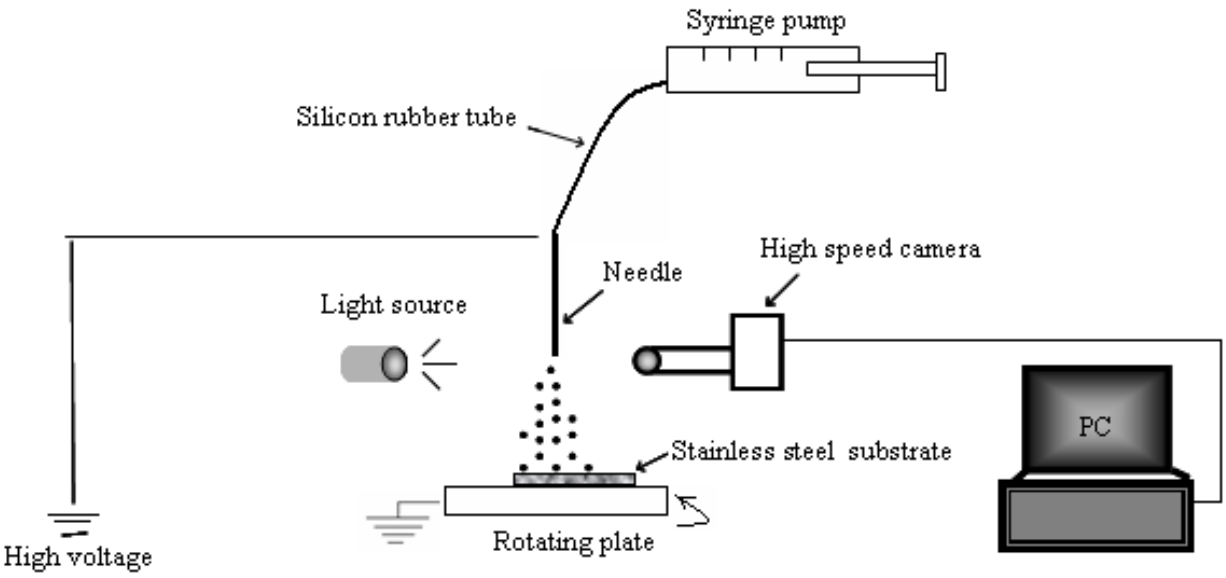


Figure 3.3. Arrangement of apparatus for electrohydrodynamic spray deposition.

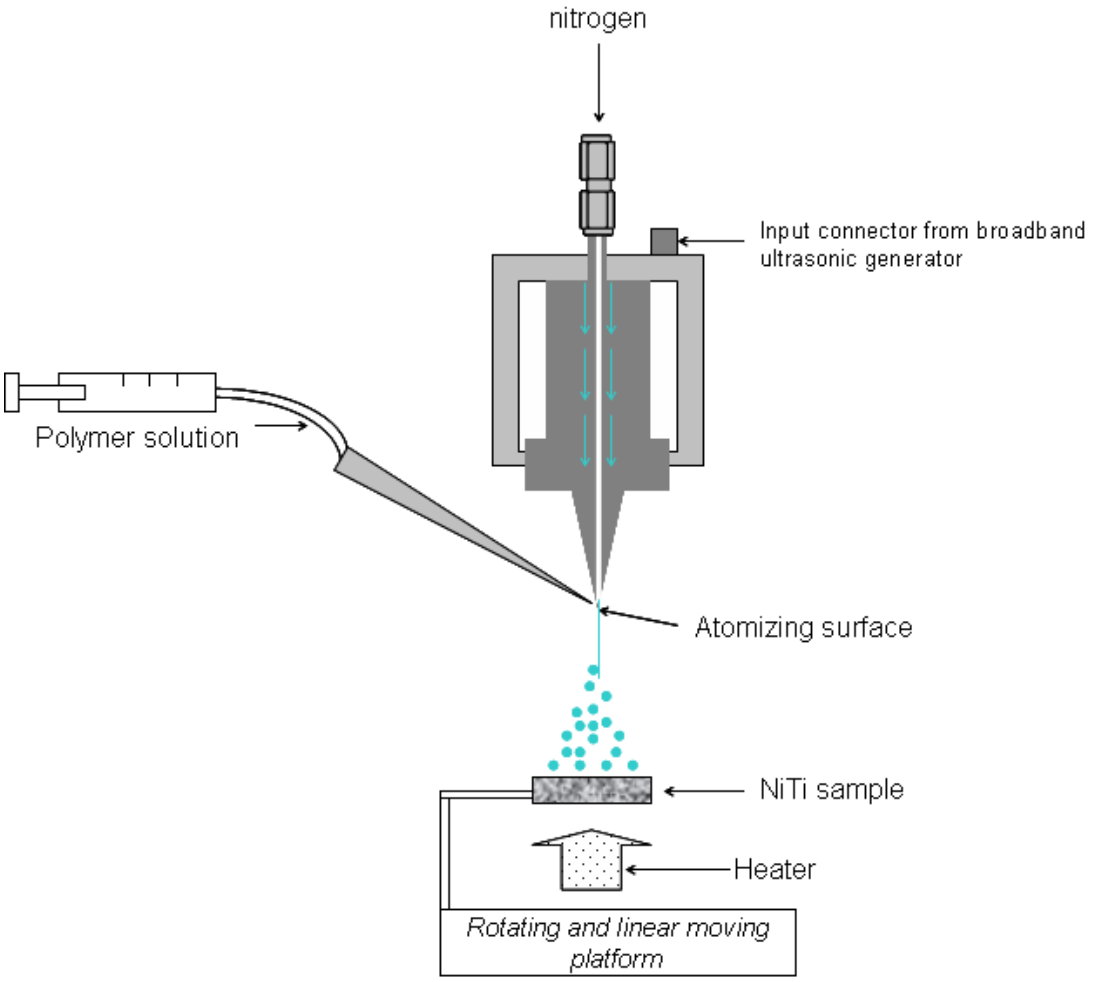


Figure 3.4. Arrangement of apparatus for ultrasonic atomization spraying.

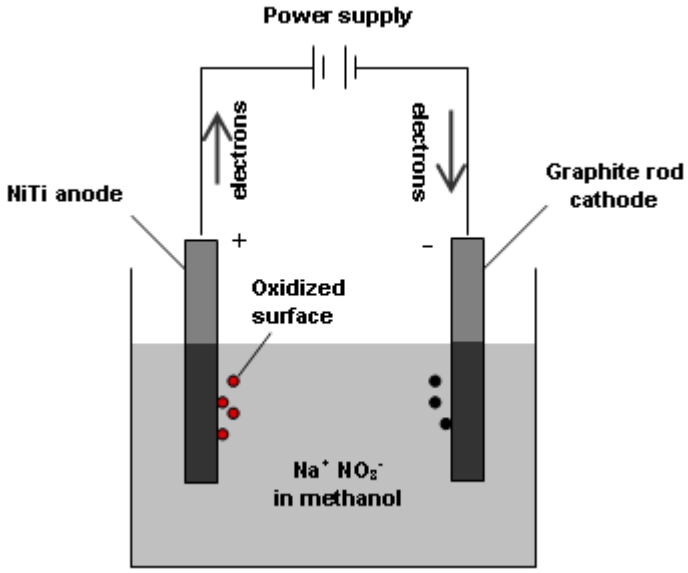


Figure 3.5. Electrochemical anodisation of NiTi alloy using sodium nitrate in methanol solution.

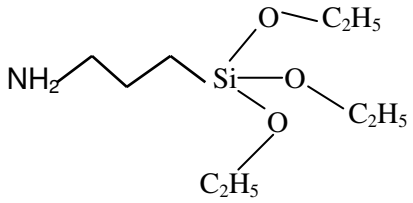


Figure 3.6. Molecular structure of 3-Aminopropyltriethoxysilane used in this study. $NH_2$ is the functional group that chemically reacts with the isocyanate.

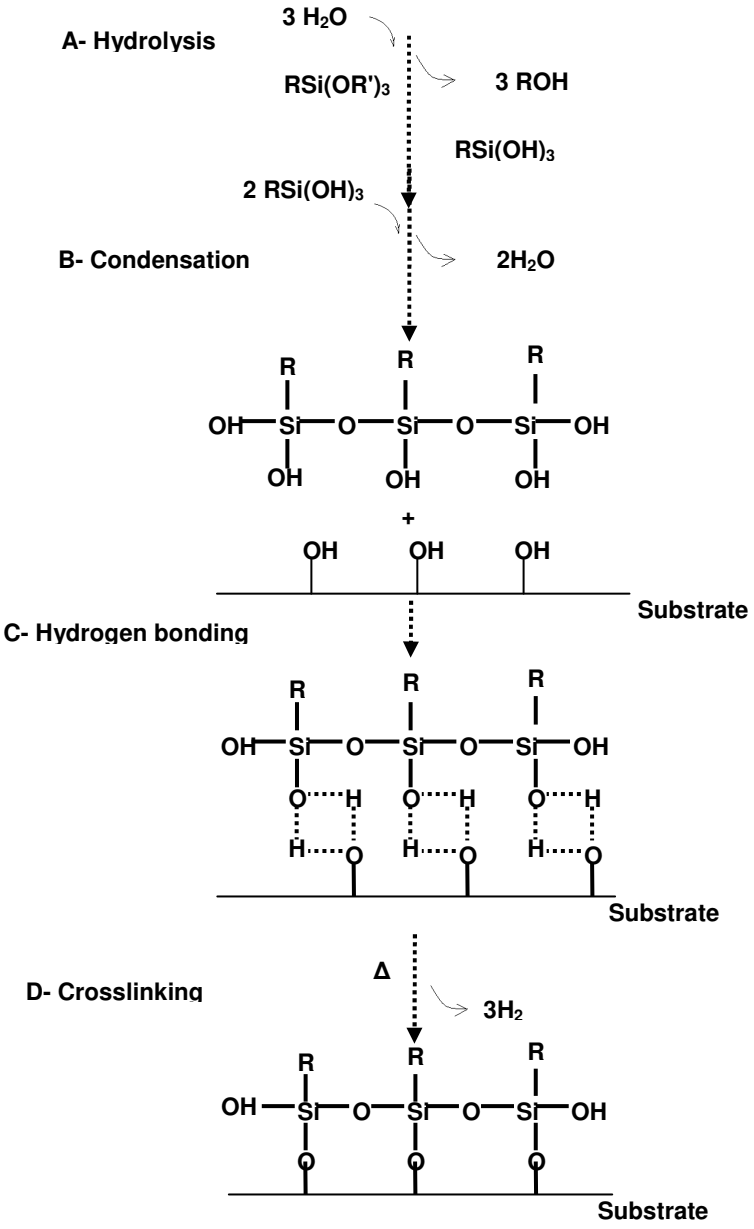


Figure 3.7. Reaction stages of organotrialkoxysilane. (A) Hydrolysis; (B) Condensation; (C) Hydrogen bonding; (D) Crosslinking.

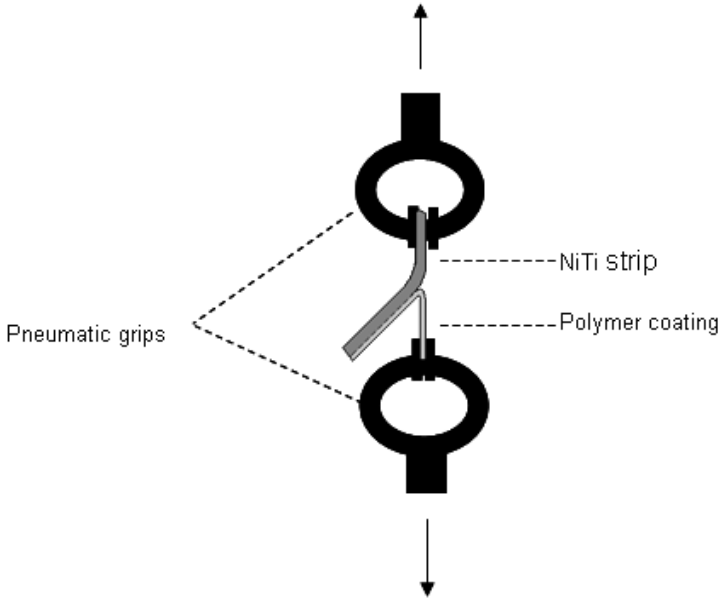


Figure 3.8. Peel test arrangement. Arrows show the moving directions of the grips.

# CHAPTER 4. Characterization of Synthesized POSS-PCU Nanocomposites

A novel range of poly(carbonate-urea)urethane nanocomposites were synthesised in our department with different levels of polyhedral oligomeric silsesquioxane (POSS) covalently bonded to poly(carbonate-urea)urethane (PCU) (Salacinski, H. J. 2005). In this study, the focus was on the improvement of the surface properties of a polymeric thin film by utilizing the inherent characteristic of POSS. A novel polyurethane system with the hard segments being molecularly modified by nanostructured molecules-POSS synthesized and characterized. The bulk properties of POSS-PCU nanocomposites were characterized by differential scanning calorimetry, gel permeation chromatography, rheometry and tensile property measurement. The surface properties of POSS-PCU was characterized by attenuated total reflectance-Fourier transform infrared spectroscopy, contact angle, atomic force microscopy, ζ-potential. This investigation forms the backbone of the research reported out in chapter 5.

## 4.1. Initial observation

As mentioned in experimental details (chapter 3), POSS-PCU nanocomposite polymers with different concentrations of POSS were synthesized. These hybrid polymers contained 0, 2, 4 and 8 wt% POSS. These nanocomposites were named PCU, POSS-PCU2, POSS-PCU4 and POSS-PCU8, respectively. The prepared PCU cast films were transparent. The POSS-PCU2 cast films containing 2% POSS are still homogeneous and transparent. The products were not homogeneous and clear with

increasing POSS, suggesting that macroscopic phase separation occurred at the scale exceeding the wavelength of visible light. POSS-PCU8 cast films containing 8% POSS were opaque. It has been previously shown that the POSS molecules also enhance the micro-phase separation between the hard and soft segments (Hsiao et al. 2000a).

## 4.2. Bulk properties of POSS-PCU

### 4.2.1. Molecular weight distribution

GPC analysis revealed thst POSS-PCU possessed a higher number average molecular weights with lower polydispersity indices of POSS-PCU as compared to the PCU. Figure 4.1 shows an overlay of the computed molecular weight distributions for POSS-PCU nanocomposites. These molecular weight distribution plots are to the same area, the y-axis being a function of weight fraction. Mn increases with increasing POSS concentration. The Mw/Mn decreases with increasing POSS concentration reaching 2.2 at 8 wt% concentration. POSS-PCU with 4 and 8 wt% POSS showed the lowest polydispersity. Chromatogram peak areas are also somewhat variable for the different samples. The POSS-PCU4 having the highest chromatogram area, PCU has the lowest areas with POSS-PCU8 being high but variable. A summary of the results obtained by GPC is given in Table 4.1.

In a study by Lacono et al. (Lacono et al. 2007) a higher POSS concentration produced high polydispersity. The high polydispersity may be likely due to the decreasing mobility of growing POSS aryl ether polymer chains causing a higher incidence of chain length fractionation**.**

Table 4.1. Selected properties of POSS-PCU hybrid nanocomposites compared with control PCU based on GPC results.

| Sample | $M_w$ | $M_n$ | Polydispersity |
|---|---|---|---|
| PCU | 77600 | 32300 | 2.5 |
| POSS-PCU2 | 107500 | 43650 | 2.5 |
| POSS-PCU4 | 91250 | 46000 | 2 |
| POSS-PCU8 | 102700 | 47000 | 2.2 |

### 4.2.2. Mechanical behaviour

The stress–strain curves of POSS-based poly(carbonate-urea)urethanes are shown in Figure 4.2. The reference PCU has been used for comparison. The maximum attainable strain of the reference PCU was about 878%. The maximum applied strains for POSS-PCU2, POSS-PCU4 and POSS-PCU8 were about 867%, 1044% and 839%, respectively. In Figure 4.2, the increase of the POSS concentration generally results in a higher modulus and a lower maximum elongation ratio.

The tensile properties of segmented polyurethane depend upon the chemical structure, the copolymer composition, and the microphase morphology (Fu et al. 2001). The obtained tensile results indicate that all of the POSS-containing hybrid polyurethanes behave like elastomeric materials. The reasons for higher modulus and a lower maximum elongation ratio with increase of the POSS concentration have been described as follows (Fu et al. 2000). First, the attachment of the rigid POSS molecules in the hard segments probably enhances the stiffness of the modified domains at the molecular level. Second, if the POSS molecules can crystallize in the hard segments, the modulus may be further increased. Finally, as some hard segments containing POSS molecules are dispersed in the polymer matrix at the molecular level, this can improve the overall modulus of the soft segment dominant matrix. The

increased cross-link density could be responsible for the decrease in the elongation at break of the materials. In a way, the POSS molecules can be considered as a compatiblizer between the hard and soft segments, which improves the miscibility between the two segments.

In comparison of the results obtained for cyclohexane chlorohydrine-POSS-polyurethane with other studies, the POSS-containing nanocomposites exhibited an increased Young's modulus and lower elongation at break with increasing Octa(propylglycidyl ether) POSS content than the control polyurethane networks (Liu et al. 2006). This increase has been interpreted on the basis of two factors: i) the nano-reinforcement of POSS cages on the polymeric matrices, and ii) the increase in cross-link density of the networks. The nano-reinforcement effect of POSS has also been reported by Fu et al. (Hsiao et al. 2000b). Inorganic POSS molecules in their hard segments of polyurethane act as nano-scale reinforcing agents. The methylsiloxy mono-functionalized POSS molecules appear to form nano-scale crystals in the hard segment domains of PU.

Fu et al. (Fu et al. 2001) found that a significant mechanical improvement was achieved by incorporating POSS molecules in PU. They also observed that the maximum attainable strain of POSS-PU was significantly higher than that of the reference polyurethane sample. They explained this observation based on the interpretation of the stress-strain behaviour in typical segmented polyurethane provided by Cella (Cella R.J. 1973) and Witsiepe (Witsiepe W.K. 1973). The hypothesis is that the initial extension may be attributed to the reversible deformation of the crystalline (hard) domains (probably 0–50% in POSS-PU-34 containing POSS

34 wt %). At strains of 50–150% in POSS-PU-34, a partly reversible reorientation of hard domains probably occurs. At higher strains, the stress is transmitted primarily through the amorphous soft segment phase.

### 4.2.3. Crystallinity

Thermal analysis has been carried out on POSS-PCU nanocomposites. DSC scans of the polyurethanes containing POSS (POSS-PCU) are illustrated in Figure 4.3. DSC analysis of samples detected the glass transition of the soft segment and the higher temperature melting thermal transition of the hard phase. Values are reported in Table 4.2. The glass transition temperature ($T_g$) gives information on the amorphous segment of the nanocomposite while the heat capacity changes ($\Delta C_p$) at the $T_g$ is a measure of the inter-molecular interaction between these molecules during this transition. In the PCU samples, a mean $T_g$ of -29 °C and a mean $\Delta C_p$ value of 0.40 J/gK was observed.

By increasing the POSS fraction in the polymer, the $T_g$ was slightly shifted at lower temperatures (Figure 4.3A) but the difeference is not significant. DSC analysis showed only minimal changes in $T_g$ for POSS nanocomposites in comparison to reference PCU. It should be noted that the control PCU and the POSS-PCU nanocomposites displayed a glass transition in the range of -29.80 to -31.79 °C; therefore, the organic-inorganic network is a typical elastomer. DSC revealed a plasticizing effect demonstrated by slightly lowered $T_g$ upon increased weight percent incorporation of POSS. The $T_g$ of the remaining hard segments was about constant despite different POSS concentrations (around 120 °C) but it appearsed as a strong transition at 8 wt% POSS concentration; which may be related to the phase separation

between the hard and soft segments within the nanocomposite (Figure 4.3B). This can describe the cloudy feature of the POSS-PCU8 films. The $T_m$ of the hard segment shifted to higher temperatures in comparison to reference the PCU, with a 12°C increase in the melting transition temperature of the hard segment for POSS-PCU8 (Table 4.2). The increase in $T_m$ of the hard segment is attributable to the increased nano-scale interactions between its constituents thus binding together the POSS-PCU nanocomposites.

Table 4.2. DSC melting temperatures and glass transition temperatures of POSS-PCU hybrid nanocomposites compared with control PCU.

| Sample | $T_g$ (°C) | $T_m$ (°C) | $C_p$ (J/gK) |
|---|---|---|---|
| PCU | -29.8 ± 0.1 | 279.7 ± 0.1 | 0.0121 |
| POSS-PCU2 | -30.4 ± 0.1 | 281.1 ± 0.1 | 0.0144 |
| POSS-PCU4 | -30.8 ± 0.1 | 286.5 ± 0.1 | 0.0203 |
| POSS-PCU8 | -31.7 ± 0.1 | 291.7 ± 0.1 | 0.0285 |

The plasticizing effect demonstrated by POSS was confirmed by lowered $T_g$ as previously reported (Iacono et al. 2007; et al 2009). The resulting drop in $T_g$ in the study by Lacono is due to the incorporation of POSS and caused by a higher fraction of lower molecular weight chains observed by increased polydispersity (Lacono et al. 2007). This is also consistent with the published literature reporting a very small effect of cores/filler molecules on $T_g$ in microcomposites. This observation may be explained by the fact that nano-cores prevent close packaging of polymer chains due to thermal rearranging which in turn results in an increase in dynamic voids within the polymer (Merkel et al. 2002a). This extra space allows for earlier segmental mobility of the polymer chain and therefore lowering the $T_g$ (Kannan et al. 2006a).

In other POSS-PU structures, however, a slight increase in $T_g$ is observed with increase in POSS concentration (Fu et al. 2000; Xu et al. 2002a; Xu et al. 2004) and interpreted as a consequence of cohesive interactions like hydrogen bonding between the siloxane cage and polar groups in the macromolecular chain. Fu et al. (Fu et al. 2000) also observed a slight increase in $T_g$ of the soft segment phase with an increase of the POSS concentration, which suggests that some hard segments along with POSS molecules may have been dispersed in the soft segment phase. This can be attributed to two causes, (i) weakening of hydrogen bonding among the hard segments in the microphase domain when the POSS molecules are incorporated into the hard segments, (ii) the POSS molecules act as compatiblizer between the soft and the hard segments, which causes an increase of the molecular restraints in the soft segments. The melting temperatures of soft segment crystals remain about constant; however, the melting point of the soft segment cannot be identified at high POSS concentrations.

This suggests that the incorporation of POSS molecules has retarded the crystallizability of soft segments, which is consistent with the notion that the miscibility between the hard and soft segments is increased by the inclusion of POSS. In other words, the incorporation of POSS molecules has weakened the interactions between the hard segments, allowing them to be dispersed more readily in the soft segment matrix (Fu et al. 2000). In the study by Liu Y. et al. (Liu et al. 2006), the hybrid nanocomposites showed an enhanced $T_g$, which increased with increasing POSS content. In POSS-containing hybrid nanocomposites, the increase in the glass transition temperature is generally interpreted on the basis of nano-reinforcement of the POSS cages in the polymer matrices, which is able to restrict the motions of the

macromolecular chains (Liu et al. 2006). In their case, the $T_g$ enhancement is not only ascribed to the nano-reinforcement of the POSS cage but also attributed to additional cross-linking between the polyurethane (PU) networks and octa(propylglycidyl ether) polyhedral oligomeric silsesquioxane.

### 4.2.4. Rheological behaviour

Figure 4.4 shows the apparent viscosity (η) versus the shear rate of the PCU with 0, 2, 4 and 8 wt% POSS. Viscosity was somewhat lower for the POSS-containing structures. POSS content has shown the same effect on the rheology of polyurethanes. It has been shown that η is somewhat lower for the POSS-containing structures (Turri et al. 2005). These results are related to lower molecular weight or to an effect of composition on Mark-Houwink parameters in polyurethanes containing POSS (Turri et al. 2005). In the study by Zheng et al. (Zhang et al. 2006), pure polyester displayed Newtonian flow behaviour, but all the resins with POSS gave shear thinning first, and as more the POSS was embedded, the shear thinning behaviour became stronger, and the viscosity increased. This can be attributed to the physical and chemical interactions between the rigid and dimensionally-large POSS cube with polyester chains.

## 4.3. Surface properties of POSS-PCU

Predictions about the interactions between biomaterial surface and adsorbed proteins can only be formulated by having an exact knowledge of the structure of the biomaterial's surface. Interaction between biological environment and foreign body material is most likely dominated by surface properties including; chemical structure of the surface, electrical properties e.g. kind and content of specific charged or polar

functional groups, hydrophilic/hydrophobic character, surface free energy, the morphology, i.e. the domain structure of a multi-component system such as crystalline and amorphous domains and the topography, i.e. the surface roughness, surface contamination of a polymer (Aiping & Tian 2006b; Altankov et al. 2003; Khorasani et al. 2006; Khorasani & Mirzadeh 2007; Klee & Hocker 1999; Safinia et al. 2005).

### 4.3.1. Surface morphology

Figure 4.5 shows the phase contrast representative AFM images of the POSS–PCU. In terms of the volume fraction of POSS and the difference in viscoelastic properties between the PCU matrix and the POSS phases. The dark continuous regions are assignable to the PCU chains of the organic–inorganic nanocomposite whilst the light regions are attributed to POSS domains (Zeng et al. 2009). It is seen that all the nanocomposites exhibited microphase-separated morphologies. For the nanocomposite containing 4 wt% of POSS, the nano-scaled POSS spherical particles with the size of 10 nm and POSS agglomerates were homogenously dispersed in the continuous PCU matrix. With increasing POSS content, some interconnected POSS microdomains began to appear (Figure 4.5D) and the quantity of the POSS microdomains was increased whereas the size of the spherical particles remained almost invariant.

### 4.3.2. Surface charge

It is obvious, that the ζ-potential of the pure PCU membrane is in the negative range only at strongly basic pH-values. If POSS is incorporated into the PCU polymer, then ζ- potentials become less positive with increasing content of POSS (Figure 4.6). The values of the points of zero charge (PZC) are listed in Table 4.3, which are estimated

from Figure 4.6. It is obvious that the ζ-potential of the pure PCU films were in the negative range if the pH value was basic. Addition of 2% POSS led only to very moderate decrease of ζ- potential curves. It is interesting to note that for both polymer films the ζ- potential was positive over a wide range up to a pH of 8.5. However, if the POSS content was further increased to 4% POSS is caused a remarkable drop of the ζ- potential. The further addition of POSS during the copolymerization process led to materials that decreased the ζ- potential to more negative values. It is remarkable to note that a POSS content of 8% generated ζ- potentials, which were negative over a wide range of pH values (pH > 4.5). These changes in the surface potential of materials as a result of the different POSS composition were also well reflected when the points of zero charge were considered. It is obvious that large changes occurred if the POSS concentration became greater than 2%. Under the pH conditions of the body, the nanocomposites containing 4 and 8 wt% POSS have negative charge while the PCU and POSS-PCU2 are positively charged.

Table 4.3. Point of zero charge (PZC) as a function of POSS content as derived from ζ-potential measurements.

| Sample | PZC ( equal to pH-value at 0 m*V*) |
|---|---|
| PCU | 8.8 |
| POSS-PCU2 | 8.5 |
| POSS-PCU4 | 7.4 |
| POSS-PCU8 | 4.5 |

Electrical properties of solid surfaces, e. g., surface charge or zeta potential may has a strong influence on protein adsorption and blood compatibility by affecting thrombogenic events at blood-polymer interface (Norde & Rouwendal 1990). The compatibility of blood with surfaces has been associated chiefly with ionic charges

based on the observation that endothelial wall, the platelets and the plasma proteins carry net anionic charges in normal physiological conditions (Bruck 1973; Klee et al. 1996). Surface charge of the polymer surface interferes with adhesion of cells. Ions present on material surfaces may interact with cell receptors to cause cell adhesion and growth, and to facilitate cell proliferation, leading to the foreign body reaction (Khorasani & Mirzadeh 2007). Blood compatibility data on polymer electrets shows that negatively charged surfaces have less of a tendency for thrombosis than positively charged ones because of electrostatic repulsion between polymer and blood components (Aiping & Tian 2006a;Murphy et al. 1970). The natural blood vessel wall has a negative ζ potential of -8 to -13 mV (Klee & Hocker 1999).

### 4.3.3. Hydrophobicity/ hydrophilicity

Contact angle measurement provides insight into the hydrophobicity as well as the surface energy of the film. The hydrophobicity of the POSS-PCU films was tested using water drop shape analysis and measured for the corresponding contact angle (θ). Surfaces with water contact angle < 90° are considered wetting whereas those with water contact angle > 90° are considered non-wetting (Wapner & Hoffman 2000). When a liquid drop is placed on a flat and smooth surface, it spreads over the surface until the mechanical and thermodynamic forces are balanced. The contact angles increased with increasing POSS content in POSS-PCU nanocomposites (Figure 4.7). It is generally agreed that the measurement of contact angle on a given solid surface is the most practical way to obtain surface energies (Wu & Nancollas 1999). The relationship of contact angle and surface energy is governed by Young's equation (Wu 1971).

$$\gamma_s = \gamma_{sl} + \gamma_l \cos\theta \quad 4.1$$

Where $\theta$ is the contact angle, $\gamma$ is the surface free energy, $\gamma_l$ is the experimentally determined surface energy (surface tension) of the liquid, $\gamma_s$ is the surface energy of the solid and $\gamma_{sl}$ is the interfacial tension between the tested solid and the probe liquid. Among the various possible thermodynamic approaches to determine $\gamma_s$ and $\gamma_{sl}$, the equation of state for solid–liquid interfacial tension has been selected for this study (Gindl et al. 2001):

$$\gamma_{sl} = \gamma_l + \gamma_s - 2\sqrt{\gamma_l \gamma_s}\, e^{-\beta(\gamma_l - \gamma_s)^2} \quad 4.2$$

Where $\beta$ is an empirical constant with an average value of $1.057\times10^{-4}$ $[(m^2\ mJ^{-1})^2]$. In combination with the Young equation, the equation of state enables the evaluation of the surface free energy of a solid ($\gamma_s$) from a single measurement of contact angle in a liquid with a known surface tension ($\gamma_l$). The surface tensions of each probe liquid are given in Table 4.4.

Table 4.4. Surface tensions of four probe liquids.

| Probe fluid | $\gamma_{l\ (mN/m)}$ | $\gamma^d_{l\ (mN/m)}$ | $\gamma^p_{l\ (mN/m)}$ |
|---|---|---|---|
| Water | 72.8 | 21.8 | 51.0 |
| Diiodomethane | 50.8 | 48.5 | 2.3 |
| Ethylene glycol | 47.7 | 29 | 19 |
| Formamide | 58.2 | 36 | 22.2 |

The results of contact angle for the POSS-PCU-coated glass slides subjected to measurements with water, diiodomethane, ethylene glycol and formamide as probe liquids are shown in Table 4.5. It appears that upon adding POSS to the system the contact angle was dramatically increased in the case of all liquids and increased with

increasing POSS content. The highest increase in water repellency was 12.7% for 8 wt % POSS with an average contact angle of 113.7° (as compared to PCU with average of 82.9°). Advancing contact angle results are very reproducible. Contact angle results shown in Table 4.5 indicate that incorporation of even a small amount of silsesquioxane strongly enhances the hydrophobicity of the surface.

Calculations for surface tension are reported in Table 4.6. The incorporation of even a small amount of POSS molecule strongly enhances the contact angles of the coated surface against all liquids. It appears that the total surface energy of polyurethanes is in any case reduced by half. The surface free energy decreased from ~ 35.1 $mNm^{-1}$ for pure PCU to as low as ~17.6 $mNm^{-1}$ when 8 % POSS was used in the polymer. The result is changed very fast in 2% POSS-modified sample, and does not significantly improve in the 2–8% POSS range.

In some studies, the surface free energies of the hybrid nanocomposites containing various percentages of POSS were calculated according to the geometric mean model (Kaelble & Uy 1970) or by the Owens–Wendt method (Owens & Wendt 1969). In this study, the calculation is based on the equation of state. Total surface free energy of POSS-containing PCU was reduced compared with pure PCU. In particular, it has been shown that the polar component is very sensitive to the presence of even a very small amount of POSS, suggesting that the inclusion of POSS moiety significantly changed the distribution of the polar groups (the urethane moieties) on the surface energy of materials; that is the POSS moiety on the surface acts as a screening agent to the polar groups of PCU (Koh et al. 2005; Liu et al. 2006). This would mean the POSS nanostructures screen the polar groups like urethanes or carboxyls and are

preferentially oriented on exposure to air (Turri et al. 2005). This value of surface free energy of all POSS-PCU (17.6-21.9 mN/m) is less than the surface free energy (~ 32.5 mN/m) of a glass slide treated with the silane coupling agent (3,3,3-trifluoropropyl)trimethoxysilane) (Koh et al. 2005). It is approaching reported values of 16 mN/m surface energy and 120° contact angle for Teflon which is a biocompatible hydrophobic materials for vascular applications.

Table 4.5. Advancing ($\theta_a$) and receding ($\theta_r$) contact angles, and hysteresis of POSS-PCU compared with control PCU. Inset: advancing and receding contact angle were measured in different probe liquids; (W) water, (D) diiodemethane, (EG) ethylene glycol and (F) formamide. (×=not available)

| Sample | $\theta_a$ | | | | $\theta_r$ | | | |
|---|---|---|---|---|---|---|---|---|
| | W | D | EG | F | W | D | EG | F |
| PCU | 82.9 | 28.1 | 67.6 | 61.7 | × | | 14.0 | × |
| POSS-PCU2 | 110.1 | 54.7 | 88.4 | 90.6 | 73.9 | 12.8 | 49.3 | 60.5 |
| POSS-PCU4 | 113.2 | 71.8 | 93.7 | 96.9 | × | × | 24.0 | × |
| POSS-PCU8 | 113.7 | 74.5 | 94.2 | 96.4 | 49.9 | 10.3 | 31.5 | 24.2 |

Table 4.6. Surface tension of POSS-PCU against PCU.

| Sample | $\gamma_s$ (mN/m) |
|---|---|
| PCU | 35.1 ± 8.1 |
| POSS-PCU2 | 21.9 ± 8.3 |
| POSS-PCU4 | 17.6 ± 4.6 |
| POSS-PCU8 | 17.6 ± 4.7 |

Increased hydrophobicity of some hybrid polymer surfaces with incorporation of POSS has also been reported in other studies (Hirao et al. 2002; Li et al. 2002; Muisener et al. 2003); (Koh et al. 2005; Li et al. 2002; Turri et al. 2005; Zeng et al. 2009) including polyurethane-based nanocomposites (Zhang et al. 2006). The

obtained findings are consistent with previously reported studies showing increased surface hydrophobicity for other POSS/polymer systems and POSS molecules with fluorinated alkyl chains attached to the POSS cage (Misra et al. 2007), PMMA blended with fluorinated POSS-terminated polymers (Koh et al. 2005), other monofunctionalized POSS-containing linear polymer systems (Liu et al. 2006, Mabry et al. 2008) or diol-functionalized POSS (Turri & Levi 2005) and octa (propylglycidyl ether)-functionalized POSS (Liu et al. 2006). The POSS moiety of the organic–inorganic hybrid which contains organosilicon and organofluorine moieties is of low free energy (Koh et al. 2005; Li et al. 2002). Surface modification as a function of POSS nano-particle concentration was also observed in contact angle studies (Misra et al. 2007; Mu et al. 2007).

Advancing/receding hysteresis is influenced by many factors such as the surface roughness, chemical heterogeneity of the surface, presence of low molecular weight species, molecular orientation, rearrangements of functional groups, changes in morphology (Morra et al. 1990; Muller et al. 2001). In a multiphase system advancing contact angle is more sensitive to the low surface energy or hydrophobic domains whereas receding contact angle is more sensitive to the high surface energy or hydrophilic domains (Schwartz & Garoff 1985; Turri & Levi 2005). POSS modification enhances both advancing angles and hysteresis. Moreover, the surfaces show different kinetic wettability behaviour, since the POSS-modified polyurethanes show a progressive increase of the hysteresis. The kinetic effects with the wetting cycles are a consequence of modifications occurring at the liquid–solid interface, evolving toward a more favourable energetic state.

Increase in the water contact angle and decrease in surface energy demonstrate the hydrophobic nature of the POSS-PCU nanocomposite surface. This has been explained partially by Misra et al. (Misra et al. 2007) using the cumulative effect of the eight hydrophobic isobutyl groups attached to the corner silicon atoms of the POSS cage. The effect is pronounced because of the higher concentration of POSS moieties on the film surface. This study attributes the increased hysteresis in the POSS containing systems to the low surface energy characteristic of POSS, which promotes its migration towards the surface, explains the hysteresis behaviour exhibited by POSS-PCU nanocomposites (Misra et al. 2007)**.** In the study by Liu Y. et al.(Liu et al. 2006), X-Ray photoelectron spectroscopy analysis revealed that the concentration of elemental Si on the surface of the hybrid composites was significantly higher than the theoretical values calculated in terms of the feed ratios. This observation suggests that an enrichment of Si-containing moiety on the surfaces exist (Koh et al. 2005;Wen et al. 1997). This result is important in understanding the improvements in surface hydrophobicity for the POSS-modified polyurethane composites.

Increase in the water contact angle and decrease in surface energy demonstrate the hydrophobic nature of the POSS-PCU nanocomposite surface which is in favour of polymer blood compatibility. This can be attributed to the low surface energy characteristic of POSS, which promotes its migration towards the surface and explains the hysteresis behaviour exhibited by POSS-PCU nanocomposites (Misra et al. 2007). The reason why incorporation of POSS decreased the surface free energy can probably be related to the surface-oriented enrichment of POSS structures bearing low-surface-tension substituents (Misra et al. 2007;Turri & Levi 2005).

Based on the previous studies, non-wettable materials have less of a tendency for thrombosis (Sharp & Taylor 1971). Biomaterial surfaces with very low polar surface energies or high dispersive surface energies favour blood compatibility. The results show that the best blood compatibility is obtained for a ratio of the dispersive and polar surface tension of nearly 12 (Klee et al. 1996).

Surface energy is one of the most influential factors on protein adsorption. Smaller interfacial energies between blood and the polymer surface imply better blood compatibility (Klee & Hocker 1999). It has been suggested that a hemocompatible surface should have a surface energy in the range of 20-25 mN/m (Gogolewski 1989).

The surface roughness as well as the chemical heterogeneity imparted by the enrichment of POSS nano-particles on the PCU surface is the other factor which may increase the hysteresis of the system. These characteristics are studied in the next section.

## 4.3.4. Surface topography

### 4.3.4.1. Surface chemical mapping

ATR-FTIR analysis provided further evidence of POSS surface enrichment. The incorporation of POSS into the PCU matrix was confirmed by spectroscopic analysis. Figure 4.8 illustrates the typical ATR-FTIR spectrum of reference PCU, and POSS-PCU hybrid nanocomposites. The control PCU showed typical wavelengths at 1736 $cm^{-1}$ indicative of the carbonyl segments of carbonate (–NHCO–;C=O), the 1512 $cm^{-1}$ wavelength is indicative of urethane carbonyl groups (–NHCOO–) and bonds in the 1240–1250 $cm^{-1}$ range show the presence of the C–O–C bonds of the CO–O–C

segments (Kannan et al. 2006b). The broad absorption band with the maximum near 3300 $cm^{-1}$ is typical for stretching vibrations of OH and N–H groups of PU (Bliznyuk et al. 2008). For the control PU, the stretching vibrations of the N-H groups occur at 3300 $cm^{-1}$, which together with the carbonyl bands at 1736 $cm^{-1}$ are indicative of the presence of urethane moieties.

Characteristic absorption bands of POSS are observed at 1080-1130 $cm^{-1}$, attributed to Si-O-Si stretching vibrations in the silsesquioxane cages (Misra et al. 2007),(Zhang et al. 1998). For the POSS-PCU hybrid nanocomposite, not only the characteristic bands of PCU, but also the absorption bands at 1109 representative of Si–O–Si stretching vibrations (Bliznyuk et al. 2008;Huang et al. 2003) were observed. The presence of the latter did not alter the existing polyurethane bonds. The characteristic 1109 absorbance is observed in the POSS-PCU2, POSS-PCU4 and POSS-PCU8 composites, with strong intensity signals. With increasing POSS concentration, the intensity of the peaks will be stronger. The absorbance band at 2250–2275 $cm^{-1}$ that is characteristic of isocyanate disappears gradually with increasing POSS concentration as expcted. It also shows POSS can self-assemble on the surface of the POSS-PCU nanocomposite. This can indicate the POSS moieties acts as a nanocore-crosslinker; which helps the completion of the reaction between the diamine and the PCU pre-polymers.

#### 4.3.4.2. Surface roughness

Increments in surface hydrophobicity may also be related to the surface roughness (Gao & McCarthy 2006). To check whether the surface roughness influenced the contact angles, and, therefore whether it influenced the surface free energies of POSS-

PCU films, AFM was used to observe the topographical images. Typical AFM topographical images of the pure PCU and hybrid POSS-PCU nanocomposite films are shown in Figure 4.9.

AFM phase imaging provides insight into the distribution of nanostructured POSS domains based on the differences in localized stiffness and modulus. The average roughness ($R_a$) provides information on the phase separation between the two phases in hybrid POSS-PCU. Incorporation of POSS in the PCU matrix leads to dramatic modification of the polymer surface, as revealed by tapping mode AFM images of the POSS-PCU nanocomposite. While the surface of the reference PCU sample, shown in Figure 4.9A, is smooth with no apparent surface features (average roughness, $R_a$, of 20 nm), the POSS-PCU blends exhibit raised features with increased surface roughness [Fig. 4.11B: POSS-PCU2, $R_a$=23 nm, Fig. 4.11C: POSS-PCU4, $R_a$=98 nm, Fig. 4.11D: POSS-PCU8, $R_a$=122 nm]. In POSS-PCU4, spherical particles were homogenously dispersed. With increasing POSS content, some interconnected POSS micro-domains appeared. More agglomerates appeared when concentration of the POSS component is up to 8wt% (POSS-PCU8).

Generally, the average roughness ($R_a$) of POSS-PCU films were very small (about 100 nm), showing highly intermingled nano-phase separated hybrid materials. It also suggests that the studied films had good surface planarity. Smaller $R_a$ and $R_q$ values have been related to improved adhesion between organic and inorganic phases (Wahab et al. 2008). Using atomic force microscopy, the degree of surface roughness showed good correlation with increasing contact angle. The average sizes of the surface protrusions were measured as the peak-to-valley ratio. As shown in Figure

4.9, images obtained from AFM revealed significant surface roughening of the POSS-PCU8 as compared to PCU with an average surface roughness of 0.12 and 0.02 μm, respectively. Surface roughnesses with $R_a$ values << 100 nm have been reported to have a very limited effect on contact angles (Neumann 1972; Schulze et al. 1989). Therefore with the Ra obtained in this study (about 100 nm), it can be concluded that surface roughness could be partially the reason for the decreasing surface free energy of the hybrid PU. The reason why incorporation of POSS decreased the surface free energy can probably be related to the surface-oriented enrichment of POSS structures bearing low-surface-tension substituents (Misra et al. 2007;Turri & Levi 2005). The same effect of POSS on surface roughness has been observed in polyurethane containing 3–20% diol functionalized POSS nano-filler (Turri & Levi 2005).

The existence of nanometer-scale surface roughness has been shown to contribute to analogous hydrophobic behaviour (Pal et al. 2005;Zhu et al. 2005), both theoretically and experimentally. It was recently shown that POSS covalently bound into polyurethanes improves dewetting, due to the increase in the nanometer-scale surface roughness as well as hydrophobic alkyl groups present in the POSS structures (Lacono et al. 2007; Turri & Levi 2005). Contact angle and surface morphology results by AFM confirm that the outermost layer of the blend film is almost covered by the POSS moieties (Koh et al. 2005). Smooth surfaces are believed to be more antithrombogenic than rough ones. Rough surfaces may have an early thrombogenic effect in contact with blood, however, enhances more rapid and firm attachment of the fibrin lining and thus endothelialization (Gogolewski 1989).

The limited effect of POSS on surface properties between 2-8% is similar to what has been indicated in previous report (Liu et al. 2006); Si enrichment on the surfaces of the hybrid composites does not increase significantly when the concentration of Octa(propylglycidyl ether) POSS is 10 %wt or more, implying that thereafter the concentration of POSS moiety on the surface was no longer increased.

A schematic view of the POSS distribution in bulk and on the surface is shown in Figure 4.10. These findings indicate that the incorporation of a small amount of POSS of the correct composition allows desired modification of surface properties, such as increased surface roughness and surface hydrophobicity and reduced surface energy. POSS moieties preferentially segregate towards the film-air surface as a consequence of the strong thermodynamic driving force to minimize the surface energy (Misra et al. 2007), (Koh et al. 2005). POSS moieties in the polymeric films prepared by blending were also shown to be highly populated on the outermost surface of the film (Koh et al. 2005). Overall dispersion and domain size of POSS in the polymer matrix is a function of various inter- and intra-molecular forces acting between POSS-POSS moieties as well as between POSS and the polymer matrix. Dispersion and compatibility of POSS in the polymer matrix can be controlled by the proper selection of organic (R) groups attached to the corner silicon atom (Misra et al. 2007).

## 4.4. Endothelialisation of hybrid POSS-PCU nanocomposites: An *in vitro* study

Two techniques have been developed in order to harvest ECs from veins. Firstly, mechanical scraping (Ryan & Maxwell 1986) and secondly enzymatic digestion using collagenase or trypsin (Jaffe et al. 1973). Mechanical scraping uses an abrasive action

to remove EC from the vascular wall which leads to significant EC damage, the possibility of contamination with smooth muscle cells and provides a poor harvest of EC (Hoshi & Mckeehan 1986;Welch et al. 1992). Enzymatic digestion using collagenase or trypsin (Jaffe et al. 1973) which has been used in this study to remove the endothelium avoids the problem of mechanical damage to the cells and provides much improved EC recovery.

### 4.4.1. Cell viability

Cell viability is the ability of the cells to survive in the presence of culture media in contact with the nanocomposite. On the other hand, cell adhesion referred to the number of cells actually adherent to the nanocomposite after the culture media was removed and the wells were gently rinsed. In order to differentiate between these two parameters, CellTiterBlue (CTB) was added to the cell adhesion assay wells only after the original culture medium had been removed and gently rinsed with PBS to ensure that only those cells which were adherent, were present. All wells contained CTB to begin with and the media was not changed for 24 hours. Fresh media was added after 24 hours and CTB added after 48 hours to investigate metabolism capacity of the cells.

Given the importance of endothelialisation in cardiovascular implants, the ability of these nanocomposites to sustain endothelialisation is studied. However, optimising the surface concentration of POSS is essential in order to promote endothelialisation following implantation as excessive amounts of silica-based molecules could hinder endothelialisation due to its high hydrophobicity (Zilla et al. 1991).

Since the bioreduction of CTB occurs via, as yet, unidentified cellular metabolites, individual calibration curves had to be constructed for HUVECs cell type and for each medium. After appropriate calibration, the CTB assay was found to be equivalent to established cell proliferation assays (Figure 4.11). The colour change from blue to pink was taken as a measure of the overall metabolizing capacity of these cells; an indicator of their viability. If these cells were physiologically dysfunctional then accordingly the amount of dye metabolised would have been decreased.

Developing a cardiovascular implant with favourable blood-material interaction would require the ECs to undergo four phases. These cells have to first remain viable within the culture medium exposed to POSS-PCU. Next, the ECs would have to adhere to the polymer surface, preferably within a short time. These adherent ECs would then need to proliferate at a steady rate in order to achieve a confluent EC monolayer. This POSS modified PCU has been tested for its cytotoxicity effects on HUVECs. This study demonstrated that this supports the adherence, growth and proliferation of HUVECs. Quantitative analysis of HUVECs attachment on POSS–PCU nanocomposites studied with CellTiterBlue (CTB) showed a significant increase in mean EC proliferation at 48 hours over baseline values. The EC attachment increased on POSS-PCU2 films compared with PCU. Upon adding more POSS, there was no significant difference found between different concentrations. This study showed that there was no significant difference between HUVECs viability on the POSS-PCU2 and POSS-PCU4 following measurement with CTB assay at 48 hours of cell culture ($P > 0.05$) as is shown in Figure 4.12. Optical microscopy images of the HUVECs on nanocomposites are shown in Figure 4.13. The cells coverage for POSS-PCU2 and POSS-PCU4 is greater than that of PCU. The morophology of the cells

confirms the proliferation of the cells after 14 days. For all the samples a spread confluent layer of cells was observed after 21 days (Figure 4.13 A-E3).

### 4.4.2. Immunostaining

Mature endothelial cells in culture have a very distinctive and well described cobblestone appearance upon confluence. Typically, they appear as flat, 1-2 μm thick, cells about 10-20 μm in diameter with a central nucleus. ECs also exhibit contact inhibition and can be seen growing in patches or clusters in sparsely seeded cultures. Immunohistochemistry is one of the most widely used tools for characterising cell types by using antibodies specific to the cell of interest. However, one significant difficulty of this technique has been the relative lack of a dependable marker for endothelial cells. Two of the most commonly used antibodies are vWF and CD31. vWF has been routinely used for endothelial identification in adult cells. Confocal microscopy was also performed in order to observe vWF expression. After seven days of culture the HUVECs seeded on the polymer were vWF positive. HUVECs thus seem to proliferate, spread, and keep their phenotype on polymer surfaces (Figure 4.14).

## 4.5. Biodegradative resistance of POSS-PCU nanocomposite

### 4.5.1. Mechanisms of degradation

When determining the suitability of a particular polymer for use *in vivo* as an implant it is vital that an assessment has been made of that polymer's susceptibility to biodegradation. This is because post-implantation interaction between the polymer and adjacent tissues may induce change in its chemical and physical properties (Salacinski et al. 2002). Chemical changes may occur by covalent bond cleavage,

crosslinking or molecular rearrangement. Physical changes include swelling, plasticisation, crystallisation or decrystallisation, creep and stress cracking. The purpose of assessment is to understand the mechanism of degradation in order to devise strategies to protect the material from such forces, thereby increasing longevity. Three modes of chemical degradation predominate *in vivo*: mineralisation, hydrolysis and oxidation.

Polyurethanes (PUs) are known to be susceptible to degradation *in vivo* (McCarthy et al. 1997). In recent years it has become apparent that polyurethanes are particularly susceptible to hydrolysis and oxidation. Stokes (Stokes et al. 1987) carried out extensive research into the mechanisms leading to cleavage of the polymer chains by studying the surface cracking of implanted polyurethanes. He postulated that this biodegradation was due to neutrophil- and monocyte-derived macrophage induced oxidation, residual stress, polyether soft-segment chemistry, molecular morphology, foreign body giant cells. Using carbonate groups instead has been shown to improve the degradative resistance of PU (Edwards et al. 1998), an effect due to the increased hydrogen bonding between all of the segments (Tang et al. 2001).

Polycarbonate urethanes are susceptible to degradation from adherent cells, hydrolysis at the carbonate linkages and to oxidation (Labow et al. 2001;Tang et al. 2001). The incorporation of silicon in the form of polydiemthylsiloxane (PDMS) either as a surface-modifying end group or by its interaction with the soft segment of the polymer (Werner & Jacobasch 1999, Barbucci et al. 2003; Mirzadeh et al. 1995) is to reduce inflammatory response *in vivo* and enhance hydrolytic and oxidative stability of such polymers (Mathur et al. 1997). The reason for this approach is that PDMS has

extreme resistance to hydrolysis and oxidation. However, the incompatibility of PDMS integration into PU has led to poor materials which display low biostability (Salacinski et al. 2002). Nanofillers substantially increase the mechanical strength of the composite. A new POSS nanocage -integrated PCU were designed and used in this study. The POSS nanocages are considered to reduce inflammatory reaction *in vivo* so it is encouraging that despite obvious oxidative and peroxidative susceptibility, the nanocages are resistant to hydrolytic enzymes and the plasma protein fractions.

The susceptibility of POSS-PCU2 to instability was assessed *in vitro* by incubating the films in biological/chemical solutions. These solutions include hydrolysis with lysosomal enzymes, plasma protein fractions (I-IV), oxidation and peroxidation and distilled water as control. Distilled water has been chosen based on the previous studies carried out by Phua et al. (Phua 1987) and Salasinski et al. (Salacinski et al. 2002b). More details of the solutions have been described in the experimental section (Chapter 3). The resistance of POSS-PCU to biodegradation forces were measured by tensile and molecular weight analysis. Initial observation of POSS-PCU2 incubated in the mentioned solutions after 70 days is shown in Figure 4.15. The samples incubated in hydrolytic and most specifically oxidative solutions appeared dark compared to other samples. That is partially because the MDI is prone to discolouration. It can be oxidized and coloured in oxidative environment. The results of stress-strain analysis of nanocomposites are summarized in Table 4.7.

### 4.5.2. The effect of serum proteins

POSS-PCU incubated in serum proteins exhibited no significant difference in tensile strength and molecular weight distribution compared to water incubated controls

(Figure 4.17 & 4.18). There were no consistent trends noted in the effect of different plasma treatments on tensile strength of POSS-PCU2 films.

Table 4.7. Stress-strain behaviour of nanocomposite.

| Sample | Stress 100% strain (MPa) | Stress 300% strain (MPa) | Stress 500% strain (MPa) |
|---|---|---|---|
| Pre-incubation | 5.675 | 11.657 | 26.485 |
| Distilled water | 3.711 | 12.091 | 23.561 |
| Cholesterol esterase | 5.999 | 10.952 | 19.316 |
| Phospholipase $A_2$ | 6.251 | 11.963 | 23.567 |
| Hydrogen peroxide | 6.170 | 11.822 | 23.674 |
| Tert-butyl peroxide | 3.245 | 6.888 | 9.688 |
| Plasma fraction I | 6.013 | 11.264 | 21.199 |
| Plasma fraction II | 6.069 | 11.736 | 23.555 |
| Plasma fraction III | 6.095 | 11.860 | 23.695 |
| Plasma fraction IV | 5.631 | 10.606 | 20.537 |

Table 4.8. Selected properties of polymers based on GPC results.

| **Sample** | **Mw** | **Mn** | **Polydispersity** |
|---|---|---|---|
| Pre-incubated | 110000 | 42900 | 2.6 |
| Distilled Water | 113500 | 45800 | 2.45 |
| t-butyl Peroxide | 53200 | 22700 | 2.35 |
| Hydrogen Peroxide | 12300 | 48300 | 2.55 |
| Cholesterol Esterase | 124500 | 48700 | 2.4 |
| Phospholipase A2 | 123500 | 51500 | 2.45 |
| Plasma Fraction I | 105000 | 43400 | 2.45 |
| Plasma Fraction II | 120500 | 50000 | 2.45 |
| Plasma Fraction III | 106500 | 44600 | 2.4 |
| Plasma Fraction IV | 118000 | 42300 | 2.4 |

### 4.5.3. Hydrolysis

Hydrolysis is the fracture of vulnerable chemical bonds with water. *In vitro* experiments have demonstrated that polyurethanes are a potent activator of monocyte-

derived macrophages (Labow et al. 1999a)and stimulate the formation of foreign body giant cells (Kao et al. 1994)- two notable features of the chronic inflammatory response. It is hypothesised that exposure to hydrolysing enzymes released following lysosomal degranulation during the chronic inflammatory reaction is a mechanism of polymer biodegradation. Cholesterol esterase (CE) (Santerre et al. 1994; Santerre et al. 1993) and more recently phospholipase $A_2$ (Labow et al. 1997) are the enzymes party in the process of hydrolytic degradation. CE preferentially attacks the ester group of the soft segment of polyurethane (Labow et al. 1999b). CE has also been observed to cause release of breakdown products from poly(ether) urethanes when used at very high concentration (Salacinski et al. 2002) whereas the specificity of phospholipase $A_2$ is unknown. Polyester polyurethanes; although are the first generation of polyurethanes to be investigated for biomedical applications; are considered unsuitable because of their hydrolytic instability (Santerre et al. 1994). Polyurethanes are also susceptible to microbial attack through enzymatic action of hydrolases such as ureases and esterases (Howard 2002).

In this study, POSS-PCU appeared resistant to both PLA and CE as judged by negligible difference in tensile strength compared to pre-incubated samples ($p > 0.05$). Stress-strain curves performed on the polymers showed no significant difference in stress-strain behaviour existed between the control, PLA, CE and plasma fractions-incubated nanocomposites. This data shows that the soft segment of the polyurethane nanocomposite remains intact in spite of accelerated degradation as illustrated by the preservation of its elastic modulus in the Table 4.7. Molecular weight distribution in the CE and PLA solutions are the same as the samples of water-incubated control

(Table 4.8). This result might be partially because POSS-PCU does not contain hydrolytically-vulnerable ester linkages.

### 4.5.4. Oxidation

*In vivo*, oxidising free radicals are generated during the inflammatory response by the respiratory burst of activated neutrophils and it is believed that this process leads to oxidation of the polymer (Hooper 2000;Zhao 1993).

Oxidation of aliphatic polymer chains usually involves four stages: initiation by hydrogen abstraction; formation of hydro-peroxide by molecular oxygen; chain reaction propagation and termination (Salacinski et al. 2002). Free radical formation may be prompted by the aqueous ions of certain transition metals such as cobalt and molybdenum (Stokes et al. 1990). Polyurethanes with soft segments that are oxidatively stable like carbonate have lower rate of biodegradation compared to ether which is prone to oxidative degradation.

In this study, POSS-PCU2 films were exposed to solutions capable of generating several oxidising free radical species including: hydroxyl (OH) species from the $H_2O_2/CoCl_2$ mixture; alkyl (OR) species from the *t*-butyl peroxide/$CoCl_2$ peroxide mixture. The pre-incubated samples generally showed a greater stress and modulus compared to all the conditioned samples. There were no significant differences between the moduli of the pre-incubated sample and $H_2O_2$-incubated samples at 100%, 300% and 500% ($P > 0.05$). Compared to pre-incubated samples, sample exposed to t-butyl peroxide/cobalt chloride showed a significant reduction in modulus at 100% ($p< 0.001$) and did not reach 500% strain because the samples fractured. It is

important to note however that in the case of t-butyl-peroxide incubated nanocomposites, samples torn at strain more than 500% indicating an apparent decrease in tensile strength of POSS-PCU2 compared to all the other samples. This degradation is supported by the GPC results (Figure 4.18).

Although according to tensile results, POSS-PCU2 appeared relatively resistant to the $H_2O_2/CoCl_2$ mixture, the results of GPC also show that both the 'biodegradative solutions' cause some decrease in the apparent molecular weight distribution compared to controls, indicating possible material degradation. However, the most substantial drop in molecular weight was for the t-butyl peroxide solution in the presence of cobalt chloride.

Clearly, POSS-PCU2 was not invulnerable to metal ion oxidative degradation. Two reasons might account for this: firstly, although the aliphatic structure of POSS-PCU2 contains a lower proportion of ether linkage in its soft segment compared to poly(ether) urethanes, some susceptible ether linkages remain. Secondly, carbonate bonds may be subject to acid catalysed hydrolysis if the pH is low enough with the formation of carbon-dioxide and alcohol. Ward has proposed such a mechanism as the main mode of biodegradation of polycarbonate polyurethanes (Ward 1995). However, the pH of the $H_2O_2$/ *t*-but peroxide mixture was 5.2±0.4; which does not approach the degree of the acidity thought necessary to promote such hydrolysis. Further studies are required to elucidate the exact mechanism-whether oxidative or hydrolytic- by which poly(carbonate) urethanes lose their chemical integrity.

The biologically abundant $H_2O_2$ system ($H_2O_2$/cobalt chloride) showed little degradation of POSS-PCU2, in contrast to t-butyl peroxide solution (t-butyl/cobalt chloride). Based on these differences and the yellowing of the samples in solutions t-butyl peroxide/cobalt chloride it can be proposed that the t-butyl peroxide systems are effective at causing degradation of the POSS nanocages-based polymers.

These results confirms that the POSS-PCU nanocomposite revealed that in spite of accelerated degradation, all samples had shown no significant difference in their strength and molecular weight distribution properties. This is an indicator of the stability of the soft phase of the POSS-integrated PCU to all forms of *in vitro* degradation with the exception of t-butyl peroxide solution in the presence of cobalt chloride as a catalyst. Thus, the POSS-PCU2 is biologically resistant after long time exposure to simulated biodegradative solutions.

In summary, the structure of a unique PCU system having inorganic POSS molecules in their hard segments as nano-scale reinforcing agent has been studied. The POSS-containing PCU networks displayed enhanced glass transition temperatures, higher modulus and lower polydispersity indices. The organic-inorganic nanocomposites displayed a significant enhancement in surface roughness, surface hydrophobicity, as well as a reduction in surface free energy compared to the control polyurethane. While microscopy, spectroscopy, contact angle analyses all indicate dramatic modification of surface properties for these nanocomposites, bulk properties are only minimally affected by incorporation of POSS in the PCU matrix. These results show the preferential orientation of POSS towards the surface. The improvement in surface properties was ascribed to the presence of the POSS moiety in the place of the polar

component of polyurethane. HUVECs viability on the nanocomposites shows that HUVECs cultured directly onto the nanocomposite exhibited optimal cell viability for up to 48 hours. This study showed that POSS-PCU is resistant to plasma proteins and hydrolytic enzyme degradation. However, POSS-PCU is vulnerable to some oxidative species. The addition of POSS nanocore/fillers to the PCU imparts a type of 'shielding' effect on the soft phase of the nanocomposite thereby preserving its elasticity and compliant properties via zones of intercalation. In addition, the extensions of these nanofillers from the hard phase into the soft phase help cross-link and bind together the entire composite as a single elastic unit. This is exemplified by the increase in $T_m$ compared to PCU. These results herein indicate the immense potential of nanofillers such as POSS in optimising the characteristics necessary in biomedical devices. Further work is necessary; to quantify the chemical changes that occur with exposure to these species, to relate these *in vitro* changes to *in vivo* performance and to consider how the chemical structure may be augmented to enhance bioresistance further.

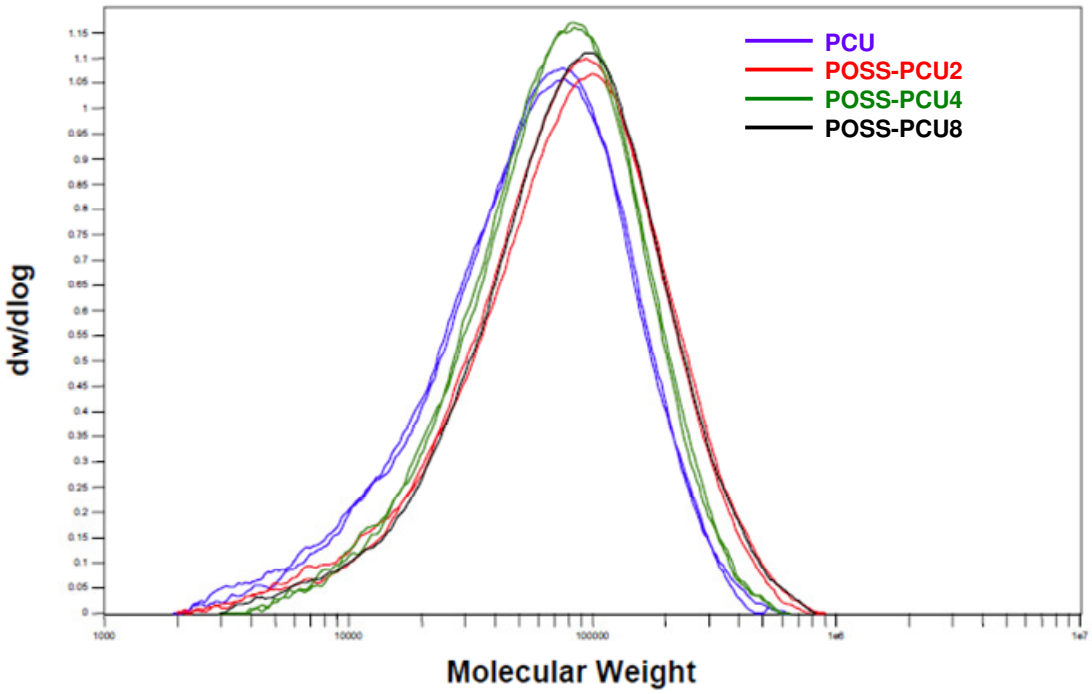


Figure 4.1. Molecular weight distribution of control PCU and POSS-PCU nanocomposites.

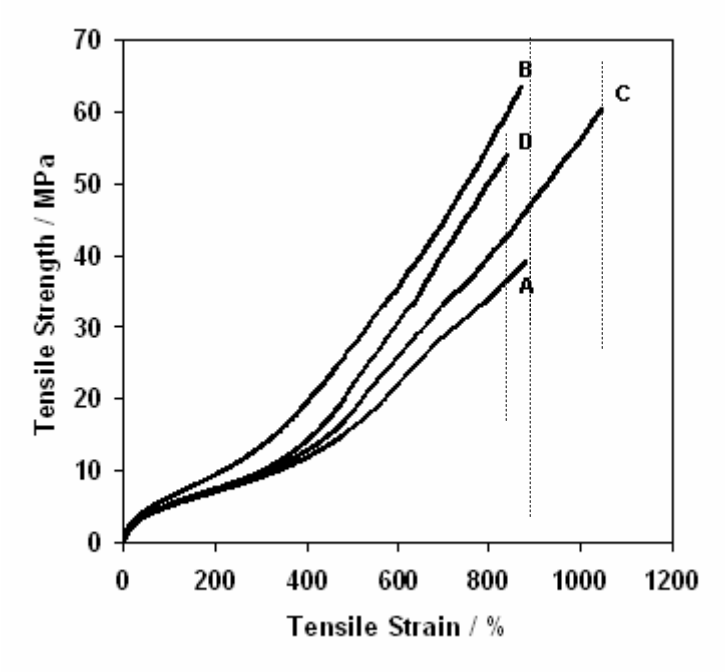


Figure 4.2. Stress–strain curves of POSS-based polyurethane nanocomposites: (A) PCU; (B) POSS-PU2; (C) POSS-PU4; (D) POSS-PU8.

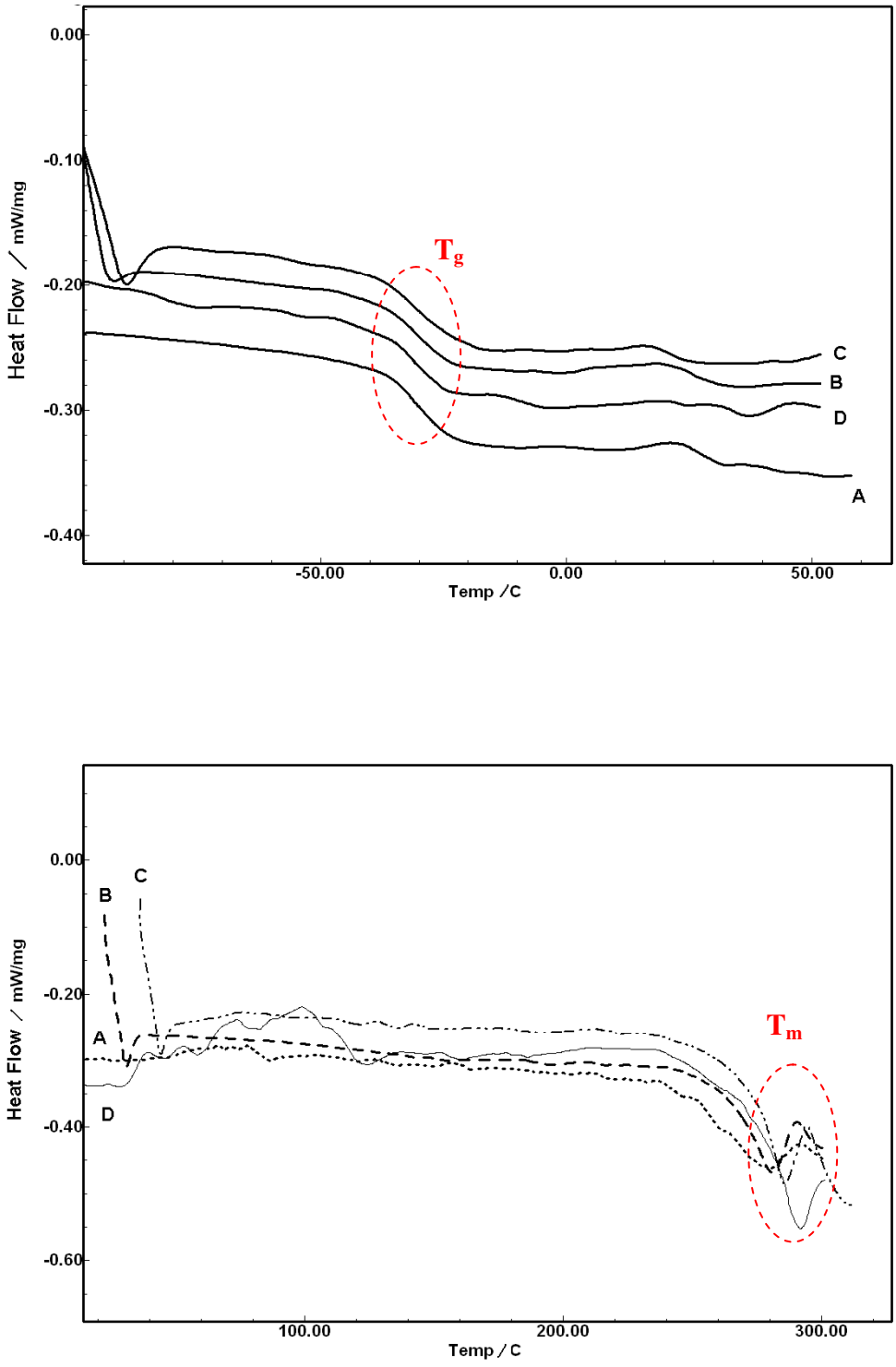


Figure 4.3. Heating DSC scans in nitrogen (10°C/min) overlay of (A) PCU as compared to (B) POSS-PCU2; (C) POSS-PCU4 and (D) POSS-PCU8. Inset: negligible change of $T_g$ and increase in $T_m$ by addition of POSS.

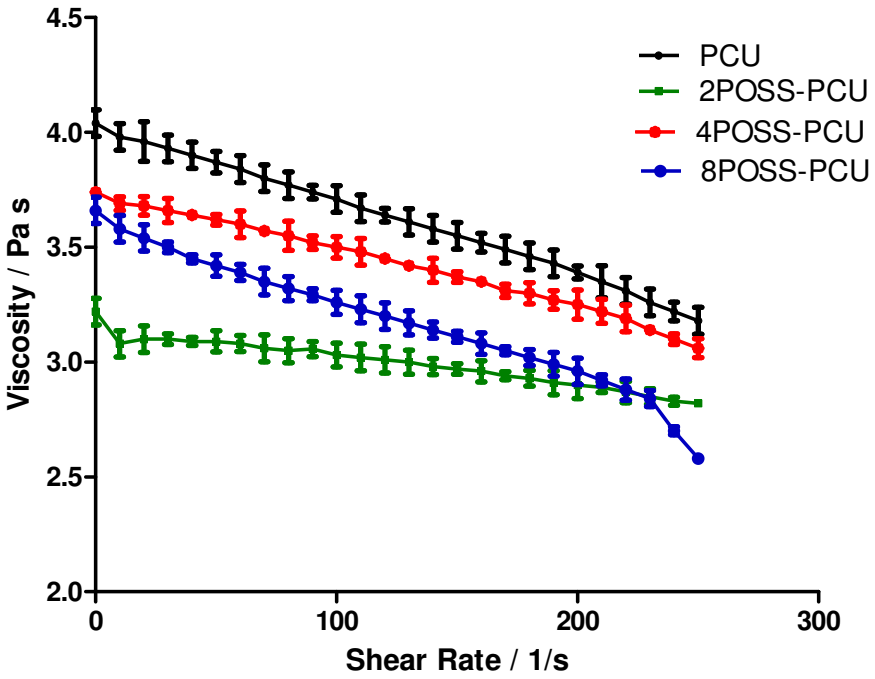


Figure 4.4. The viscosity of control PCU and POSS-PCU nanocomposites as a function of shear rate at 25 °C.

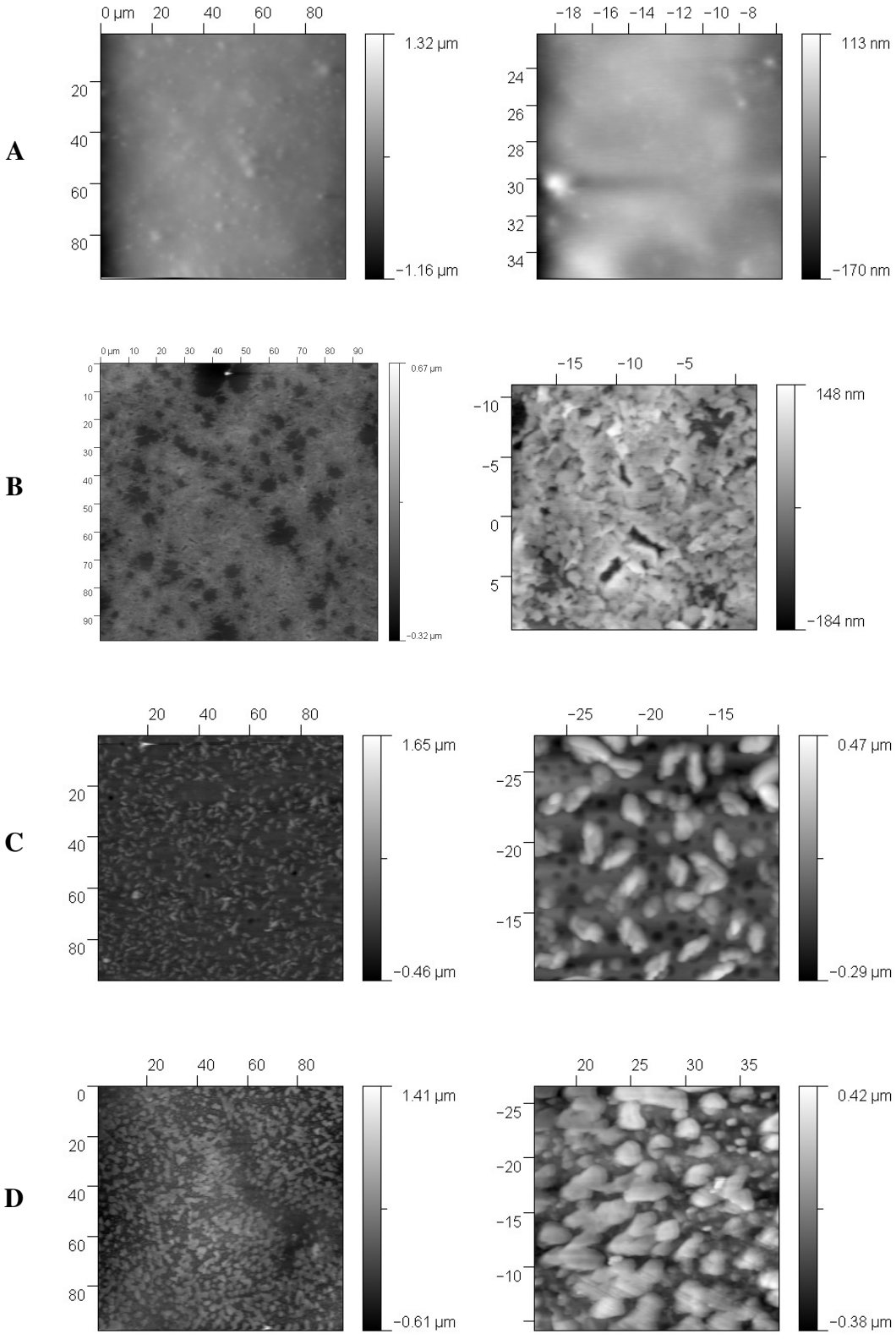


Figure 4.5. AFM phase contrast micrographs of (A) PCU; (B) POSS-PCU2; (C) POSS-PCU4; and (D) POSS-PCU8.

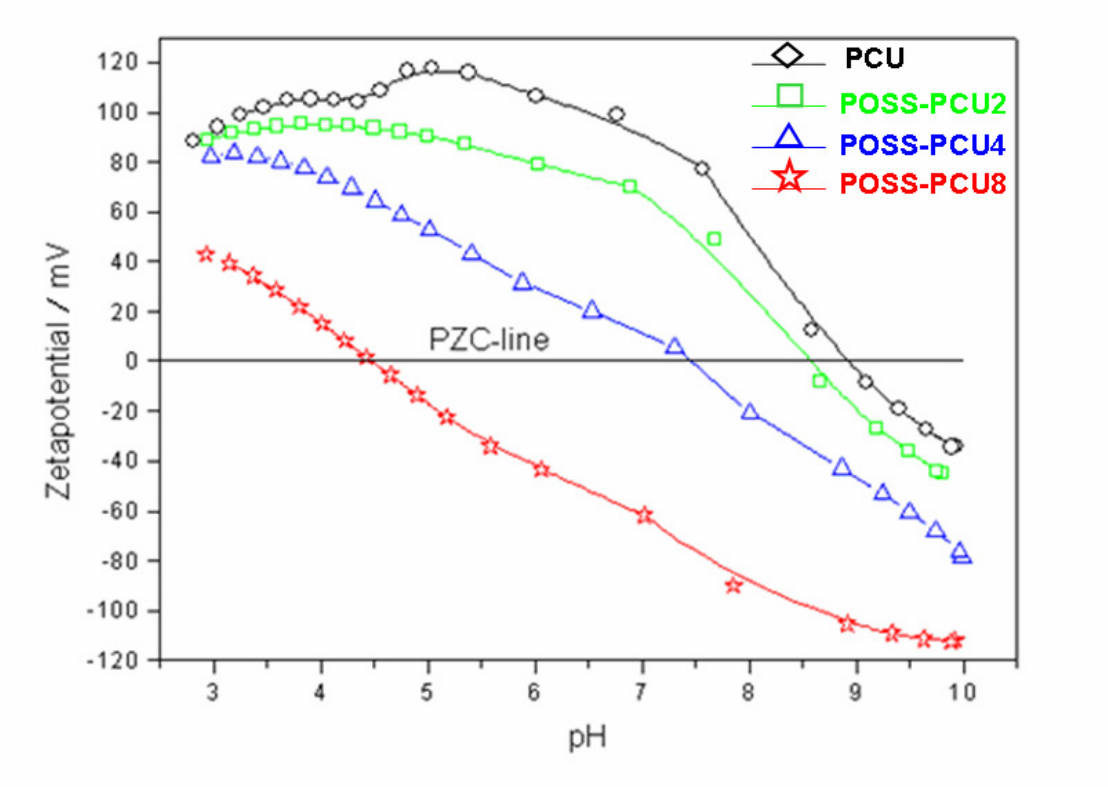


Figure 4.6. ζ-potentials of control PCU and POSS-PCU nanocomposites in dependence of pH value of electrolyte solution. Inset: surface charge shifts towards negative values by addition of POSS.

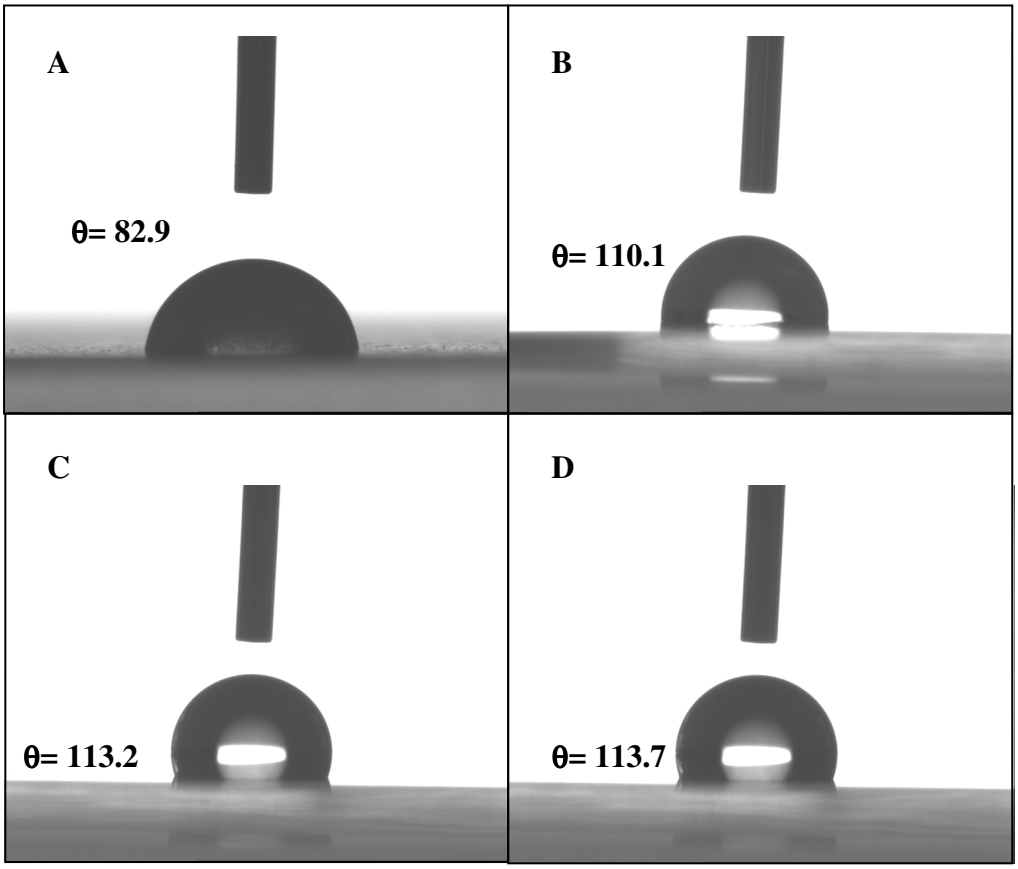


Figure 4.7. Water contact angle images on the surface of: (A) PCU; (B) POSS-PCU2; (C) POSS-PCU4; and (D) POSS-PCU8.

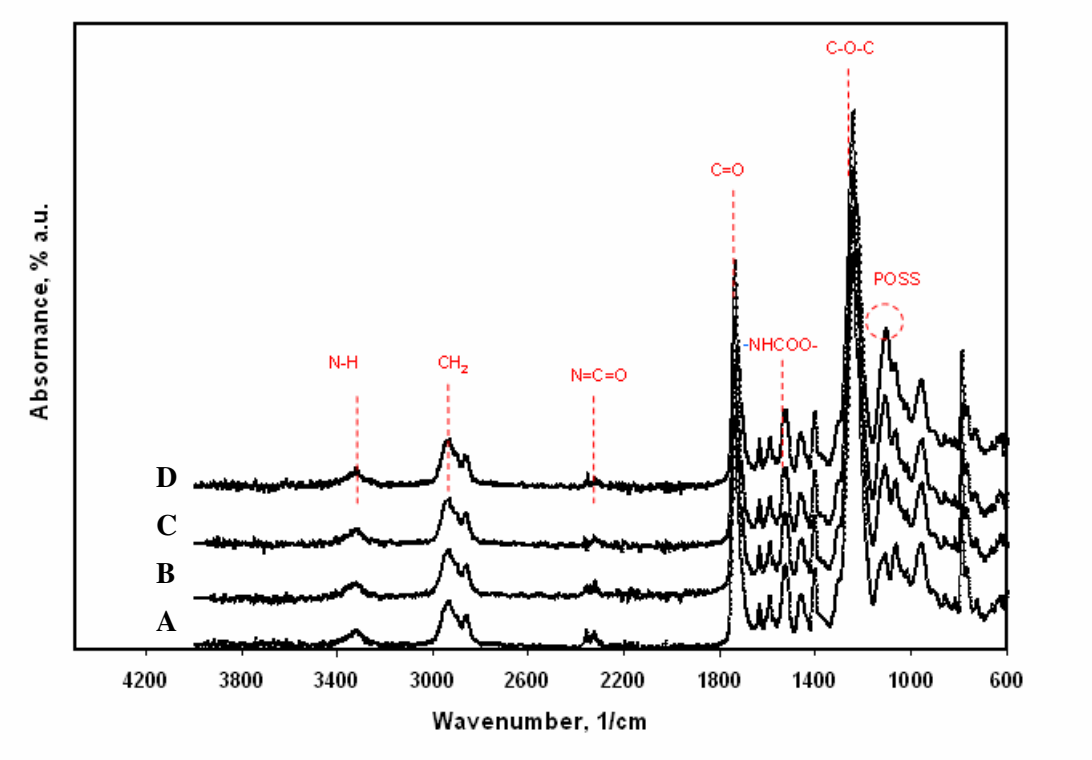


Figure 4.8. FT-IR spectra of: (A) PCU; (B) POSS-PU2; (C) POSS-PU4; and (D) POSS-PU8.

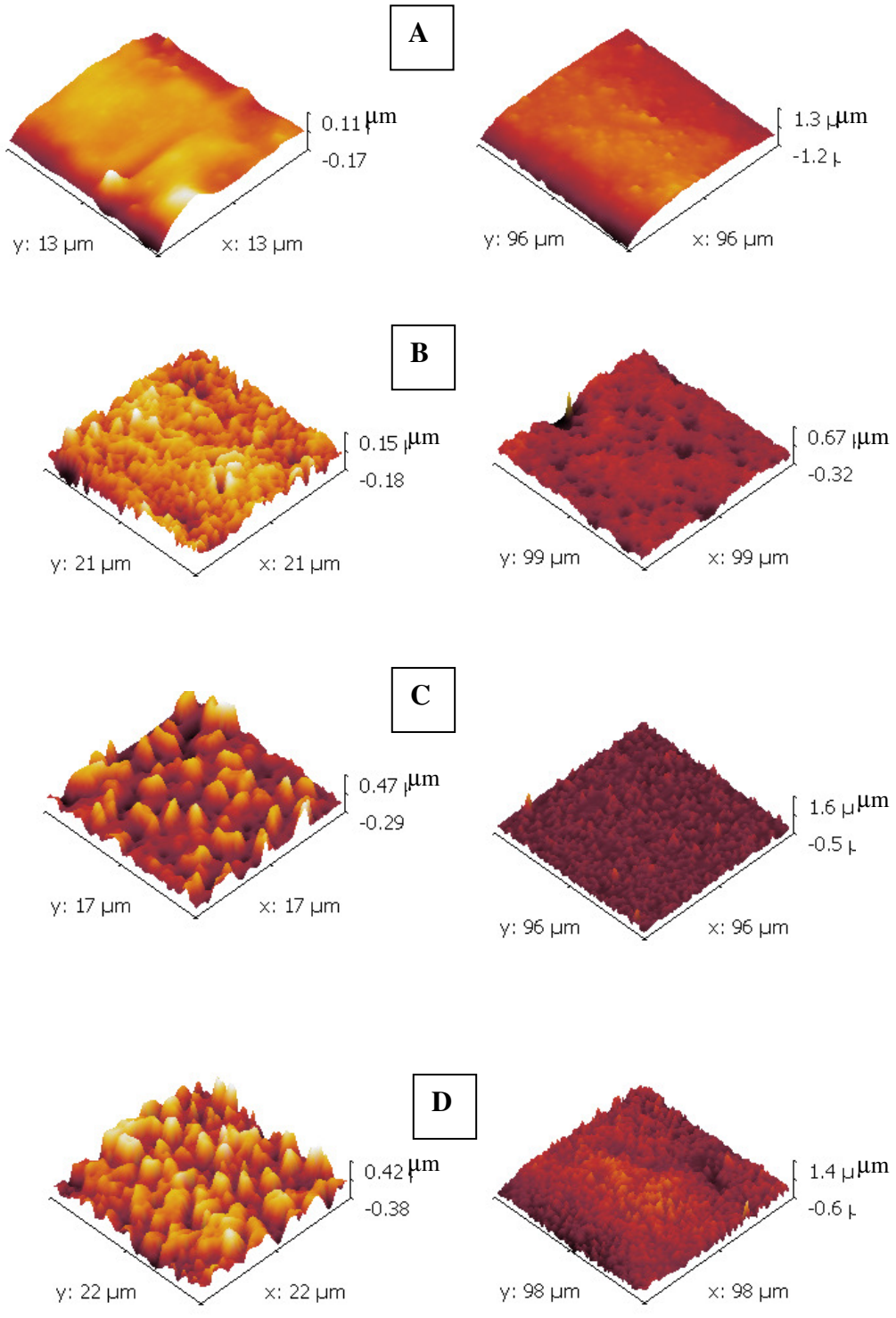


Figure 4.9. AFM topography images of (A) PCU; (B) POSS-PCU2; (C) POSS-PCU4 (D) POSS-PCU8. Inset: increase of surface roughness by addition of POSS.

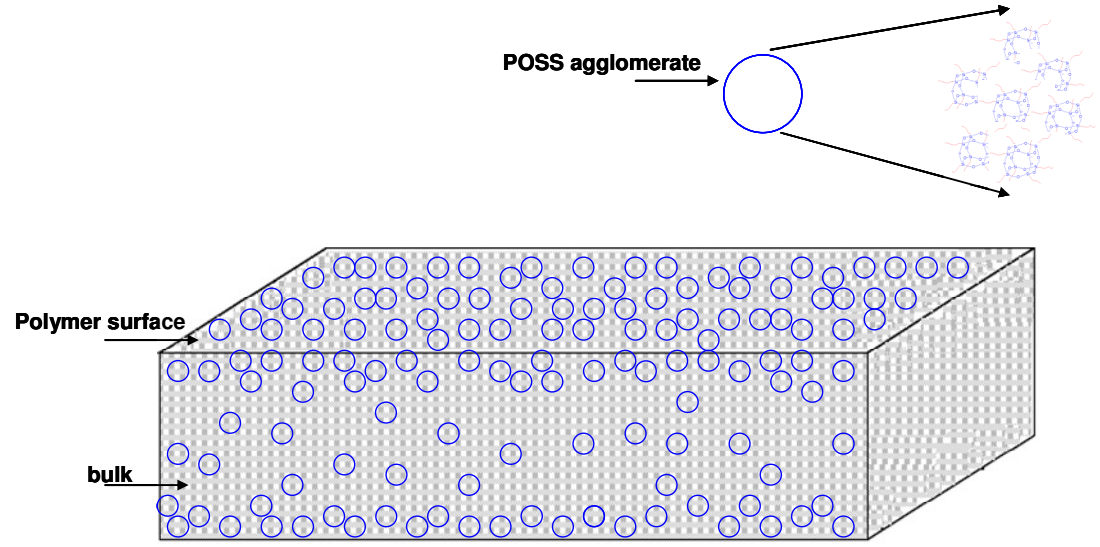


**(A)**

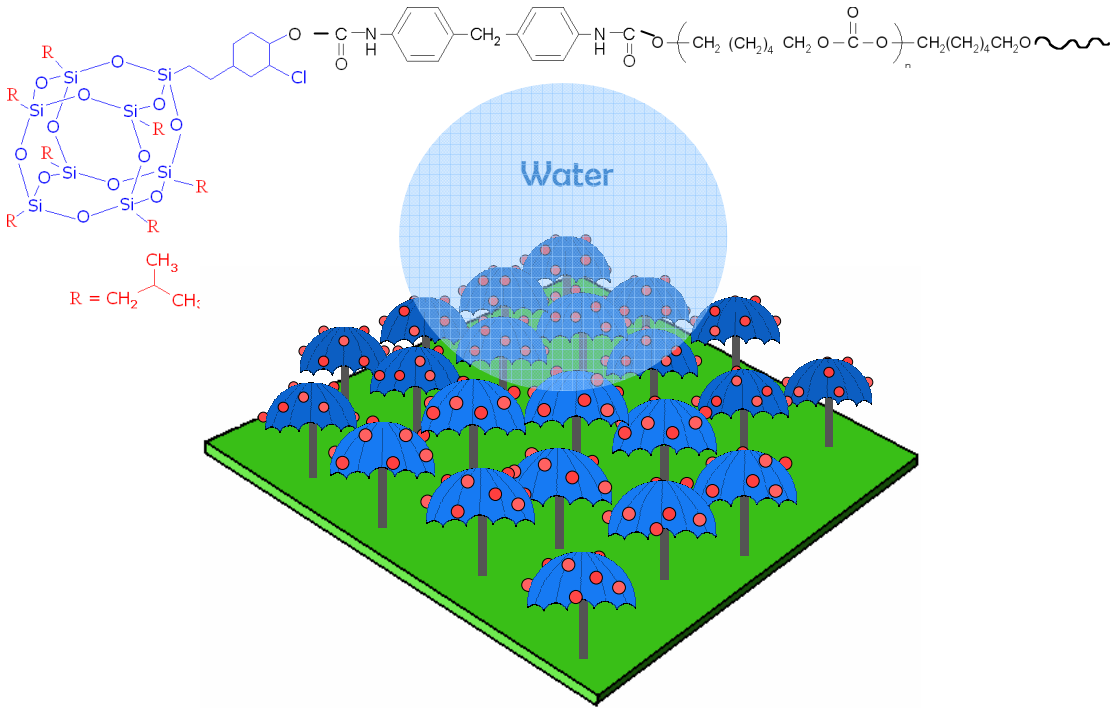


**(B)**

Figure 4.10. (A) Schematic representation of bulk versus surface distribution of POSS nano-particles in POSS-PCU nanocomposite. (B) Preferential segregation of POSS moieties towards the film-air surface. POSS behaves like umbrella which make the surface hydrophobic.

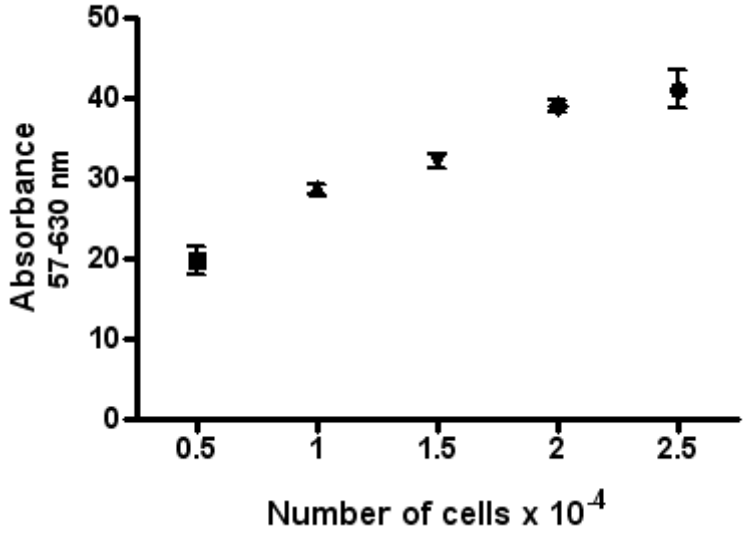


Figure 4.11. CellTiter Blue standard calibration curve for HUVECs.

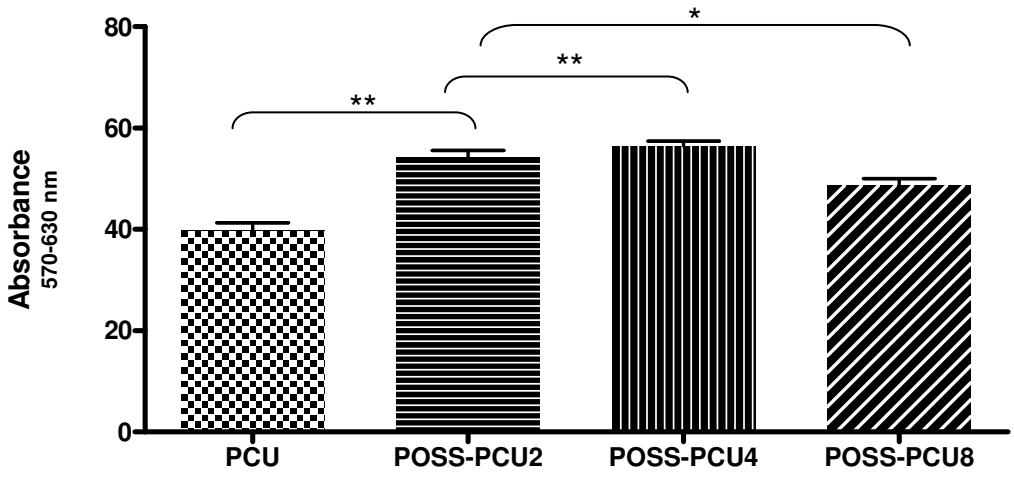


Figure 4.12. Cell viability test using CellTiter-Blue assay for HUVECs exposed to POSS-PCU nanocomposites and control PCU for 48 h.

Keys:

** $p < 0.01$ significant against PCU.

** $p < 0.01$ significant against POSS-PCU4

* $p < 0.01$ Significantly decreased against POSS-PCU2 and POSS-PCU4.

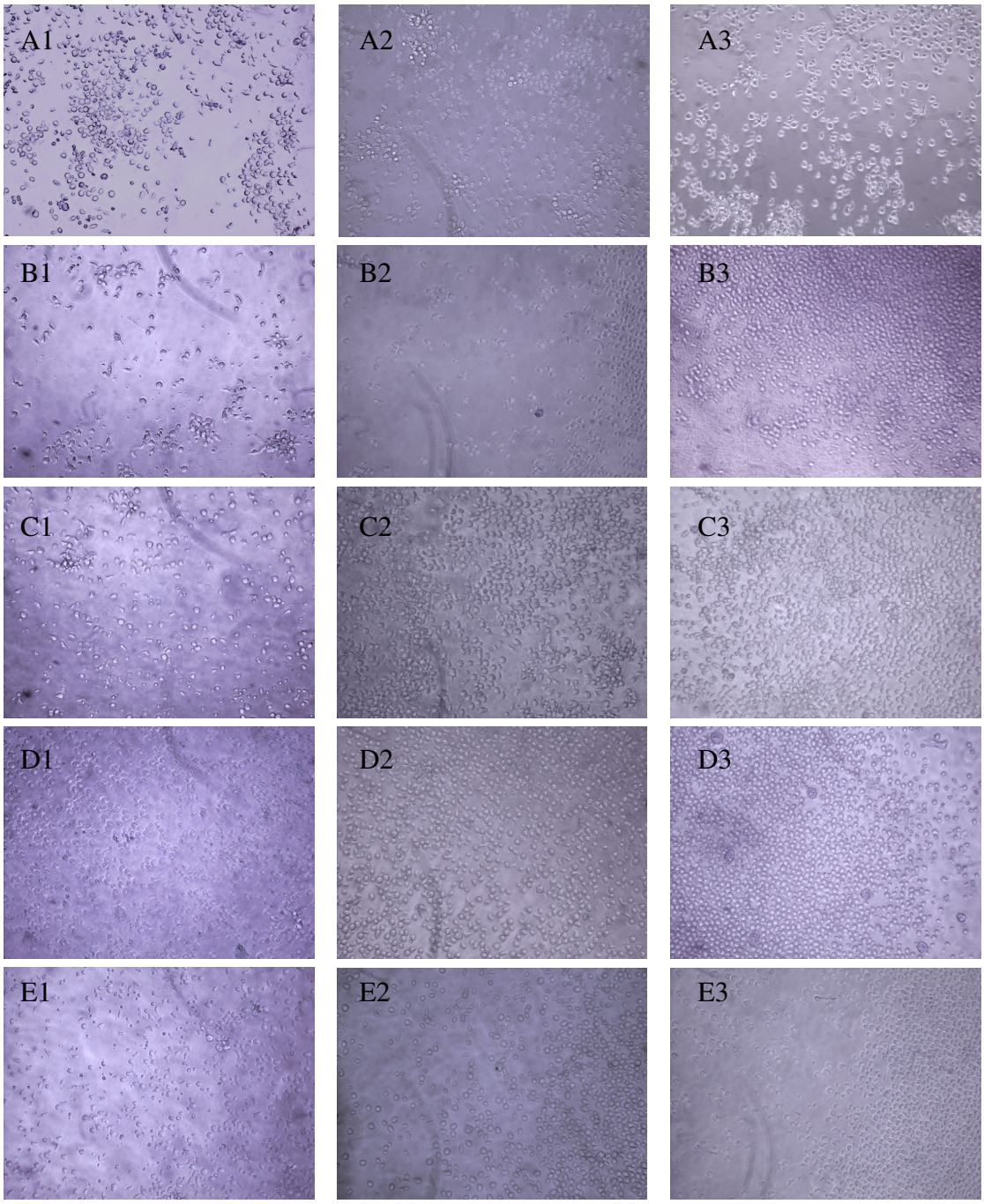


Figure 4.13. Morphological evolution of ECs seeded on TCP (A1–3); PCU (B1-3); POSS-PCU2 (C1-3); POSS-PCU4 (D1-3); and POSS-PCU8 (E1-3) by optical phase contrast microscopy. EPCs at 7 days (A-E1), 14 days (A-E2) and 21 days (A-E3). TCP were used as a control. Insets: A-E1)typical round shape cells, A-E2 & A-E3) differentiation and proliferation of cells. Objective × 20.

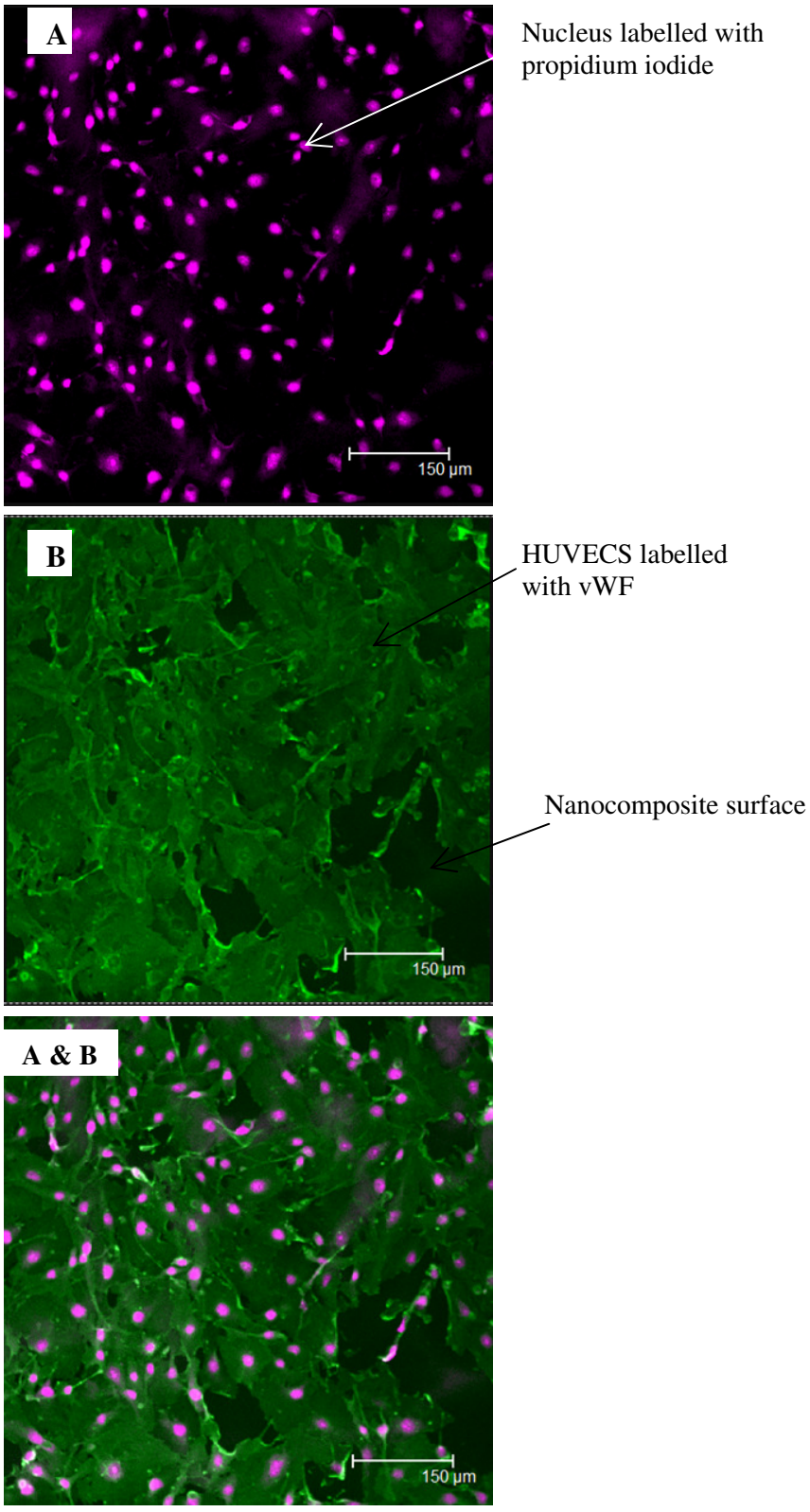


Figure 4.14. Cytoskeleton visualization (A) and cell phenotype characterization $vWF^{+}$ (B) by confocal microscopy after 48 hours of culture on POSS-PCU2, objective ×20.

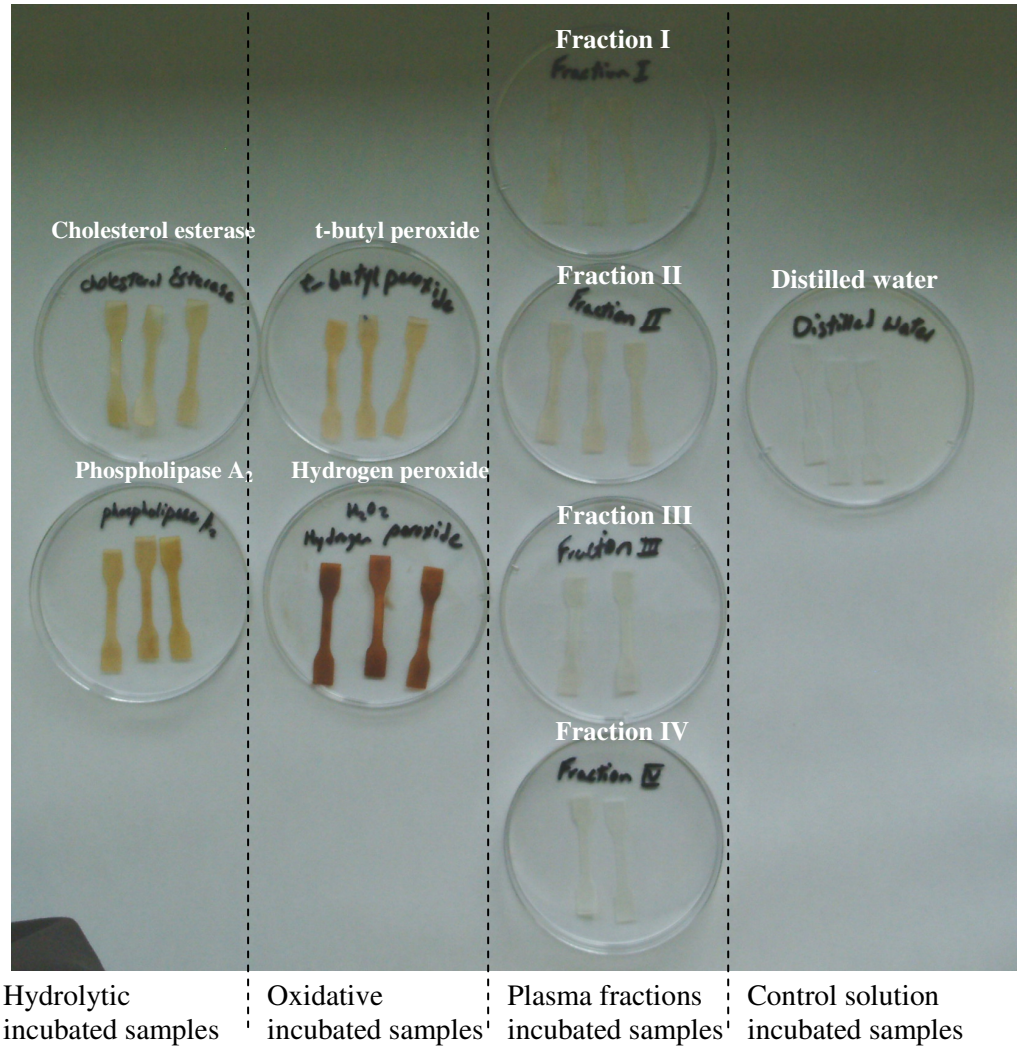


Figure 4.15. Initial observation of POSS-PCU2 following 70 days immersion in different degradative solutions.

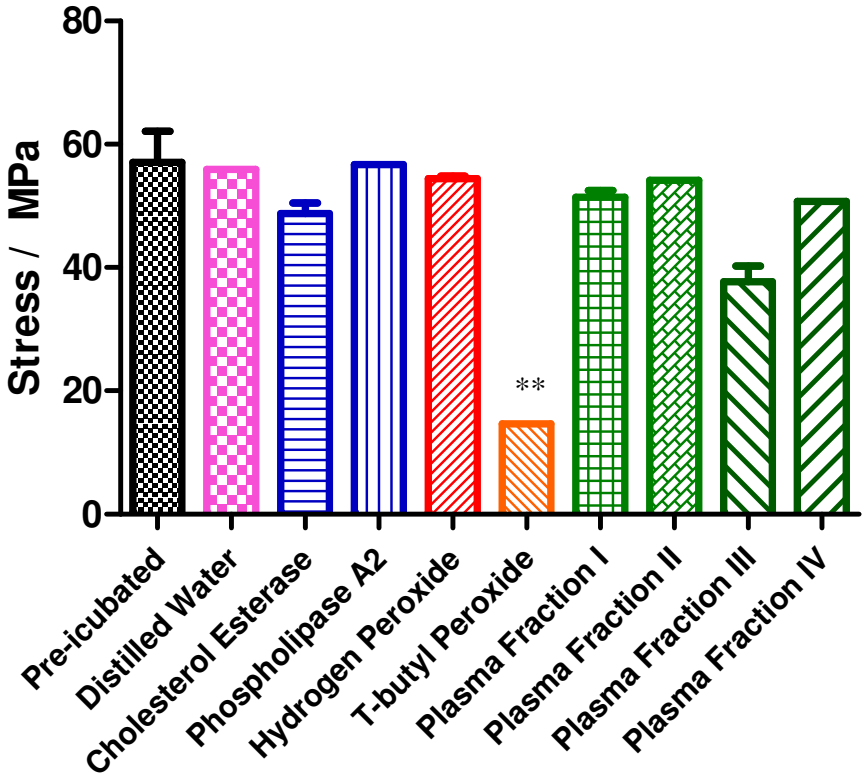


Figure 4.16. Ultimate tensile strength of POSS-PCU2 following 70 days immersion in different media.

** p< 0.05 significant against pre-incubated.

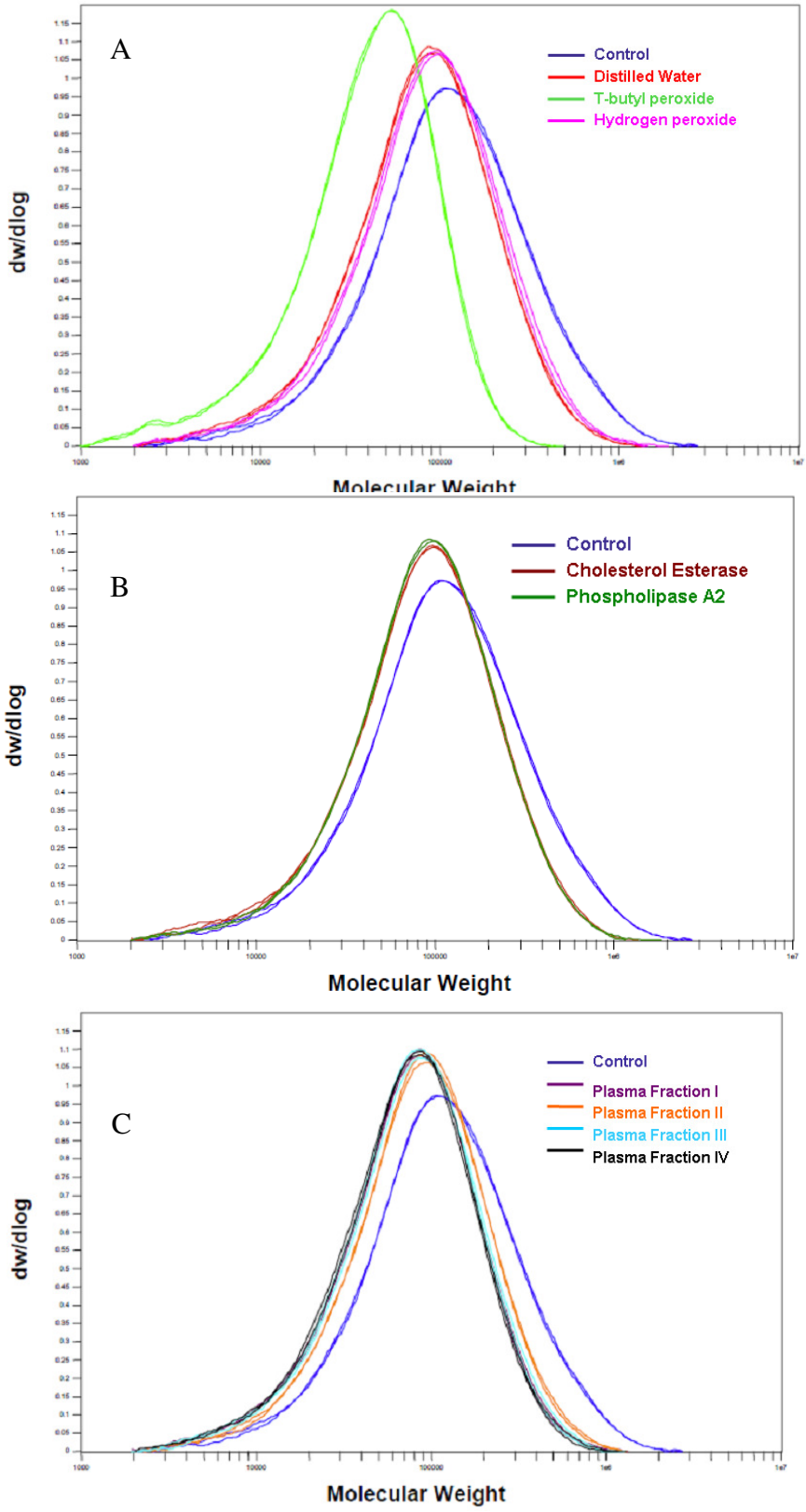


Figure 4.17. Molecular weight distribution of POSS-PCU2 nanocomposites following 70 days immersion in different media: (A) hydrolytic solutions; (B) plasma fractions; and (C) oxidative/peroxidative solutions.

# CHAPTER 5. Coating Stainless Steel and NiTi with POSS-PCU

In this chapter the electrohydrodynamic spraying and ultrasonic atomization spraying of POSS-PCU2 nanocomposite polymer developed and investigated for coating metallic stent materials. The experimental details of these thechniques were given in Chapter 3. The results are compared with data from samples made by simply casting the metal with the polymer.

Based on the results in Chapter 4, POSS-PCU2 was chosen for this part of the work. In this research, electrohydrodynamic spraying of POSS-PCU2 solution on a stainless steel substrate over a wide rang of applied voltage and flow rates was investigated and the effect of varying the polymer concentration in the solution and the electrospraying time on the coating has been studied. Ultrasonic atomization spraying was also assessed for coating NiTi with POSS-PCU2. This coating technique was optimised using different variables such as nanocomposite concentration, applied voltage and flow rate. The structural features of the POSS-PCU2 films were assessed using microscopy. Films were also tensile tested. These results are reported and compared with cast-coated films.

## 5.1. Casting

POSS-PCU2 films were prepared by brushing polymer solution on NiTi/stainless steel. By adding different amounts of polymer solution, different films with different thicknesses were prepared. Further structural characterization will be discussed in comparison with other techniques in the following sections.

## 5.2. Electrohydrodynamic spraying set up

The stable cone-jet mode EHDA used to deposit the nanocomposite polymer allowed the formation of films on a rotating stainless steel substrate. An electrostatic field is created between the positively charged needle and the earthed stainless steel collector. A rotating plate was used to ensure even spreading of droplets generated by EHDA and a balance between deposition and drying time, which leads to the formation of film instantaneously with uniform thickness. The centre of rotation of the plate was slightly off-set to the exit of the needle so that all droplets do not collect in the centre while rotating (Figure 5.1).

### 5.2.1. Solution characterization

The effect of the polymer concentration on the properties relevant to electrohydrodynamic spraying is shown in Table 5.1. As expected, the viscosity of the solution increased with increasing polymer concentration. Polymer concentration slightly increases the surface tension of the solutions. High polymer concentrations also result in higher electrical conductivity. The aromatic rings in MDI are more likely to be responsible for the electrical conductivity. The extra electrons of the double bonds which are free to move throughout the structure could account for the electrical conductivity in the solution. The first report of metallic conductivity in doped polymers (Friend et al. 1999) has lead to the development of a number of conductive polymers which were based on molecules containing aromatic rings, such as poly(p-phenylene) and poly(pyrrole) (Nicholson 2006).

### 5.2.2. Mode selection map

Figure 5.2 shows the different spraying modes observed for 15 wt% polymer solutions at different applied voltages. Figure 5.2A shows the dripping mode in which drops take the shape of regular spheres, eventually detaching from the capillary due to gravity. Figure 5.2B exhibits the unstable cone-jet mode where visually the cone appears and disappears intermittently, in contrast, the stable cone-jet mode was obtained for the solution at 5.6 kV (Figure 5.2C). In the stable cone-jet mode the solution exits the capillary in the form of a cone with a jet emanating from the cone apex. Figure 5.2D exhibits rim emission mode in which an irregular jet comes out of the capillary in random directions. Figure 5.2E represents a jet exiting the needle in the precession mode with spiral-like rotating around the capillary. The increase in the flow rate forms the multi-rim emission with several jets exiting (Figure 5.2F). Overall, as the polymer concentration is increased, the stable cone-jet mode region expands and covers a larger range of flow rates and voltages.

Table 5.1. Physical properties of POSS-PCU2 nanocomposite polymer solution, the values are mean of three readings; DMAC: N, N-dimethylacetamide.

| **UCL-Nano/ DMAC** | **Density ($kg/m^3$)** | **Viscosity (mPa s)** | **Surface tension (mN/m)** | **Electrical conductivity (µS/m)** |
|---|---|---|---|---|
| **10%** | 955 | 936 | 33 | 2.1 |
| **15%** | 964 | 2930 | 36 | 2.6 |
| **20%** | 1100 | 3960 | 40 | 3.3 |
| **DMAC** | 937 | 1.2 | 34 | 0.2 |

The mode of spraying for applied voltage versus flow rate in the range of 1-10 kV and 1-10 µl/s was investigated to establish the best spraying conditions for the polymer

solutions. Thus, mode selection maps were established for three concentrations of polymer: 10 wt%, 15 wt% and 20 wt% (Figure 5.3). At a fixed flow rate, the spraying mode changes at different applied voltages. It shows several electrospraying modes such as, dripping, unstable cone-jet, stable cone-jet, rim emission, precession and multi-rim emission. As shown in Figure 5.3A, the 10%wt polymer solution was too dilute for film formation and the envelope for stable cone-jet mode spraying was only obtained at higher flow rates in a small applied voltage envelope, making process control very difficult. The solution containing 20 wt% of polymer had the largest stable cone-jet mode region (Figure 5.3B) but a small amount of polymer blocked the silicon rubber tube connected to the needle, and this made it difficult to maintain the electrospray. Decreasing the polymer concentration to 15%wt avoided blockage and spraying conditions of 5.8 kV and 4 µl/s were chosen for 15 wt% solution as these resulted in the homogenous film forming conditions (Figure 5.3B).

## 5.3. Ultrasonic atomization spraying

This method utilizes vibrations, supplied by a voltage applied through an ultrasonic generator, to create capillary waves, with small wave length and high frequency, on the surface of a liquid. Tehrefore, there are so many variables to optimise the procedure of atomization.

### 5.3.1. Parameter optimisation

Varying parameters of the atomization process permitted the modification of the patterns present on the surface and the thickness. Sprayed films were prepared for different parameter values in accordance with the Taguchi method (Taguchi 1986) (Table 5.2). Here, the Taguchi method allowed three parameters to be investigated

with three levels of variability (polymer flow rate, voltage, and time) and five parameters with two levels of variability (temperature, distance from nozzle, polymer concentration, gas flow rate, and drying conditions) in 12 experiments. In contrast, to test all contribution of variables, 59 ($3^3 + 2^5$) experiments would be required.

Table 5.2: Taguchi orthogonal array method for parameter testing.

| Sample Number | Polymer Flow Rate ($m^3/h$) | Applied Voltage (V) | Time of spraying (hour) | Temp. (°C) | Distance of the substrate from Nozzle (mm) | Polymer Conc. (wt%) | Gas Flow $\times 10^{-4}$ ($N/m^2$) | Drying Condition |
|---|---|---|---|---|---|---|---|---|
| **1** | 10 | 11 | 1 | 37 | 90 | 2 | 4 | Oven |
| **2** | 10 | 15 | 3 | 57 | 90 | 2 | 3 | Room |
| **3** | 10 | 20 | 2 | 37 | 90 | 5 | 3 | Room |
| **4** | 10 | 11 | 3 | 37 | 70 | 2 | 4 | Room |
| **5** | 15 | 15 | 2 | 57 | 90 | 2 | 3 | Oven |
| **6** | 15 | 20 | 1 | 37 | 70 | 5 | 4 | Oven |
| **7** | 15 | 15 | 3 | 57 | 70 | 5 | 4 | Room |
| **8** | 15 | 11 | 1 | 57 | 70 | 5 | 3 | Room |
| **9** | 18 | 20 | 2 | 37 | 90 | 5 | 4 | Oven |
| **10** | 18 | 11 | 2 | 57 | 70 | 5 | 4 | Room |
| **11** | 18 | 20 | 3 | 57 | 70 | 2 | 3 | Oven |
| **12** | 18 | 15 | 1 | 37 | 90 | 2 | 3 | Oven |

## 5.4. Film characterization

### 5.4.1. Surface morphology

Surface morphologies of the films deposited on stainless steel prepared from the 15% polymer solution are shown in Figure 5.4, after 1 hour, 2 hours and 3 hours of electrospraying. These reveal their very uniform non-porous films were produced by this method after 1 hour of electrospraying, while the films prepared after 2 and 3 hours showed a porous structure. The shorter the electrospraying time, the thinner the

layer thickness and the denser the deposited film (Figures 5.4D-F). Similar results have been reported in other studies (Nguyen & Djurado 2001). It is known that droplets generated during spraying will have varying spreading times on a substrate due to surface tension between the substrate and the spraying medium (Chen et al. 1996). The surface energy of the metallic substrate is greater than that of the polymer solution. The accumulation of polymer results in reduced surface energy on the deposited substrate. When deposition time and layer thickness are increased, the droplets spread slowly on the surface of the denser preceding layer, which has smaller surface energy than stainless steel, leading to the formation of a porous top layer. With a deposition time of 3 hours, the top surface is very porous.

The thickness of EHDA films deposited in this work increased parabolically with electrospraying time (Figure 5.5). Electrosprayed film thickness was about 50 μm after spraying for 2 hours. It can be concluded that as the film thickness increased, the stability of the cone-jet mode was affected. This is because the polymer coat acted as a dielectric layer in the electric field and this made droplet deposition and thickness control difficult (Pareta & Edirisinghe 2006).

The use of a Taguchi orthogonal array allowed for the seven different parameters in ultrasonic atomization spraying to be altered and assessed with minimal experimentation. The results of SEM are shown in Figure 5.6. The most striking observation from the SEM images below is the presence of dried polymer residue on the surface of samples 3, 6, 7, 8, 9 and 10, all of which are sprayed using a polymer concentration of 5 wt%. It is also possible to determine the polymer droplet size, and therefore the surface smoothness from the SEM images. This was achieved by

averaging the diameter of particles at ×160 magnification for each sample. Droplet size was assessed by measuring the diameter of 10 visible droplets from the SEM images and taking the average. The results are shown in Table 5.3.

Table5. 3. Droplet sizes of 12 samples sprayed with POSS-PCU2 with different parameters.

| Sample | Droplet size Distribution (μm) | Mean Droplet Size (μm) |
|---|---|---|
| 1 | 62 – 137 | 99 |
| 2 | 97 – 165 | 131 |
| 3 | 56 – 125 | 91 |
| 4 | 46 – 88 | 67 |
| 5 | 90 – 145 | 118 |
| 6 | 46 – 125 | 85 |
| 7 | 115 – 159 | 137 |
| 8 | 55 – 157 | 106 |
| 9 | 66 – 106 | 86 |
| 10 | 71 – 179 | 125 |
| 11 | 73 – 228 | 151 |
| 12 | 78 – 108 | 93 |

It is obvious to see that the droplet size is related to the spraying temperature (Figure 5.7). This graph clearly shows that a lower spraying temperature leads to a smaller droplet diameter. The graph clearly show that lower spraying temperatures lead to a reduced droplet diameter (p value = $10^{-6}$; p value < 0.001 shows significant difference), and therefore, by extension, a more irregular surface morphology. Samples 1, 3, 4, 6, 9 and 12 were all sprayed at 37°C and showed a smaller mean droplet diameter, and therefore a less smooth surface when compared with samples sprayed at 57°C. An unpaired, 2-tailed T-test showed that this result is statistically significant (p value= $10^{-6}$; p value < 0.001). Sample 12 was deemed to have the most favourable surface morphology as there was minimal polymer residue and a small

mean droplet size. Parameter testing was performed to ascertain the optimal parameters for spraying stents with POSS-PCU2 by ultrasonic atomization spraying. The SEM images show that polymer residue forms when a polymer concentration of 5 wt% is used. This is most probably due to incomplete spraying. At higher polymer concentrations, the viscosity is higher and it is therefore more difficult to create capillary waves with high enough amplitude to break up into droplets. This leads to 'spitting' of larger drops which, when once the solvent has evaporated, result in residue. This residue could break-off if implanted and cause hypersensitivity reactions and thrombus formation. A polymer concentration of 2 wt% seems to be more compatible with ultrasonic atomization spraying and spraying with this concentration leads to minimal residue formation, and is thus more suitable for use in stent coatings. The surface smoothness was assessed by measuring the mean diameter of droplets. A smaller mean droplet diameter results in a more uneven surface. This may be because at higher temperatures the solvent evaporates quicker, whereas at lower temperatures, the slower solvent evaporation allows a degree of cohesion to occur before all of the solvent evaporates, reducing the mean droplet diameter. A lower spraying temperature therefore leads to a more uneven surface. An uneven surface also aids in 'trapping' circulating endothelial progenitor cells (Cabanlit et al. 2007b). A more uneven surface may therefore aid endothelial healing and reduce the risk of late thrombosis.

### 5.4.2. Mechanical properties

The tensile strength of the cast films is shown in Figure 5.8. The results show the nanocomposite polymer behaves like elastomer. The tensile strength of the films varied between 40-57 $N/mm^2$.

The stress-strain curves of electrosprayed polymer films within the thickness range of 30 µm to 100 µm are given in Figure 5.9. The maximum attainable strain was 300%. The results demonstrated a thickness dependent stress–strain relationship at the size scale of a coronary stent; the typical thickness of a stent is 100 µm (De Beule et al. 2007). These results agree well with SEM images. As shown in Figure 5.9, tensile strength was inversely proportional to the film thickness and this could be due to the presence of increased porosity at higher film thicknesses.

The ultrasonic prepared polymer films were prepared according to the parameters shown in Table 5.4. These films were used for further characterization. The times were varied to alter the thickness of the polymer coating.

Table 5.4. Set of parameters used for films preparation for tensile testing and ICP/MS.

| **Parameter** | **Value** |
|---|---|
| Polymer solution flow rate | 18ml/hr |
| Applied voltage | 15 V |
| Time of spraying | 0.5, 2, 2.5 , 3 hours |
| Temperature of the chamber | 37°C |
| Distance of substrate from spray nozzle | 9cm |
| Polymer solution concentration | 2 wt% |
| Gas flow rate | 0.3 bar |
| Drying condition of the sprayed films | Oven (60° C) |

Tensometry of cast and ultrasonic sprayed samples of different thicknesses was performed and the results are shown in Figure 5.10. The results show that, at 49 and 68 µm, the maximum tensile stress before breaking for both cast and sprayed samples were very similar, with a mean maximum stress of 45±2 MPa for cast samples and 44±2 MPa for sprayed samples. However, there wasis a more difference between cast and sprayed samples at 23 and 31 µm, with a mean maximum stress of 38±3 MPa for cast samples and 33±4 MPa for sprayed samples. The mean elongation at break for cast POSS-PCU2 samples was 530%, whereas that of sprayed samples was 556%.

## 5.5. Comparison of endothelialisation of sprayed and cast films

### 5.5.1. Cell adhesion and proliferation

Alamar Blue (AB) is a non-toxic, simple assay which quantifies cell viability, cell proliferation and cytotoxicity. This aqueous dye is stable in solution and will not affect cell metabolism when added to cell culture media. Cell metabolism results in chemical reduction of colourimetric oxidation reduction indicators incorporated into the dye; resarfurin and resazurin. This colour change may be measured using a colorimetric machine.

The calibration study reveals a linear increase of absorbance with the number of cells (Figure 5.11) showing that the amount of dye metabolised by the cells is an indicator of the number of cell adherent in this case. The colour change from blue to pink was taken as a measure of the overall metabolizing capacity of these cells. After appropriate calibration, the AB assay was found to be equivalent to established cell proliferation assays. AB cell viability assay showed that sprayed films promoted cell adhesion and cell viability. Quantitative analysis of HUVECs attachment on POSS–

PCU2 studied with AB showed a significant increase in mean endothelial cells attachment at 72 hours compared with cast films (Figure 5.12).

### 5.5.2. Cell morphology

SEM images also confirmed the endothelial cells adhered to POSS-PCU2 films (Figure 5.13). HUVECs were adherent to polymer films at 72 hours. SEM clearly visualised the presence of optimal cell – polymer interactions with the formation of numerous filopodia at its surface, flattened ECs and no rounded cells. Cell morphology was consistent with healthy metabolizing cell spread across the films. This suggests that these ECs were capable of morphogenesis and had the ability to proliferate well.

Cells were shown to adhere to both cast and sprayed films. Although cast films although showed a good percentage of cell coverage after 72 hours, coverage was still less than for the sprayed POSS-PCU2 film, which was fully covered by HUVECs. Surface area of the POSS-PCU2 films covered by cells appeared to be greater on sprayed samples compared to cast film. The surface morphology of POSS-PCU2 sprayed films was shown to have a rough undulating surface (Figure 5.13A). AB cell viability assay showed that sprayed films promoted cell adhesion and cell viability.

Ultrasonic atomization spraying therefore created a favourable surface roughness, and ECs adhered well to the nanocomposite surface. So, it can be concluded that ultrasonic atomization spraying provided a surface that encouraged endothelial progenitor cells growth (EPCs) and migration. Uneven surfaces have been shown to promote EPC growth and migration and in the case of vascular stents, an uneven

surface also aids in 'trapping' circulating EPCs (Cabanlit et al. 2007a). Cell metabolism increased between 8 and 72 hours for both those seeded onto tissue culture plastic (TCP) or polymer. Based on the results, this coating technique offers versatility of architecture and supports endothelial cell adherence and proliferation. So spraying the POSS-PCU nanocomposite provides a suitable technology for stent coating applications.

In summary, electrohydrodynamic and ultrasonic atomization spraying approaches have been applied to POSS-PCU nanocomposite polymer coating for metallic stents. POSS-PCU can be successfully subjected to electrospraying and ultrasonic atomization spraying. In this research, polymer stent coatings have been formed with nearly linear control over the film thickness with electrospray deposition time. This has possible application for stent design, especially in smaller stents including coronary and peripheral arterial applications. The tensile strength of the films varies as a function of coating thickness and therefore it is of immense importance to be able to control the film thickness while forming. As a comparison, poly(styrene-b-isobutylene-b-styrene) (SIBS), the polymer used on the Taxus™ stent, has a reported tensile strength of 9.4MPa (the tensile strength repoted > 20 MPa in this study) and an elongation at break of 592% (elongation at break > 400% in this study) and the stress to strain failure of arteries and veins is up to 260% (Antony, Puskas, & Kontopoulou 2003; Lee & Haut 1992). POSS-PCU2, whether cast or sprayed has comparable mechanical properties to the SIBS polymer, which is currently widely used as coronary stents and the stress to strain failure is far superior to that of arteries and veins. Surface morphology revealed that POSS-PCU coated stents by spraying would

have a surface morphology that promotes EPC growth and therefore improve the healing process.

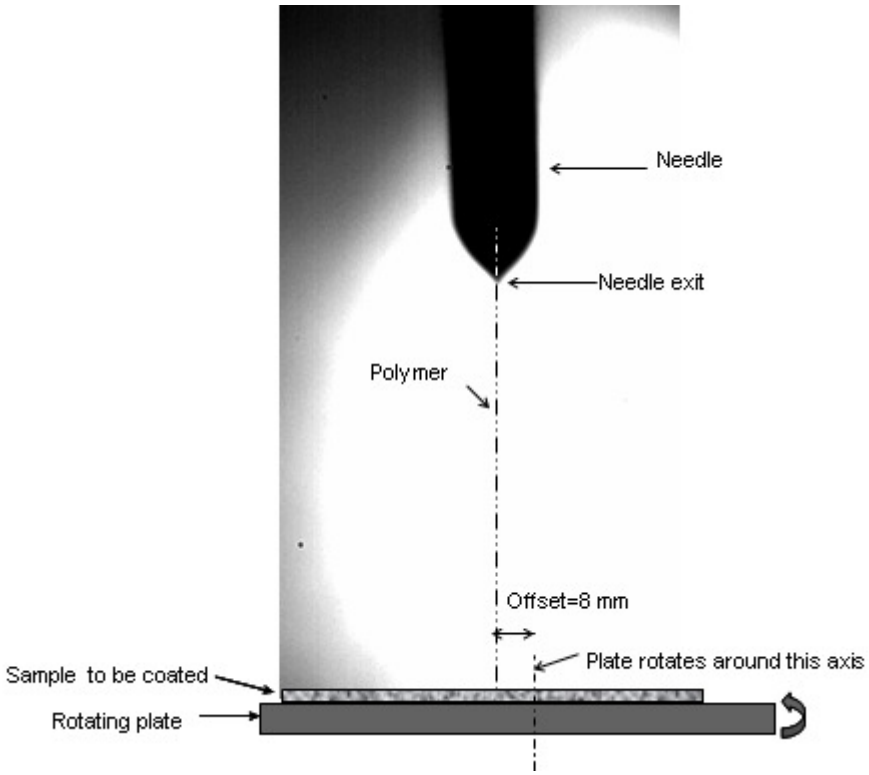


Figure 5.1. The electrohydrodynamic spraying set up for stainless steel coating.

The rotating centre is 8 mm away from the jet.

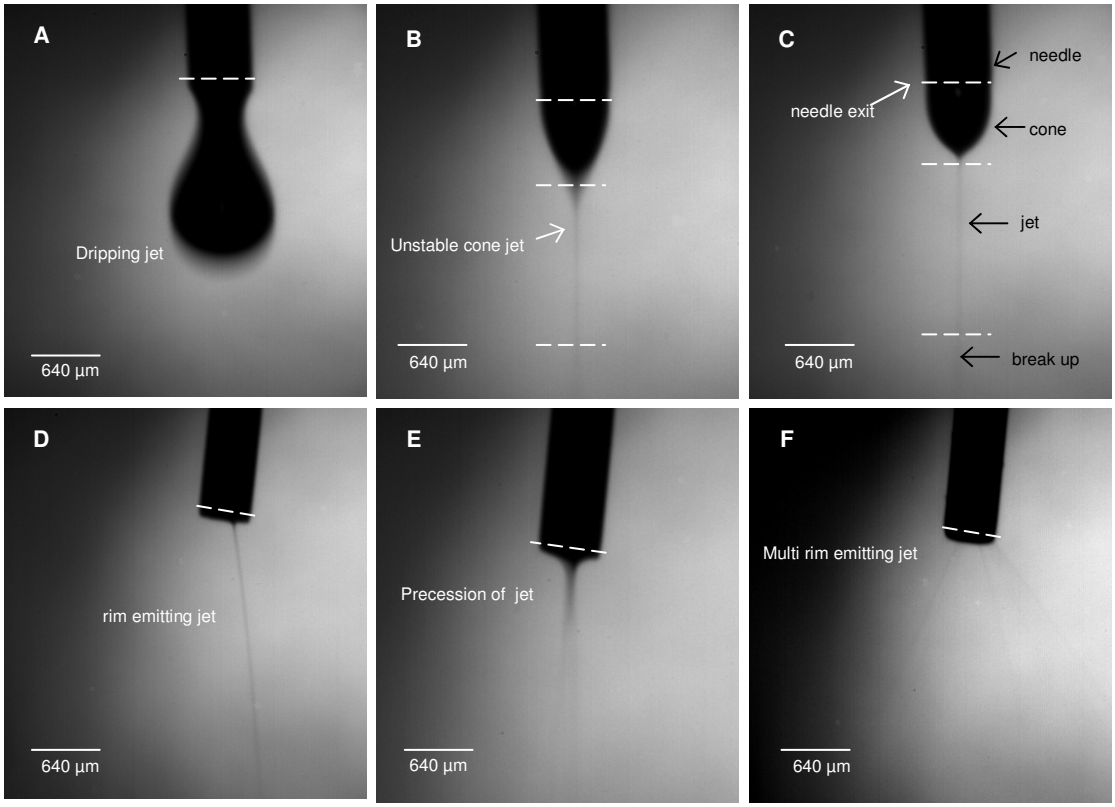


Figure 5.2. Electrohydrodynamic spraying modes obtained from 10 wt% polymer solution at a flow rate of 8 µl/s; (A) dripping mode at 4 kV; (B) unstable cone-jet mode at 5.6 kV; (C) stable cone-jet mode at 6.1 kV; (D) rim emission at 5.8 kV; (E) Precession mode at 8.2 kV; and (F) multi rim emission at 9.5 kV.

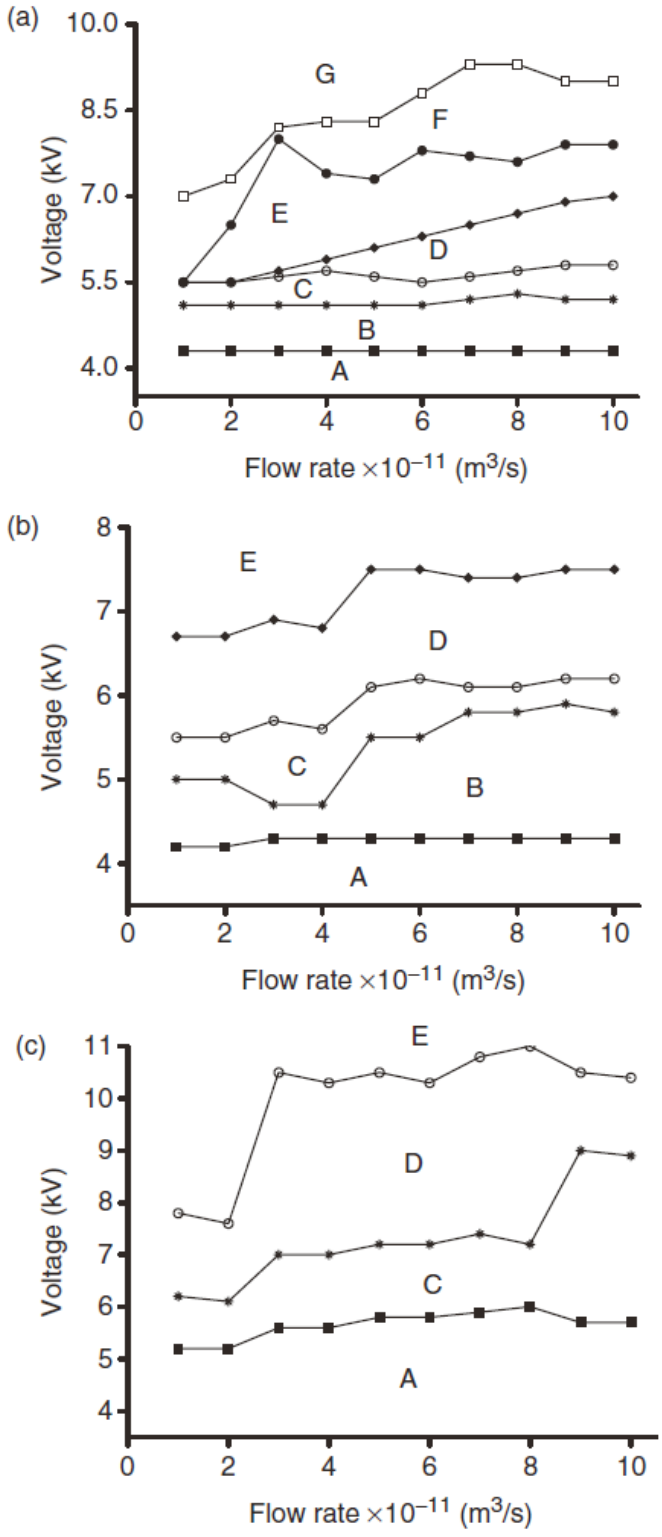


Figure 5.3. Mode Selection map for: (a) 10wt%; (b) 15 wt%; and (c) 20 wt% polymer solution (needle diameter: 300 μm, distance from the substrate: 250mm). The different modes presented are: (A) dripping mode; (B) unstable cone-jet mode; (C) stable cone-jet mode; (D) rim emission mode; (E) precession mode; (F) multi-rim emission.

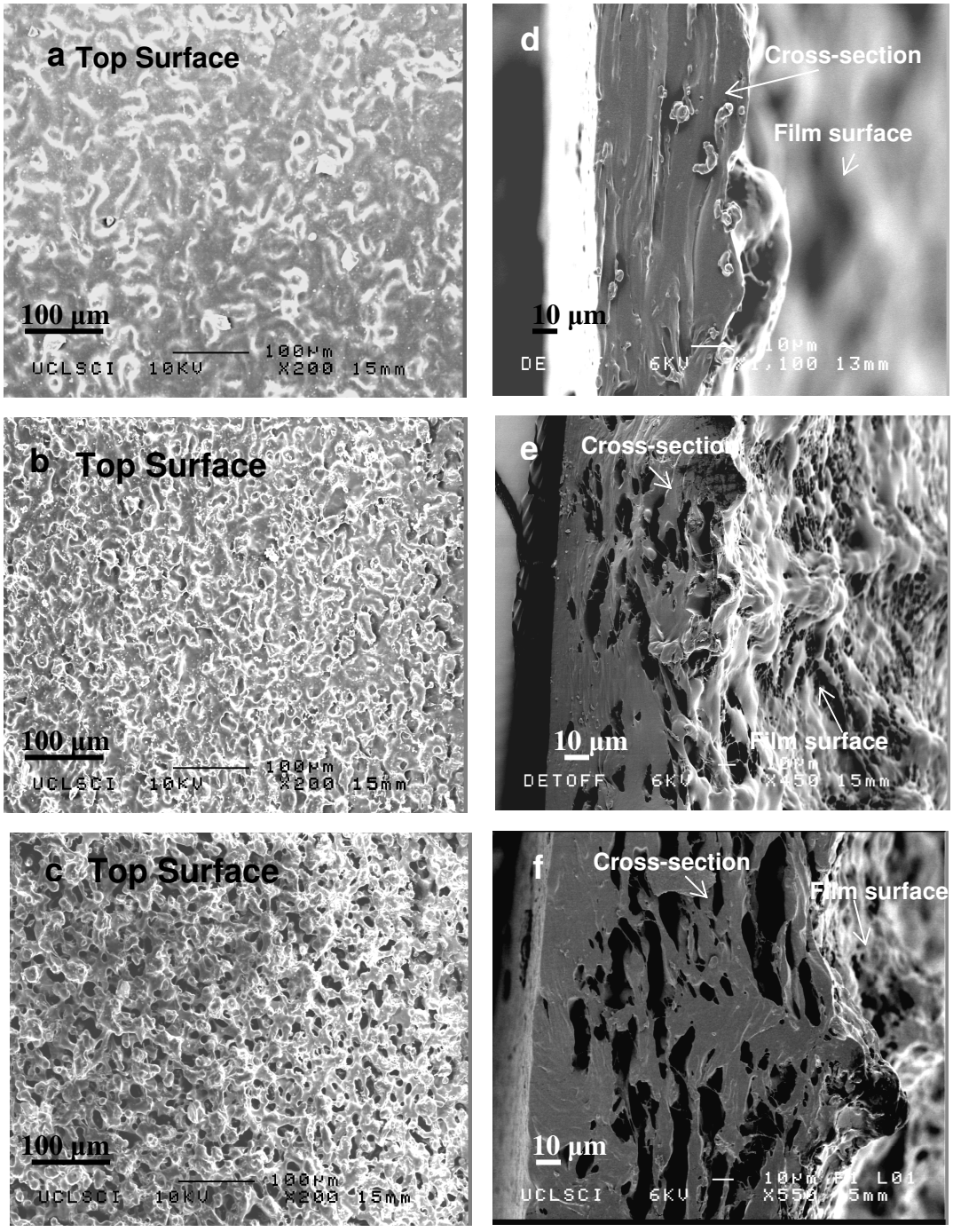


Figure 5.4. Morphology of the electrosprayed films after (a, d) 1 hour, (b, e) 2 hours, (c, f) 3 hours.

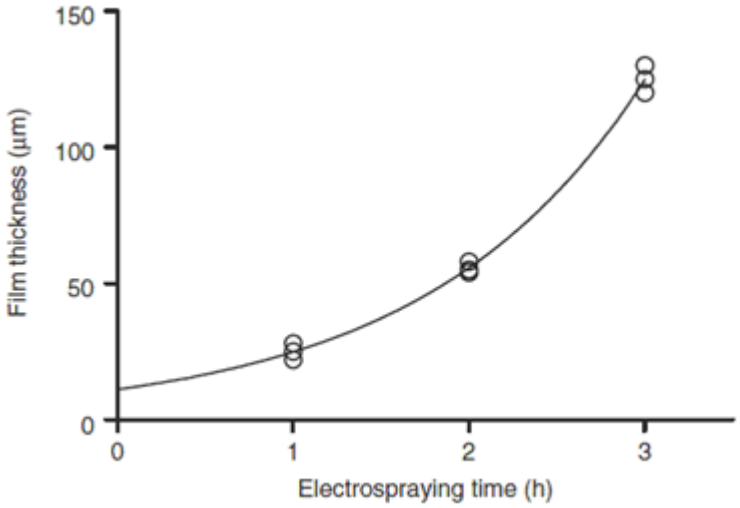


Figure 5.5. Film thickness as a function of electrospraying time.

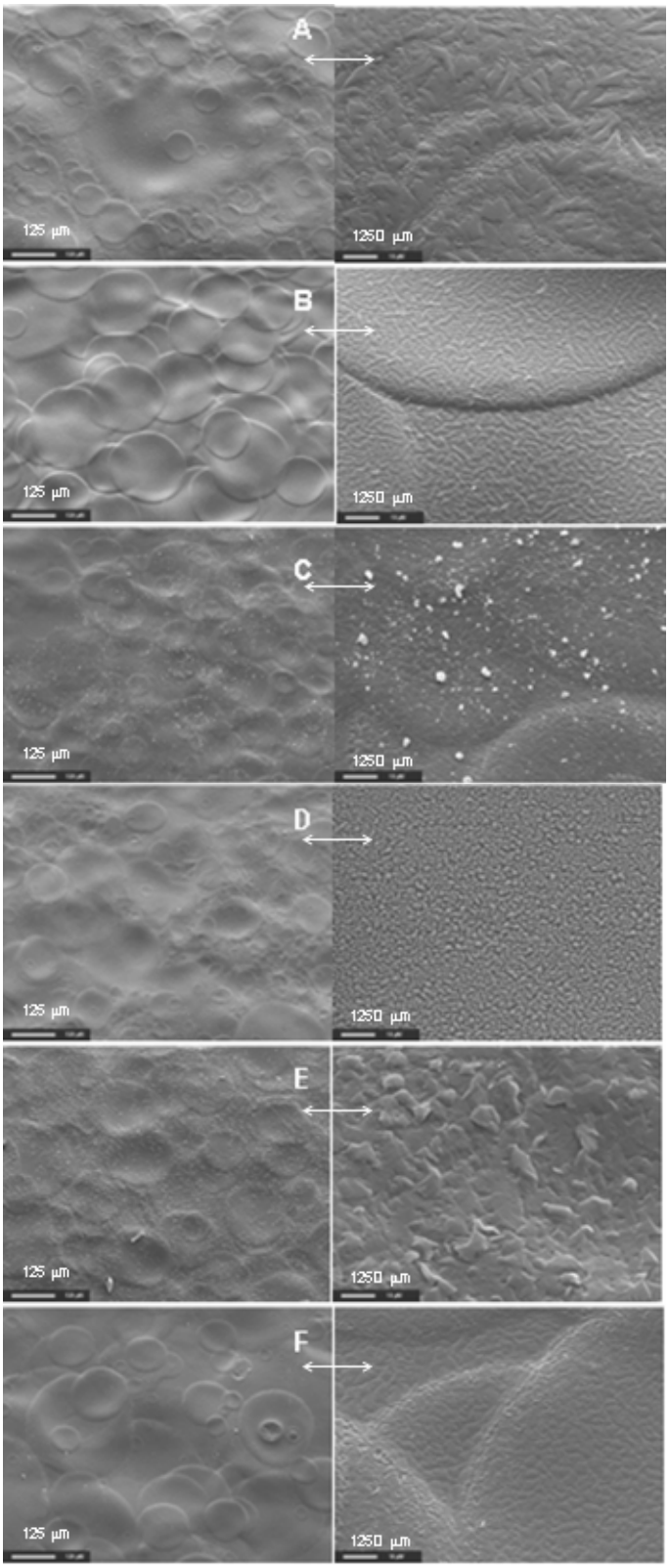


Figure 5.6. SEM images of polymer films. Each sample is displayed at left) ×160 and right) ×1250 magnifications (A-F represent sample numbers 1-6 respectively as defined in Table 5.2). Continued

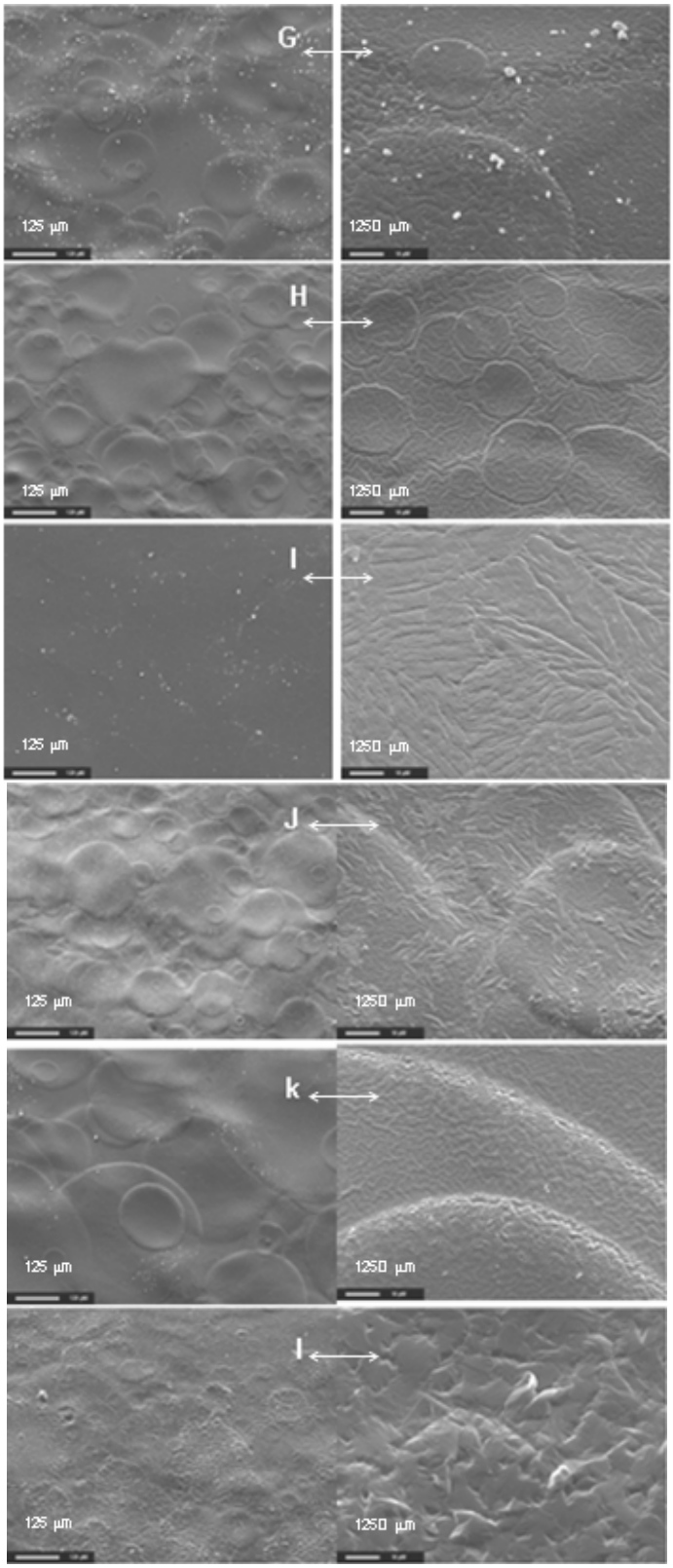


Figure 5.6. SEM images of polymer films. Each sample is displayed at left) ×160 and right) ×1250 magnifications (G-I represent sample numbers 7-12 respectively as defined in Table 5.2).

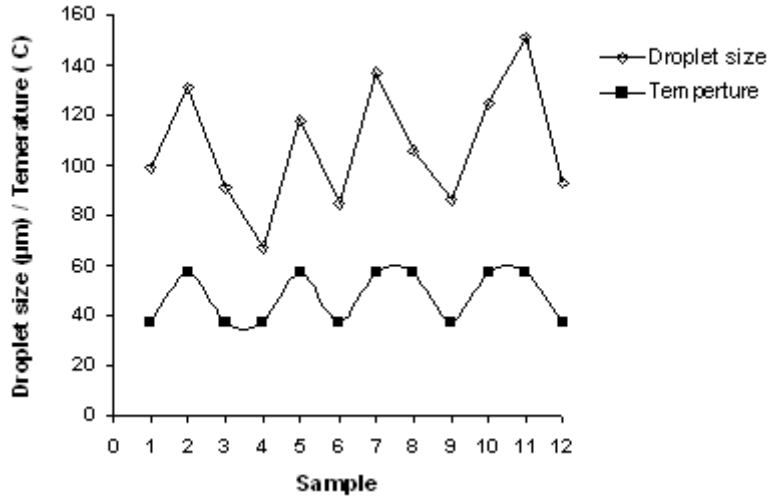


Figure 5.7. Graph showing the relationship between spraying temperature and mean polymer droplet diameter.

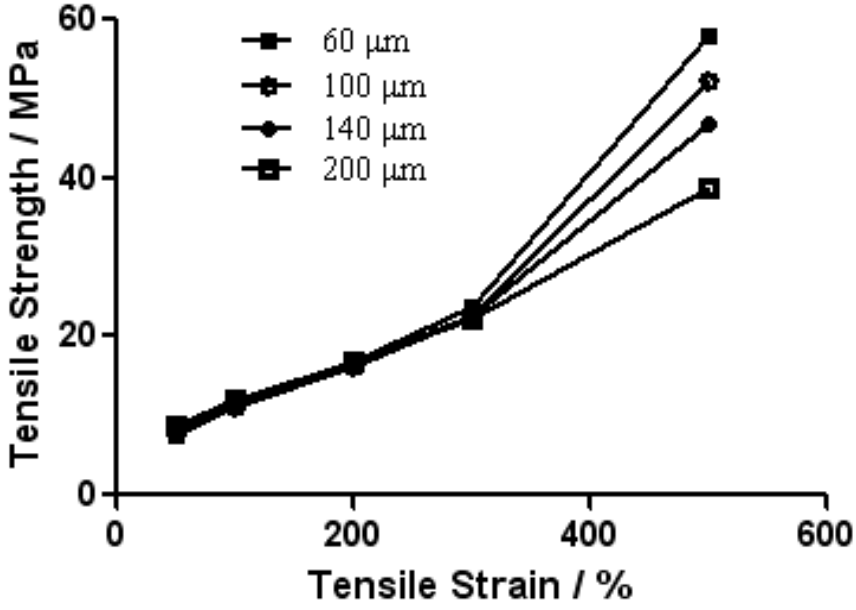


Figure 5.8. Tensile strength of cast films.

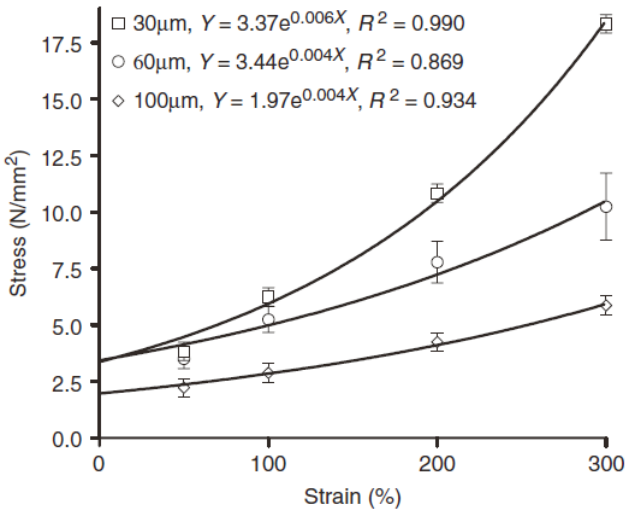


Figure 5.9. Comparison of tensile stress between films prepared by electrohydrodynamic spraying with different thicknesses.

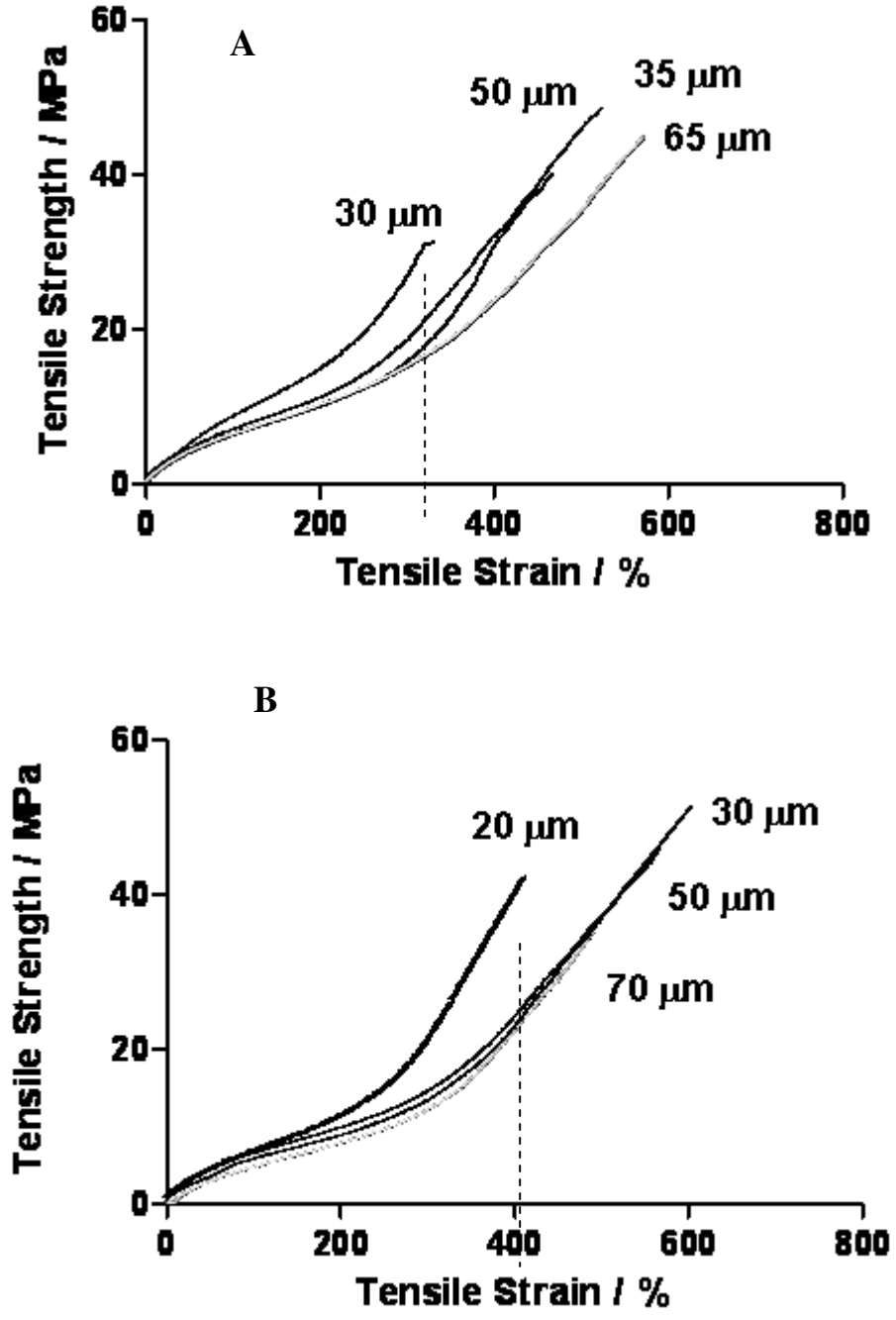


Figure 5.10. Comparison of tensile stress between films with different thicknesses. Films prepared by: (A) casting; and (B) ultrasonic atomization spraying.

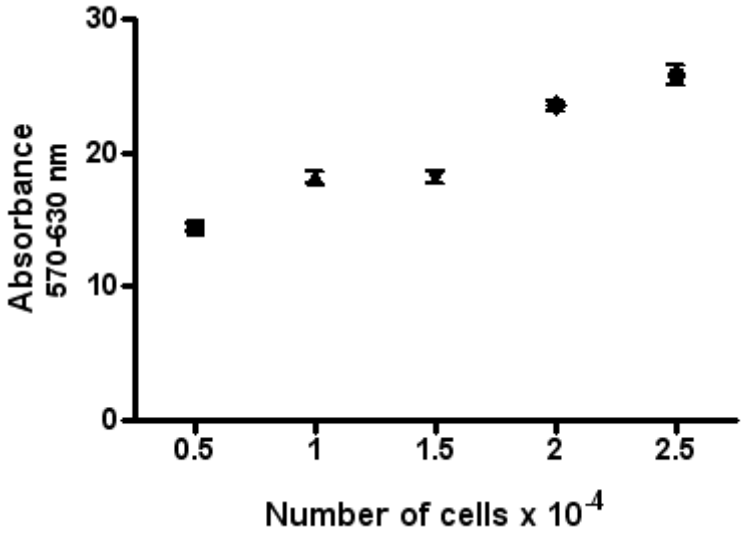


Figure 5.11. Alamar Blue standard calibration curve for HUVECs.

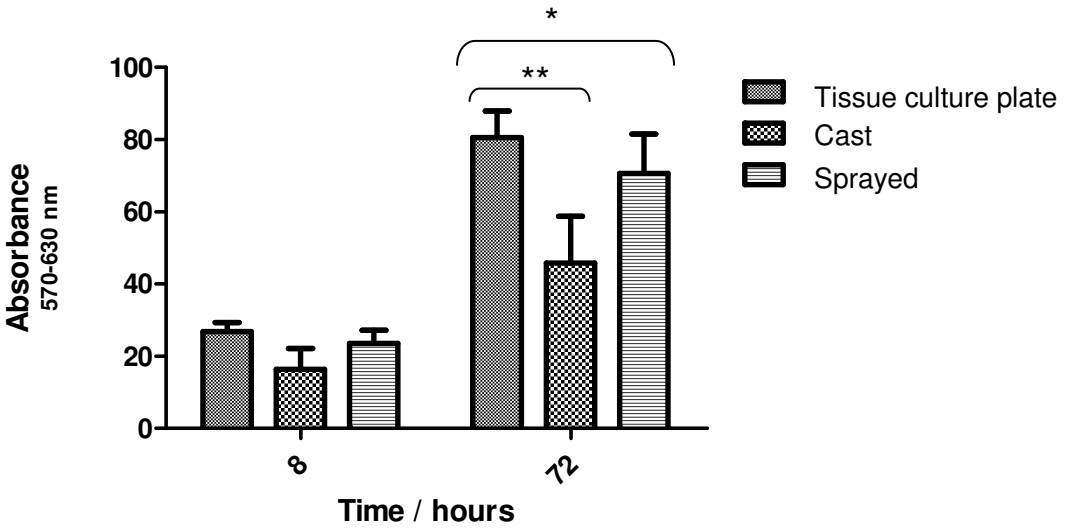


Figure 5.12. Alamar Blue viability assay on HUVECs exposed to POSS-PCU2 nanocomposite for 8 and 72 h.

Keys:

** $p<0.05$ Significant against cast.

- $p>0.05$ Not significant against sprayed.

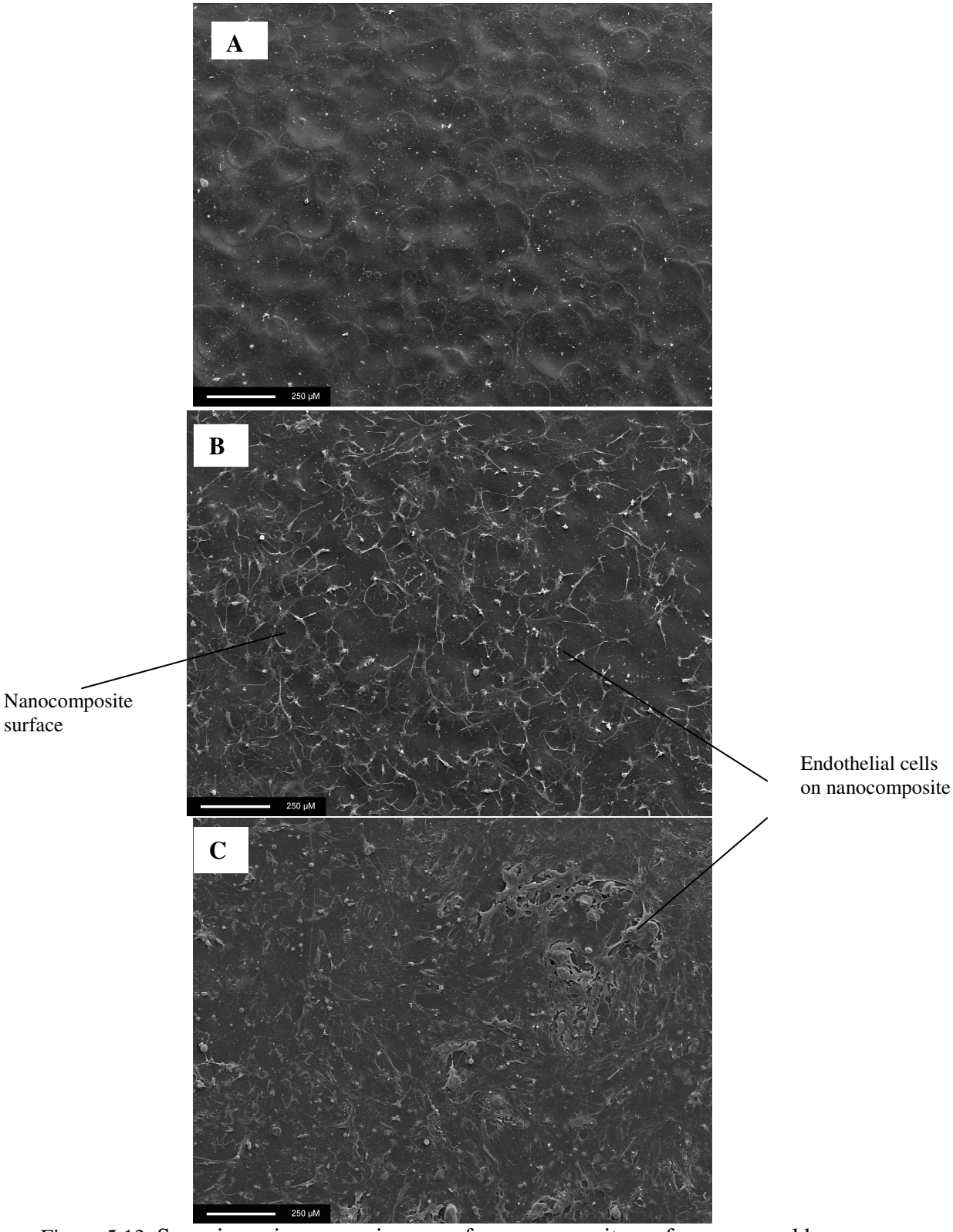


Figure 5.13. Scanning microscopy images of nanocomposite surface prepared by ultrasonic atomization (A). HUVECs adhered to nanocomposite after 24 hours on film surface prepared by casting (B); and ultrasonic atomization spraying (C). Inset: Images show that the percentage of cell coverage on sprayed film is more than that on the cast film.

# CHAPTER 6. Surface Modification of NiTi to Enhance Bonding of Nanocomposite

This chapter presents an innovative approach to self-expanding coronary stent preparation. The aim of this work was to coat NiTi stent alloy with POSS-PCU2 and increase the stability of the coating. In prolonged applications in the human body, the corrosion of the NiTi alloy can result in the release of deleterious ions which leads to unwanted biological reactions. Coating the NiTi surface with POSS-PCU can enhance surface resistance, reduce Ni release and therefore improve biocompatibility. Failure of the coating *in vivo*, reduces the efficiency and imparts even more complexity to the implant including formation of debris which can induce thrombus formation.

In the Chapter 4, POSS-PCU hybrid nanocomposites with different formulations were been characterised in terms of bulk properties and most importantly surface properties which affect the blood/tissue interaction *in vivo*. POSS-PCU2 has been chosen for the stent coating stents application. In Chapter 5, electrohydrodynamic spraying and ultrasonic atomization spraying methods were investigated in order to apply POSS-PCU nanocomposite polymer to metallic stents (Bakhshi et al. 2008). Both these investigations in the previous chapters involved choosing the material and coating technique with ideal characteristics for coating stent technology.

This research describes surface modification to promote bond strength between the POSS-PCU2 nanocomposite and the surface of NiTi strips. The aim is to develop protocols with the potential for effective bonding of the nanocomposite polymer to

NiTi in the development of stents; including coronary or peripheral stents. In this work the stability and the integrity of the POSS-PCU2 coating in pseudo-physiological solutions is also evaluated to determine whether the surface modification applied retains its effectiveness long-term. Prior to deposition the NiTi was surface modified. The peel strength of the deposit was studied before and after degradation of the coating.

## 6.1. NiTi alloy superelastic properties

Figure 6.1 shows the stress-strain curve obtained for the NiTi strip. In the first loading cycle, the specimen was tensioned to a stress of approximately 650 MPa before being unloaded. This stress was high enough to induce a full transformation, with a stress-strain curve following a nonlinear loop that is characteristic of the superelastic response of Nitinol. This behaviour confirms that the material is fully superelastic at room temperature. Quantitative analysis of the stress-strain curve shows that the Young's modulus of the material varies greatly across its superelastic strain range.

## 6.2. Surface characterization of NiTi after surface modification

### 6.2.1. Assessment of oxide layer thickness

At the end of the anodisation process, the sample surface appeared dark brown and was free of cracks, which is an indication of oxygen efficiency. Figure 6.2 shows the cross-sectional views of the NiTi strips before and after anodisation. After anodisation, the thickness of the strip increased by 20 μm and this indicates the formation of a uniform oxide layer (Figure 6.2B). The measurement of the thickness of this layer was estimated up to the curvature which leads to the base of the metallic strips. These measurements compare well with the 17μm reported by Cheng et al.

(Cheng et al. 2005) who used a similar process and deposition time. However, these values are significantly higher than those achieved using other methods of preparing oxide layers on NiTi alloys. For example, oxide layers with a thickness of ~0.5µm have been prepared using solution-based oxidation with hydrogen peroxide (Hu et al. 2007). Furthermore, much finer oxide coatings (2 nm) can be prepared by controlling the partial pressure of oxygen in a selective oxidation process, but this requires more sophisticated equipment including the use of atmospheric sensors (Pohl et al. 2008).

A current density of $3\times10^{-2}$ mA/mm$^2$ was selected for the anodization process. This value was selected based on previous studies (Cheng et al. 2005), although the thickness of the NiTi strips in this application is much thicker (2mm compared to 0.5mm). With the anodisation process lasting for three hours, it was anticipated that during this procedure the anode potential rises with time and can reach a value of 1.15V, and these measurements have been used as indicators of coating thickness. It is postulated that $TiO_2$ is formed as a result of hydrolysis and polycondensation of titanium methoxide in the presence of water (Cheng et al. 2005). Even if the surface layer is nickel oxide, it still provides a suitable platform for binding of aminosilane, since an oxide layer is required for silanisation. Electrolytic methods have been used to coat surfaces of NiTi alloys. For example thin tantalum coatings on NiTi alloys enhance resistance to corrosion when placed in a 3.5% NaCl solution (El Abedin et al. 2005).

Figure 6.2C shows the thickness of the modified NiTi strip was reduced by ~5µm after heat treatment at 600°C for 1hr; compared with the thickness before heating. Hence on heating, densification occurs and the thickness of the coating is reduced.

The structure of these coatings (Figure 6.2) shows the existence of micro to nanoscaled pores within the coating layer. Some pores are still evident in the post-heated coating, which means that an optimal heating temperature or time is desired. The aging of the oxide layers by heat treatment is also believed to reduce the ion dissolution and improve its alloy biocompatibility, which makes the material ideal for its application (Wisbey et al. 1991). However, it should be noted that the mechanical response of the material is affected by heat treatment. A study of this effect has been carried out previously (Liu et al. 2008). It showed that the material's austenite phase formation end temperature, which is critical to superelastic response, increases after heat treatment and is a function of heat treatment time and temperature. Careful management of the heat treatment process can be used to optimise the mechanical response of the material for the requirements of an intravascular device. Simply by changing the temperature and duration of the heat treatment, one can optimise the procedure to maintain superelastic properties of the NiTi (Liu et al. 2008).

### 6.2.2. Surface topography

The surface morphology varies markedly between anodised and anodised-heat modified strips (Figure 6.3). Anodized samples present micro-scaled topographical variations of the surface which consist of valley and mountain like features. Upon thermal oxidation which reinforces the initial oxidation process from the anodisation procedure, smaller sized nano-scaled peaks develop which make the surface more even. This is largely due to coalescence of the oxide layer, which results in a more homogenous surface.

### 6.2.3. Surface chemical mapping

The oxygen (O) peak in the spectrum obtained for anodized NiTi confirms the presence of an oxide layer through anodisation (Figure 6.4B). The O peak observed has the same order of intensity as the titanium peak; the major alloying element of NiTi. The intensity of the Ni peak is less than that of the Ti peak which favours biocompatibility since it reduces the risk of nickel release.

As described earlier in experimental details (Chapter 3), the silanisation process involves four steps; namely, hydrolysis, condensation, hydrogen bonding and crosslinking. Control of each step will affect the efficiency of the whole process. To optimise the silanisation process, a few parameters were altered such as hydrolysis time, concentration of silane solution and pH. These parameters were changed in accordance to the Taguchi method (Taguchi 1986) as shown in Table 6.1. The Taguchi method for parameter optimisation allows the effect of multiple parameters on a performance characteristic to be assessed in a condensed set of experiments. For example, in the Table 6.1, the Taguchi method has allowed three parameters with two levels of variability (hydrolysis time, concentration of silane solution, pH) to be assessed in four experiments. In contrast, to test all variables, eight ($2^3$) would be required.

Table 6.1. Orthogonal Arrays for parameter testing.

| Experimental Number | Parameters | | |
|---|---|---|---|
| | Concentration of silane solution/ vol% | pH | Deposition time/ min |
| 1 (A) | 2 | 4 | 15 |
| 2 (B) | 2 | 8 | 60 |
| 3 ( C) | 5 | 4 | 60 |
| 4 (D) | 5 | 8 | 15 |

Key: The amount of Si in Table 6.2 is calculated according to the experiments in Table 6.1.

The chemical composition of the NiTi surface after different silane modification conditions is compared in Table 6.2. The strip under modification (A) is rich in Si uniformly in all regions whereas hardly any Si could be detected on all the regions selected for the rest of the surface by SEM/EDX. Energy dispersive X-ray analysis (EDX) analysis on the whole surface showed Si peaks of moderate intensity indicating that a 5% silane solution at pH=4 and 1 hour deposition results in a rather uniform silane film. The hydrophobic siloxane layer is usually ten molecular layers thick (up to 800 nm), depending on the silane concentration (Sundararajan & van Ooij 2000; van Ooij et al. 2006).

The chemistry of the NiTi surface after each step of surface treatment has been studied by X-ray Photoelectron Spectroscopy (XPS). In contrast to EDX, XPS has much higher surface sensitivity (probing depth in the nm rather than mm range). Figure 6.5 shows typical XPS survey spectra of the surfaces of the NiTi strip. The analysis of all observed peak intensities in the survey XP spectra allows a quantification of the elemental composition of the surface region probed by XPS. The surfaces of four samples were analysed: NiTi alloy as received, NiTi after anodisation, NiTi after heat treatment at 600 °C and NiTi after silanisation. Relative atom concentrations (at %) of all elements found are summarized in Table 6.3.

The as-received sample showed a surface dominated by a relatively thick layer of carbon and oxygen. There was a clear preference for a 'capping' layer of $TiO_2$. Nickel was detected at low levels, due to attenuation by the carbon/oxygen/titanium over layers. Analysis of the C(1s) and O(1s) high resolution scans suggest a large degree of hydrocarbon contamination on the surface together with carbide. Survey

scan revealed that the surface also consisted of N, Na, Cl, Ca and Si. The Si content on the surface was due to the lubricant; which disappeared after cleaning and anodisation. The presence of C may be attributed to surface contamination by carbon-containing molecules absorbed from the environment.

Table 6.2. Composition of the Si compositions (in wt.%) measured by EDX for different silane modification scenarios. A) 2%, 15min, pH=4; B) 2%, 1hour, pH=8; C) 5%, 1hour, pH=4; D) 5%, 15min, pH=8;

| Spectrum | A | B | C | D |
|---|---|---|---|---|
| Spectrum 1 | 1.68 | 1.33 | 0.48 | × |
| Spectrum 2 | 3.11 | × | 0.31 | 0.68 |
| Spectrum 3 | 0.89 | × | 0.94 | × |
| Spectrum 4 | 0.62 | 0.58 | 0.90 | 0.53 |
| Average | 1.57 | 0.48 | 0.66 | 0.30 |

Key: × Si is not detectable because the silane concentration in that area was lower than the range detectable by EDX.

Table 6.3. Surface composition obtained from the quantification of the XPS survey spectra.

| Element | NiTi alloy (As received) | | Anodized NiTi | | Heated treated NiTi at 600°C | | Silanised NiTi | |
|---|---|---|---|---|---|---|---|---|
| | At. % | BE eV | At. % | BE eV | At. % | BE eV | At. % | BE eV |
| O 1s | 34.47 | 530.41 | 46.62 | 530.03 | 48.89 | 530.01 | 49.36 | 530.034 |
| C 1 s | 54.15 | 284.912 | 27.39 | 285.03 | 25.44 | 285.51 | 28.31 | 285.34 |
| N 1s | 1.04 | 399.91 | 1.01 | 398.53 | 0.96 | 399.51 | 3.36 | 400.34 |
| Si 2s | 3.99 | 152.91 | × | × | × | × | 3.98 | 153.84 |
| Ti 2p | 3.34 | 458.41 | 10.24 | 458.03 | 12.72 | 458.51 | 7.51 | 458.34 |
| Ni 2p | 1.00 | 855.41 | 4.76 | 855.53 | 4.84 | 855.01 | 6.85 | 855.34 |
| Ca 2p | | | 0.86 | 384.03 | 0.26 | 347.01 | 0.64 | 346.84 |
| Na KLL | 1.41 | 495.41 | 8.22 | 495.53 | 5.19 | 496.51 | | |

Key: × is not detectable. BE: Binding energy

The dominant elements after anodisation process were O, C, Ti. The anodized sample showed a surface more enriched in Ti compared to the NiTi as received. Ni content had also increased, but not as much as Ti. Titanium is again in a $TiO_2$ like form, but exhibited broadening to low binding energy, possibly due to a lower oxidation state of titanium (e.g. Ti(III)). Other elements present on the surface were: N, Ca, Cl and Na. The Na content was much higher than in the NiTi as received. This might be because of the anodisation has been done in sodium nitrate solution in methanol. Si was not detected in the sample after cleaning and anodisation.

The heat treated sample again showed preference for Ti (as $TiO_2$) at the surface. C, N, Na, Ca, Cl and Si were also present. Ni was present as Ni(II), the shape of the spectrum was characteristic of NiO. It is worth noting that the heat treatment process had affected the Ti content more than Ni. The surface Ti concentration of the heat treated sample could be as high as 12.72 at%. These results suggest that the anodized sample was covered by a titanium oxide film. The silanised sample showed preference for Ti (as $TiO_2$) at the surface. No sodium was detected. N (1s) intensity was increased. High resolution scans of N(1s) level revealed two nitrogen states, 399.4 and 401.2 eV. The former may be characteristic of $NH_x$-like species, whereas the latter is more than likely associated with a surface bond. This is because of the $NH_2$ group in 3-aminopropyltriethoxysilane used in the silanisation process. Detection of the Si signal also indicates silanisation has occurred.

The coating method had three steps where the anodisation process involved the formation of an oxide layer which then reacted with 3-aminopropyltriethoxysilane. The final step involved the binding of the free isocyanate groups in the polyurethane

nanocomposite with the free amine groups of the 3-aminopropyltriethoxysilane. The schematic illustration of these bonding mechanisms between the reagents and NiTi strips is shown in Figure 6.6.

## 6.3. Bonding strength

The approach employed was based on the ASTM D413 standard, which is used to determine the force per unit width required to separate a rubber layer from a flexible substrate such as fabric, fibre, wire, or sheet metal ( 2007). The standard describes methods for peeling the strip with the unpeeled portion held to give $\alpha^{\circ}$ separation with moving grips. The adhesion strength is equal to the mean force recorded during the test.

The cross section of the polymer coatings deposited by EHDA and casting on modified NiTi are compared in Figure 6.7. Castings (Figure 6.7A) produced a more uniform coating than electrospraying (Figure 6.7B, C). In addition, in the case of electrosprayed coatings the thickness could be varied very effectively by adjusting the spraying time. Peel strength data (Figure 6.8) confirmed that a significant improvement in adhesion could be achieved by using the described modification procedures in experimental details (Chapter3). Analysis of the data showed that above an extension of 25 mm the load required to remove the polymer from the modified strip for all the samples was, on average, three times greater than that for the control.

There was no significant difference between the bonding strength as a result of the different coating methods (Figure 6.8). Considering EHDA deposition, the peel strength of the 100 μm thick polymer coating was slightly greater than that for the 50

μm thick coating. It should be noted that below an extension of 10 mm, all the curves of the modified specimens showed a positive slope. In this range the applied load was not high enough to break the bond between the polymer and the strip; however, the applied extension caused the exposed polymer (i.e. the polymer that was manually peeled from the strip) to strain. The initial region of the curve should be ignored and it is not significant to the overall peel strength measured. It is possible to apply a coating thickness of < 10 μm, however such specimens were difficult to handle for peel strength testing. So, the specimen thickness used in this study was increased to facilitate peel strength testing. The proposed surface treatment can be applied to a range of strut/wire thickness. Yin Y. et al. (Yin et al. 2009) used the same peel test technique for assessment of bond strength of the coating on metal surfaces.

Stainless steel is another metal widely used in the construction of commercially available coronary stents. To see how surface treatment utilized in this work may influence the functionality of stainless steel; the same protocol for surface treatment was applied on stainless steel substrates. Upon applied silanisation process, a about three times improvement in the bond strength observed compared to the non-treated stainless steel. The results show that this surface treatment protocol is still effective when stainless steel material is used as the stent for coating. Results are shown in Appendix B.

## 6.4. Coating durability

The susceptibility of POSS-PCU2 coated-NiTi to instability was assessed *in vitro* by incubating the coated strips that had been modified in biological/chemical solutions, as were un-modified samples. These solutions included hydrolysis with lysosomal

enzymes, plasma protein fractions (I-IV), oxidation and peroxidation with distilled water as control. More details of the solutions have been described in experimental details (Chapter 3).

The surface topography of the aged samples is shown in Figure 6.9. Topographic and structural changes due to aging can influence the adhesion properties of the coating, leading to coating failures. The nanocomposite polymer coating incubated in distilled water characteristically showed a smooth and uniform surface (Figure 6.9A). Also, no cracks or failure of the coatings were observed for the polymer coating subjected to hydrolysis (Figures 6.9B, C). The coating exposed to plasma fractions still appeared uniform, which indicates sufficient interfacial adhesion (Figures 6.9D, E). Pores or surface cracking was visible on the surface of the nanocomposite exposed to oxidative degradation (Figure 6.9F). Incubation of the POSS-PCU in oxidative environment such as t-butyl peroxide in the presence of cobalt chloride as the catalyst resulted in increased surface degradation (crack formation). This effect was more pronounced with the $H_2O_2$ systems (figure 6.9G). Therefore, the nanocomposite coating incubated in oxidative solutions did not exhibit the required resistance to oxidative environment. As summary of the results are shown in Table 6.4.

Three modes of chemical degradation predominate *in vivo*: mineralisation, hydrolysis and oxidation. In recent years it has become apparent that polyurethanes are particularly susceptible to the latter two processes, both of which lead to the phenomenon of environmental stress cracking.

POSS-PCU appeared resistant to both PLA and CE as judged by a lack of environmental surface cracking (ESC). ESC was observed in POSS-PCU2 exposed to the $H_2O_2/CoCl_2$ mixture, and most particularly to the t-butyl peroxide mixture. Zhao et al proposed that plasma proteins were able to act as ESC promoters in poly(ether)urethanes, although the mechanism of action remains unknown (Zhao 1991). Notably, POSS-PCU showed no ESC compared to water incubated controls.

Table 6.4. Effect of aging solution on POSS-PCU2 coating surface.

| Solution | Surface cracks observed in SEM images |
|---|---|
| $H_2O$ | - |
| Plasma fraction I | - |
| Plasma fraction II | - |
| Plasma fraction III | - |
| Plasma fraction IV | - |
| Phospholipase $A_2$ | + |
| cholesterol esterase | + |
| hydrogen peroxide/cobalt chloride | |
| tert-butyl peroxide/cobalt chloride | |

The $H_2O_2$ (Co) solution provides an oxidative reaction comparable to that observed in the functional activity of the inflammatory cells in response to some biomaterials (Hooper 2000). However, a solution concentration of 1.63 M $H_2O_2$ -which is very high compared to that reported by Lee et al. (Lee 2007), which is < 20µmol- was used.

Some biomaterials influence the functional activity of inflammatory cells, so an increase in release of hydrogen peroxide by cells is observed (Hooper 2000). In some instances, material-mediated inflammatory responses may even cause degradation of the material itself (via oxidative products released by implant-associated

inflammatory cells) (Tang 1995). *In vivo*, such degradation is caused or enhanced by the action of metabolic products such as hydrogen ions, lysosomal enzymes and peroxides released from the adherent leukocytes and foreign body giant cells at the cell-polymer interface (Zhao 1991). In the study by Lee *et al.* (Lee 2007) hydrogen peroxide generated by activated macrophages and neutrophils, in a lipopolysaccharide model of acute inflammation was imaged using peroxalate nanoparticles. Although $H_2O_2$ (Co) solution provides an oxidative reaction comparable to that observed in the respiratory burst of adherent macrophages and foreign-body giant cells (Zhao 1993), the concentration used in this work (1.63 M $H_2O_2$) was very high compared to that reported by Lee et al (Lee 2007), which is < 20µm.

In this study, peel strength analysis showed that, in spite of accelerated degradation, the coating showed no significant difference in adhesion properties between the control, hydrolytic and plasma-degraded nanocomposites (Figure 6.10). This is an indicator of the stability of the surface modification applied and coating durability to these types of *in vitro* degradation. When compared to the similar experiments performed on non-modified NiTi, the modified NiTi showed significantly greater stability in a degradative environment. In fact, the non-modified specimens lost their polymer coating completely after a few weeks. The surface modification proposed retained its effectiveness to promote coating adhesion to the NiTi. It is important to note however that in the case of $H_2O_2$ and t-butyl-peroxide-degraded nanocomposites, a decrease in peel strength was observed. Therefore, except in aggressive oxidative environments, the polymer coating on the modified NiTi stent alloy withstands effects of biological environments without any signs of instability or delamination.

The problem of delamination is particularly challenging with stent coating applications, and requires full consideration of the interface between the coating and the underlying substrate. Ruptures and cracks could be problematic by inducing fast restenosis and uneven surface structures are a major cause of thrombogenic events with stent implants (Unger et al. 2007). Therefore, coatings are expected to minimize the risk of bare metal parts getting into direct contact with tissue throughout the stent lifetime. A few studies have investigated the effect of mechanical strain forces encountered during stent deployment. They have examined the integrity of the coating on the stent by studying any sign of cracking or delamination of the coating after balloon expansion and implantation (Chen et al. 2005; Cho et al. 2008; Hanefeld et al. 2006c; Richard et al. 2005; Sternberg et al. 2007; Unger, Westedt, Hanefeld, Wombacher, Zimmermann, Greiner, Ausborn, & Kissel 2007; Wang et al. 2008; Westedt et al. 2006; Zhang et al. 2006).

## 6.5. Corrosion resistance

As described in detail in Experimental details (Chapter 3), three set of NiTi strips were chosen for corrosion resistance studies. The first group was surface modified NiTi strip coated with POSS-PCU2 according to the method which was shown to lead to a much greater resistance to decay in peel strength compared to untreated NiTi. The second group was untreated NiTi strip coated with POSS-PCU2. Bare NiTi strips were chosen as the control. The Ni release from all three groups in plasma fraction I and Dulbecco's modified Eagles' medium (DMEM) was measured by Inductively Coupled Plasma Mass Spectroscopy (ICP-MS).

The Ni release tests (Figure 6.11) clearly showed the effect of coating NiTi samples with POSS-PCU2, even after one hour. In both media, Ni release was much greater from the bare NiTi samples, reaching 1521ng/mL in the plasma fraction and 1784 ng/mL in DMEM after 3 days compared to 3.15 ng/mL and 4.16 ng/mL, respectively, for surface treated sprayed NiTi samples (p value = $3 \times 10^{-8}$, p value < 0.001 which shows a significant difference). In addition, there is also a difference between untreated POSS-PCU2 coated NiTi samples and surface treated samples. After 3 hours, the amount of Ni released from untreated sprayed samples was higher than the amount released from surface treated samples, 31.27 ng/mL and 13.77 ng/mL released from untreated NiTi samples in plasma fraction and DMEM, respectively, compared with 3.514 and 4.163 from surface treated samples (p value = $5 \times 10^{-6}$; p value < 0.001 which shows a significant difference). It is also important to note that the POSS-PCU coated samples (both treated and untreated), not only reduced the amount of Ni released, but also significantly reduced the rate at which it was released, shown by the minimal change in Ni concentration between 1 hour (6.89±1.97 ng/mL) and 72 hours (13.32±8.70 ng/mL). This is compared to an increase in Ni concentration of more than 1300 ng/mL between 1 hour and 72 hours. Based on these results it is clear that coating with POSS-PCU2 reduced the amount of Ni released to a negligible amount. Surface treatment process of the NiTi strips before coating helped this effect further. This process increased the strength of the bond between polymer and NiTi and thereby increased the corrosion resistance. This is of great importance as the release of Ni from NiTi can result in tissue damage and therefore delay healing and increase the risk of thrombus formation (Berger-Gorbet et al. 1996b; Heintz et al. 2001b).

In summary, an approach for depositing the POSS-PCU2 onto NiTi self-expandable stent is outlined. This involves pre-modification of the metal alloy and electrohydrodynamic polymer deposition. The effective surface modification protocol has been deduced. The coating has the potential to protect the materials surface, mitigate corrosion and increase the longevity of the device *in vivo*. The results of peel strength have shown that a three-fold increase in the bond strength of the POSS-PCU2 to the metal alloy can be readily achieved upon surface modification. Comparative *in vitro* degradation of the coating on modified and non-modified NiTi was carried out and demonstrated the ability of the coating to remain integral with the stent after long period (70 days) of exposure to biological environments under static conditions. It is also indicated how the adhesion strength of the POSS-PCU2 coating changes post-exposure to physiological solutions comprised of hydrolytic, oxidative, peroxidative and biological media. This part of the study shows that the modified NiTi presents far greater resistance to decay in peel strength compared to the non-modified NiTi. Ni release profiles showed the dramatic effect that POSS-PCU had on the corrosion resistance of NiTi samples. It is clear that coating with POSS-PCU reduced the amount of Ni released to a negligible level. This effect was exaggerated by surface treatment of NiTi before coating. This process increased the strength of the bond between polymer and NiTi and thereby increases the corrosion resistance. This is of great importance as the release of Ni from NiTi can result in tissue damage and therefore delays healing and increases the risk of thrombus formation (Berger-Gorbet et al. 1996a; Heintz et al. 2001a).

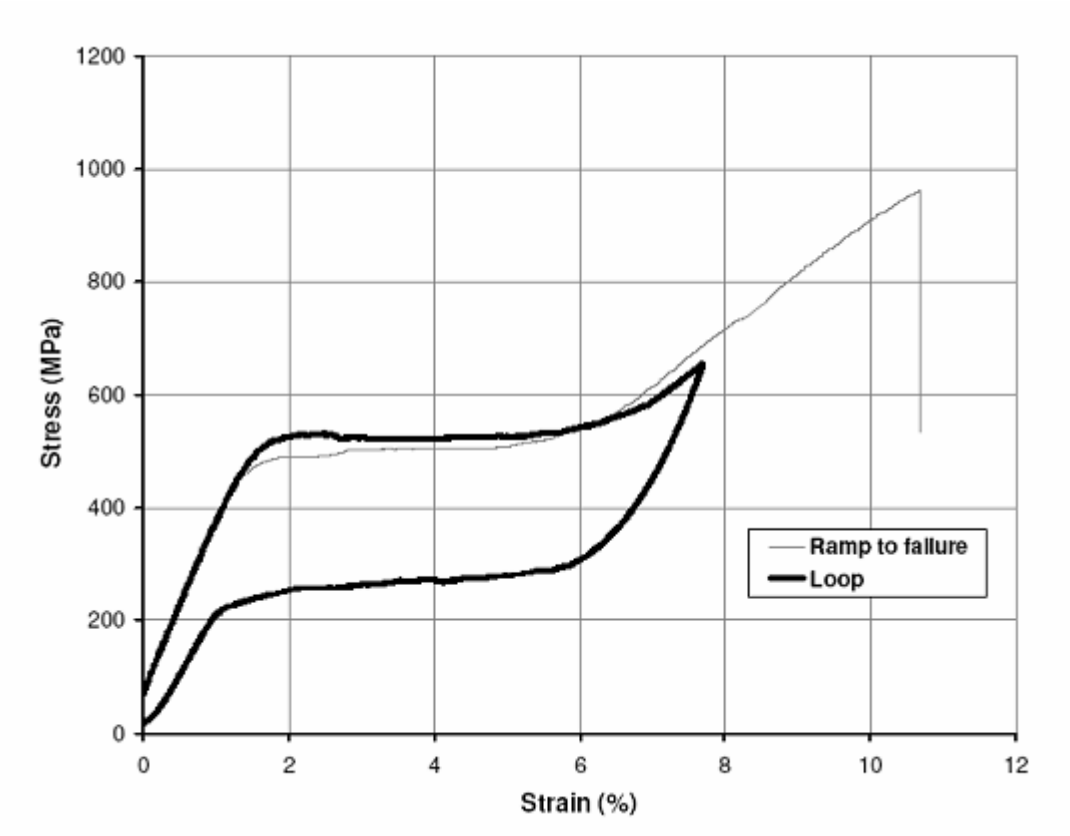


Figure 6.1. Mechanical response of NiTi strip.

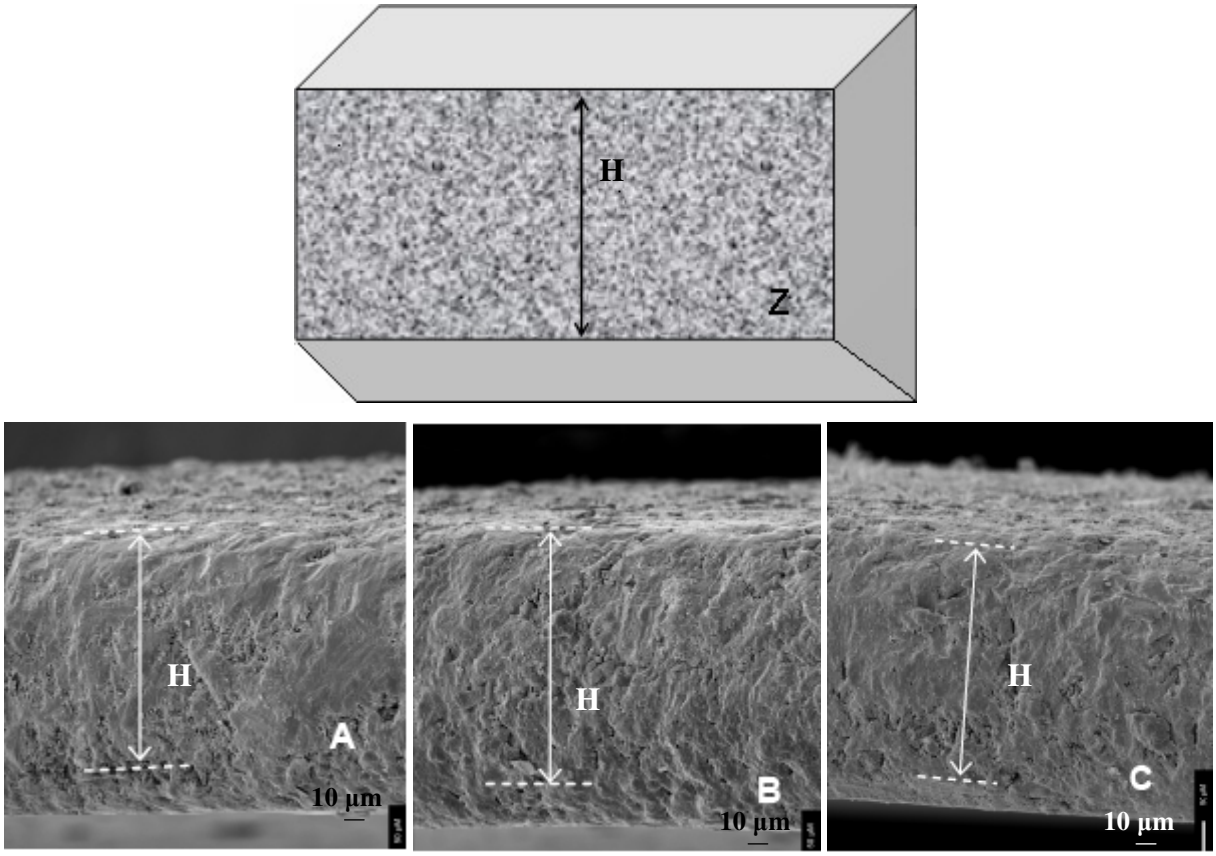


Figure 6.2. Scanning electron micrographs showing the cross-sections of oxide coating on NiTi: (A) before anodisation; (B) after anodisation followed by; (C) heat treatment at 600 °C for 1 h. (Z) schematic view of the NiTi strip. H= thickness of the NiTi strip in different stages of surface treatment.

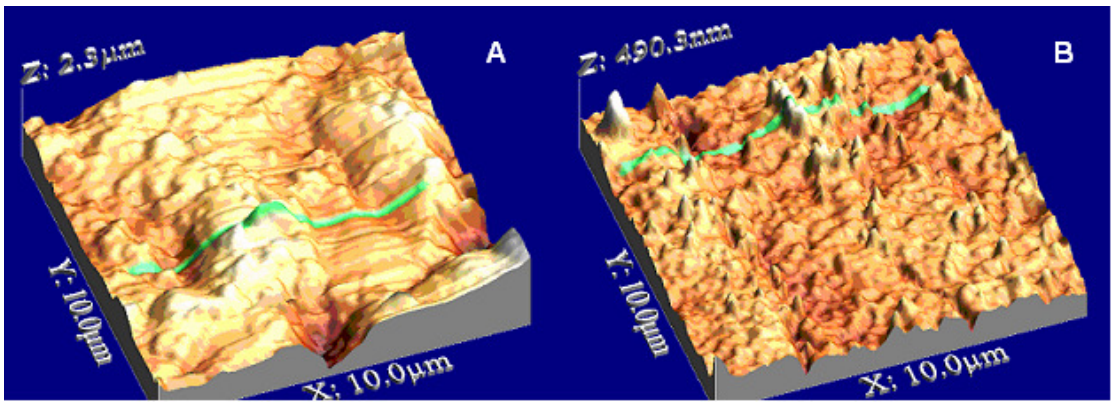


Figure 6.3. Topography of anodized NiTi samples: (A) before heat treatment; (B) after heat treatment at 600°C. The scale in left image is in µm and in the right image is in nm.

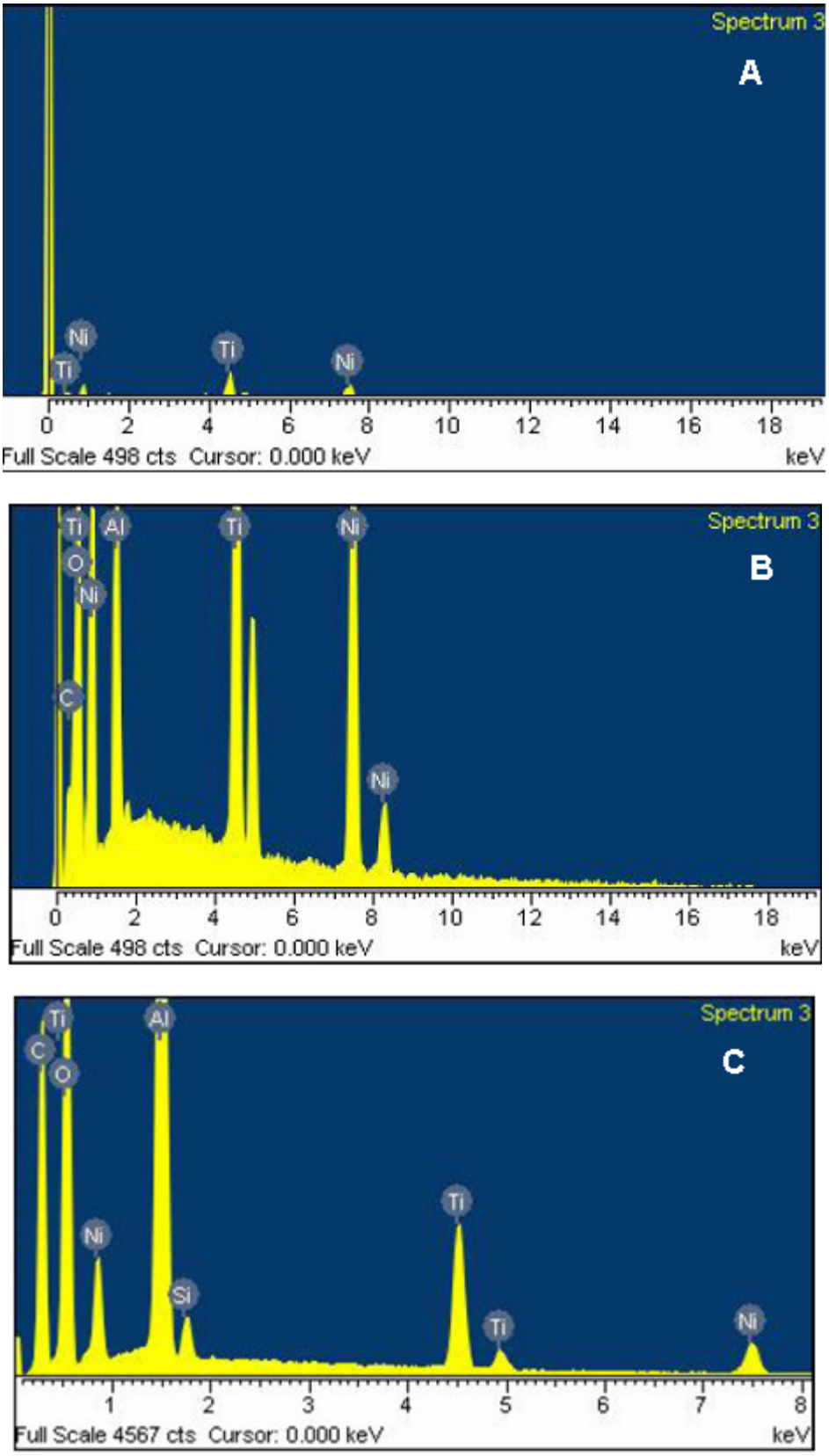


Figure 6.4. Energy dispersive X-ray spectra of the treated NiTi: (A) as supplied before treatment; (B) after anodisation; and (C) after silanisation.

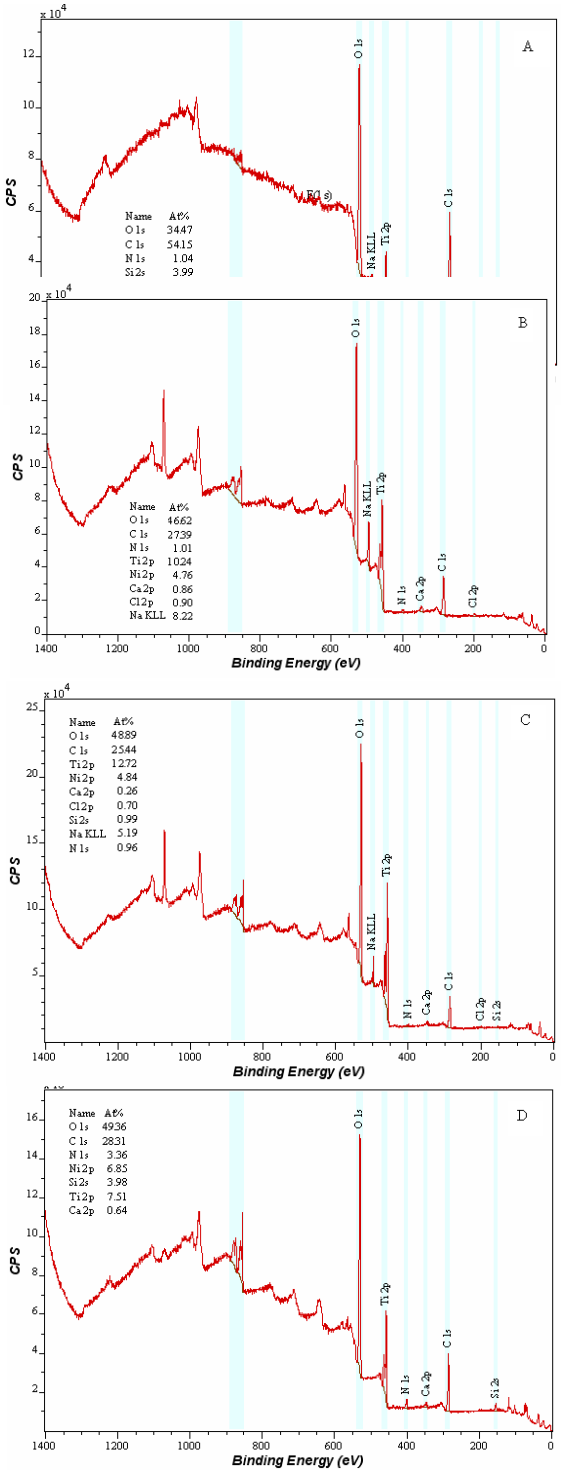


Figure 6.5. XPS survey spectra of the surface of NiTi : (A) NiTi alloy as received; (B)anodized NiTi; (C) heat treated at 600°C; and (D) Silanised NiTi. Key: cps=counts per second. The emission occurs from different orbital with different binding energies for the core levels.

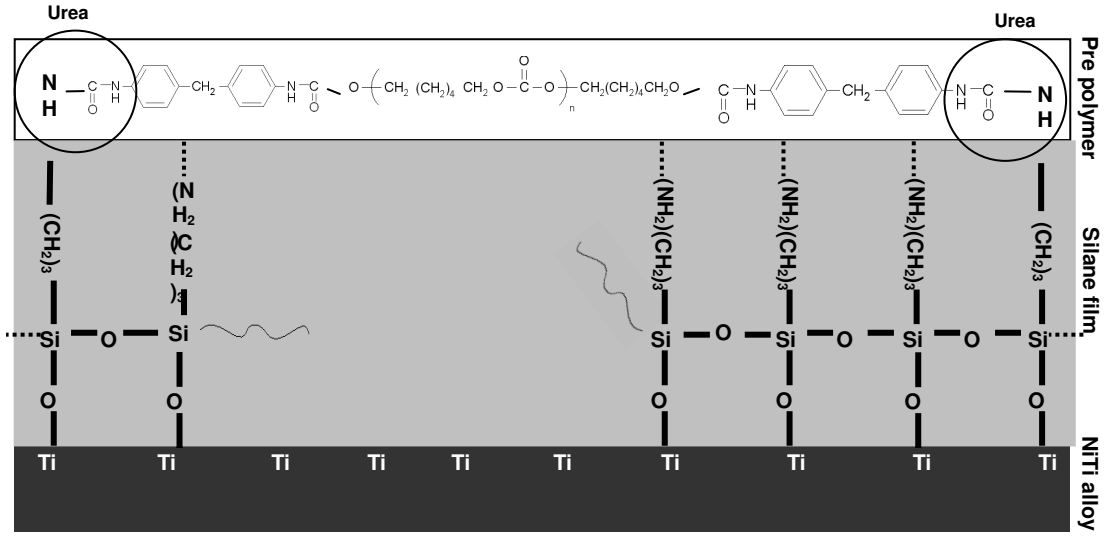


Figure 6.6. Schematic illustration of the bonding mechanism between activated silane solution and NiTi.

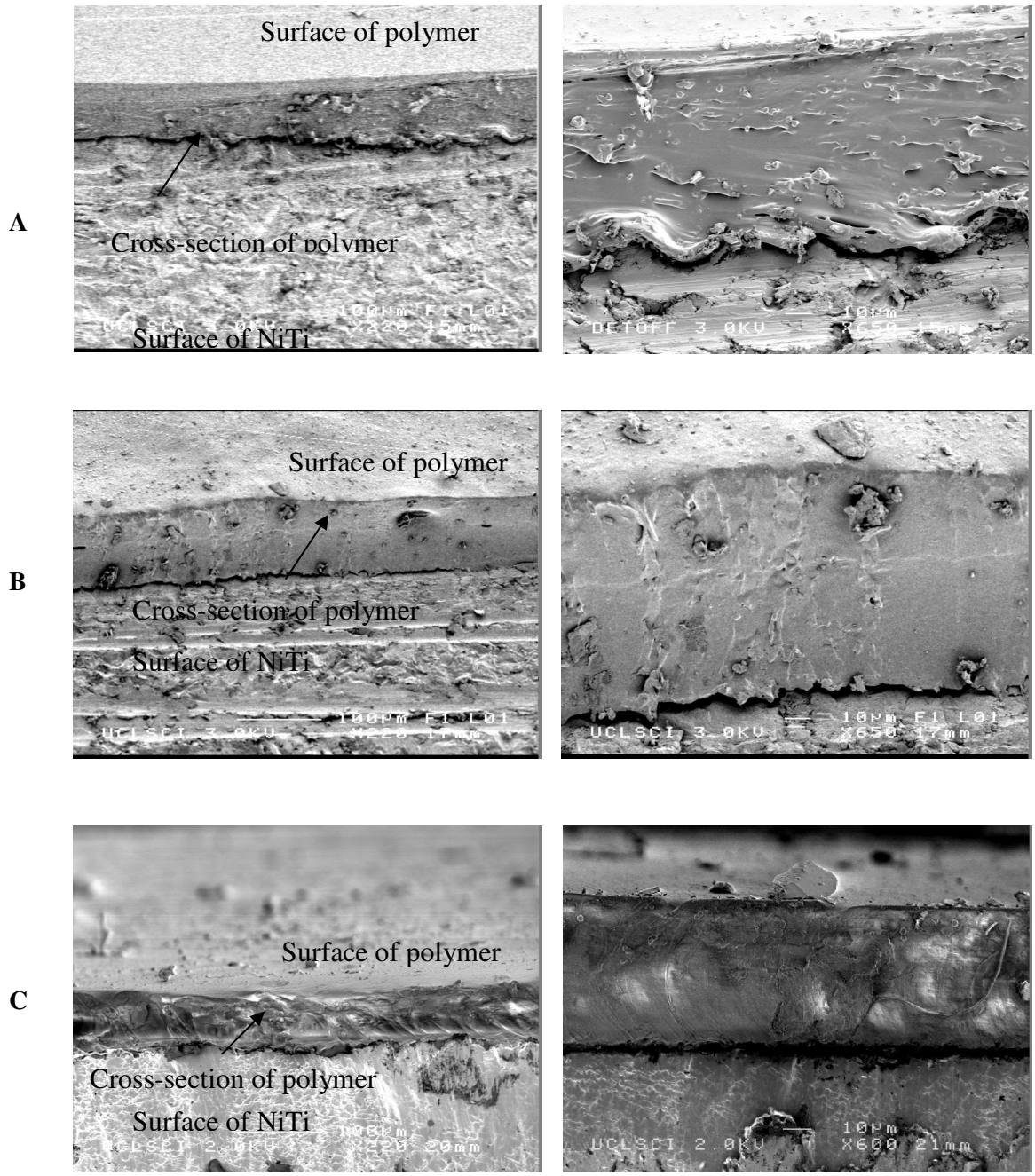


Figure 6.7. Scanning electron micrographs showing cross-sections of treated, coated NiTi strip: (A) casting; (B) electrosprayed; 100 μm thick polymer coating; (C) electrosprayed, 50 μm thick polymer coating.

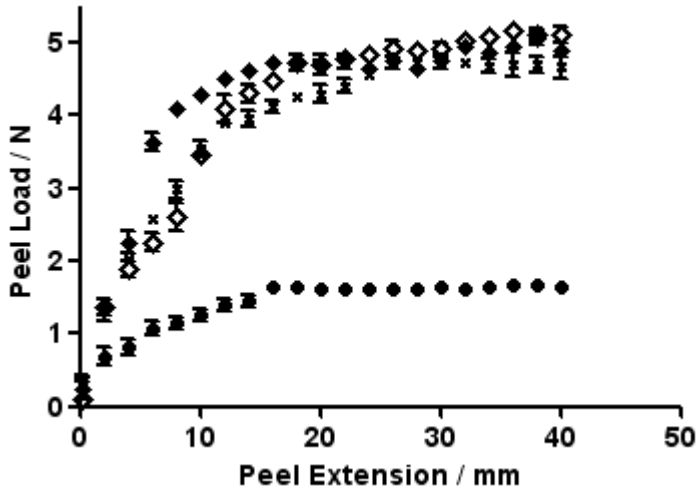


Figure 6.8. Peel strength test results for untreated and treated NiTi strip: (◊) 100 μm electrosprayed coating on treated NiTi; (×) 50 μm electrosprayed coating on treated NiTi; (♦) casting on treated NiTi; (●) Untreated NiTi. Inset: greater bond strength between polymer and treated NiTi compared to untreated NiTi.

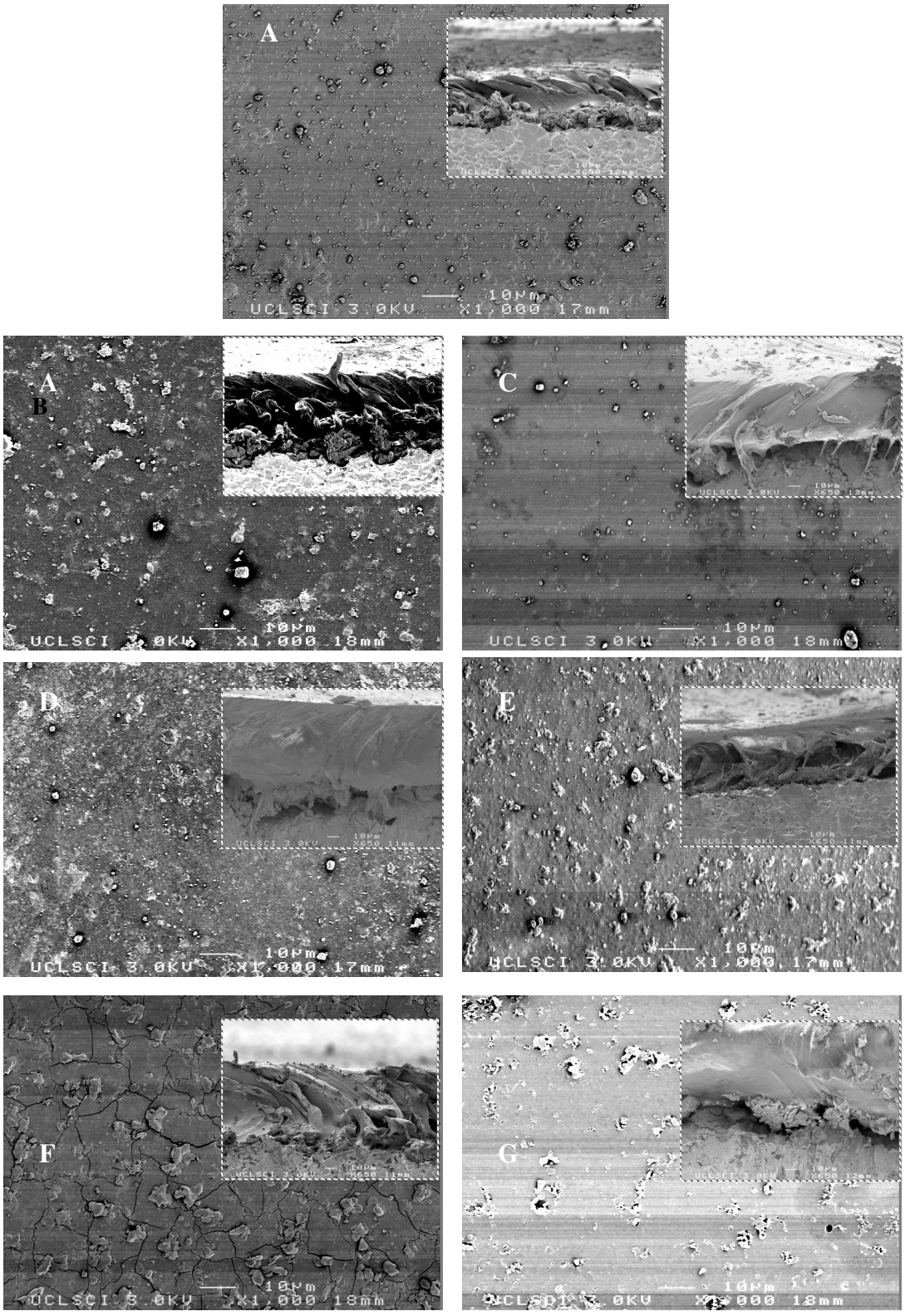


Figure 6.9. Typical scanning electron micrographs of post-incubated POSS-PCU2 nanocomposite polymer coating on NiTi in: (A) distilled water; (B) Cholesterol Esterase; (C) Phospholipase A2; (D) Plasma fraction II; (E) Plasma fraction III; (F) $H_2O_2$ ; and G) t-butyl peroxide after 70 days. Inserts show cross-sections.

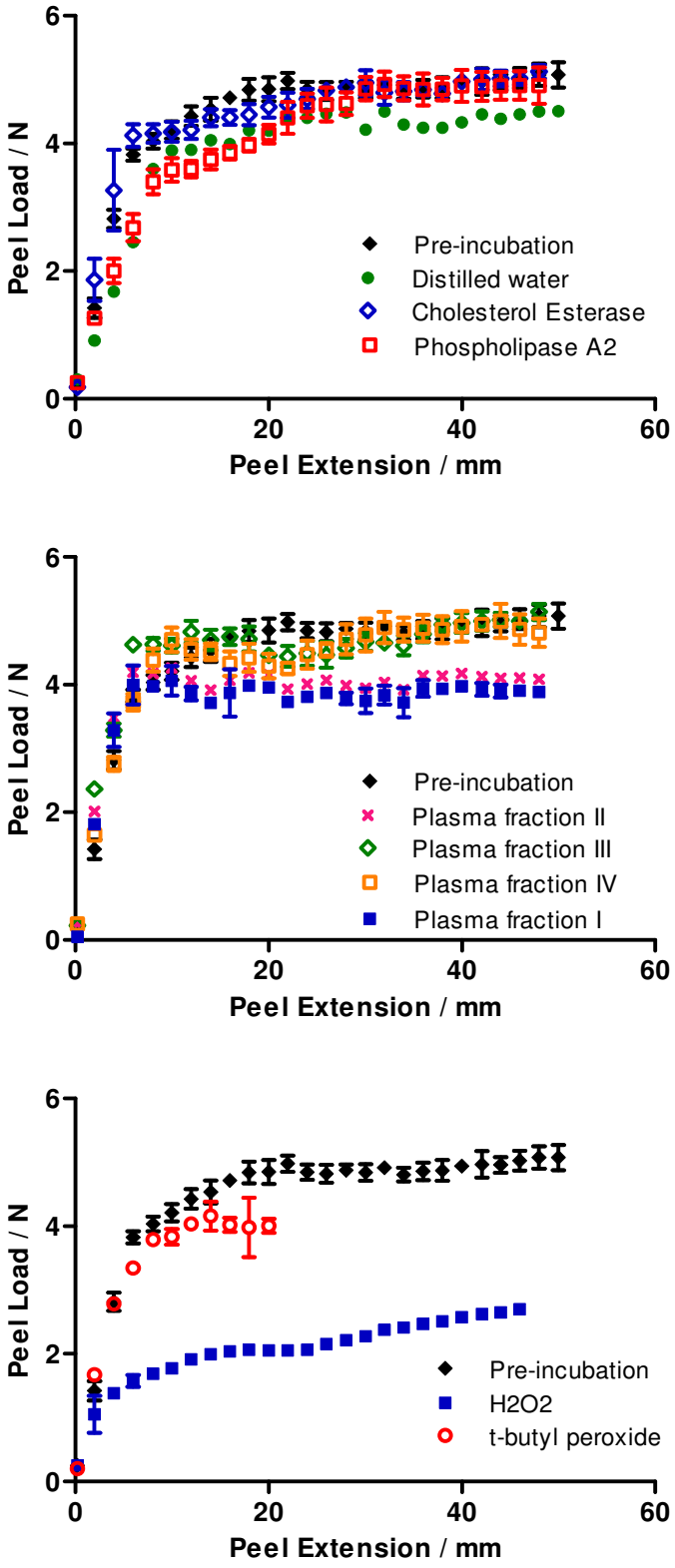


Figure 6.10. Peel strength test of coated NiTi strip following 70 days immersion in different media. A) hydrolytic solutions, B) plasma fractions and C) oxidative/peroxidative solutions.

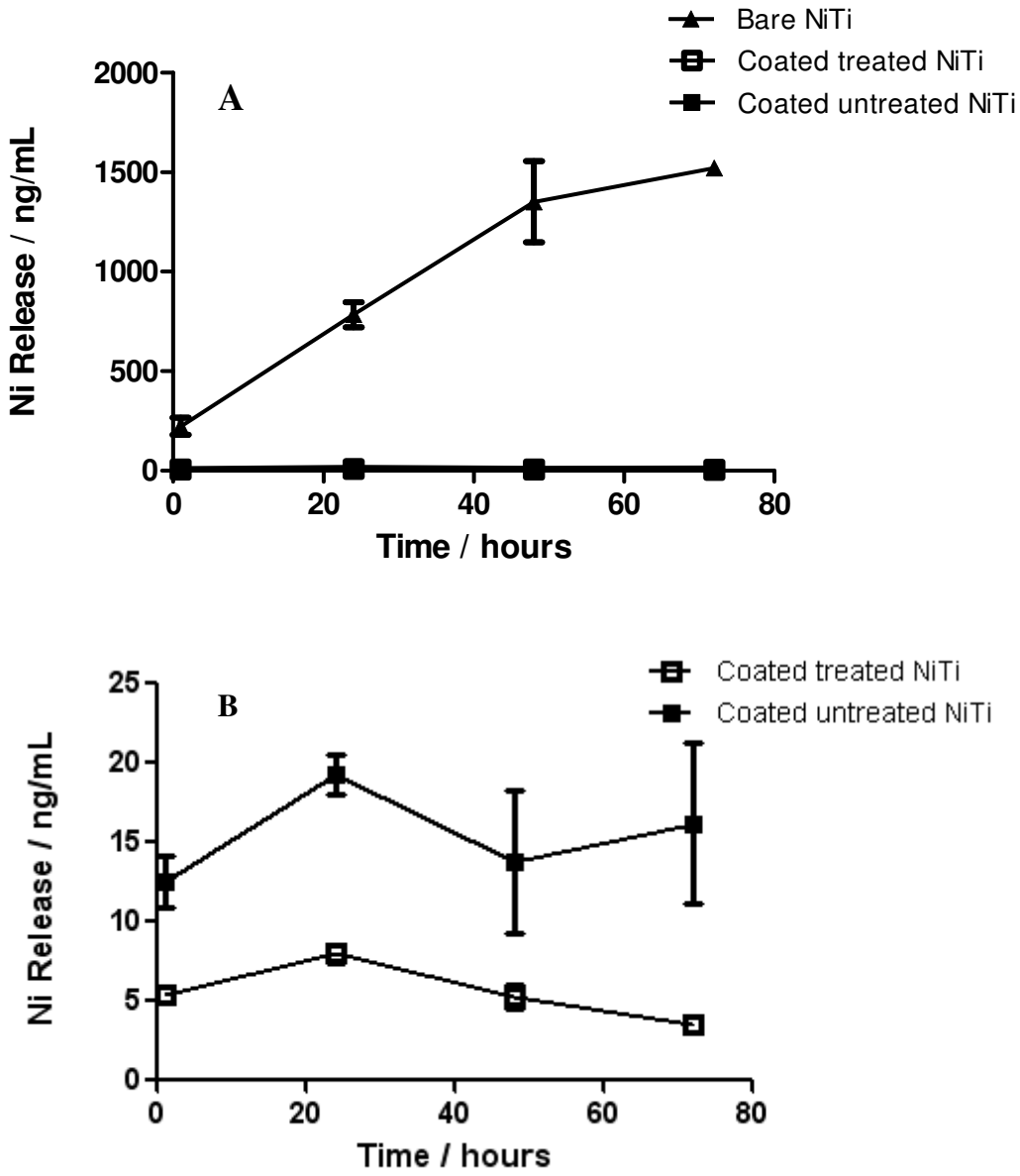


Figure 6.11. Ni release profiles from NiTi strips obtained from mass spectroscopy. Strips were incubated in DMEM. Inset: A) negligible Ni release from coated NiTi compared with bare NiTi; B) less Ni release from coated treated NiTi compared with coated untreated NiTi.

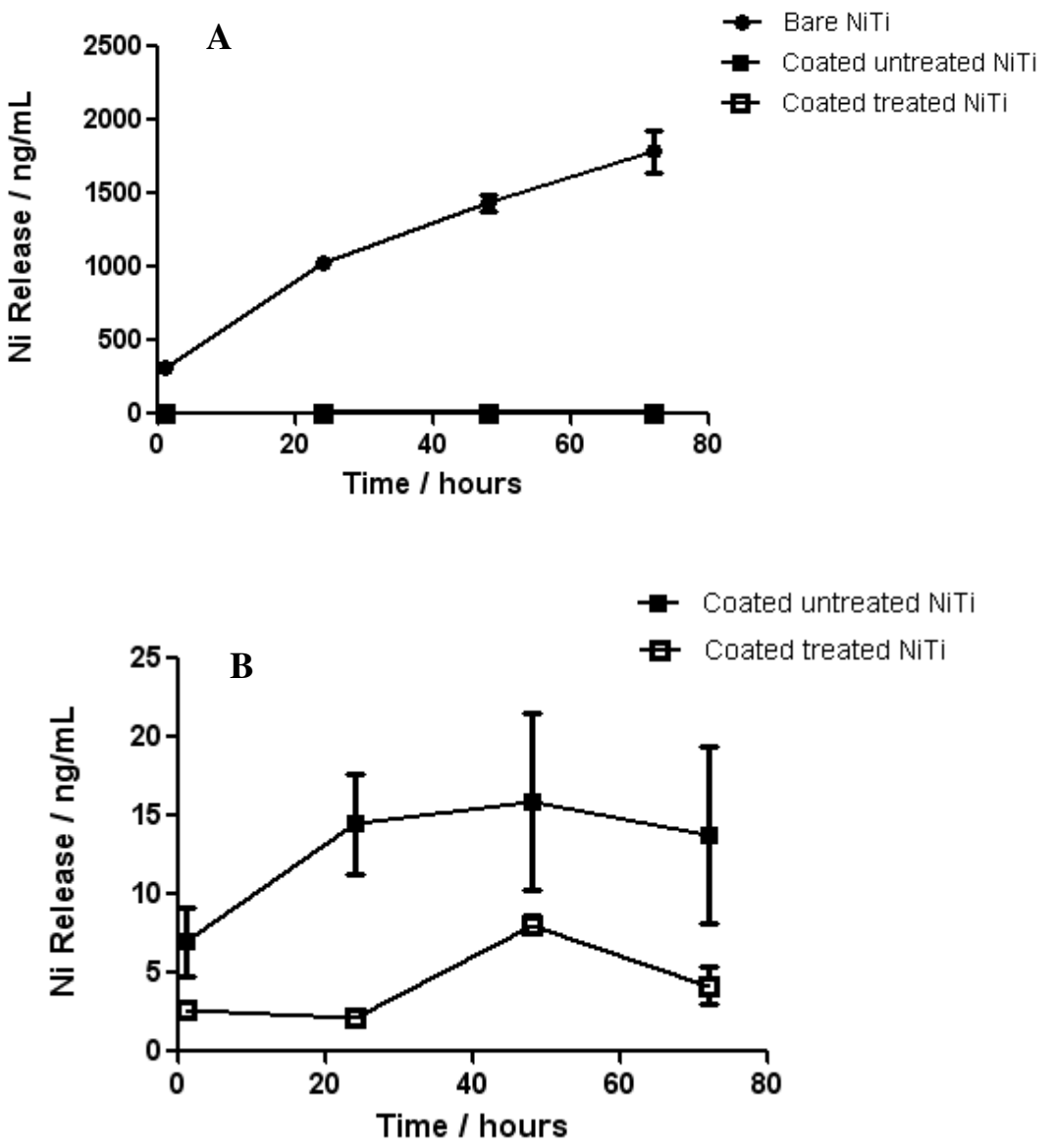


Figure 6.12. Ni release profiles from NiTi strips obtained from mass spectroscopy. Strips were incubated in plasma fraction I. Inset: A) negligible Ni release from coated NiTi compared with bare NiTi; B) less Ni release from coated treated NiTi compared with coated untreated NiTi.

# CHAPTER 7. Conclusions and Future Work

## 7.1. Conclusions

The investigations carried out in this research resulted in the following major conclusions:

- As discussed in the literature review, the development of the polymeric coatings of stents, including coronary or peripheral stents, is currently limited by the problem of thrombosis/restenosis. In this thesis, a suitable material was sought for the coating of metallic stent materials and a new nanocomposite based on poly(carbonate-urea)urethane which incorporated silsesquioxane nanocages was discovered for this purpose.

- The development of an ideal stent coating involves identifying the right polymer and then optimising its coating technique on the metallic stent. The POSS addition to the primary PCU increased the strength of the polymer with great homogeneity throughout the polymer as compared with PCU only. Contact angle analysis showed that the POSS nanocube linked up to the hard segment of PCU, increasing the hydrophobicity characteristics of PCU and reducing the surface energy. The surface charge of the polymer shifted towards negative values by the addition of POSS during the polymerisation of PCU. Compared to bulk properties, the surface properties of PCU differed most upon the addition of POSS. This showed preferential orientation of nanocages towards the surface.

- *In vitro* degradation studies revealed that POSS-PCU was resistant to a broad range of hydrolytic enzymes and plasma proteins whilst retaining its viscoelastic properties. GPC, SEM and stress-strain studies demonstrated that POSS nanocores shield the soft segment(s) of the polyurethane, responsible for its elasticity, from different forms of degradation, principally hydrolysis and plasma protein fractions. These nanocomposites hence provide an optimal method, by which these polymers may be strengthened and improved in biostability whilst maintaining their elasticity, making them ideal materials for the development of cardiovascular implant.

- The biocompatibility of the novel nanocomposite polymer for a coating at the vascular interface was assessed for its potential as a substrate that will support the appropriate cellular activity. At a cellular level, cytocompatibility studies were conducted using endothelial cells. The parameters studied were viability, adhesion and confluence morphology. Cells were able to survive for up to three days in a POSS-PCU medium without any evidence of toxicity. The analysis showed that the films of nanocomposite polymer were not toxic but also can be successfully seeded with endothelial cells. It also indicated that, once seeded, the endothelial cells remain viable and proliferate for a period of three days. These results suggest that once placed *in vivo*, POSS-PCU coatings would allow endothelialisation without causing any adverse effects on the host.

- On studying the behaviour of POSS-PCU and the cells, the results revealed that with increasing concentrations of POSS, the polymer's potential for cell adhesion properties increased compared to PCU alone. Interestingly, there was no significant difference in cells adhesion with further increase of POSS (POSS-PCU2 versus

POSS-PCU4). It is postulated that this behaviour was attributable to its inherent surface roughness as a result of POSS integration. This was confirmed on AFM studies which showed that surface roughness was directly proportional to POSS content.

- Having identified POSS-PCU as a suitable material for a cardiovascular stent coating, the optimal coating technique was determined. Using stainless steel and NiTi materials, different methods -including electrospraying and dip-coating- were used to coat the metals with POSS-PCU. In addition, the optimum experimental parameters necessary to create an even coating were determined. Materiasls made using a variety of parameter conditions were subjected to stress-strain testing and SEM to optimise a consistent and reproducible procedure. It was also found that ultrasonic spraying produced a surface morphology with potential for endothelial cells adhesion compared to the casting technique. This finding is in favour of endothelialisation of the stents following implantation. So it is anticipated that adhesion and proliferation of a layer of endothelial cells on coating would help prevent problems such as the development of intimal hyperplasia.

- A new surface modification technique to enhance the bonding between nanocomposite polymer and NiTi was developed. This involved a surface modification to promote bond strength between the POSS-PCU nanocomposite and the surface of NiTi. The surface modification introduced enhances the potential of the coating to protect the materials surface, mitigate corrosion and increase the longevity of the device *in vivo*. This is of great importance as the release of Ni from NiTi can increase the risk of thrombus formation.

- These combined results suggest that the nanocomposite is suitable for further development in the production of a coronary stents coating.

### 7.2. Future work

With the culmination of this work, the early stages of developing a coating of stent with POSS-PCU is completed. Considering the investigations carried out in this thesis and the results obtained, the following recommendations for further work are made.

⇨ In-vitro degradation in pseudo-physiological solutions, coating adhesion and corrosion resistance was already investigated in the present work. A future study for evaluation of the coating integrity with the stent over the lifespan of the device involves the coating durability after accelerated durability testing. This study would estimate the durability of POSS-PCU on Nitinol and stainless steel stents under pulsating flow conditions and physiologic loading simulating blood pressure conditions in the human body.

⇨ The investigation of coating durability after expansion to the largest labelled diameter is also suggested to simulate stent deployment. 6% deformation of the NiTi/25% deformation of the stainless steel stent should be done by mounting the stent on a balloon. The following experiments are suggested to study the stent after deployment:

- Surface topography by AFM on deformed and un-deformed samples.

- Surface morphology, smoothness of the surface before and after dilation should be investigated by SEM to track the signs of delamination or destruction after expansion.
- Structural changes after expansion should be observed by XPS for metal compounds on the surface and cracks on the surface.

⇨ The two main coating techniques used, i.e. electrohydrodynamic spraying and ultrasonic atomization spraying should be compared upon deployment to see which will be less influenced by expansion.

⇨ Coating thickness on stent should be investigated by variable angle spectroscopic ellipsometry or by AFM. Some studies applied a scratch system to the coating equipped with surface profiler which can read the thickness.

⇨ Some characteristics of the nanocomposite should be investigated after sterilization. Sterilization techniques include using ethylene oxide, radiation, chemicals and heat. The following experiments should be done after sterilisation:

- Molecular weight of the polymer by GPC.
- Mechanical properties by tensometer.
- Degree of crystallinity before and after sterilization by DSC or wide angle X-ray diffraction.
- Contact angle measurement.

The characteristics of the coatings need to be investigated before and after sterilization. In this case, the coated stent should be mounted on a balloon and sterilized with ethylene oxide. The sterilized coated stent should be examined by SEM and compared with pre-sterilization coated stent.

⇨ One clear limitation of this study was the fact that EC adhesion was studied under static conditions, and the possible influence of pulsating flow was not recognized. A next step is the evaluation of the EC attachment on coated-stent exposed to the circulated flow of ECs in an *in vitro* flow circuit model during further experiments.

⇨ The assessment of vascular smooth muscle cells adhesion, apoptosis and growth should also be done by SEM and fluorescent microscopy.

⇨ It is also suggested to investigate the potential for the development of a device with the aim of achieving *in-situ* endothelialisation once implanted. Human peripheral blood contains both circulating endothelial cells and endothelial progenitor cells. Further investigations are being carried out to improve and optimize the endothelial progenitor cells extraction and growth methods, employing magnetic beads to isolate $CD34^+$ or $CD133^+$ cells. Circulating endothelial cells are being isolated from human peripheral blood and characterized by fluorescent-activated cell sorting and immunohistochemistry. The next step should be to seed the isolated cells on the nanocomposite following extracted from human blood and to investigate endothelial-like properties on the nanocomposite after 14 days of culture.

⇨ Haemocompatibility of the coated stent in a closed-loop system under whole blood flow is recommended. Hydrophobicity and smoothness, negative charges of the surface investigated in this study are complementary tests to discuss the results for thrombogenicity. TCP and unloaded stent can be used as negative and positive control, respectively. The set of experiments for haemocompatibility assessment should include:

- Thromboelastography.
- Platelet adhesion and spreading by immunofluorescent microscope.
- Activated partial thromboplastin time (APTT).
- Fibrinogen adsorption test by ELISA.
- Anticoagulant activity of the surface using factor Xa chromogenic assay.

⇨ Comparison of POSS-PCU in terms of haemocompatibility/biological properties with commercially available polymers for coatings is recommended. Stents should be compared with different coatings like poly(ethylene-co-vinylacetate) and polybutylmethacrylate (PEVA/PBMA), or poly(styrene-b-isobutylene-b-styrene) (SIBS); which are the polymers used in the construction of commercially available DES.

⇨ Although the *in vitro* experiments on POSS-PCU with different POSS concentrations presented here are promising, further *in vivo* investigations, from a broad experimental study based on a sheep model, would need to be performed before concluding on its overall biocompatibility and for its potential

use in the stents coatings setting. The result for up to 7-month implantation is recommended.

References

Standard Test Methods for Rubber Property—Adhesion to Flexible Substrate. [ASTM D413]. 2007.

2009, *Cardiovascular News International. First do no harm – the Genous stent. http://www.orbusneich.com/news/media/0701-04%20CardioVascular%20News%20Issue%204%20Jan%202007.pdf 2007.*

A.M.Gañán-Calvo, J.Dávila, & A.Barrero 1997, "Current and droplet size in the electrospraying of liquids. Scaling laws", *Journal of Aerosol Science*, vol. 28, no. 2, pp. 249-275.

Ahn, Y. K., Jeong, M. H., Kim, J. W., Kim, S. H., Cho, J. H., Cho, J. G., Park, C. S., Juhng, S. W., Park, J. C., & Kang, J. C. 1999, "Preventive effects of the heparin-coated stent on restenosis in the porcine model", *Catheterization and Cardiovascular Interventions*, vol. 48, no. 3, pp. 324-330.

Aiping, Z. & Tian, C. 2006c, "Blood compatibility of surface-engineered poly(ethylene terephthalate) via o-carboxymethylchitosan", *Colloids Surf.B Biointerfaces.*, vol. 50, no. 2, pp. 120-125.

Aiping, Z. & Tian, C. 2006a, "Blood compatibility of surface-engineered poly(ethylene terephthalate) via o-carboxymethylchitosan", *Colloids Surf.B Biointerfaces.*, vol. 50, no. 2, pp. 120-125.

Airoldi, F., Colombo, A., Tavano, D., Stankovic, G., Klugmann, S., Paolillo, V., Bonizzoni, E., Briguori, C., Carlino, M., Montorfano, M., Liistro, F., Castelli, A., Ferrari, A., Sgura, F., & Di, M. C. 2004, "Comparison of diamond-like carbon-coated stents versus uncoated stainless steel stents in coronary artery disease", *Am.J.Cardiol.*, vol. 93, no. 4, pp. 474-477.

Albertini, B., Passerini, N., & Rodriguez, L. 2005, "Evaluation of ultrasonic atomization as a new approach to prepare ionically cross-linked chitosan microparticles", *J Pharm Pharmacol*, vol. 57, pp. 821-829.

Alivisatos, A. P. 1996, "synthesis of nanoparticles", *Science*, vol. 271, p. 933.

Altankov, G., Richau, K., & Groth, T. 2003, "The role of surface zeta potential and substratum chemistry for regulation of dermal fibroblasts interaction", *Materialwissenschaft und Werkstofftechnik*, vol. 34, no. 12, pp. 1120-1128.

Antony, P., Puskas, J. E., & Kontopoulou, M. 2003, "Investigation of the rheological and mechanical properties of a polystyrene-polyisobutylene-polystyrene triblock copolymer and its blends with polystyrene", *Polymer Engineering and Science*, vol. 43, no. 1, pp. 243-253.

Austin, G. E., Ratliff, N. B., Hollman, J., Tabei, S., & Phillips, D. F. 1985, "Intimal proliferation of smooth muscle cells as an explanation for recurrent coronary artery stenosis after percutaneous transluminal coronary angioplasty", *J.Am.Coll.Cardiol.*, vol. 6, no. 2, pp. 369-375.

Autio, I., Malo-Ranta, U., Kallioniemi, O. P., & Nikkari, T. 1989, "Cultured bovine aortic endothelial cells secrete factor(s) chemotactic for aortic smooth muscle cells", *Artery*, vol. 16, no. 2, pp. 72-83.

AW Neumann, G. R. J. 1972, "Thermodynamics of contact angles", *Journal of colloid and interface science*, vol. 38, no. 2, p. 341.

B.K.Ku & S.S.Kim 2002, "Electrospray characteristics of highly viscous liquids.", *Journal of Ae7rosol Science*, vol. 33, no. 10, pp. 1361-1378.

Bakhshi, R., Edirisinghe, M. J., Darbyshire, A., Ahmad, Z., & Seifalian, A. M. 2008, "Electrohydrodynamic jetting behaviour of polyhedral oligomeric silsesquioxane nanocomposite", *J Biomater Appl.*, vol. [Epub ahead of print].

Barbucci, R., Magnani, A., Lamponi, S., Pasqui, D., & Bryan, S. 2003, "The use of hyaluronan and its sulphated derivative patterned with micrometric scale on glass substrate in melanocyte cell behaviour", *Biomaterials*, vol. 24, no. 6, pp. 915-926.

Beatrice, A., Nadia, P., & Lorenzo, R. 2005, "Evaluation of ultrasonic atomization as a new approach to prepare ionically cross-linked chitosan microparticles", *Journal of Pharmacy and Pharmacology*, vol. 57, no. 7, pp. 821-830.

Berger, H. L. 2006, "Using ultrasonic spray nozzles to coat drug-eluting stents", *Med.Device Technol.*, vol. 17, no. 9, pp. 44-49.

Berger-Gorbet, M., Broxup, B., Rivard, C., & Yahia, L. H. 1996a, "Biocompatibility testing of NiTi screws using immunohistochemistry on sections containing metallic implants", *J.Biomed.Mater.Res.*, vol. 32, no. 2, pp. 243-248.

Berger-Gorbet, M., Broxup, B., Rivard, C., & Yahia, L. H. 1996b, "Biocompatibility testing of NiTi screws using immunohistochemistry on sections containing metallic implants", *J.Biomed.Mater.Res.*, vol. 32, no. 2, pp. 243-248.

Berroeta, C., Benbara, A., Provenchere, S., Ajzenberg, N., Benessiano, J., Depoix, J. P., Desmonts, J. M., Iung, B., & Philip, I. 2006, "A comparison of bilateral with single internal mammary artery grafts on postoperative mediastinal drainage and transfusion requirement", *Anesth.Analg.*, vol. 103, no. 6, pp. 1380-1385.

Bertrand, M. E., Rupprecht, H. J., Urban, P., & Gershlick, A. H. 2000, "Double-blind study of the safety of clopidogrel with and without a loading dose in combination with aspirin compared with ticlopidine in combination with aspirin after coronary stenting : the clopidogrel aspirin stent international cooperative study (CLASSICS)", *Circulation*, vol. 102, no. 6, pp. 624-629.

Bittner, B. & Kissel, T. 1999, "Ultrasonic atomization for spray drying: a versatile technique for the preparation of protein loaded biodegradable microspheres", *Journal of Microencapsulation*, vol. 16, no. 3, pp. 325-341.

Blanco-Prieto, M. J., Campanero, M. A., Besseghir, K., Heimgatner, F., & Gander, B. 2004, "Importance of single or blended polymer types for controlled in vitro release and plasma levels of a somatostatin analogue entrapped in PLA/PLGA microspheres", *J Contr Rel.* pp. 437-438.

Bliznyuk, V. N., Tereshchenko, T. A., Gumenna, M. A., Gomza, Y. P., Shevchuk, A. V., Klimenko, N. S., & Shevchenko, V. V. 2008, "Structure of segmented poly(ether urethane)s containing amino and hydroxyl functionalized polyhedral oligomeric silsesquioxanes (POSS)", *Polymer*, vol. 49, no. 9, pp. 2298-2305.

Blum, F. D., Meesiri, W., Kang, H. J., & Gambogi, J. E. 1991, "Hydrolysis, Adsorption, and Dynamics of Silane Coupling Agents on Silica Surfaces", *Journal of Adhesion Science and Technology*, vol. 5, no. 6, pp. 479-496.

Bruck, S. D. 1973, "Intrinsic Semiconduction, Electronic Conduction of Polymers and Blood Compatibility", *Nature*, vol. 243, no. 5407, pp. 416-417.

Cabanlit, M., Maitland, D., Wilson, T., Simon, S., Wun, T., Gershwin, M. E., & Van de, W. J. 2007b, "Polyurethane shape-memory polymers demonstrate functional biocompatibility in vitro", *Macromol.Biosci.*, vol. 7, no. 1, pp. 48-55.

Carter, A. J., Scott, D., Laird, J. R., Bailey, L., Kovach, J. A., Hoopes, T. G., Pierce, K., Heath, K., Hess, K., Farb, A., & Virmani, R. 1998, "Progressive vascular remodeling and reduced neointimal formation after placement of a thermoelastic self-expanding nitinol stent in an experimental model", *Cathet.Cardiovasc.Diagn.*, vol. 44, no. 2, pp. 193-201.

Casscells, W. 1992, "Migration of smooth muscle and endothelial cells. Critical events in restenosis", *Circulation*, vol. 86, no. 3, pp. 723-729.

Cella R.J. 1973, "Morphology of segmented polyester thermoplastic elastomers", *Journal of polymer science part c-polymer symposium* no. 42, pp. 727-740.

Chen, C. H., Kelder, E. M., vanderPut, P. J. J. M., & Schoonman, J. 1996, "Morphology control of thin LiCoO2 films fabricated using the electrostatic spray deposition (ESD) technique", *Journal of Materials Chemistry*, vol. 6, no. 5, pp. 765-771.

Chen, M. C., Liang, H. F., Chiu, Y. L., Chang, Y., Wei, H. J., & Sung, H. W. 2005, "A novel drug-eluting stent spray-coated with multi-layers of collagen and sirolimus", *J.Control Release*, vol. 108, no. 1, pp. 178-189.

Cheng, F. T., Shi, P., & Man, H. C. 2005, "Nature of oxide layer formed on NiTi by anodic oxidation in methanol", *Materials Letters*, vol. 59, no. 12, pp. 1516-1520.

Chiacchio, M. A., Borrello, L., Di Pasquale, G., Pollicino, A., Bottino, F. A., & Rescifina, A. 2005, "Synthesis of functionalized polyhedral oligomeric silsesquioxane (POSS) macromers by microwave assisted 1,3-dipolar cycloaddition", *Tetrahedron*, vol. 61, no. 33, pp. 7986-7993.

Cho, H. H., Han, D. W., Matsumura, K., Tsutsumi, S., & Hyon, S. H. 2008, "The behavior of vascular smooth muscle cells and platelets onto epigallocatechin gallate-releasing poly(l-lactide-co-epsilon-caprolactone) as stent-coating materials", *Biomaterials*, vol. 29, no. 7, pp. 884-893.

Choi, J., Harcup, J., Yee, A. F., Zhu, Q., & Laine, R. M. 2001, "Organic/inorganic hybrid composites from cubic silsesquioxanes", *Journal of the American Chemical Society*, vol. 123, no. 46, pp. 11420-11430.

Christensen, K., Larsson, R., Emanuelsson, H., Elgue, G., & Larsson, A. 2001, "Heparin coating of the stent graft - effects on platelets, coagulation and complement activation", *Biomaterials*, vol. 22, no. 4, pp. 349-355.

Christensen, K., Larsson, R., Emanuelsson, H., Elgue, G., & Larsson, A. 2005, "Improved blood compatibility of a stent graft by combining heparin coating and abciximab", *Thromb.Res.*, vol. 115, no. 3, pp. 245-253.

Cloupeau, M. & Prunet-Foch, B. 1989, "Electrostatic spraying of liquids in cone-jet mode", *J.Electrostatics*, vol. 22, pp. 135-159.

Cloupeau, M. & Prunet-Foch, B. 1990, "Electrostatic spraying of liquids: main functioning modes", *J.Electrostatics*, vol. 25, pp. 165-184.

Colombo, A. & Karvouni, E. 2000, "Biodegradable stents : "fulfilling the mission and stepping away"", *Circulation*, vol. 102, no. 4, pp. 371-373.

Cook, S., Walker, A., Hugli, O., Togni, M., & Meier, B. 2007, "Percutaneous coronary interventions in Europe: prevalence, numerical estimates, and projections based on data up to 2004", *Clin.Res.Cardiol.*, vol. 96, no. 6, pp. 375-382.

Cui, D., Tian, F., Ozkan, C. S., Wang, M., & Gao, H. 2005, "Effect of single wall carbon nanotubes on human HEK293 cells", *Toxicol.Lett.*, vol. 155, no. 1, pp. 73-85.

Danzi, G. B., Capuano, C., Sesana, M., Di Blasi, A., Predolini, S., & Antoniucci, D. 2002, "Patterns of in-stent restenosis after placement of NIR gold-coated stents in unselected patients", *Catheterization and Cardiovascular Interventions*, vol. 55, no. 2, pp. 157-162.

De Beule, M., Mortier, P., Belis, J., Van Impe, R., Verhegghe.B., & Veddonck, P. 2007, "plasticity as a lifesaver in the design of cardiovascular stents", *Key Engineering Materials Vols*, vol. 340-341, pp. 841-846.

De Scheerder, I., Sohier, J., Wang, K., Verbeken, E., Zhou, X., & Froyen, L. 2000, "Metallic surface treatment using electrochemical polishing decreases thrombogenicity and neointimal hyperplasia of coronary stents", *Journal of Interventional Cardiology*, vol. 13, no. 3, pp. 179-185.

Deepa, N. & Venkatraman, S. 2009, "Effect of pore size and interpore distance on endothelial cell growth on polymers", *Journal of Biomedical Materials Research.Part A*, vol. 87, no. 3.

Dijkstra, T. W., Duchateau, R., van Santen, R. A., Meetsma, A., & Yap, G. P. A. 2002, "Silsesquioxane models for geminal silica surface silanol sites. A spectroscopic investigation of different types of silanols", *Journal of the American Chemical Society*, vol. 124, no. 33, pp. 9856-9864.

DIN 53504: "Testing of rubber; determination of tensile strength at break, tensile stress at yield, elongation at break and stress values in a tensile test", Deutsches Institut Fur Normung E.V. (German National Standard) / 01-May-1994 / 7 pages.

Dorros, G., Cowley, M. J., Simpson, J., Bentivoglio, L. G., Block, P. C., Bourassa, M., Detre, K., Gosselin, A. J., Gruntzig, A. R., Kelsey, S. F., Kent, K. M., Mock, M. B., Mullin, S. M., Myler, R. K., Passamani, E. R., Stertzer, S. H., & Williams, D. O. 1983, "Percutaneous transluminal coronary angioplasty: report of complications from the National Heart, Lung, and Blood Institute PTCA Registry", *Circulation*, vol. 67, no. 4, pp. 723-730.

Edelman, E. R., Seifert, P., Groothuis, A., Morss, A., Bornstein, D., & Rogers, C. 2001, "Gold-coated NIR stents in porcine coronary arteries", *Circulation*, vol. 103, no. 3, pp. 429-434.

Edirisinghe, M. J. & Jayasinghe, S. N. 2004, "Electrohydrodynamic atomization of a concentrated nano-suspension", *International Journal of Applied Ceramic Technology*, vol. 1, no. 2, pp. 140-145.

Edwards, A., Carson, R. J., Szycher, M., & Bowald, S. 1998, "In vitro and in vivo biodurability of a compliant microporous vascular graft", *J.Biomater.Appl.*, vol. 13, no. 1, pp. 23-45.

El Abedin, S. Z., Welz-Biermann, U., & Endres, F. 2005, "A study on the electrodeposition of tantalum on NiTi alloy in an ionic liquid and corrosion behaviour of the coated alloy", *Electrochemistry Communications*, vol. 7, no. 9, pp. 941-946.

Farb, A., Sangiorgi, G., Carter, A. J., Walley, V. M., Edwards, W. D., Schwartz, R. S., & Virmani, R. 1999, "Pathology of acute and chronic coronary stenting in humans", *Circulation*, vol. 99, no. 1, pp. 44-52.

Fattori, R. & Piva, T. 2003b, "Drug-eluting stents in vascular intervention", *Lancet*, vol. 361, no. 9353, pp. 247-249.

Felder, Ch. B., Blanco-Prieto, M. J., Heizmann, J., Merkle, H. P., & Gander, B. 2003, "Ultrasonic atomization and subsequent polymer desolvation for peptide and protein microencapsulation into biodegradable polyesters", *J Microencapsulation*, vol. 20, pp. 553-567.

Fenn, J. B., Mann, M., Meng, C. K., Wong, S. F., & Whitehouse, C. M. 1989, "Electrospray ionization for mass spectrometry of large biomolecules", *Science*, vol. 246, no. 4926, pp. 64-71.

Friend, R. H., Gymer, R. W., Holmes, A. B., Burroughes, J. H., Marks, R. N., Taliani, C., Bradley, D. D. C., dos Santos, D. A., Bredas, J. L., Logdlund, M., & Salaneck, W. R. 1999, "Electroluminescence in conjugated polymers", *Nature*, vol. 397, no. 6715, pp. 121-128.

Frye, C. L. & Collins, T. 1970, "Oligomeric silsesquioxanes, (HSiO3/2)n.", *J.Am.Chem.Soc.*, vol. 92, pp. 5586-5588.

Fu, B. X., Hsiao, B. S., Pagola, S., Stephens, P., White, H., Rafailovich, M., Sokolov, J., Mather, P. T., Jeon, H. G., Phillips, S., Lichtenhan, J., & Schwab, J. 2001, "Structural development during deformation of polyurethane containing polyhedral oligomeric silsesquioxanes (POSS) molecules", *Polymer*, vol. 42, no. 2, pp. 599-611.

Fu, B. X., Zhang, W., Hsiao, B. S., Rafailovich, M., Sokolov, J., Johansson, G., Sauer, B. B., Phillips, S., & Balnski, R. 2000, "Synthesis and characterization of segmented polyurethanes containing polyhedral oligomeric silsesquioxanes nanostructured molecules", *High Perform.Polym.*, vol. 12, pp. 565-571.

Furchgott, R. F. & Zawadzki, J. V. 1980, "The obligatory role of endothelial cells in the relaxation of arterial smooth muscle by acetylcholine", *Nature*, vol. 288, no. 5789, pp. 373-376.

Gaikwads, G., Reddy, V. C., & Pandita, B. 2005, "Ultrasonic atomisation : A novel technique for surface coatings", *Surface coatings international.Part B, Coatings transactions*, vol. 88, no. 3, pp. 189-196.

Galli, M., Bartorelli, A., Bedogni, F., DeCesare, N., Klugmann, S., Maiello, L., Miccoli, F., Moccetti, T., Onofri, M., Paolillo, V., Pirisi, R., Presbitero, P., Sganzerla, P., Viecca, M., Zerboni, S., & Lanteri, G. 2000, "Italian BiodivYsio open registry (BiodivYsio PC-coated stent): study of clinical outcomes of the implant of a PC-coated coronary stent", *J.Invasive.Cardiol.*, vol. 12, no. 9, pp. 452-458.

Galli, M., Sommariva, L., Prati, F., Zerboni, S., Politi, A., Bonatti, R., Mameli, S., Butti, E., Pagano, A., & Ferrari, G. 2001, "Acute and mid-term results of

phosphorylcholine-coated stents in primary coronary stenting for acute myocardial infarction", *Catheter.Cardiovasc.Interv.*, vol. 53, no. 2, pp. 182-187.

Gao, F., Tong, Y. H., Schricker, S. R., & Culbertson, B. M. 2001, "Evaluation of neat resins based on methacrylates modified with methacryl-POSS, as potential organic-inorganic hybrids for formulating dental restoratives", *Polymers for Advanced Technologies*, vol. 12, no. 6, pp. 355-360.

Gao, H. J., Ji, B. H., Jager, I. L., Arzt, E., & Fratzl, P. 2003, "Materials become insensitive to flaws at nanoscale: Lessons from nature", *Proceedings of the National Academy of Sciences of the United States of America*, vol. 100, no. 10, pp. 5597-5600.

Gao, L. & McCarthy, T. J. 2006, "The "Lotus Effect" Explained: Two Reasons Why Two Length Scales of Topography Are Important", *Langmuir*, vol. 22, no. 7, pp. 2966-2967.

Ghalanbor, Z., Marashi, S. A., & Ranjbar, B. 2005, "Nanotechnology helps medicine: nanoscale swimmers and their future applications", *Med.Hypotheses*, vol. 65, no. 1, pp. 198-199.

Gindl, M., Sinn, G., Gindl, W., Reiterer, A., & Tschegg, S. 2001, "A comparison of different methods to calculate the surface free energy of wood using contact angle measurements", *Colloids and SurfacesA: Physicochemical and Engineering Aspects*, vol. 181, pp. 279-287.

Gogolewski, S. 1989, "Selected topics in biomedical polyurethanes. A review", *Colloid & Polymer Science*, vol. 267, pp. 757-785.

Gutensohn, K., Beythien, C., Bau, J., Fenner, T., Grewe, P., Koester, R., Padmanaban, K. & Kuehnl, P. 2000, " In Vitro Analyses of Diamond-like Carbon Coated Stents: Reduction of Metal Ion Release, Platelet Activation, and Thrombogenicity ", Thrombosis Research, vol 99, no. 6, pp. 577-585.

Gruenzig, A. R. 1978, "Transluminal dilation of coronary artery stenoses.", *Lancet*, vol. 1, no. 8058, p. 263.

Gruntzig, A. R., Senning, A., & Siegenthaler, W. E. 1979, "Nonoperative dilatation of coronary-artery stenosis: percutaneous transluminal coronary angioplasty", *N.Engl.J.Med.*, vol. 301, no. 2, pp. 61-68.

Gunn, J. & Cumberland, D. 1999, "Does stent design influence restenosis?", *Eur.Heart J.*, vol. 20, no. 14, pp. 1009-1013.

Habal, M. B. 1984, "The biologic basis for the clinical application of the silicones. A correlate to their biocompatibility", *Arch.Surg.*, vol. 119, no. 7, pp. 843-848.

Haddad, T. S., Stapleton, R., Jeon, H. G., Mather, P. T., Lichtenhan, J. D., & Phillips, S. 1999, "Nanostructured hybrid organic/inorganic materials. Silsesquioxane modified plastics", *Abstracts of Papers of the American Chemical Society*, vol. 217, p. U608.

Hanefeld, P., Westedt, U., Wombacher, R., Kissel, T., Schaper, A., Wendorff, J. H., & Greiner, A. 2006a, "Coating of poly(p-xylylene) by PLA-PEO-PLA triblock copolymers with excellent polymer-polymer adhesion for stent applications", *Biomacromolecules*, vol. 7, no. 7, pp. 2086-2090.

Hao, Y. 1979, "A simple method for the preparation of human serum albumin", *Vox Sang.*, vol. 36, no. 5, pp. 313-320.

Hartman R.P.A, Borra J.-P, Brunner D.J, Marijnissen J.C.M, & Scarlett B 1999, "The evolution of electrohydrodynamic sprays produced in the cone-jet mode, a physical model", *Journal of Electrostatics*, vol. 47, no. 3, pp. 143-170.

Hartman, R. P. A., Brunner, D. J., Camelot, D. M. A., Marijnissen, J. C. M., & Scarlett, B. 1999, "Electrohydrodynamic atomization in the cone-jet mode physical modeling of the liquid cone and jet.", *Journal of Aerosol Science*, vol. 30, no. 7, pp. 823-849.

Heintz, C., Riepe, G., Birken, L., Kaiser, E., Chakfe, N., Morlock, M., Delling, G., & Imig, H. 2001b, "Corroded nitinol wires in explanted aortic endografts: an important mechanism of failure?", *J.Endovasc.Ther.*, vol. 8, no. 3, pp. 248-253.

Herring, M., Gardner, A., & Glover, J. 1978, "A single-staged technique for seeding vascular grafts with autogenous endothelium", *Surgery*, vol. 84, no. 4, pp. 498-504.

Hirao, A., Koide, G., & Sugiyama, K. 2002, "Synthesis of novel well-defined chain-end- and in-chain-functionalized polystyrenes with one, two, three, and four perfluorooctyl groups and their surface characterization", *Macromolecules*, vol. 35, no. 20, pp. 7642-7651.

Hoffman, D. W., Roy, R., & Komarneni, S. 1984, "Diphasic Xerogels, A New Class of Materials - Phases in the System Al2O3-Sio2", *Journal of the American Ceramic Society*, vol. 67, no. 7, pp. 468-471.

Hofma, S. H., Whelan, D. M., van Beusekom, H. M., Verdouw, P. D., & van der Giessen, W. J. 1998, "Increasing arterial wall injury after long-term implantation of two types of stent in a porcine coronary model", *Eur.Heart J.*, vol. 19, no. 4, pp. 601-609.

Hooi, J. D., Kester, A. D., Stoffers, H. E., Rinkens, P. E., Knottnerus, J. A., & van Ree, J. W. 2004, "Asymptomatic peripheral arterial occlusive disease predicted cardiovascular morbidity and mortality in a 7-year follow-up study", *J.Clin.Epidemiol.*, vol. 57, no. 3, pp. 294-300.

Hooper, K. A. 2000, "Characterization of the inflammatory response to biomaterials using a rodent air pouch model", *Journal of Biomedical Materials Research*, vol. 50, no. 3, pp. 365-374.

Hoshi, H. & Mckeehan, W. L. 1986, "Isolation, Growth Requirements, Cloning, Prostacyclin Production and Life-Span of Human Adult Endothelial-Cells in Low Serum Culture-Medium", *In Vitro Cellular & Developmental Biology*, vol. 22, no. 1, pp. 51-56.

Hou, G., Mulholland, D., Gronska, M. A., & Bendeck, M. P. 2000, "Type VIII collagen stimulates smooth muscle cell migration and matrix metalloproteinase synthesis after arterial injury", *Am.J.Pathol.*, vol. 156, no. 2, pp. 467-476.

Howard, G. T. 2002, "Biodegradation of polyurethane: a review", *International Biodeterioration & Biodegradation*, vol. 49, no. 4, pp. 245-252.

Hsiao, B. S., White, H., Rafailovich, M., Mather, P. T., Jeon, H. G., Phillips, S., Lichtenhan, J., & Schwab, J. 2000a, "Nanoscale reinforcement of polyhedral oligomeric silsesquioxane (POSS) in polyurethane elastomer", *Polymer International*, vol. 49, no. 5, pp. 437-440.

Hu, T., Chu, C. L., Yin, L. H., Pu, Y. P., Dong, Y. S., Guo, C., Sheng, X. B., Chung, J. C. Y., & Chu, P. K. 2007, "In vitro biocompatibility of titanium-nickel alloy with

titanium oxide film by H2O2 oxidation", *Transactions of Nonferrous Metals Society of China*, vol. 17, no. 3, pp. 553-557.

Huang, J., Best, S. M., Bonfield, W., Brooks, R. A., Rushton, N., Jayasinghe, S. N., & Edirisinghe, M. J. 2004, "In vitro assessment of the biological response to nano-sized hydroxyapatite", *Journal of Materials Science: Materials in Medicine*, vol. 15, no. 4, pp. 441-445.

Huang, J., He, C., Xiao, Y., Mya, K., Dai, J., & Siow, Y. P. 2003, "Polyimide/POSS nanocomposites: interfacial interaction, thermal properties and mechanical properties", *Polymer*, vol. 44, pp. 4491-4499.

Iacono, S., Budy, S. M., Mabry, J. M., & Smith, D. W. 2007, "Synthesis, characterization, and properties of chain terminated polyhedral oligomeric silsesquioxane-functionalized perfluorocyclobutyl aryl ether copolymers", *Polymer*, vol. 48, no. 16, pp. 4637-4645.

Isayeva, I. S. & Kennedy, J. P. 2004, "Amphiphilic membranes crosslinked and reinforced by POSS", *Journal of Polymer Science Part A-Polymer Chemistry*, vol. 42, no. 17, pp. 4337-4352.

J.M.López-Herrera, A.Barrero, A.López, I.G.Loscertales, & M.Márquez 2003, "Coaxial jets generated from electrified Taylor cones. Scaling laws", *Journal of Aerosol Science*, vol. 34, no. 5, pp. 535-552.

Jaffe, E. A., Nachman, R. L., ecker, C. G., & Miinick, R. 1973, "Culture of human endothelial cells derived from umbilical veins: identification by morphologic and immunologic criteria", *The Journal of Clinical Investigation*, vol. 52, pp. 2745-2756.

Jaworek, A. & Krupa, A. 1999b, "Classification of the modes of EHD spraying", *Journal of Aerosol Science*, vol. 30, no. 7, pp. 873-893.

Jaworek, A. & Krupa, A. 1999c, "Jet and drops formation in electrohydrodynamic spraying of liquids. A systematic approach", *Experiments in Fluids*, vol. 27, no. 1, pp. 43-52.

Jaworek, A. & Krupa, A. 1999a, "Classification of the modes of EHD spraying", *Journal of Aerosol Science*, vol. 30, no. 7, pp. 873-893.

Jayasinghe, S., Edirisinghe, M., & De Wilde, T. 2002, "A novel ceramic printing technique based on electrostatic atomization of a suspension", *Materials Research Innovations*, vol. 6, no. 3, pp. 92-95.

Jayasinghe, S. N. & Edirisinghe, M. J. 2004a, "Electrostatic atomisation of a ceramic suspension", *Journal of the European Ceramic Society*, vol. 24, no. 8, pp. 2203-2213.

Jayasinghe, S. N. & Edirisinghe, M. J. 2002, "Effect of viscosity on the size of relics produced by electrostatic atomization", *Journal of Aerosol Science*, vol. 33, no. 10, pp. 1379-1388.

Jayasinghe, S. N. & Edirisinghe, M. J. 2004b, "Electrically forced jets and microthreads of high viscosity dielectric liquids", *Journal of Aerosol Science*, vol. 35, no. 2, pp. 233-243.

Joner, M., Finn, A. V., Farb, A., Mont, E. K., Kolodgie, F. D., Ladich, E., Kutys, R., Skorija, K., Gold, H. K., & Virmani, R. 2006, "Pathology of drug-eluting stents in humans: delayed healing and late thrombotic risk", *J.Am.Coll.Cardiol.*, vol. 48, no. 1, pp. 193-202.

Joshi, M. & Butola, B. S. 2004, "Polymeric nanocomposites - Polyhedral oligomeric silsesquioxanes (POSS) as hybrid nanofiller", *Journal of Macromolecular Science-Polymer Reviews*, vol. C44, no. 4, pp. 389-410.

K.Tang & A.Gomez 1994a, "On the structure of an electrostatic spray of monodisperse droplets.", *Phys.Fluids*, vol. 6, no. 7, p. 2317.

Kaelble, D. H. & Uy, K. C. 1970, "A Reinterpretation of Organic Liquid-Polytetrafluoroethylene Surface Interactions", *Journal of Adhesion*, vol. 2, p. 50-&.

Kandzari, D. E., Tcheng, J. E., & Zidar, J. P. 2002, "Coronary artery stents: evaluating new designs for contemporary percutaneous intervention", *Catheter.Cardiovasc.Interv.*, vol. 56, no. 4, pp. 562-576.

Kang, H. J., Kim, D. J., Park, S. J., Yoo, J. B., & Ryu, Y. S. 2007, "Controlled drug release using nanoporous anodic aluminum oxide on stent", *Thin Solid Films*, vol. 515, no. 12, pp. 5184-5187.

Kannan, R. Y., Salacinski, H. J., Odlyha, M., Butler, P. E., & Seifalian, A. M. 2006b, "The degradative resistance of polyhedral oligomeric silsesquioxane nanocore integrated polyurethanes: an in vitro study", *Biomaterials*, vol. 27, no. 9, pp. 1971-1979.

Kao, W. J., Zhao, Q. H., Hiltner, A., & Anderson, J. M. 1994, "Theoretical analysis of in vivo macrophage adhesion and foreign body giant cell formation on polydimethylsiloxane, low density polyethylene, and polyetherurethanes", *J.Biomed.Mater.Res.*, vol. 28, no. 1, pp. 73-79.

Khorasani, M. T. & Mirzadeh, H. 2007, "Effect of oxygen plasma treatment on surface charge and wettability of PVC blood bag - In vitro assay", *Radiation Physics and Chemistry*, vol. 76, no. 6, pp. 1011-1016.

Khorasani, M. T., Moemenbellah, S., Mirzadeh, H., & Sadatnia, B. 2006, "Effect of surface charge and hydrophobicity of polyurethanes and silicone rubbers on L929 cells response", *Colloids Surf.B Biointerfaces.*, vol. 51, no. 2, pp. 112-119.

Kickelbick, G. 2003, "Concepts for the incorporation of inorganic building blocks into organic polymers on a nanoscale", *Prog.Polym.Sci.*, vol. 28, pp. 83-114.

Kidane, A. G., Salacinski, H., Tiwari, A., Bruckdorfer, K. R., & Seifalian, A. M. 2004, "Anticoagulant and antiplatelet agents: their clinical and device application(s) together with usages to engineer surfaces", *Biomacromolecules.*, vol. 5, no. 3, pp. 798-813.

Kim, G. M., Qin, H., Fang, X., Sun, F. C., & Mather, P. T. 2003, "Hybrid epoxy-based thermosets based on polyhedral oligosilsesquioxane: Cure behavior and toughening mechanisms", *Journal of Polymer Science Part B-Polymer Physics*, vol. 41, no. 24, pp. 3299-3313.

Kim, S. K., Heo, S. J., Koak, J. Y., Lee, J. H., Lee, Y. M., Chung, D. J., Lee, J. I., & Hong, S. D. 2007, "A biocompatibility study of a reinforced acrylic-based hybrid denture composite resin with polyhedraloligosilsesquioxane", *J.Oral Rehabil.*, vol. 34, no. 5, pp. 389-395.

Kirkpatrick, J. E. 1999, "Symptoms in peripheral artery disease", *J.Insur.Med.*, vol. 31, no. 1, pp. 37-38.

Klee, D. & Hocker, H. 1999, "Polymers for biomedical applications: Improvement of the interface compatibility", *Biomedical Applications: Polymer Blends*, vol. 149, pp. 1-57.

Klee, D., Severich, B., & Hocker, H. 1996, "Correlation between chemical and physical surface properties and blood compatibility of PPE/EVA-blends", *Macromolecular Symposia*, vol. 103, pp. 19-29.

Klugherz, B. D., Song, C., DeFelice, S., Cui, X., Lu, Z., Connolly, J., Hinson, J. T., Wilensky, R. L., & Levy, R. J. 2002, "Gene delivery to pig coronary arteries from stents carrying antibody-tethered adenovirus", *Hum.Gene Ther*, vol. 13, no. 3, pp. 443-454.

Koh, K., Sugiyama, S., Morinaga, T., Ohno, K., Tsujii, Y., Fukuda, T., Yamahiro, M., Iijima, T., Oikawa, H., Watanabe, K., & Miyashita, T. 2005, "Precision synthesis of a fluorinated polyhedral oligomeric silsesquioxane-terminated polymer and surface characterization of its blend film with poly(methyl methacrylate)", *Macromolecules*, vol. 38, no. 4, pp. 1264-1270.

Komarneni, S. 1992, "Nanocomposites", *Journal of Materials Chemistry*, vol. 2, no. 12, pp. 1219-1230.

Kornowski, R., Hong, M. K., Tio, F. O., Bramwell, O., Wu, H., & Leon, M. B. 1998, "In-stent restenosis: contributions of inflammatory responses and arterial injury to neointimal hyperplasia", *J.Am.Coll.Cardiol.*, vol. 31, no. 1, pp. 224-230.

Koster, R., Vieluf, D., Kiehn, M., Sommerauer, M., Kahler, J., Baldus, S., Meinertz, T., & Hamm, C. W. 2000, "Nickel and molybdenum contact allergies in patients with coronary in-stent restenosis", *Lancet*, vol. 356, no. 9245, pp. 1895-1897.

Kubik, T., Bogunia-Kubik, K., & Sugisaka, M. 2005, "Nanotechnology on duty in medical applications", *Curr.Pharm.Biotechnol.*, vol. 6, no. 1, pp. 17-33.

Kunlin J. 1949, "The treatment of arterial obstruction by vein grafting.", *Arch Mal Coeur*, vol. 42, pp. 371-375.

Kuntz, R. E., Gibson, C. M., Nobuyoshi, M., & Baim, D. S. 1993, "Generalized model of restenosis after conventional balloon angioplasty, stenting and directional atherectomy", *J.Am.Coll.Cardiol.*, vol. 21, no. 1, pp. 15-25.

Kuntz, R. E., Hinohara, T., Safian, R. D., Selmon, M. R., Simpson, J. B., & Baim, D. S. 1992, "Restenosis after directional coronary atherectomy. Effects of luminal diameter and deep wall excision", *Circulation*, vol. 86, no. 5, pp. 1394-1399.

Kuo, S. W., Lin, H. C., Huang, W. J., Huang, C. F., & Chang, F. C. 2006, "Hydrogen bonding interactions and miscibility between phenolic resin and octa(acetoxystyryl) polyhedral oligomeric silsesquioxane (AS-POSS) nanocomposites", *Journal of Polymer Science Part B-Polymer Physics*, vol. 44, no. 4, pp. 673-686.

Labow, R. S., Meek, E., & Santerre, J. P. 1999b, "Synthesis of cholesterol esterase by monocyte-derived macrophages: a potential role in the biodegradation of poly(urethane)s", *J.Biomater.Appl.*, vol. 13, no. 3, pp. 187-205.

Labow, R. S., Meek, E., & Santerre, J. P. 2001, "Hydrolytic degradation of poly(carbonate)-urethanes by monocyte-derived macrophages", *Biomaterials*, vol. 22, no. 22, pp. 3025-3033.

Labow, R. S., Santerre, J. P., & Waghray, G. 1997, "The effect of phospholipids on the biodegradation of polyurethanes by lysosomal enzymes", *Journal of Biomaterials Science-Polymer Edition*, vol. 8, no. 10, pp. 779-795.

Lacono, S. T., Budy, S. M., Mabry, J. M., & Smith, D. W. 2007, "Synthesis, characterization, and surface morphology of pendant polyhedral oligomeric silsesquioxane perfluorocyclobutyl aryl ether copolymers", *Macromolecules*, vol. 40, no. 26, pp. 9517-9522.

Lafont, A., Guzman, L. A., Whitlow, P. L., Goormastic, M., Cornhill, J. F., & Chisolm, G. M. 1995, "Restenosis after experimental angioplasty. Intimal, medial, and adventitial changes associated with constrictive remodeling", *Circ.Res.*, vol. 76, no. 6, pp. 996-1002.

Lahann, J., Klee, D., Thelen, H., Bienert, H., Vorwerk, D., & Hocker, H. 1999a, "Improvement of haemocompatibility of metallic stents by polymer coating", *Journal of Materials Science-Materials in Medicine*, vol. 10, no. 7, pp. 443-448.

Laine, R. M. 2005, "Nanobuilding blocks based on the [OSiO1.5](x) (x=6, 8, 10) octasilsesquioxanes", *Journal of Materials Chemistry*, vol. 15, no. 35-36, pp. 3725-3744.

Lang, R. J. 1962, "Ultrasonic Atomization of Liquids", *J.Acoust.Soc.Am.*, vol. 34, no. 1, pp. 6-8.

Lee, A. & Lichtenhan, J. D. 1998, "Viscoelastic responses of polyhedral oligosilsesquioxane reinforced epoxy systems", *Macromolecules*, vol. 31, no. 15, pp. 4970-4974.

Lee, A. & Lichtenhan, J. D. 1999, "Thermal and viscoelastic property of epoxy-clay and hybrid inorganic-organic epoxy nanocomposites", *Journal of Applied Polymer Science*, vol. 73, no. 10, pp. 1993-2001.

Lee, D. 2007, " In vivo imaging of hydrogen peroxide with chemiluminescent nanoparticles.", *nature materials*, vol. 6, pp. 765-769.

Lee, M. C. & Haut, R. C. 1992, "Strain rate effects on tensile failure properties of the common carotid artery and jugular veins of ferrets", *J.Biomech.*, vol. 25, no. 8, pp. 925-927.

Leon, M. B. 2007, "Late thrombosis a concern with drug-eluting stents", *J.Interv.Cardiol.*, vol. 20, no. 1, pp. 26-29.

Leu, C. M., Chang, Y. T., & Wei, K. H. 2003, "Polyimide-side-chain tethered polyhedral oligomeric silsesquioxane nanocomposites for low-dielectric film applications", *Chemistry of Materials*, vol. 15, no. 19, pp. 3721-3727.

Lewis, A. L., Furze, J. D., Small, S., Robertson, J. D., Higgins, B. J., Taylor, S., & Ricci, D. R. 2002, "Long-term stability of a coronary stent coating post-implantation", *J.Biomed.Mater.Res.*, vol. 63, no. 6, pp. 699-705.

Li, G. Z., Wang, L. C., Ni, H. L., & Pittman, C. U. 2001b, "Polyhedral oligomeric silsesquioxane (POSS) polymers and copolymers: A review", *Journal of Inorganic and Organometallic Polymers*, vol. 11, no. 3, pp. 123-154.

Li, G. Z., Yamamoto, T., Nozaki, K., & Hikosaka, M. 2000a, "Studies on morphology of single crystals of ladder-like polyphenylsilsesquioxane (PPSQ) by polarized optical

microscopy", *Macromolecular Chemistry and Physics*, vol. 201, no. 12, pp. 1283-1285.

Li, G. Z., Yamamoto, T., Nozaki, K., & Hikosaka, M. 2000b, "Studies on morphology of single crystals of ladder-like polyphenylsilsesquioxane (PPSQ) by polarized optical microscopy", *Macromolecular Chemistry and Physics*, vol. 201, no. 12, pp. 1283-1285.

Li, X., Andruzzi, L., Chiellini, E., Galli, G., Ober, C. K., Hexemer, A., Kramer, E. J., & Fischer, D. A. 2002, "Semifluorinated Aromatic Side-Group Polystyrene-Based Block Copolymers: Bulk Structure and Surface Orientation Studies", *Macromolecules*, vol. 35, no. 21, pp. 8078-8087.

Lichtenhan, J. & Hibrid Plastics 2003, "Economic and commercialisation of nanostructured hybrid chemicals", *Organic/inorganic hybrid materials*.

Lichtenhan, J. D. 1995, "Polyhedral Oligomeric Silsesquioxanes - Building-Blocks for Silsesquioxane-Based Polymers and Hybrid Materials", *Comments on Inorganic Chemistry*, vol. 17, no. 2, pp. 115-130.

Lichtenhan, J. D., Haddad, T. S., Schwab, J. J., Carr, M. J., Chaffee, K. P., & Mather, P. T. 1998, "The next generation of silicon-based plastics: Polyhedral oligomeric silsesquioxane (POSS) nanocomposites", *Abstracts of Papers of the American Chemical Society*, vol. 215, p. U410.

Liu, C. L., Chu, P. K., Lin, G. Q., & Qi, M. 2006, "Anti-corrosion characteristics of nitride-coated AISI 316L stainless steel coronary stents", *Surface & Coatings Technology*, vol. 201, no. 6, pp. 2802-2806.

Liu, H. & Zheng, S. 2005, "Polyurethane Networks Nanoreinforced by Polyhedral Oligomeric Silsesquioxane", *Macromol.Rapid Commun.*, vol. 26, pp. 196-200.

Liu, H. Z., Zheng, S. X., & Nie, K. M. 2005, "Morphology and thermomechanical properties of organic-inorganic hybrid composites involving epoxy resin and an incompletely condensed polyhedral oligomeric silsesquioxane", *Macromolecules*, vol. 38, no. 12, pp. 5088-5097.

Liu, X. P., Wang, Y. N., Yang, D. Z., & Qi, M. 2008, "The effect of ageing treatment on shape-setting and superelasticity of a nitinol stent", *Materials Characterization*, vol. 59, no. 4, pp. 402-406.

Liu, Y. H., Ni, Y., & Zheng, S. X. 2006, "Polyurethane networks modified with octa(propylglycidyl ether) polyhedral oligomeric silsesquioxane", *Macromolecular Chemistry and Physics*, vol. 207, no. 20, pp. 1842-1851.

Loeffler, J. P., View, M., & Calif 1999, *Polymer coated stent structure.*, 5897911 (patent).

Loeffler, J. P. *Passive perfusion stent delivery system*, US 5891154, Advanced Cardiovascular System, Inc., (patent).

Lozano, A., Amaveda, H., Barreras, F., Jorda, X., & Lozano, M. 2003, "High frequency ultrasonic atomization with pulsed excitation. 2003;125:941-45", *J Fluids Eng.*, vol. 125, pp. 941-945.

Luscher, T. F., Steffel, J., Eberli, F. R., Joner, M., Nakazawa, G., Tanner, F. C., & Virmani, R. 2007, "Drug-eluting stent and coronary thrombosis: biological mechanisms and clinical implications", *Circulation*, vol. 115, no. 8, pp. 1051-1058.

Mabry, J. M., Vij, A., acono, S. T., & iers, B. D. 2008, "Fluorinated Polyhedral Oligomeric Silsesquioxanes (F-POSS)", *Angew.Chem.Int.Ed.*, vol. 47, pp. 4137-4140.

Maciel, G. E., Sullivan, M. J., & Sindorf, D. W. 1981, "Carbon-13 and silicon-29 nuclear magnetic resonance spectra of solid poly(methylsiloxane) polymers.", *Macromolecules*, vol. 14, pp. 1607-1608.

Madbouly, S. A., Otaigbe, J. U., Nanda, A. K., & Wicks, D. A. 2007, "Rheological behavior of POSS/polyurethane-urea nanocomposite films prepared by homogeneous solution polymerization in aqueous dispersions", *Macromolecules*, vol. 40, no. 14, pp. 4982-4991.

Mani, G., Feldman, M. D., Patel, D., & Agrawal, C. M. 2007, "Coronary stents: A materials perspective", *Biomaterials*, vol. 28, no. 9, pp. 1689-1710.

Mathur, A. B., Collier, T. O., Kao, W. J., Wiggins, M., Schubert, M. A., Hiltner, A., & Anderson, J. M. 1997, "In vivo biocompatibility and biostability of modified polyurethanes", *J.Biomed.Mater.Res.*, vol. 36, no. 2, pp. 246-257.

Mayer, B., Erdmann, J., & Schunkert, H. 2007, "Genetics and heritability of coronary artery disease and myocardial infarction", *Clin.Res.Cardiol.*, vol. 96, no. 1, pp. 1-7.

McCarthy, S. J., Meijs, G. F., Mitchell, N., Gunatillake, P. A., Heath, G., Brandwood, A., & Schindhelm, K. 1997, "In-vivo degradation of polyurethanes: transmission-FTIR microscopic characterization of polyurethanes sectioned by cryomicrotomy", *Biomaterials*, vol. 18, no. 21, pp. 1387-1409.

McFadden, E. P., Stabile, E., Regar, E., Cheneau, E., Ong, A. T., Kinnaird, T., Suddath, W. O., Weissman, N. J., Torguson, R., Kent, K. M., Pichard, A. D., Satler,

L. F., Waksman, R., & Serruys, P. W. 2004, "Late thrombosis in drug-eluting coronary stents after discontinuation of antiplatelet therapy", *Lancet*, vol. 364, no. 9444, pp. 1519-1521.

McGillicuddy, F. C., Lynch, I., Rochev, Y. A., Burke, M., Dawson, K. A., Gallagher, W. M., & Keenan, A. K. 2006b, "Novel "plum pudding" as potential drug-eluting stent coatings : Controlled release of fluvastatin", *Journal of Biomedical Materials Research Part A*, vol. 79A, no. 4, pp. 923-933.

Merkel, T. C., Freeman, B. D., ontak, R. J., , Z., nnau, I., akin, P., & ll, A. J. 2002a, "Ultrapermeable, Reverse-Selective Nanocomposite Membranes.", *Science*, vol. 296, no. 19.

Merkel, T. C., Freeman, B. D., Spontak, R. J., He, Z., Pinnau, I., Meakin, P., & Hill, A. J. 2002b, "Ultrapermeable, reverse-selective nanocomposite membranes", *Science*, vol. 296, no. 5567, pp. 519-522.

Meurice, T., Bauters, C., Hermant, X., Codron, V., VanBelle, E., McFadden, E. P., Lablanche, J., Bertrand, M. E., & Amouyel, P. 2001, "Effect of ACE inhibitors on angiographic restenosis after coronary stenting (PARIS): a randomised, double-blind, placebo-controlled trial", *The Lancet*, vol. 357, no. 9265, pp. 1321-1324.

Mintz, G. S., Popma, J. J., Pichard, A. D., Kent, K. M., Satler, L. F., Hong, M. K., & Leon, M. B. 1996, "Intravascular Ultrasound Assessment of the Mechanisms and Predictors of Restenosis Following Coronary Angioplasty", *J.Invasive.Cardiol.*, vol. 8, no. 1, pp. 1-14.

Mirzadeh, H., Katbab, A. A., Khorasani, M. T., Burford, R. P., Gorgin, E., & Golestani, A. 1995, "Cell attachment to laser-induced AAm- and HEMA-grafted

ethylene-propylene rubber as biomaterial: in vivo study", *Biomaterials*, vol. 16, no. 8, pp. 641-648.

Misra, R., Fu, B. X., & Morgan, S. E. 2007, "Surface energetics, dispersion, and nanotribomechanical behavior of POSS/PP hybrid nanocomposites", *Journal of Polymer Science Part B-Polymer Physics*, vol. 45, no. 17, pp. 2441-2455.

Moreau, J. J. E., Vellutini, L., Man, M. W. C., & Bied, C. 2003b, "Shape-controlled bridged silsesquioxanes: Hollow tubes and spheres", *Chemistry-A European Journal*, vol. 9, no. 7, pp. 1594-1599.

Morra, M., Occhiello, E., & Garbassi, F. 1990, "Knowledge About Polymer Surfaces from Contact-Angle Measurements", *Advances in Colloid and Interface Science*, vol. 32, no. 1, pp. 79-116.

Mu, J. F., Liu, Y. H., & Zheng, S. X. 2007, "Inorganic-organic interpenetrating polymer networks involving polyhedral oligomeric silsesquioxane and poly(ethylene oxide)", *Polymer*, vol. 48, no. 5, pp. 1176-1184.

Muisener, P. A. V. O., Jalbert, C. A., Yuan, C. G., Baetzold, J., Mason, R., Wong, D., Kim, Y. J., & Koberstein, J. T. 2003, "Measurement and modeling of end group concentration depth profiles for omega-fluorosilane polystyrene and its blends", *Macromolecules*, vol. 36, no. 8, pp. 2956-2966.

Muller, B., Riedel, M., Michel, R., De Paul, S. M., Hofer, R., Heger, D., & Grutzmacher, D. 2001, "Impact of nanometer-scale roughness on contact-angle hysteresis and globulin adsorption", *Journal of Vacuum Science & Technology B*, vol. 19, no. 5, pp. 1715-1720.

Murphy, J. G., Schwartz, R. S., Edwards, W. D., Camrud, A. R., Vlietstra, R. E., & Holmes, D. R., Jr. 1992, "Percutaneous polymeric stents in porcine coronary arteries. Initial experience with polyethylene terephthalate stents", *Circulation*, vol. 86, no. 5, pp. 1596-1604.

Murphy, P. V., Lacroix, A., Merchant, S., & Bernhard, W. 1970, "Development of Blood Compatible Polymers Using Electret Effect - Orpl", *Abstracts of Papers of the American Chemical Society* p. 4.

Nanda, A. K., Wicks, D. A., Madbouly, S. A., & Otaigbe, J. U. 2006, "Nanostructured polyurethane/POSS hybrid aqueous dispersions prepared by homogeneous solution polymerization", *Macromolecules*, vol. 39, no. 20, pp. 7037-7043.

Neumann, D., Fisher, M., Tran, L., & Matisons, J. G. 2002, "Synthesis and characterization of an isocyanate functionalized polyhedral oligosilsesquioxane and the subsequent formation of an organic-inorganic hybrid polyurethane", *J.Am.Chem.Soc.*, vol. 124, no. 47, pp. 13998-13999.

Nguyen, T. & Djurado, E. 2001, "Deposition and characterization of nanocrystalline tetragonal zirconia films using electrostatic spray deposition", *Solid State Ionics*, vol. 138, no. 3-4, pp. 191-197.

Nicholson, J. W. 2006, "Special topics in polymer chemistry", *J.Mater.Chem.*, vol. 16, pp. 3867-3874.

Norde, W. & Rouwendal, E. 1990, "Streaming Potential Measurements As A Tool to Study Protein Adsorption-Kinetics", *Journal of colloid and interface science*, vol. 139, no. 1, pp. 169-176.

Oaten, M. & Choudhury, N. R. 2005, "Silsesquioxane-Urethane Hybrid for Thin Film Applications", *Macromolecules*, vol. 38, no. 15, pp. 6392-6401.

Okner, R., Oron, M., Tal, N., Mandler, D., & Domb, A. J. 2007a, "Electrocoating of stainless steel coronary stents for extended release of Paclitaxel", *Materials Science & Engineering C-Biomimetic and Supramolecular Systems*, vol. 27, no. 3, pp. 510-513.

Ong, A.T.L., McFadden, E.P., Regar, E., de Jaegere, P.T., van Domburg, R.T. , & Serruys, P.W. 2005, " Late Angiographic Stent Thrombosis (LAST) Events With Drug-Eluting Stents", *J Am Coll Cardiol*, vol 45, pp. 2088-2092.

Owens, D. K. & Wendt, R. C. 1969, "Estimation of Surface Free Energy of Polymers", *Journal of Applied Polymer Science*, vol. 13, no. 8, p. 1741-&.

Pal, S., Weiss, H., Keller, H., & Muller-Plathe, F. 2005, "Effect of nanostructure on the properties of water at the water-hydrophobic interface: A molecular dynamics simulation", *Langmuir*, vol. 21, no. 8, pp. 3699-3709.

Pan, C. J., Tang, J. J., Shao, Z. Y., Wang, J., & Huang, N. 2007a, "Improved blood compatibility of rapamycin-eluting stent by incorporating curcumin", *Colloids Surf.B Biointerfaces.*, vol. 59, no. 1, pp. 105-111.

Pan, Ch. J., Tang, J. J., weng, Y. J., Wang, J., & Huang, N. 2006, "Preparation, characterization and anticoagulation of curcumin-eluting controlled biodegradable coating stents", *Journal of Controlled Release*, vol. 116, pp. 42-49.

Pareta, R., Brindley, A., Edirisinghe, M. J., Jayasinghe, S. N., & Luklinska, Z. B. 2005, "Electrohydrodynamic atomization of protein (bovine serum albumin)", *Journal of Materials Science-Materials in Medicine*, vol. 16, no. 10, pp. 919-925.

Pareta, R. & Edirisinghe, M. J. 2006, "A novel method for the preparation of starch films and coatings", *Carbohydrate Polymers*, vol. 63, no. 3, pp. 425-431.

Park, J. C., Park, B. J., Lee, D. H., Suh, H., Kim, D. G., & Kwon, O. H. 2002a, "Evaluation of the cytotoxicity of polyetherurethane (PU) film containing zinc diethyldithiocarbamate (ZDEC) on various cell lines", *Yonsei Med.J*, vol. 43, no. 4, pp. 518-526.

Park, S. J., Lee, C. W., Hong, M. K., Kim, J. J., Park, S. W., Tahk, S. J., Jang, Y. S., Seung, K. B., Yang, J. Y., & Jeong, M. H. 2002b, "Comparison of gold-coated NIR stents with uncoated NIR stents in patients with coronary artery disease", *Am.J.Cardiol.*, vol. 89, no. 7, pp. 872-875.

Patel, R. R., Mohanraj, R., & Pittman, C. U. 2006, "Properties of polystyrene and polymethyl methacrylate copolymers of polyhedral oligomeric silsesquioxanes: A molecular dynamics study", *Journal of Polymer Science Part B-Polymer Physics*, vol. 44, no. 1, pp. 234-248.

Pavanetto, F., Genta, I., Giunchedi, P., & Conti, B. 1993, "Evaluation of spray drying as a method for polylactide and polylactide-co-glycolide microsphere preparation", *J Microencapsulation*, vol. 10, pp. 487-497.

Petrenko, Y. A., Gorokhova, N. A., Tkachova, E. N., & Petrenko, A. Y. 2005, "The reduction of Alamar Blue by peripheral blood lymphocytes and isolated mitochondria", *UKRAINSKII BIOKHIMICHESKII ZHURNAL*, vol. 77, no. 5, pp. 100-105.

Phillips, S. H., Haddad, T. S., & Tomczak, S. J. 2004, "Developments in nanoscience: polyhedral silsesquioxane (POSS)-polymers oligomeric", *Current Opinion in Solid State & Materials Science*, vol. 8, no. 1, pp. 21-29.

Phua, S. K. 1987, "Biodegradation of a polyurethane in vitro", *Journal of Biomedical Materials Research*, vol. 21, pp. 231-246.

Pohl, M., Glogowski, T., Kuhn, S., Hessing, C., & Unterumsberger, F. 2008, "Formation of titanium oxide coatings on NiTi shape memory alloys by selective oxidation", *Materials Science and Engineering A-Structural Materials Properties Microstructure and Processing*, vol. 481, pp. 123-126.

Poncin, P. & Proft, J. "Stent tubing:underestanding the desired attributes.".

Prati, F., Di, M. C., Moussa, I., Reimers, B., Mallus, M. T., Parma, A., Lioy, E., & Colombo, A. 1999, "In-stent neointimal proliferation correlates with the amount of residual plaque burden outside the stent: an intravascular ultrasound study", *Circulation*, vol. 99, no. 8, pp. 1011-1014.

R.P.A.Hartman, D.J.Brunner, D.M.A.Camelot, J.C.M.Marijnissen, & B.Scarlett 2000, "jet break up in electrohydrodynamic atomization in the cone jet mode.", *Journal of Aerosol Science*, vol. 31, no. 1, pp. 65-95.

Ramani, K., Weinder, W., & Kumar, G. 1998, "Silicon sputtering as a surface treatment to titanium alloy for bonding with PEKEKK.", *International Journal of Adhesion and Adhesives*, vol. 18, no. 6, pp. 401-412.

Regar, E., Serruys, P. W., Bode, C., Holubarsch, C., Guermonprez, J. L., Wijns, W., Bartorelli, A., Constantini, C., Degertekin, M., Tanabe, K., Disco, C., Wuelfert, E., &

Morice, M. C. 2002, "Angiographic findings of the multicenter Randomized Study With the Sirolimus-Eluting Bx Velocity Balloon-Expandable Stent (RAVEL): sirolimus-eluting stents inhibit restenosis irrespective of the vessel size", *Circulation*, vol. 106, no. 15, pp. 1949-1956.

Regar, E., Sianos, G., & Serruys, P. W. 2001, "Stent development and local drug delivery", *British Medical Bulletin*, vol. 59, pp. 227-248.

Richard, R. E., Schwarz, M., Ranade, S., Chan, A. K., Matyjaszewski, K., & Sumerlin, B. 2005, "Evaluation of acrylate-based block copolymers prepared by atom transfer radical polymerization as matrices for paclitaxel delivery from coronary stents", *Biomacromolecules.*, vol. 6, no. 6, pp. 3410-3418.

Rogers, C. & Edelman, E. R. 1995, "Endovascular stent design dictates experimental restenosis and thrombosis", *Circulation*, vol. 91, no. 12, pp. 2995-3001.

Rosamond, W., Flegal, K., Furie, K., Go, A., Greenlund, K., Haase, N., Hailpern, S. M., Ho, M., Howard, V., Kissela, B., Kittner, S., Lloyd-Jones, D., McDermott, M., Meigs, J., Moy, C., Nichol, G., O'Donnell, C., Roger, V., Sorlie, P., Steinberger, J., Thom, T., Wilson, M., & Hong, Y. 2008, "Heart disease and stroke statistics--2008 update: a report from the American Heart Association Statistics Committee and Stroke Statistics Subcommittee", *Circulation*, vol. 117, no. 4, pp. e25-146.

Ryan, U. S. & Maxwell, G. 1986, "Isolation, culture, and subculture of bovine pulmonary artery endothelial cells: Mechanical methods", *Methods in Cell Science*, vol. 10, no. 1, pp. 3-5.

Safinia, L., Datan, N., Hohse, M., Mantalaris, A., & Bismarck, A. 2005, "Towards a methodology for the effective surface modification of porous polymer scaffolds", *Biomaterials*, vol. 26, no. 36, pp. 7537-7547.

Salacinski, H. J., Odlyha, M., Hamilton, G., & Seifalian, A. M. 2002a, "Thermo-mechanical analysis of a compliant poly(carbonate-urea)urethane after exposure to hydrolytic, oxidative, peroxidative and biological solutions", *Biomaterials*, vol. 23, no. 10, pp. 2231-2240.

Salacinski, H. J., Tai, N. R., Carson, R. J., Edwards, A., Hamilton, G., & Seifalian, A. M. 2002b, "In vitro stability of a novel compliant poly(carbonate-urea)urethane to oxidative and hydrolytic stress", *J.Biomed.Mater.Res.*, vol. 59, no. 2, pp. 207-218.

Salacinski, H., Hancook, S., and Seifalian, A. M.. Polymer for use in conduits, medical devices and biomedical surface modification. [Int. App. PCT/GB2005/000489].2005.

Sanchez, C., Soler-Illia, G. J. D. A., Ribot, F., Lalot, T., Mayer, C. R., & Cabuil, V. 2001a, "Designed hybrid organic-inorganic nanocomposites from functional nanobuilding blocks", *Chemistry of Materials*, vol. 13, no. 10, pp. 3061-3083.

Santerre, J. P., Labow, R. S., & Adams, G. A. 1993, "Enzyme-biomaterial interactions: effect of biosystems on degradation of polyurethanes", *J.Biomed.Mater.Res.*, vol. 27, no. 1, pp. 97-109.

Santerre, J. P., Labow, R. S., Duguay, D. G., Erfle, D., & Adams, G. A. 1994, "Biodegradation evaluation of polyether and polyester-urethanes with oxidative and hydrolytic enzymes", *J.Biomed.Mater.Res.*, vol. 28, no. 10, pp. 1187-1199.

Schulze, R. D., Possart, W., Kamusewitz, H., & Bischof, C. 1989, "Youngs Equilibrium Contact-Angle on Rough Solid-Surfaces .1. An Empirical Determination", *Journal of Adhesion Science and Technology*, vol. 3, no. 1, pp. 39-48.

Schurmann, K., Vorwerk, D., Uppenkamp, R., Klosterhalfen, B., Bucker, A., & Gunther, R. W. 1997, "Iliac arteries: Plain and heparin-coated dacron-covered stent-grafts compared with noncovered metal stents - An experimental study", *Radiology*, vol. 203, no. 1, pp. 55-63.

Schwartz, L. W. & Garoff, S. 1985, "Contact-Angle Hysteresis on Heterogeneous Surfaces", *Langmuir*, vol. 1, no. 2, pp. 219-230.

Schwartz, R. S., Topol, E. J., Serruys, P. W., Sangiorgi, G., & Holmes, D. R., Jr. 1998, "Artery size, neointima, and remodeling: time for some standards", *J.Am.Coll.Cardiol.*, vol. 32, no. 7, pp. 2087-2094.

Semiz, E., Ermis, C., Yalcinkaya, S., Sancaktar, O., & Deger, N. 2003, "Comparison of initial efficacy and long-term follow-up of heparin-coated Jostent with conventional NIR stent", *Jpn.Heart J.*, vol. 44, no. 6, pp. 889-898.

Serruys, P. W., Sianos, G., van der, G. W., Bonnier, H. J., Urban, P., Wijns, W., Benit, E., Vandormael, M., Dorr, R., Disco, C., Debbas, N., & Silber, S. 2002, "Intracoronary beta-radiation to reduce restenosis after balloon angioplasty and stenting; the Beta Radiation In Europe (BRIE) study", *Eur.Heart J.*, vol. 23, no. 17, pp. 1351-1359.

Sharkawi, T., Leyni-Barbaz, D., Chikh, N., & McMullen, J. N. 2005a, "Evaluation of the in vitro drug release from resorbable biocompatible coatings for vascular stents", *Journal of Bioactive and Compatible Polymers*, vol. 20, no. 2, pp. 153-168.

Sharp, V. W. & Taylor, B. C. 1971, "Experience with Negatively Charged Polyure thane-Backed Velours", *J.BIOMED.MATER.RES.SYMPOSIUM*, vol. 1, pp. 75-81.

Sheth, S., Litvack, F., Dev, V., Fishbein, M. C., Forrester, J. S., & Eigler, N. 1996, "Subacute thrombosis and vascular injury resulting from slotted-tube nitinol and stainless steel stents in a rabbit carotid artery model", *Circulation*, vol. 94, no. 7, pp. 1733-1740.

Silver, J. H., Lin, J. C., Lim, F., Tegoulia, V. A., Chaudhury, M. K., & Cooper, S. L. 1999, "Surface properties and hemocompatibility of alkyl-siloxane monolayers supported on silicone rubber: effect of alkyl chain length and ionic functionality", *Biomaterials*, vol. 20, no. 17, pp. 1533-1543.

Smith, S. C., Jr., Feldman, T. E., Hirshfeld, J. W., Jr., Jacobs, A. K., Kern, M. J., King, S. B., III, Morrison, D. A., O'Neill, W. W., Schaff, H. V., Whitlow, P. L., Williams, D. O., Antman, E. M., Adams, C. D., Anderson, J. L., Faxon, D. P., Fuster, V., Halperin, J. L., Hiratzka, L. F., Hunt, S. A., Nishimura, R., Ornato, J. P., Page, R. L., & Riegel, B. 2006, "ACC/AHA/SCAI 2005 Guideline Update for Percutaneous Coronary Intervention--summary article: a report of the American College of Cardiology/American Heart Association Task Force on Practice Guidelines (ACC/AHA/SCAI Writing Committee to Update the 2001 Guidelines for Percutaneous Coronary Intervention)", *Circulation*, vol. 113, no. 1, pp. 156-175.

Sobel, B. E. 2001, "Acceleration of restenosis by diabetes: pathogenetic implications", *Circulation*, vol. 103, no. 9, pp. 1185-1187.

Stefanadis, C., Toutouzas, K., Vlachopoulos, C., Stratos, C., Kallikazaros, I., Karayannakos, P., Gravanis, M. M., Robinson, K., & Toutouzas, P. 1996, "Stents wrapped in autologous vein: an experimental study", *J.Am.Coll.Cardiol.*, vol. 28, no. 4, pp. 1039-1046.

Sternberg, K., Kramer, S., Nischan, C., Grabow, N., Langer, T., Hennighausen, G., & Schmitz, K. P. 2007, "In vitro study of drug-eluting stent coatings based on poly(L-lactide) incorporating cyclosporine A - drug release, polymer degradation and mechanical integrity", *J.Mater.Sci.Mater.Med.*, vol. 18, no. 7, pp. 1423-1432.

Stoeckel, D., Pelton, A., & Duerig, T. 2004, "Self-expanding nitinol stents: material and design considerations", *Eur.Radiol.*, vol. 14, no. 2, pp. 292-301.

Stokes, K., Urbanski, P., & Cobian, K. 1987, "New test methods for the evaluation of stress cracking and metal catalyzed oxidation in implanted polymers", *Polyurethanes in biomedical engineering* pp. 109-128.

Stokes, K., Urbanski, P., & Upton, J. 1990, "The in vivo auto-oxidation of polyether polyurethane by metal ions", *J.Biomater.Sci.Polym.Ed*, vol. 1, no. 3, pp. 207-230.

Su, J. W., Fu, S. J., Gwo, S., & Lin, K. J. 2008, "Fabrication of porous carbon nanotube network", *Chem.Commun.* pp. 5631-5632.

Sundararajan, G. P. & van Ooij, W. J. 2000, "Silane based pretreatments for automotive steels", *Surface Engineering*, vol. 16, no. 4, pp. 315-320.

Suresh, S., Zhou, W. S., Spraul, B., Laine, R. M., Ballato, J., & Smith, D. W. 2004, "Novel fluoropolymer functionalized silsesquioxanes for nanoscale architecture of hybrid composites", *Journal of Nanoscience and Nanotechnology*, vol. 4, no. 3, pp. 250-253.

Suzuki, T., Kopia, G., Hayashi, S., Bailey, L. R., Llanos, G., Wilensky, R., Klugherz, B. D., Papandreou, G., Narayan, P., Leon, M. B., Yeung, A. C., Tio, F., Tsao, P. S., Falotico, R., & Carter, A. J. 2001, "Stent-based delivery of sirolimus reduces neointimal formation in a porcine coronary model", *Circulation*, vol. 104, no. 10, pp. 1188-1193.

Svedman, C., Tillman, C., Gustavsson, C. G., Moller, H., Frennby, B., & Bruze, M. 2005, "Contact allergy to gold in patients with gold-plated intracoronary stents", *Contact Dermatitis*, vol. 52, no. 4, pp. 192-196.

Taguchi, G. Introduction to quality engineering, quality resources. Asian Productivity Organisation, NY . 1986. Asian Productivity Organisation, NY.
Tamai, H., Igaki, K., Kyo, E., Kosuga, K., Kawashima, A., Matsui, S., Komori, H., Tsuji, T., Motohara, S., & Uehata, H. 2000, "Initial and 6-month results of biodegradable poly-l-lactic acid coronary stents in humans", *Circulation*, vol. 102, no. 4, pp. 399-404.

Tan, L., Dodd, R. A., & Crone, W. C. 2003, "Corrosion and wear-corrosion behavior of NiTi modified by plasma source ion implantation", *Biomaterials*, vol. 24, no. 22, pp. 3931-3939.

Tanabe, K., Serruys, P. W., Grube, E., Smits, P. C., Selbach, G., van der Giessen, W. J., Staberock, M., de, F. P., Muller, R., Regar, E., Degertekin, M., Ligthart, J. M.,

Disco, C., Backx, B., & Russell, M. E. 2003, "TAXUS III Trial: in-stent restenosis treated with stent-based delivery of paclitaxel incorporated in a slow-release polymer formulation", *Circulation*, vol. 107, no. 4, pp. 559-564.

Tang, K. & Gomez, A. 1995, "generation of monodisperse water droplets from electrospray in a corona-assisted cone jet mode.", *J.Coll.Inter.Sci.*, vol. 175, pp. 326-332.

Tang, L. 1995, "Inflammatory responses to biomaterials.", *American journal of clinical pathology*, vol. 103, no. 4, pp. 500-528.

Tang, Y. W., Labow, R. S., & Santerre, J. P. 2001, "Enzyme-induced biodegradation of polycarbonate-polyurethanes: dependence on hard-segment chemistry", *J.Biomed.Mater.Res.*, vol. 57, no. 4, pp. 597-611.

Tesoro, G. & Wu, Y. L. 1991, "Silane Coupling Agents - the Role of the Organofunctional Group", *Journal of Adhesion Science and Technology*, vol. 5, no. 10, pp. 771-784.

Tran, H. V., Hung, R. J., Loy, D. A., Wheeler, D. R., Byers, J., Conley, W., & Willson, C. G. 2001, "Synthesis of siloxanes and silsesquioxanes for 157 nm lithography", *Abstracts of Papers of the American Chemical Society*, vol. 221, p. U337.

Turri, S. & Levi, M. 2005, "Wettability of Polyhedral Oligomeric Silsesquioxane Nanostructured Polymer Surfaces.", *Macromol.Rapid Commun.*, vol. 26, pp. 1233-1236.

Turri, S., Levi, M., & Properties 2005, "Structure, Dynamic Properties, and Surface Behavior of Nanostructured Ionomeric Polyurethanes from Reactive Polyhedral Oligomeric Silsesquioxanes", *Macromolecules*, vol. 38, no. 13, pp. 5569-5574.

Unger, F., Westedt, U., Hanefeld, P., Wombacher, R., Zimmermann, S., Greiner, A., Ausborn, M., & Kissel, T. 2007, "Poly(ethylene carbonate): a thermoelastic and biodegradable biomaterial for drug eluting stent coatings?", *J.Control Release*, vol. 117, no. 3, pp. 312-321.

Unverdorben, M., Sattler, K., Degenhardt, R., Fries, R., Abt, B., Wagner, E., Koehler, H., Scholz, M., Ibrahim, H., Tews, K. H., Hennen, B., Daemgen, G., Berthold, H. K., & Vallbracht, C. 2003, "Comparison of a silicon carbide coated stent versus a noncoated stent in humans: the Tenax- versus Nir-Stent Study (TENISS)", *J.Interv.Cardiol.*, vol. 16, no. 4, pp. 325-333.

Vaina, S. & Serruys, P. W. 2006, "Progressive stent technologies: new approaches for the treatment of cardiovascular diseases", *Expert.Opin.Drug Deliv.*, vol. 3, no. 6, pp. 783-797.

Valgimigli, M., van Mieghem, C.A.G.; Ong, A.T.L.; Aoki, J.; Rodriguez Granillo, G.A.; McFadden, E.P.; Kappetein, A.P. de Feyter, P.J. ; Smits, P.C.; Regar, E.; Van der Giessen, W.J.; George Sianos, MD, PhD; Peter de Jaegere, MD, PhD; Ron T. Van Domburg, PhD; Patrick W. Serruys 2005, " Short- and Long-Term Clinical Outcome After Drug-Eluting Stent Implantation for the Percutaneous Treatment of Left Main Coronary Artery Disease", *Circulation.vol* 111, pp. 1383-1389.

van der Giessen, W. J., Lincoff, A. M., Schwartz, R. S., van Beusekom, H. M., Serruys, P. W., Holmes, D. R., Jr., Ellis, S. G., & Topol, E. J. 1996, "Marked

inflammatory sequelae to implantation of biodegradable and nonbiodegradable polymers in porcine coronary arteries", *Circulation*, vol. 94, no. 7, pp. 1690-1697.

van Domburg, R. T., Foley, D. P., de Jaegere, P. P., de, F. P., van den, B. M., van der, G. W., Hamburger, J., & Serruys, P. W. 1999, "Long term outcome after coronary stent implantation: a 10 year single centre experience of 1000 patients", *Heart*, vol. 82 Suppl 2, p. II27-II34.

Vaina, S. & Serruys, P.W. 2006, " Progressive stent technologies: new approaches for the treatment of cardiovascular diseases", *Expert Opin. Drug Deliv, vol 3, no. 6, pp.783-797.*

van Ooij, W. J., Zhu, D., Palanivel, V., Lamar, J. A., & Stacy, M. 2006, "Overview: The Potential of silanes for chromate replacement in metal finishing industries.", *Silicon Chemistry*, vol. 3, pp. 11-30.

Venkatraman, S. & Boey, F. 2007, "Release profiles in drug-eluting stents: issues and uncertainties", *J.Control Release*, vol. 120, no. 3, pp. 149-160.

Venkatraman, S., Boey, F., & Lao, L. 2008, "Implanted cardiovascular polymers: Natural, synthetic and bio-inspired.", *Progress in Polymer Science*, vol. 33, pp. 853-874.

Virmani, R., Farb, A., Guagliumi, G., & Kolodgie, F. D. 2004, "Drug-eluting stents: caution and concerns for long-term outcome", *Coron.Artery Dis.*, vol. 15, no. 6, pp. 313-318.

vom, D. J., Haager, P. K., Grube, E., Gross, M., Beythien, C., Kromer, E. P., Cattelaens, N., Hamm, C. W., Hoffmann, R., Reineke, T., & Klues, H. G. 2002,

"Effects of gold coating of coronary stents on neointimal proliferation following stent implantation", *Am.J.Cardiol.*, vol. 89, no. 7, pp. 801-805.

Vrolix, M. C., Legrand, V. M., Reiber, J. H., Grollier, G., Schalij, M. J., Brunel, P., Martinez-Elbal, L., Gomez-Recio, M., Bar, F. W., Bertrand, M. E., Colombo, A., & Brachman, J. 2000, "Heparin-coated Wiktor stents in human coronary arteries (MENTOR trial). MENTOR Trial Investigators", *Am.J.Cardiol.*, vol. 86, no. 4, pp. 385-389.

Wada, K., Watanabe, N., Yamada, K., Kondo, T., & Mitsudo, T. 2005, "Synthesis of novel starburst and dendritic polyhedral oligosilsesquioxanes", *Chemical Communications* no. 1, pp. 95-97.

Wahab, M. A., Mya, K. Y., & He, C. B. 2008, "Synthesis, morphology, and properties of hydroxyl Terminated-POSS/polyimide low-k nanocomposite films", *Journal of Polymer Science Part A-Polymer Chemistry*, vol. 46, no. 17, pp. 5887-5896.

Waller, B. F., Pinkerton, C. A., Orr, C. M., Slack, J. D., VanTassel, J. W., & Peters, T. 1991, "Morphological observations late (greater than 30 days) after clinically successful coronary balloon angioplasty", *Circulation*, vol. 83, no. 2 Suppl, p. I28-I41.

Wang, G. X., Luo, L. L., Yin, T. Y., Li, Y., Jiang, T., Ruan, C. G., Guidoin, R., Chen, Y. P., & Guzman, R. 2009, "Ultrasonic atomization and subsequent desolvation for monoclonal antibody (mAb) to the glycoprotein (GP) IIIa receptor into drug eluting stent", *Journal of Microencapsulation*.

Wang, X., Zhang, X., Castellot, J., Herman, I., Iafrati, M., & Kaplan, D. L. 2008, "Controlled release from multilayer silk biomaterial coatings to modulate vascular cell responses", *Biomaterials*, vol. 29, no. 7, pp. 894-903.

Wapner P.G. & Hoffman W.P. 2000, "Utilization of surface tension and wettability in the design and operation of microsensors", *Sensors and actuators b-chemical* no. 1-2, pp. 60-67.

Ward RS 1995, "Surface modification prior to surface formation. Control of polymer surface properties via bulk modification", *MedPlast Biomater* pp. 34-41.

Watanabe, H., Matsuyama, T., & Yamamoto, H. 2003, "Experimental study on electrostatic atomization of highly viscous liquids", *Journal of Electrostatics*, vol. 57, no. 2, pp. 183-197.

Welch, M., Durrans, D., Carr, H. M. H., Vohra, R., Rooney, O. B., & Walker, M. G. 1992, "Endothelial cell seeding: a review", *Annals of Vascular Surgery [0890-5096] Welch Year: 1992 Volume: 6 Issue: 5 Page: 473*, vol. 6, no. 5, pp. 473-484.

Wen, J. M., Somorjai, G., Lim, F., & Ward, R. 1997, "XPS study of surface composition of a segmented polyurethane block copolymer modified by PDMS end groups and its blends with phenoxy", *Macromolecules*, vol. 30, no. 23, pp. 7206-7213.

Werner, C. & Jacobasch, H. J. 1999, "Surface characterization of polymers for medical devices", *Int.J.Artif.Organs*, vol. 22, no. 3, pp. 160-176.

Westedt, U., Wittmar, M., Hellwig, M., Hanefeld, P., Greiner, A., Schaper, A. K., & Kissel, T. 2006, "Paclitaxel releasing films consisting of poly(vinyl alcohol)-graft-

poly(lactide-co-glycolide) and their potential as biodegradable stent coatings", *J.Control Release*, vol. 111, no. 1-2, pp. 235-246.

Whelan, D. M., van der Giessen, W. J., Krabbendam, S. C., van Vliet, E. A., Verdouw, P. D., Serruys, P. W., & van Beusekom, H. M. 2000, "Biocompatibility of phosphorylcholine coated stents in normal porcine coronary arteries", *Heart*, vol. 83, no. 3, pp. 338-345.

Whitehouse, C. M., Dreyer, R. N., Yamashita, M., & Fenn, J. B. 1985, "Electrospray interface for liquid chromatographs and mass spectrometers", *Anal.Chem.*, vol. 57, no. 3, pp. 675-679.

Whittaker, D. R. & Fillinger, M. F. 2006, "The engineering of endovascular stent technology: a review", *Vasc.Endovascular.Surg.*, vol. 40, no. 2, pp. 85-94.

Wieneke, H., Sawitowski, T., Wnendt, S., Fischer, A., Dirsch, O., Karoussos, I. A., & Erbel, R. 2002, "Stent coating: a new approach in interventional cardiology", *Herz*, vol. 27, no. 6, pp. 518-526.

Windecker, S., Mayer, I., De, P. G., Maier, W., Dirsch, O., De, G. P., Wu, Y. P., Noll, G., Leskosek, B., Meier, B., & Hess, O. M. 2001a, "Stent coating with titanium-nitride-oxide for reduction of neointimal hyperplasia", *Circulation*, vol. 104, no. 8, pp. 928-933.

Wisbey, A., Gregson, P. J., Peter, L. M., & Tuke, M. 1991, "Effect of surface-treatment on the dissolution of titanium-based implant materials", *Biomaterials*, vol. 12, no. 5, pp. 470-473.

Witsiepe W.K. 1973, "Segmented polyester thermoplastic elastomers", *Advances in chemistry series* no. 129, pp. 39-60.

Wohrle, J., Al-Khayer, E., Grotzinger, U., Schindler, C., Kochs, M., Hombach, V., & Hoher, M. 2001, "Comparison of the heparin coated vs the uncoated Jostent--no influence on restenosis or clinical outcome", *Eur.Heart J.*, vol. 22, no. 19, pp. 1808-1816.

Wood, W. R. & Loomis, A. L. 1927, "The Physical and Biological Effects of High F Frequency Sound-Waves of Great Intensity", *Philos.Mag.*, vol. 49, no. 22, pp. 417-437.

Wu, S. 1971, "Calculation of interfacial tension in polymer systems", *Journal of polymer science : Part C*, vol. 34, pp. 19-39.

Wu, W. & Nancollas, G. H. 1999, "Determination of interfacial tension from crystallization and dissolution data: a comparison with other methods", *Advances in Colloid and Interface Science*, vol. 79, no. 2-3, pp. 229-279.

Xiao, Z., Théroux, P, 1998, " Platelet Activation With Unfractionated Heparin at Therapeutic Concentrations and Comparisons With a Low-Molecular-Weight Heparin and With a Direct Thrombin Inhibitor", *Circulation.*, vol 97, pp. 251-256

Xu, H., Kuo, S., Huang, C., & Chang, F. 2004, "Characterization of Poly(vinyl pyrrolidone-*co*isobutylstyryl polyhedral oligomeric silsesquioxane) Nanocomposites", *Journal of Applied Polymer Science*, vol. 91, pp. 2208-2215.

Xu, H., Kuo, S., Lee, S., & Chang, F. 2002a, "Preparations, Thermal Properties, and Tg Increase Mechanism of Inorganic/Organic Hybrid Polymers Based on Polyhedral Oligomeric Silsesquioxanes", *Macromolecules*, vol. 35, pp. 8788-8793.

Xu, H. Y., Kuo, S. W., Huang, C. F., & Chang, F. C. 2002b, "Poly(acetoxystyrene-co-isobutylstyryl POSS) nanocomposites: Characterization and molecular interaction", *Journal of Polymer Research-Taiwan*, vol. 9, no. 4, pp. 239-244.

Yasuda, K., Bando, Y., Yamaguchi, S., Nakamura, M., Oda, A., & Kawase, Y. 2005, "Analysis of concentration characteristics in ultrasonic atomization by droplet diameter distribution", *Ultrason Sonochem.*, vol. 12, pp. 37-41.

Yeo, Y. & Park, K. 2004, "A new microencapsulation method using an ultrasonic atomizer based on interfacial solvent exchange", *Journal of Controlled Release*, vol. 100, pp. 379-388.

Yin, Y., Wise, S. G., Nosworthy, N. J., Waterhouse, A., & Bax, D. V. 2009, "Covalent immobilisation of tropoelastin on a plasma deposited interface for enhancement of endothelialisation on metal surfaces", *Biomaterials*, vol. 30, pp. 1675-1681.

Zaremba, C. M., Belcher, A. M., Fritz, M., Li, Y. L., Mann, S., Hansma, P. K., Morse, D. E., Speck, J. S., & Stucky, G. D. 1996, "Critical transitions in the biofabrication of abalone shells and flat pearls", *Chemistry of Materials*, vol. 8, no. 3, pp. 679-690.

Zeng, K., Wang, L., Zheng, S. X., & Qian, X. F. 2009, "Self-assembly behavior of hepta(3,3,3-trifluoropropyl) polyhedral oligomeric silsesquioxane-capped poly(epsilon-caprolactone) in epoxy resin: Nanostructures and surface properties", *Polymer*, vol. 50, no. 2, pp. 685-695.

Zhang, Ch., Babonneau, F., Bonhomme, Ch., Laine, R. M., Soles, Ch. L., Hristov, A., & Yee, A. F. 1998, "Highly Porous Polyhedral Silsesquioxane Polymers. Synthesis and Characterization", *J.Am.Chem.Soc.*, vol. 120, no. 33, pp. 8380-8391.

Zhang, G., Fandrey, C., Naqwi, A., & Wiedmann, T. S. 2008, "High-frequency ultrasonic atomization for drug delivery to rodent animal models-optimal particle size for lung inhalation of difluoromethylornithine", *Experimental Lung Research*, vol. 34, pp. 209-223.

Zhang, H. B. & Edirisinghe, M. J. 2006, "Electrospinning zirconia fiber from a suspension", *Journal of the American Ceramic Society*, vol. 89, no. 6, pp. 1870-1875.

Zhang, H. B., Edirisinghe, M. J., & Jayasinghe, S. N. 2006, "Flow behaviour of dielectric liquids in an electric field", *Journal of Fluid Mechanics*, vol. 558, pp. 103-111.

Zhang, H. B., Jayasinghe, S. N., & Edirisinghe, M. J. 2006, "Electrically forced microthreading of highly viscous dielectric liquids", *Journal of Electrostatics*, vol. 64, no. 6, pp. 355-360.

Zhang, S. L., Zou, Q. C., & Wu, L. M. 2006, "Preparation and characterization of polyurethane hybrids from reactive polyhedral oligomeric silsesquioxanes", *Macromolecular Materials and Engineering*, vol. 291, no. 7, pp. 895-901.

Zhang, Z., Cao, X., Zhao, X., Withers, S. B., Holt, C. M., Lewis, A. L., & Lu, J. R. 2006, "Controlled delivery of antisense oligodeoxynucleotide from cationically modified phosphorylcholine polymer films", *Biomacromolecules.*, vol. 7, no. 3, pp. 784-791.

Zhao, Q. 1991, "Foreign-body giant cells and polyurethane biostability : In vivo correlation of cell adhesion and surface cracking", *Journal of Biomedical Materials Research*, vol. 25, pp. 177-183.

Zhao, Q. H. 1993, "Human plasma a2-macroglobulin promotes in vitro oxidative stress cracking of Pellethane 2363-80A: In vivo and in vitro correlations.", *Journal of Biomedical Materials Research*, vol. 27, pp. 379-389.

Zheng, L., Farris, R. J., & Coughlin, E. B. 2001, "Novel polyolefin nanocomposites: Synthesis and characterizations of metallocene-catalyzed polyolefin polyhedral oligomeric silsesquioxane copolymers", *Macromolecules*, vol. 34, no. 23, pp. 8034-8039.

Zhu, L. B., Xiu, Y. H., Xu, J. W., Tamirisa, P. A., Hess, D. W., & Wong, C. P. 2005, "Superhydrophobicity on two-tier rough surfaces fabricated by controlled growth of aligned carbon nanotube arrays coated with fluorocarbon", *Langmuir*, vol. 21, no. 24, pp. 11208-11212.

Zilla, P., Fasol, R., Deutsch, M., Fischlein, T., Minar, E., Hammerle, A., Krupicka, O., & Kadletz, M. 1987, "Endothelial cell seeding of polytetrafluoroethylene vascular grafts in humans: a preliminary report", *J.Vasc.Surg.*, vol. 6, no. 6, pp. 535-541.

Zilla, P., Fasol, R., Grimm, M., Fischlein, T., Eberl, T., Preiss, P., Krupicka, O., von, O. U., & Deutsch, M. 1991, "Growth properties of cultured human endothelial cells on differently coated artificial heart materials", *J.Thorac.Cardiovasc.Surg.*, vol. 101, no. 4, pp. 671-680.